SOLID-STATE NMR ANALYSIS OF EXCIPIENTS AND DRUG-EXCIPIENT INTERACTIONS IN THE AMORPHOUS STATE

BY

DIANA M. SPERGER

Submitted to the graduate degree program in Pharmaceutical Chemistry and the Graduate Faculty of the University of Kansas in partial fulfillment of the requirements for the degree of Doctor of Philosophy.

Chairperson

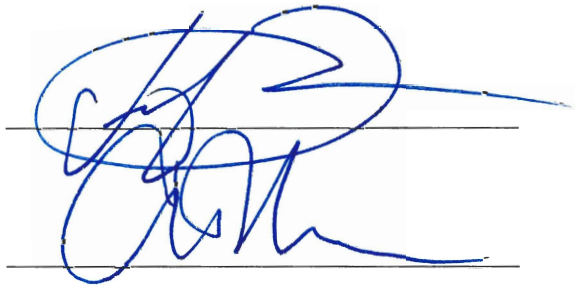

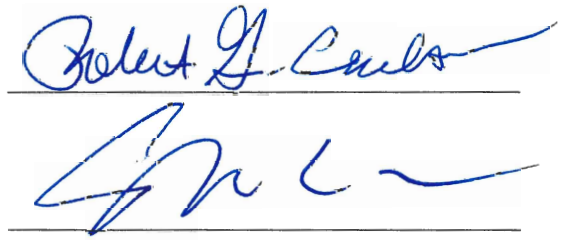

Committee members

Date Defended: August 18, 2010

The Dissertation Committee for Diana M. Sperger

certifies that this is the approved version of the following dissertation:

SOLID-STATE NMR ANALYSIS OF EXCIPIENTS AND DRUG-EXCIPIENT INTERACTIONS IN THE AMORPHOUS STATE

Chairperson

Date approved: August 26, 2010

Abstract

Solid-state NMR (SSNMR) experiments were used to investigate numerous aspects of pharmaceutically relevant amorphous materials, such as structure, molecular weight, water content, interactions with other molecules, and molecular mobility. This dissertation highlights the benefit of using SSNMR in conjunction with other techniques to gain a fuller understanding of the solid-state properties of amorphous pharmaceutical samples.

The application of SSNMR to the analysis of polysaccharide-based excipients was demonstrated. Excipients that were studied included the following: alginic acid and sodium alginate, carrageenans, starch and derivatives, microcrystalline cellulose, and cellulose-based derivatives such as hydroxyethylcellulose, (HEC), hydroxypropylcellulose (HPC), and hydroxypropylmethylcellulose (HPMC). Results showed that although the peaks in the SSNMR spectra of these samples were broad, the resolution was sufficient for accurate form identification and differentiation. Relaxation measurements provided unique information on starch derivatives. A linear correlation between T_1, the peak area of new signals, and the extent of hydrolysis of starch derivatives was observed.

Experiments to explore the potential for SSNMR parameters to be correlated to functionally related characteristics of sodium alginate were performed. The ability to detect variations in monomer content among different grades was demonstrated. Hydration was found to increase the resolution of signals in the SSNMR spectra. Differences in intrinsic viscosity and molecular weight of samples with similar monomer content were correlated to SSNMR relaxation times.

The hydrogen-bonding networks of the crystalline forms and the melt-quenched amorphous form of indomethacin were analyzed using SSNMR. Disruptions of this network when intimately mixed with PVP or HPMC were detected. SSNMR data supported the conclusion that indomethacin forms hydrogen bonds with PVP and HPMC at the expense of forming hydrogen bonds with other indomethacin molecules.

The miscibility and mobility of indomethacin amorphous solid dispersions was probed using SSNMR relaxation measurements. Based on relaxation values, indomethacin appeared to form a miscible amorphous solid dispersion with HPMC at all conditions studied and with PVP in solvent-evaporated mixtures. Melt-quenched indomethacin:PVP mixtures appeared only partially miscible by SSNMR relaxation measurements, suggesting that better mixing was achieved using solvent evaporation. The mobility of amorphous indomethacin was significantly reduced in the presence of both PVP and HPMC.

Dedicated to:

My mother, Charlene, for teaching me the value of education, the importance of hard work, and how to be a strong, independent, and successful woman.

Acknowledgements

First, I would like to express my gratitude to my advisor, Dr. Eric Munson, for his guidance and support throughout my time at the University of Kansas. I admire his passion for research, his scientific capabilities, and perhaps most of all the way he always looks out for his students. Whether it is a new instrument, a faster computer, the chance to attend a conference, an internship opportunity, or some time off to deal with personal/family issues, he always makes sure his students have what they need in order to succeed. For this genuine care and concern, I am truly grateful.

I would also like to thank Dr. Valentino Stella, Dr. Jennifer Laurence, Dr. Sue Lunte, and Dr. Robert Carlson for taking time out of their busy schedules and agreeing to serve on my dissertation committee. In particular, I must especially thank Drs. Stella and Laurence for reading this dissertation in its entirety and providing excellent feedback. Dr. Stella's willingness to serve as chairperson of my committee and as a substitute mentor to the Munson lab members over the past few months is also very much appreciated and will certainly not be forgotten.

Thank you to all past and present members of the Munson group: Dr. Dewey Barich, Dr. Bob Berendt, Elodie Dempah, Eric Gorman, Dr. Joe Lubach, Ben Nelson, Sarah Pyszczynski, and Dr. Loren Schieber. I am grateful for the professional and personal relationships I have made with each of you. Thank you, Bob, for being an exceptionally good friend and lab mate over the past six years. I don't think I could have survived the stress of classes, the long nights/weekends in lab, or the general frustrations

associated with graduate school without you. I would like to thank Joe and Loren for training me on the instruments when I first joined the group, teaching me the ways of the lab, and helping me whenever I needed them. I also must acknowledge Ben for his ability to fix broken instruments and for creating a method of doing nitrogen fills that no longer required me to drag heavy dewars around. Sarah and Elodie, thank you for joining the group and increasing the female-to-male ratio of the Munson lab. I am thankful for the friendship I have developed with each of you over the past three years and wish you both all the best as you complete your graduate career at the University of Kentucky.

Many thanks to the staff members who have made day-to-day operations much easier: Nicole Brooks, Karen Hall, Nancy Helm, Ann Heptig, and Richard Walker. In particular, I would like to thank Nicole, Nancy, and Ann for their friendship. Thank you for your genuine interest in how things were going for me both personally and professionally, for all the jokes and funny conversations we have shared, and for being there to listen whenever I just needed someone to talk to. The multiple cups of coffee I drink each day just won't be the same without you.

I am also extremely grateful for the Madison and Lila Self Graduate Fellowship, a program that would not be possible without the generosity of Al and Lila Self. The lessons I have learned during the skill sessions will surely contribute to my success in the future. Thank you to the following people who were instrumental in creating such a fine development program: Jimmy Morrison, Howard Mossberg, Cathy Dwigans, Sharon Graham, and Patty Dannenberg.

My time here at the University of Kansas would not have been nearly as enjoyable without the many wonderful colleagues and friends I have had the pleasure of making. In addition to the previously mentioned Munson lab members, I would like to especially thank (in no particular order) the following students and alumni for their friendship over the years: Courtney Kuhnline, Dr. Kelly Desino, Natalie Ciaccio, Maria (Thorson) Feeney, Taryn Bagby, Shuang Cai, Dr. Brooke Barrett, Mary Krause, Talia Martin, Jessica Creamer, Bo Pornputtapitak, Chuda Chittasupho, Supang Khondee, Dr. Laura Peek, Dr. Becky Bross, Dr. Celeste Frankenfeld, Dr. Amber Young, Dr. Pallabi Mitra, Dr. Katie Mitchell-Koch, Ester Bedard, Dr. Allyn Kaufmann, Dr. Sandipan Sinha, Dr. Erik Rytting, Ryan Funk, Stephen Goldman, Leon van Haandel, Josh Woods, Dr. Justin Pennington, Dr. Kwame Nti-Addae, Dr. Aditya Wakankar, Dr. Raja Thyagarajapuram, Dr. Prakash Manikwar, Barlas Buyuktimkin, Ahmed Badawi, Dr. Reza Esfandiary, Drew Vartia, Randy Logan, Justin Thomas, Dr. Aaron Markham, Dr. Pradyot Nandi, Dr. David Fischer, Dr. Dan Mudra, Dr. Bill Marinaro, Dr. Maulik Trivedi, and Dr. Gary Gerstenecker. Special thanks to Courtney for being such a great friend and allowing me to stay at her apartment during this last crazy month of graduate school, and to Kelly for providing excellent advice, friendship, and baked goods over the years.

Additionally, I must thank my friends who live in or near Kansas City and have provided a much needed escape from the stresses of graduate school: Ryan and Andrea Box, John Coleman, Greg and Megan Davey, Derek Gathright, Mike and Maggie Kolb, Brett and Erin Lambert, Tiffany Nixon, Katye Okerstrom, Will Potts, Mandy and Steven Riemer, Josh Roberts, Steve Stone, and Kate Theurer. In particular, I would like to thank

John for providing many wonderful memories of good times spent in the War Room. Thank you, Greg and Megan, for your friendship and constant support. To Mandy, Megan, and Tiffany: You are three fabulous ladies and I will miss our girls' nights together. I would also like to thank Tom and Ann Davey for the numerous Thanksgiving and Easter holidays spent at their home in Omaha. Thank you all for opening your hearts and welcoming me into your lives.

Thank you to my former Pfizer colleagues and friends for supporting my decision to return to graduate school. I am particularly grateful to fellow Jayhawks Dr. Amy Antipas and Dr. Ravi Shanker for encouraging me to come to Kansas. Also, thank you to Dr. Meg Landis, Dr. Gene Fiese, Alison Mutchler, LT Louie, Brenda Ramos, Lisa Yuhas, and Daryl Simmons for being great friends and for frequently checking in on me during the course of my graduate career.

Finally, thank you to those near and dear to my heart. To my best friends Rebecca Bulas Hazelton and Kim Hewitt Cooper: Thank you for always believing in me. I love you both like sisters. Tim Davey, you have been an amazing source of love and support. Thank you for your calming influence and for always being there for me. Mom, thank you for instilling into me a strong work ethic and desire to succeed. Dad, thank you for being my biggest fan. I would not have been able to make it through the past six years without you cheering me on. Tom and Patrick, thanks for being the best brothers I could have ever asked for. I am so grateful to have been blessed with a wonderful family and unbelievable support system. I love you all very much and would not be where I am today without you.

Table of Contents

Chapter 1

Introduction

1.1 Objectives

The overall purpose of this study was to assess whether solid-state NMR (SSNMR) spectroscopy could be used to analyze the structure and structure/function relationships of drugs, excipients, and drug-excipient mixtures. This work can be divided into two major parts: 1) detection of variability in excipient structural properties and correlation of SSNMR parameters to functionally related characteristics of excipients, and 2) analysis of the structure, physical stability, and mobility of amorphous drugs alone and formulated with excipients. In the following sections, a brief background on the importance of studying pharmaceutical solids will be given, and differences between crystalline and amorphous solid forms will be explained. The motivation for studying the amorphous state will be discussed, and common analytical methods used to characterize amorphous forms will be presented.

1.2 Pharmaceutical Solids

It is estimated that 90% of pharmaceuticals are formulated for oral drug delivery.[1] Oral administration is convenient and easy, which results in high patient compliance. While formulations for oral drug delivery can include solutions and suspensions, the majority are marketed in the solid state as tablets or capsules. Solid oral dosage forms offer the advantage of a longer shelf life, as the chemical degradation rates of drugs are

typically much slower in the solid state than in solution. Also, compared to other oral dosage forms, solid-state formulations are easier to store, transport, and handle. Furthermore, the relatively low cost of manufacturing makes solid oral dosage forms an attractive choice for pharmaceutical companies.

Solid oral dosage forms are composed of two major components: the active pharmaceutical ingredient (API) and other ingredients known as excipients. The API typically does not possess the proper material characteristics such as flow and compressibility required for manufacturing tablets of high quality, and if the API is highly potent, the size of the dose to be delivered is typically too small for producing reasonably sized tablets. Excipients are added to alleviate these problems, and can serve as binders, disintegrants, lubricants, dissolution modifiers, wetting agents, stabilizing agents, coating agents, and even as flavoring and coloring agents.[2-3]

In the following sections, the possible physical forms of the API and excipients will be described. These solid forms have a direct impact on the properties and performance characteristics of the formulation, such as the dissolution rate, physical and chemical stability, and manufacturability of the dosage form.[4] Thus, it is important to be able to detect any form changes in the API, even in the presence of excipients. Similarly, it is equally as important to detect variations in excipients and to ensure that the same form of an excipient is consistently used during formulation.

1.3 Solid-state Forms

In general, solid forms of drugs and excipients are grouped into two major classes, crystalline and amorphous. Crystalline solids are ones in which the component molecules are arranged in a highly ordered fashion. In amorphous materials, the long-range order present in crystalline solids does not exist.

1.3.1 The crystalline state

In a crystalline solid, the molecules are arranged into a three-dimensional lattice having long-range order. The smallest building block of a crystal structure is the unit cell, which repeats in three directions. The molecules in a crystal pack together to minimize void space, and are often stabilized by intermolecular non-covalent interactions such as hydrogen bonding.[5-6]

It is possible and quite common for molecules to pack into multiple conformational arrangements in the crystal lattice, resulting in different crystal structures for the same chemical compound. These different crystal structures are known as polymorphs, and can differ from one another in terms of melting point, density, solubility, and stability.[4] Most small molecule drugs and some commonly used excipients such as lactose and mannitol display polymorphism.[7] When multiple polymorphs of a substance exist at a given temperature and pressure, only one will be the most thermodynamically stable form. All others will be referred to as metastable forms and will eventually convert to the most thermodynamically stable form over time.

The thermodynamic stability relationship between polymorphs can be defined as either monotropic or enantiotropic.[8] In a monotropic system, one polymorph is the most thermodynamically stable form at all temperatures. In an enantiotropic system, the relative stability of polymorphs changes with temperature. As stability is represented by free energy, which is directly related to solubility, one common way to determine the type of relationship that exists is by creating a van't Hoff plot.[4] Theoretical van't Hoff plots for a monotropic and enantiotropic system are shown in Figures 1.1a and 1.1b, respectively. If the relative solubility difference does not change with temperature, a monotropic relationship exists; conversely, if the relative solubility inverts at some temperature, the relationship is defined as enantiotropic.

Additionally, crystalline solids can occur as solvates or salts.[9] A crystal form is termed a solvate when molecules of solvent are incorporated into the crystal lattice. When the solvent molecule is water, the solvate is termed a hydrate, and is commonly seen in pharmaceuticals. Salt forms can be prepared for compounds that have acidic or basic ionizable functional groups, and are typically used when the free acid or free base form of the drug displays poor solubility. Like polymorphs, solvates and salts will have different physicochemical properties than the unsolvated and free acid or free base forms.

These different types of crystal forms thereby give the pharmaceutical scientist a wealth of options when selecting the API and excipients to be included in a formulation. However, the choice is not limited to crystalline forms. The other major class of solid forms, the amorphous state, presents the pharmaceutical scientist with other options for formulation consideration.

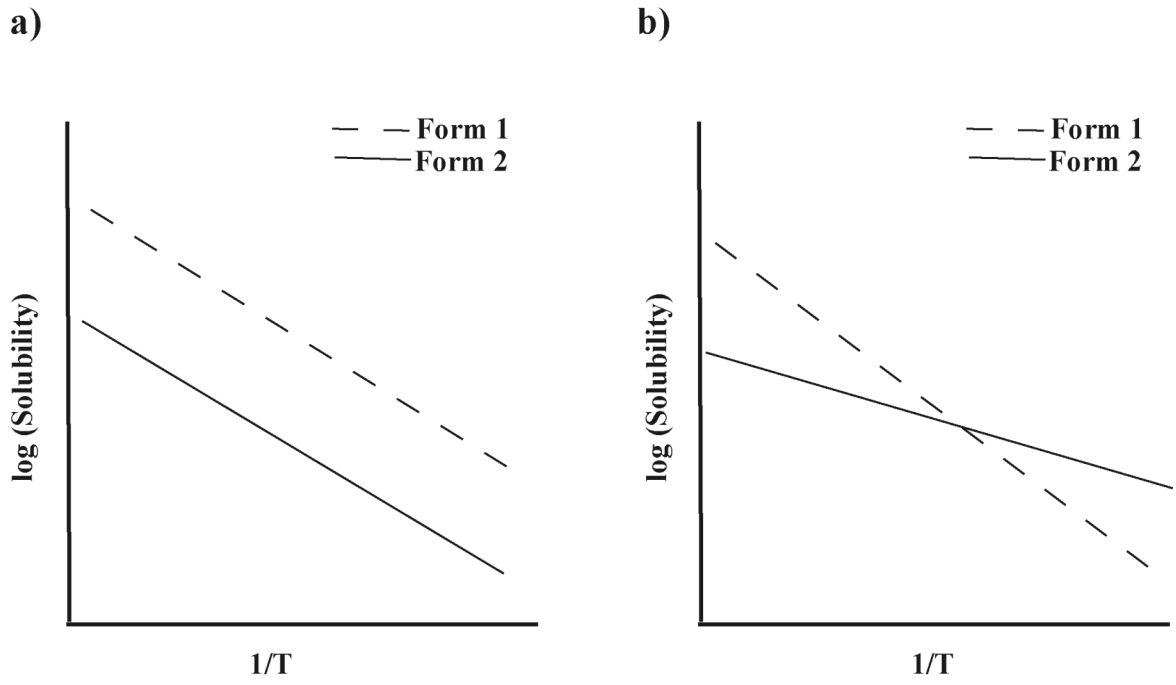

Figure 1.1. Theoretical van't Hoff plots for two polymorphs related (a) monotropically, and (b) enantiotropically.

1.3.2 The amorphous state

Amorphous solids are highly disordered materials that do not display the long-range order seen in crystalline materials. The amorphous form is sometimes referred to as a "glass" and can be viewed as an extension of the liquid state below the melting point of the crystalline solid. Compared to its crystalline counterpart, the amorphous form represents a higher energy, thermodynamically metastable (less stable) state.[10-11]

A graphical representation of the thermodynamic relationship between the liquid, amorphous, and crystalline states is shown in Figure 1.2. The enthalpy of a crystalline solid increases slowly with temperature until the melting temperature (T_m) is reached. At this point, a significant jump in enthalpy occurs as the material experiences a solid-liquid phase transition. If the liquid is rapidly cooled to a temperature below T_m such that it does not have sufficient time to crystallize, an amorphous solid, or "supercooled liquid", will be formed. The enthalpy of the supercooled liquid could theoretically continue to decrease with temperature at a constant rate, resulting in an eventual intersection with that of the crystalline solid. The temperature at which this intersection would occur is known as the Kauzmann temperature (T_K).[12-13] Below T_K, the supercooled liquid would theoretically have an enthalpy lower than that of the crystal. However, before this critical temperature is reached, there is a transition or change in the rate of enthalpy decrease that occurs. The point at which this transition occurs is known as the glass transition temperature (T_g). Here, the amorphous material changes from a supercooled liquid with low viscosity to a

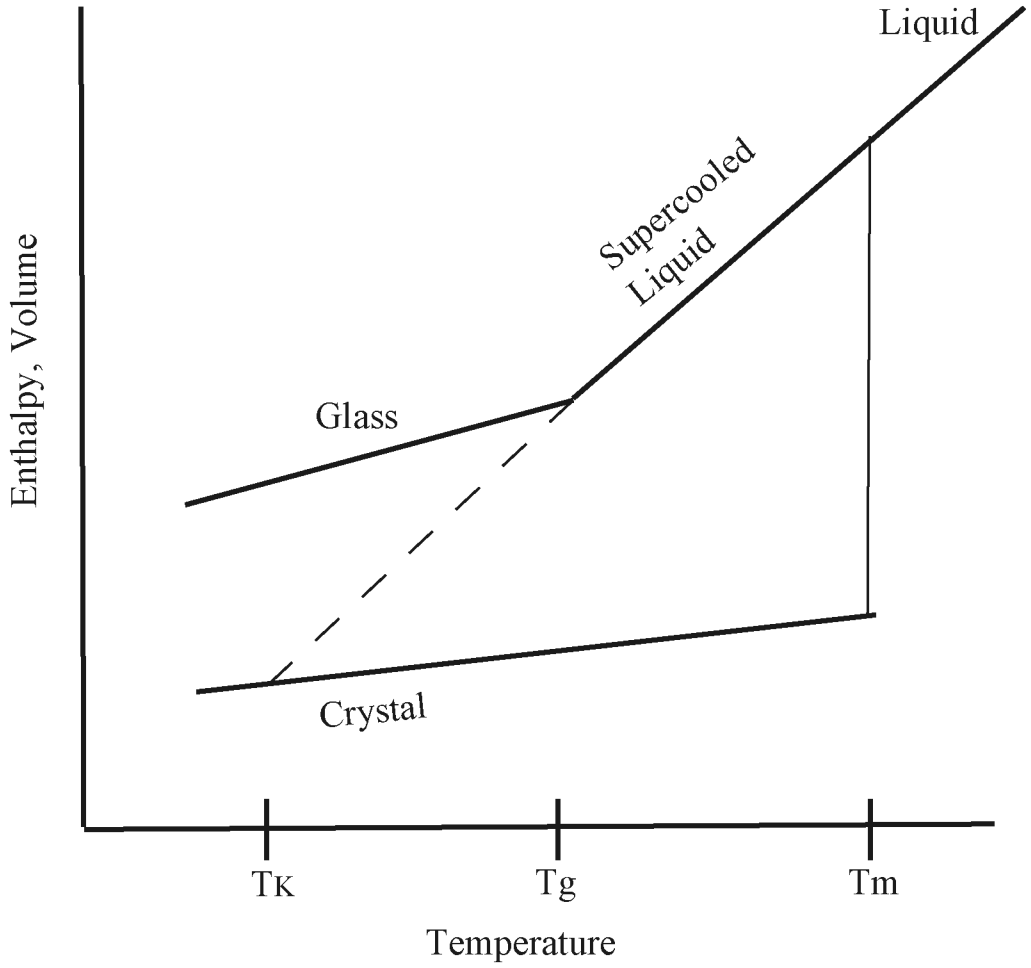

Figure 1.2. Graphical depiction of the thermodynamic relationship between the liquid, crystalline, and amorphous states. The changes in enthalpy that occur with temperature for each state are shown.

glass with much greater viscosity.

The glass transition temperature is one of the most important properties of the amorphous state. At temperatures below T_g, the amorphous form is considered to be in the glassy state. In the glassy state, the molecules lack motion and are essentially frozen in place. Above T_g, the amorphous form is commonly referred to as being in the rubbery state, and the molecules possess enough configurational motion to flow. Physicochemical properties such as physical stability will differ for these two states.[4] Thus, an understanding of where the boundary (T_g) between the glassy and rubbery states occurs is of great importance to the pharmaceutical scientist.

1.4 Occurrence of Amorphous Materials in Pharmaceuticals

The amorphous form is sometimes present as a physical impurity produced during the development or manufacturing of a crystalline solid. In these cases, the amorphous material is viewed as an undesired, unintentionally produced solid form because the physical and/or chemical degradation of the amorphous form can affect the therapeutic integrity of the drug product. However, in many cases, amorphous solids are intentionally selected for use in pharmaceutical dosage forms. Three major uses of amorphous solids and situations in which the pharmaceutical scientist will encounter the amorphous form are outlined below.

1.4.1 Naturally derived excipients

Many excipients used by the pharmaceutical industry are natural polymers. For example, starches and celluloses, the most abundant natural polymers on earth, are extensively used as excipients in pharmaceutical formulations. Polysaccharides such as starch and cellulose offer a wide variety and range of physicochemical properties, as well as the possibility for structurally modified derivatives to be created.[14] Other commonly used polysaccharide-based excipients include, but are certainly not limited to, alginates, carrageenans, derivatives of starch such as maltodextrin, and derivatives of cellulose such as hydroxypropylmethylcellulose (HPMC).

Polymers intrinsically exist as either fully amorphous forms or as semi-crystalline materials. In semi-crystalline polymers, both amorphous and crystalline regions exist; however, although crystalline regions can exist among amorphous zones, a completely crystalline polymer possessing long-range order will never be encountered. Fully amorphous polymers do not melt and thus will not exhibit a T_m but rather will have a T_g at which the material softens. Semi-crystalline polymers will have a T_g corresponding to the amorphous regions but will also have a T_m at the point at which the ordered regions of the polymer break up. The T_g for amorphous polymers does not typically occur as a sharp transition but rather as a broad transition spanning over a wide range of temperatures. The molecular weight, thermal history, chemical composition, and water content of the polymer can all have an effect on the T_g. These parameters vary greatly for naturally derived excipients, which can result in differences in physicochemical properties, structure, and functional behavior in formulations.

1.4.2 Amorphous APIs

Over the past decade, there has been elevated interest in the use of amorphous forms of small molecule active pharmaceutical ingredients (APIs) as a means of improving oral bioavailability. In theory, the amorphous form represents the most energetic solid state of a material. Thus, when prepared in the amorphous state, poorly soluble APIs will exhibit higher solubility and dissolution rates than their crystalline counterparts.[15]

Amorphous forms of small molecule drugs can be generated in various ways. Common routes to the amorphous state include cooling of the melt, precipitation from solution via rapid solvent evaporation, and mechanical disruption of the crystal lattice.[16-17] There are advantages and disadvantages associated with each of these methods.

Preparation of the amorphous state from the melt involves rapid cooling, or quenching, of the melt e.g., by immersion in liquid nitrogen. Quenching of the melt prohibits the molecules from arranging themselves into an ordered crystal lattice upon solidification. This technique is often the first to be evaluated when trying to render an API amorphous, as it is fast and often successful. However, one major drawback of this method is that it cannot be used for compounds that degrade at temperatures close to the melting point.

Solvent-evaporation methods involve the removal of solvent, either slowly or rapidly, resulting in formation of an amorphous solid. This type of method avoids the potential for thermal degradation that exists when using the melt-quench method. This technique can be achieved through the use of rotary evaporation or spray drying. In both cases, the API is first dissolved in an organic solvent. When using rotary evaporation, the

solvent is efficiently removed by lowering the pressure above the bulk liquid, which in turn lowers the boiling point of the solvent. With spray drying, the solution is passed through a spray nozzle, or atomizer, to create small droplets that are then dried by passing through a hot gas. The biggest disadvantages of these methods are that they require the use of large quantities of organic solvent when scaled up for manufacturing, and the potential for residual organic solvent to be present in the final product is always a risk.

The third type of method involves mechanical disruption, which can be achieved through grinding of the crystalline material.[18] Grinding induces stress in the crystal lattice, resulting in bond breakage, deformations, and eventual transformation to the amorphous state. In order to dissipate the heat that can be produced by grinding, the process can be performed at liquid nitrogen temperatures and is thus referred to as cryogrinding. Although issues that accompany other techniques are avoided, drawbacks do exist. First, mechanical disruption as a route to the amorphous state will unfortunately not be successful for every API. Additionally, the length of grinding time needed to create completely amorphous material can vary dramatically, ranging from just a couple of minutes for some compounds to over an hour for others.

No matter which method is used, the amorphous form that is produced is thermodynamically metastable and will eventually transform to a more stable crystal form through nucleation and crystal growth.[4,11] Thus, all benefits of increased solubility and dissolution rate are lost. As discussed in section 1.3.2, amorphous solids have higher mobility and hence greater propensity to recrystallize when in the rubbery state than when in the glassy state. However, even when stored at temperatures below T_g, the non-

equilibrium glassy state can "relax" toward the equilibrium supercooled liquid state, as shown in Figure 1.3. This process is referred to as structural or enthalpic relaxation, and occurs as the glassy state anneals, or ages, at a temperature (T_a) below that of the T_g.[19-20] During aging, enthalpy and free volume decrease while structural order increases. Once the amorphous compound has fully relaxed, crystallization can occur. Thus, the production of a stable amorphous API that is not prone to crystallization over the normal shelf life of a product (~2 years) is a challenging task for the pharmaceutical scientist.

1.4.3 Amorphous solid dispersions

Amorphous solid dispersions are processed mixtures of the API in the amorphous state with a water-soluble, amorphous polymeric excipient. The preparation of a solid dispersion is a formulation strategy used to counter the tendency for recrystallization and maintain the performance benefits of the amorphous form.[21] The T_g of an amorphous solid dispersion typically falls between that of the amorphous API and the amorphous polymer. The ability of polymers to physically stabilize the amorphous API has been attributed to many factors, such as preferential API-polymer interactions and reduced molecular mobility.[11]

Amorphous solid dispersions can be classified based upon the degree of molecular mixing that exists. Maximum stabilization of the amorphous API will only be achieved if the drug and excipient are intimately mixed on the molecular level. When the solid dispersion consists of a single phase of API and polymer, it is defined as a "miscible" system. In a "partially miscible" system, multiple amorphous phases with different API to

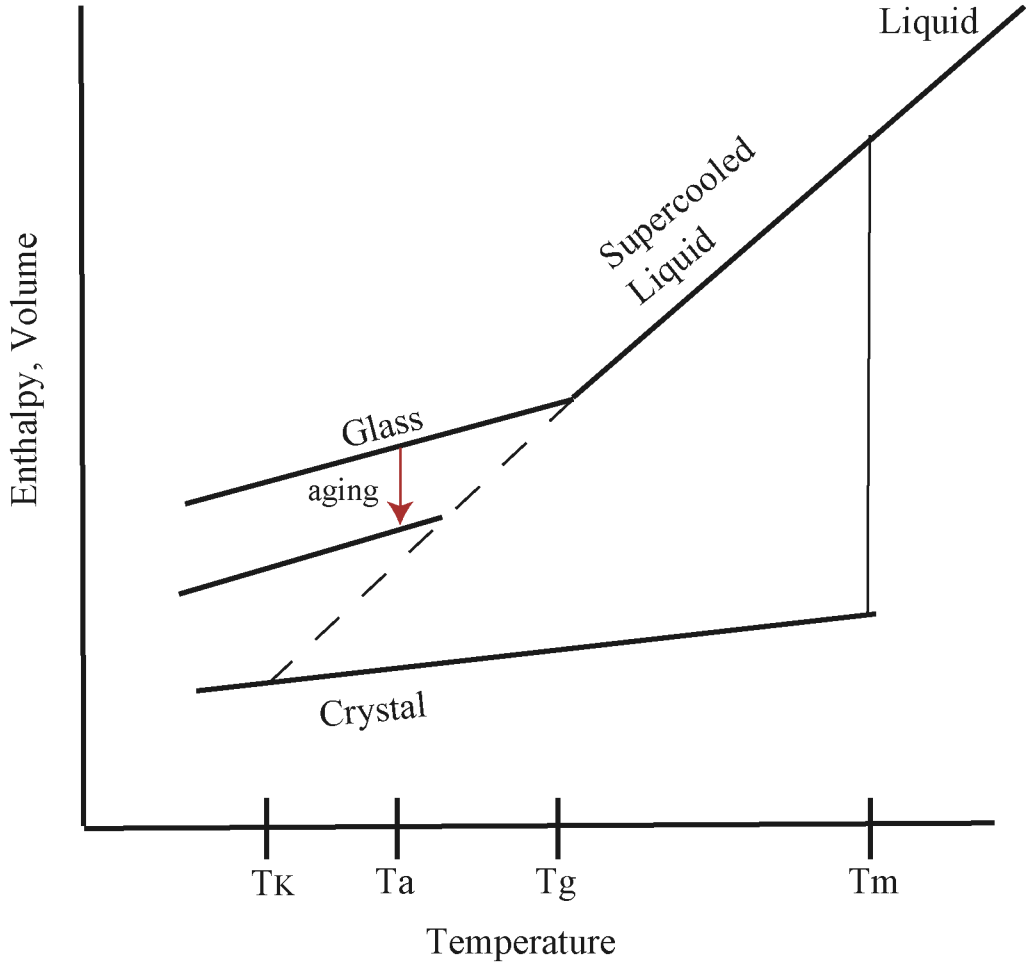

Figure 1.3. Graphical depiction of the thermodynamic relationship between the liquid, crystalline, and amorphous states. The structural relaxation that occurs during aging of the glassy amorphous state is shown.

polymer ratios are present. When the API and excipient are completely "immiscible", the system is fully phase separated into the individual amorphous components. These variations in composition will result in differences in physical stability between these systems, which makes an understanding of the degree of mixing that occurs during preparation of amorphous solid dispersions extremely important.

Frequently used pharmaceutically acceptable polymers for the creation of amorphous solid dispersions include polyvinylpyrollidone (PVP) and various hydroxypropylmethylcellulose (HPMC) derivatives. Amorphous solid dispersions can be prepared using the same methods outlined in section 1.4.2, with the only difference being that the starting material is now a mixture of both API and polymer.

1.5 Characterization of Amorphous Solids

Amorphous solids can be characterized using a wide variety of analytical methods. These methods can be classified as thermal, crystallographic, or spectroscopic techniques. Each analytical tool offers unique information about the amorphous state.

Thermal analysis refers to any method in which the sample is heated and a change in some physical property is monitored. The most commonly used thermal methods for the analysis of amorphous solids are thermogravimetric analysis (TGA) and differential scanning calorimetry (DSC). In TGA, the sample is heated and any change in mass that occurs is monitored. Thus, this technique is commonly used to determine the amount of

solvent or any volatile component associated with an amorphous material. In a DSC experiment, the difference in heat flow between a reference and a sample is measured. DSC can detect both endothermic (e.g., melting) and exothermic (e.g., crystallization) events. Additionally, DSC is often used to determine the T_g of amorphous materials. A measure of the rate and extent of enthalpic relaxation of the amorphous form can also be performed using DSC experiments.[19]

Powder X-Ray diffraction (PXRD) is the crystallographic technique most often used for the analysis of pharmaceutical solids. As discussed in section 1.3.1, crystalline solids are highly ordered. This highly ordered array of atoms and molecules enables the crystal to act as a three-dimensional diffraction grating for X-rays, resulting in distinct diffraction patterns that are unique to each crystal structure. In amorphous solids, long-range order does not exist. Therefore, amorphous materials do not give a definitive X-ray pattern, but rather produce a diffuse "halo". Observation of a large halo and lack of sharp peaks in a PXRD diffraction pattern is currently the most widely accepted method for determining the presence of amorphous material.

Spectroscopic methods used for the analysis of amorphous solids include infrared (IR), Raman, and SSNMR spectroscopy. IR and Raman spectroscopy are complementary techniques that monitor changes in the vibrational energy states of a molecule. These energy states are extremely sensitive to changes in structure, conformation, and chemical environment, making IR and Raman spectra quite useful for the identification of different solid forms. SSNMR spectroscopy monitors changes in the local electronic environment of the nuclei present in the sample of interest. The signals in the SSNMR spectrum of a

crystalline material will occur as sharp peaks, while peaks in the SSNMR spectrum of an amorphous form will be much broader. Additionally, SSNMR spectroscopy can be used to examine the molecular dynamics of solids through the use of relaxation measurements, and thus can be useful for determining the mobility of molecules in the amorphous state.[22-23]

1.6 Overview of Thesis Work

The previous sections have provided an introduction to pharmaceuticals in the solid state, the motivation for the pharmaceutical scientist to study the amorphous form, and a brief outline of some of the common analytical methods used for amorphous material characterization. In this section, the chapters in this dissertation are described.

1.6.1 Solid-state NMR spectroscopy and applications to pharmaceuticals

Chapter 2 provides an overview of SSNMR spectroscopy, including the basic theory behind the technique, its limitations, and advantages it provides over other analytical tools. Specifically, the areas in which SSNMR spectroscopy can add a wealth of information to the current understanding of API and excipients in the amorphous state will be highlighted.

1.6.2 Structural characterization of polymeric excipients

In Chapter 3, the information gained from SSNMR spectroscopy of a wide variety of polysaccharide-based excipients obtained from various suppliers will be presented. The potential to use SSNMR parameters such as chemical shift (peak position), relative peak areas and intensities, and relaxation times for the identification of different excipient forms and detection of variations in excipient structure will be demonstrated.

1.6.3 Correlation of SSNMR parameters to excipient properties that affect functionality

Whereas Chapter 3 provides a survey of the structural information gained from SSNMR analysis of various excipients, Chapter 4 focuses on how SSNMR parameters can be correlated to functionally related characteristics of excipients. Sodium alginate was the model excipient chosen for this study. The analysis of composition, molecular weight, and water content variations in this excipient using SSNMR analysis will be presented.

1.6.4 Detection of drug-excipient interactions in amorphous solid dispersions

Chapter 5 describes how SSNMR spectroscopy can be used to gain insight into the nature of stabilizing interactions that occur in amorphous solid dispersions. Specifically, the poorly water-soluble drug indomethacin was prepared with polymeric excipients such as PVP and HPMC. Differences in hydrogen bonding arrangements between these systems will be discussed, and comparisons to physical mixtures will be presented.

1.6.5 Insights into miscibility and mobility of amorphous solid dispersions

Chapter 6 builds upon the data in Chapter 5 and describes the ability of SSNMR relaxation measurements to be used for determination of both miscibility and mobility in amorphous solid dispersions of indomethacin and PVP or HPMC. Results from variable temperature SSNMR studies that were performed in order to examine the effect of temperature on miscibility and mobility will also be presented.

1.7 References

1. Hillery AM. 2001. Advanced drug delivery and targeting: an introduction. In Hillery AM, Lloyd AW, Swarbrick J, editors. Drug delivery and targeting for pharmacists and pharmaceutical scientists, Ed., New York: Taylor and Francis Inc. p 63-81.

2. Kottke MK, Rudnic EM. 2002. Tablet dosage forms. In Banker GS, Rhodes CT, editors. Modern Pharmaceutics, 4th ed., New York: Marcel Dekker Inc. p 287-333.

3. Rowe RC, Sheskey PJ, Owens SC. 2006. Handbook of pharmaceutical excipients. 5th ed., Washington DC: American Pharmacists Association. p 918.

4. Byrn SR, Pfeiffer RR, Stowell JG. 1999. Solid-state chemistry of drugs. Second ed., West Lafayette, IN: SSCI, Inc. p 574.

5. Reutzel SM, Etter MC. 1992. Evaluation of the conformational, hydrogen bonding, and crystal packing preferences of acyclic imides. J Phys Org Chem 5(1):44-54.

6. Kistenmacher TJ, Marsh RE. 1972. Crystal and molecular structure of an antiinflammatory agent, indomethacin, 1-(p-chlorobenzoyl)-5-methoxy-2-methylindole-3-acetic acid. J Am Chem Soc 94:1340-1345.

7. Kirk JH, Dann SE, Blatchford CG. 2007. Lactose: a definitive guide to polymorph determination. Int J Pharm 334:103-114.

8. Burger A, Ramberger R. 1979. On the polymorphism of pharmaceuticals and other molecular crystals. I. Theory of thermodynamic rules. Mikrochimica Acta 2:259-271.

9. Brittain HG. 2007. Polymorphism and solvatomorphism 2005. J Pharm Sci 96(4):705-728.

10. Hancock BC, Zografi G. 1997. Characteristics and significance of the amorphous state in pharmaceutical systems. J Pharm Sci 86(1):1-12.

11. Bhugra C, Pikal MJ. 2008. Role of thermodynamic, molecular, and kinetic factors in crystallization from the amorphous state. J Pharm Sci 97(4):1329-1349.

12. Kauzmann W. 1948. The nature of the glassy state and the behavior of liquids at low temperatures. Chemical Reviews 43:219-256.

13. Hancock BC, Christensen K. 1998. Estimating the critical molecular mobility temperature (Tk) of amorphous pharmaceuticals. Pharm Res 15:1649-1651.

14. Marchessault RH, Ravenelle F, Zhu XX. 2006. Polysaccharides for Drug Delivery and Pharmaceutical Applications. ed., Washington, DC: American Chemical Society

15. Hancock BC, Parks M. 2000. What is the true solubility advantage for amorphous pharmaceuticals? Pharm Res 17(4):397-404.

16. Patterson JE, James MB, Forster AH, Lancaster RW, Butler JM, Rades T. 2005. The influence of thermal and mechanical preparative techniques on the amorphous state of four poorly soluble compounds. J Pharm Sci 94(9):1998-2012.

17. Patterson JE, James MB, Forster AH, Lancaster RW, Butler JM, Rades T. 2007. Preparation of glass solutions of three poorly water soluble drugs by spray drying, melt extrusion and ball milling. Int J Pharm 336:22-34.

18. Wildfong PLD, Hancock BC, Moore MD, Morris KR. 2006. Towards an understanding of the structurally based potential for mechanically activated disordering of small molecule organic crystals. J Pharm Sci 95(12):2654-2656.

19. Hancock BC, Shamblin SL, Zografi G. 1995. Molecular mobility of amorphous pharmaceutical solids below their glass transition temperatures. Pharm Res 12(6):799-806.

20. Liu J, Rigsbee DR, Stotz C, Pikal MJ. 2002. Dynamics of pharmaceutical amorphous solids: the study of enthalpy relaxation by isothermal microcalorimety. J Pharm Sci 91(8):1853-1862.

21. Vasconcelos T, Sarmento B, Costa P. 2007. Solid dispersions as strategy to improve oral bioavailability of poor water soluble drugs. Drug Discov Today 12(23/24).

22. Lubach JW, Xu D, Segmuller BE, Munson EJ. 2007. Investigation of the effects of pharmaceutical processing upon solid-state NMR relaxation times and implications to solid-state formulation stability. J Pharm Sci 96(4):777-787.

23. Forster AH, Apperley D, Hempenstall J, Lancaster RW, Rades T. 2003. Investigation of the physical stability of amorphous drug and drug/polymer melts using variable temperature solid state NMR. Pharmazie 58:761-762.

Chapter 2

Solid-state NMR Spectroscopy and Applications to Pharmaceuticals

2.1 Introduction

In Chapter 1, the nature of the amorphous state and its relevance to pharmaceuticals was presented. Methods commonly used to characterize amorphous solids were briefly outlined. The purpose of this chapter is twofold: 1) to provide a general overview of the basic theory of SSNMR, and 2) to highlight the aspects of SSNMR particularly pertinent for analysis of the systems to be discussed in this dissertation. For a comprehensive, detailed explanation of NMR theory, the reader is directed to other sources.[1-2]

2.2 Basic Theory of NMR Spectroscopy

All nuclei contain protons, which carry a charge, and neutrons, which have no charge. The combination of these gives each nucleus a characteristic spin quantum number, denoted as *I*. Some nuclei have integral spin quantum numbers (*I*=1, 2, 3...), some have fractional spin quantum numbers (*I*=1/2, 3/2, 5/2…), and some have a spin quantum number of zero (*I*=0) and cannot be observed by NMR. In this dissertation, only commonly observed NMR active nuclei with $I = 1/2$, such as ^{1}H and ^{13}C, will be discussed.

In the absence of an external magnetic field, nuclei with $I = 1/2$ will have two degenerate spin states. When an external magnetic field, B_0, is applied, the spin states will become non-degenerate, as shown in Figure 2.1. The magnetic moment of the lower energy state (α) is aligned with B_0, but that of the higher energy

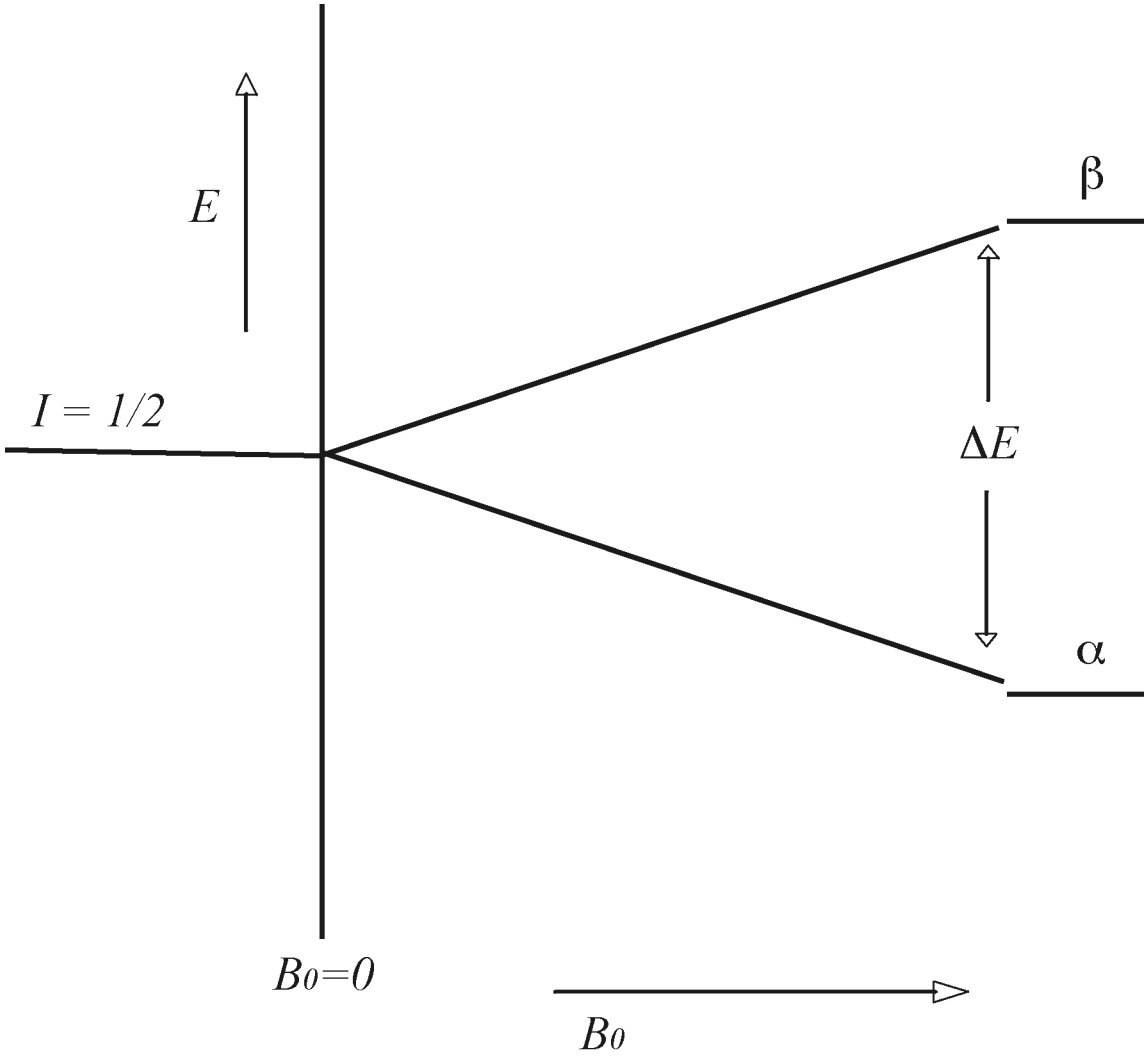

Figure 2.1 Splitting of nuclear spin states in an external magnetic field.

state (β) is aligned against B_0. The population difference between these two states is governed by the Boltzmann distribution:

$$\Delta N_0 = Ne^{\Delta E/k_B T}$$

In this equation, N is equal to the number of nuclei present, $\Delta E = \gamma \hbar B_0$, k_B is the Boltzmann constant, and T is temperature. An excess of spins will exist in the lower energy state and the magnitude of this excess will depend on the strength of B_0.

Nuclei are charged, and a spinning charge will have a magnetic moment, which can be visualized as a tiny bar magnet. The torque produced by the external magnetic field will cause the nuclei to precess at a rate proportional to the strength of the external magnetic field and the magnetogyric ratio (γ), a unique constant for each nucleus. For example, a ^{1}H nucleus placed in a magnetic field of 7.05 T will have a Larmor frequency of 300 MHz, while a ^{13}C nucleus placed in the same field will have a Larmor frequency of 75 MHz.

In Fourier transform (FT) NMR spectroscopy, the nuclei are perturbed from equilibrium by applying a radio frequency (RF) pulse, and the precessing spins create an alternating current in a coil surrounding the sample. The resulting signal, or free induction decay (FID), is collected, amplified, and processed to produce the NMR spectrum. As shown in Figure 2.1, increasing the strength of B_0 results in a greater ΔE, which thereby produces a bigger population difference. This larger population difference results in a larger NMR signal. Stronger magnetic fields therefore generate stronger signals in NMR spectroscopy.

Differences in the local electronic environments surrounding the nuclei in a molecule cause the nuclei to experience slight differences in the magnetic field. The nuclei then resonate at slightly different frequencies. Therefore, each unique nucleus will produce a characteristic signal located in a specific region of the NMR spectrum. This difference in peak position for different nuclei is referred to as the chemical shift. Chemical shifts are measured in parts per million (ppm) with respect to a reference signal.

2.3 Solid-state NMR Spectroscopy

Solution-state NMR is viewed as the most powerful tool for structural elucidation of organic compounds. Highly resolved, sharp signals can be achieved because the rapid tumbling of molecules in solution averages out most of the contributions that cause line broadening. When applied to solids, however, conventional solution-state NMR techniques produce only a broad, featureless NMR spectrum. The rigidity of molecules in the solid state leads to two major causes of line broadening, chemical shift anisotropy (CSA) and dipolar couplings. Additionally, the lack of molecular motion results in long spin-lattice relaxation times (T_1). This increases the amount of time it takes to collect an NMR spectrum in the solid state. Furthermore, the low natural abundance of nuclei such as ^{13}C requires a large number of transients to be averaged together in order to produce an NMR spectrum with a sufficient signal to noise (S/N) ratio. These drawbacks have traditionally limited the application of SSNMR, particularly in the pharmaceutical

industry, where high-throughput techniques are often preferred. Advances in experimental techniques used to overcome the problems outlined above have improved the efficiency of SSNMR spectroscopy and the quality of data it provides. These advances and the specific issues they address will be outlined in the following sections.

2.3.1 Chemical shift anisotropy and magic-angle spinning

In solids, the chemical shift is dependent on the orientation of the molecules in the magnetic field. This effect of orientation dependence is referred to as chemical shift anisotropy (CSA). In solution, the rapid molecular tumbling of small molecules averages the CSA effect to zero. Since molecules in the solid state are rigid, their orientation is relatively fixed with respect to the magnetic field, resulting in a distribution of chemical shifts known as a powder pattern, the width of which may be 200 ppm or more. This orientation dependence of the chemical shift is best described in terms of a chemical shielding tensor, σ_{obs}, which can be divided into an isotropic and an anisotropic component, as shown below:

$$\sigma_{obs} = \sigma_{iso} + \sigma_{aniso}\,(3\cos^2\theta - 1)\sigma_{iso}$$

In solution, only the isotropic chemical shift is observed. In solids, the contribution from the anisotropic shielding tensor can be eliminated if the sample is spun at an angle θ such that the $(3\cos^2\theta - 1)$ term equals zero. The angle at which this is achieved has a value of 54.74° and is referred to as the magic angle.[3-4] When spun at the magic angle, the orientation dependence of the solid sample is significantly reduced, and the isotropic

chemical shift is observed. If the rate of sample spinning is less than the width of the powder pattern for individual resonances, spinning sideband artifacts may occur in the spectrum. High magic-angle spinning (MAS) speeds can help to reduce the presence of these artifacts. For instance, the SSNMR spectra presented in this dissertation were collected using MAS spinning frequencies ranging from 3-4.5 kHz. In order to completely eliminate spinning sidebands, a pulse sequence for the total oppression of spinning sidebands (TOSS) can be implemented.[5] Use of MAS and TOSS will result in a SSNMR spectrum consisting of just the isotropic chemical shifts.

2.3.2 Dipolar coupling and high-power proton decoupling

The other major source of line broadening in solids is dipolar coupling. Dipolar couplings are through-space interactions between the magnetic moments of two or more nuclei. The magnetic moment of one nucleus can affect and interact with the neighboring magnetic field of another nucleus. Dipolar coupling can be homonuclear or heteronuclear. In solution, small molecule homonuclear ^{1}H-^{1}H dipolar couplings are averaged to zero due to fast molecular motion. However, homonuclear ^{1}H-^{1}H dipolar coupling is present in solids due to the lack of molecular tumbling. For this reason, ^{1}H NMR is not often used for solids, and nuclei such as ^{13}C are more commonly studied. While homonuclear ^{13}C-^{13}C dipolar coupling is not an issue due to the improbable chance of two ^{13}C nuclei being in close proximity, heteronuclear dipolar couplings between the ^{1}H and ^{13}C nuclei still need to be overcome. This can be achieved through the use of high power ^{1}H decoupling sequences, such as two-pulse phase modulated (TPPM) or Spinal-64.[6] During acquisition,

a decoupling field at the ^{1}H Larmor frequency is applied, which causes the ^{1}H nuclei to rapidly flip between the α and β states. This effectively averages the dipolar interactions to zero.

2.3.3 Low sensitivity and cross polarization

Another hurdle to overcome in order to collect a ^{13}C SSNMR spectrum is inherently low sensitivity, as the ^{13}C nucleus is only 1.1% naturally abundant. For this reason, a technique known as cross polarization (CP) is often implemented.[7-8] In CP, bulk magnetization is transferred from the abundant ^{1}H nuclear spins to those of the dilute ^{13}C spins. This process results in a four-fold gain in sensitivity per scan for the ^{13}C nuclei because it is proportional to the magnetogyric ratio, which is 4:1 for ^{1}H and ^{13}C nuclei. Additionally, CP makes it possible to acquire and average more transients in the same time period, as the relaxation times are now governed by the ^{1}H T_1 values, which are significantly shorter than T_1 values for ^{13}C. This significantly decreases the amount of time it takes to collect a high quality ^{13}C SSNMR spectrum.

2.3.4 Combination of techniques

The techniques outlined above must be used in unison to achieve a ^{13}C SSNMR spectrum with linewidths, resolution, and signal approaching what is observed in solution. As shown in Figure 2.2a, implementing MAS alone does not provide much gain. Decoupling without MAS also results in an uninformative spectrum, as shown in Figure

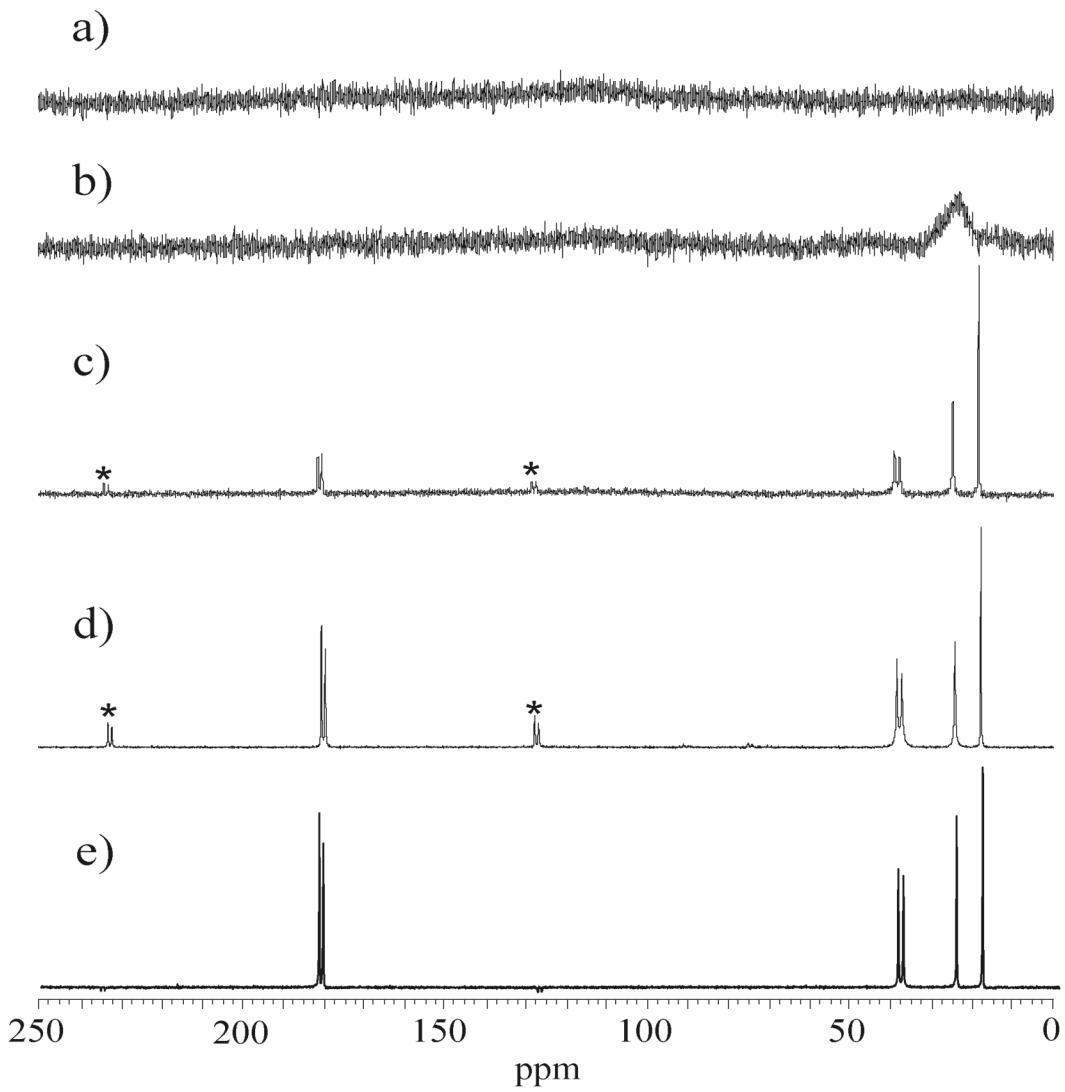

Figure 2.2. Solid-state ^{13}C NMR spectra of 3-methylglutaric acid (MGA) obtained at 75 MHz: (a) with MAS at 4 kHz, no decoupling, (b) with high-power decoupling, no MAS, (c) with both MAS at 4 kHz and high-power decoupling, (d) same as (c) with cross polarization, and (e) same as (d) with the implementation of TOSS. ∗Denotes spinning sidebands.

2.2b. Resolved signals, shown in Figure 2.2c, are not observed until MAS and decoupling are combined. The spectrum shown in Figure 2.2d demonstrates the sensitivity gain provided by the implementation of cross polarization. Finally, the addition of TOSS, as shown in Figure 2.2e, reduces the intensity of the spinning sidebands.

2.4 Applications of SSNMR Spectroscopy to Pharmaceuticals

SSNMR spectroscopy is a non-destructive, powerful technique for obtaining both structural and dynamic information on a wide variety of solid samples. The physical state of the solid (crystalline or amorphous), polymorphs, and presence of drug-excipient interactions can be detected using SSNMR spectroscopy. Additionally, SSNMR spectroscopy is inherently a quantitative technique, meaning that under appropriate experimental conditions, peak areas can be used to quantitate the different components that are present in the solid sample. Several reviews devoted to the application of SSNMR in pharmaceutical research have been reported.[9-13] The purpose of the following sections is not to provide a comprehensive review of SSNMR spectroscopy applications, but rather to present the specific aspects of this powerful technique that are necessary for an understanding of the work to be presented in Chapters 3-6 of this dissertation.

2.4.1 Structural information

The isotropic ^{13}C chemical shift is the most important parameter for the obtainment of valuable structural information because it is very sensitive to changes in local

environment. In a general sense, the regions of a ^{13}C SSNMR spectrum can be broken down as follows: peaks from 200-220 ppm are due to ketone carbonyls, 160-180 ppm are due to carboxylic acid derivatives, 100-160 ppm are from aromatic and olefinic carbons, 50-100 ppm are due to sp3-hybridized carbons attached to heteroatoms, and 10-40 ppm are from aliphatic carbons attached to other carbons and/or hydrogens. This is demonstrated in Figure 2.3, which shows the ^{13}C SSNMR spectrum and peak assignments for crystalline aspirin. The ester carbonyl (peak 8) is furthest upfield, followed by the carboxylic acid (peak 7). The carbons in the aromatic ring give peaks (1-6) located between 100 and 160 ppm while the methyl group (peak 9) is furthest downfield at ~20 ppm.

Another piece of valuable structural information that can be obtained from the ^{13}C SSNMR spectrum of a crystalline compound is the number of crystallographically inequivalent molecules in the unit cell. These independent molecules experience different environments in the unit cell; therefore, the same carbon nucleus in the different molecules will, in theory, have a different chemical shift. For example, two polymorphs of the drug molecule indomethacin, α and γ, have different packing arrangements, which results in a different number of crystallographically inequivalent molecules per unit cell.[14-15] This is reflected in the ^{13}C SSNMR spectra, shown in Figure 2.4. The γ form has one crystallographically inequivalent molecule in the unit cell, resulting in one isotropic chemical shift for each carbon nucleus, as shown in Figure 2.4a. Conversely, the crystal structure of the α form is known to have three crystallographically inequivalent molecules per unit cell, resulting in the splitting of the peaks observed in Figure 2.4b.

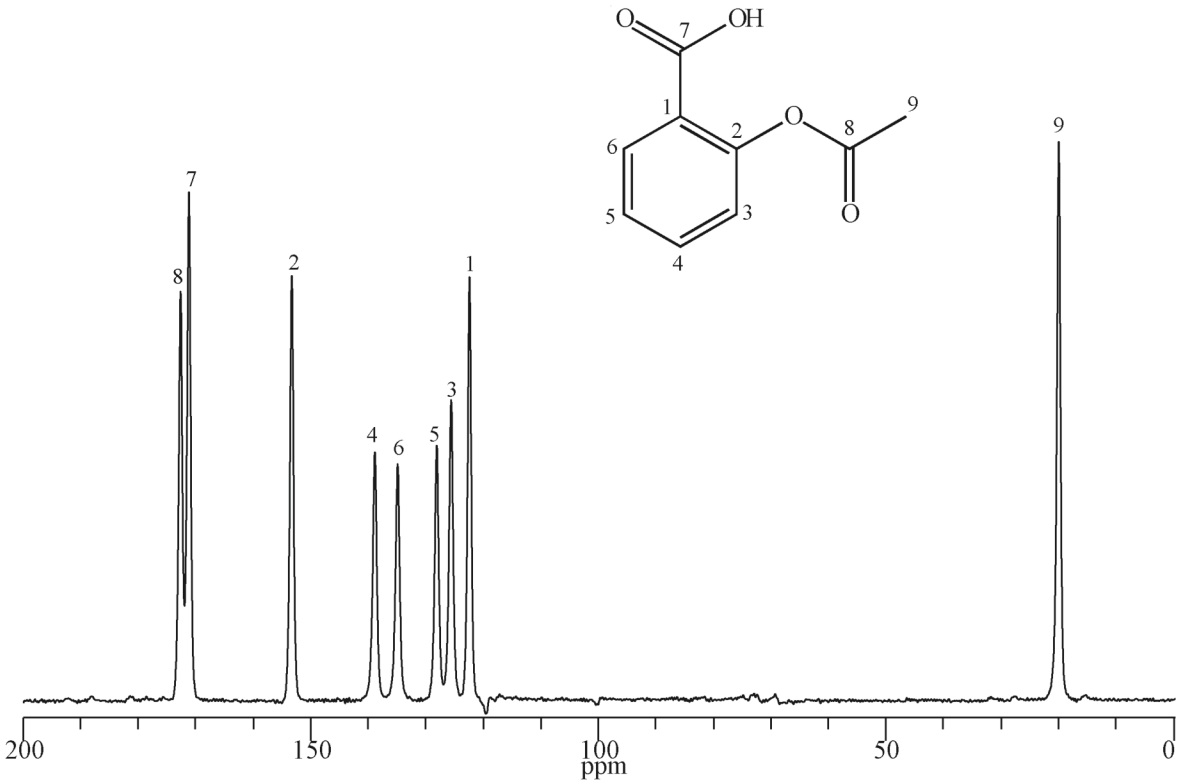

Figure 2.3. ^{13}C Solid-state NMR spectrum of crystalline aspirin. Structure and peak assignments are given.

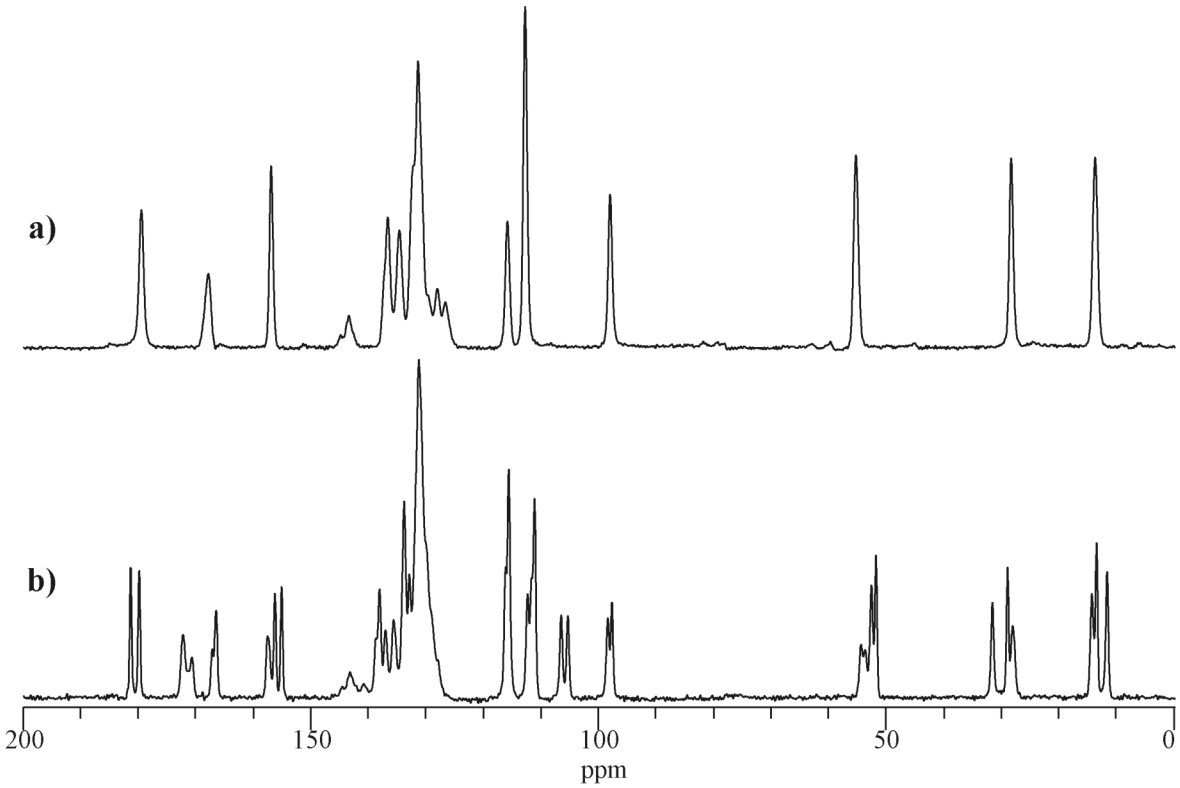

Figure 2.4. ^{13}C Solid-state NMR spectra of indomethacin polymorphs: (a) γ form, and (b) α form. The splitting of peaks in the α form is due to the greater number of crystallographically inequivalent molecules in the unit cell.

Once the chemical shifts are assigned to the different carbon sites in the molecule, detailed structural information can be obtained. For instance, important information on the structure of a molecule in the solid state can be obtained by comparing the ^{13}C NMR spectrum acquired in the solid state to that collected in solution. A detectable change in the chemical shift indicates that some modification in the environment of that carbon occurred upon passing from the solution to the solid state. The most common of these modifications are hydrogen-bonding interactions, which, as stated in Chapter 1, are often found in crystalline solids. An example of this is seen with indomethacin. Apperley and co-workers observed a significant shift of the carboxylic acid peak of indomethacin from the solution state to the solid state.[16] The chemical shift in solution was 172 ppm, but in the solid state NMR spectrum of the γ form it shifted substantially to 179 ppm. Hydrogen bonding between the carboxylic acid groups in the γ form is known to occur[14], and is the cause of this change in chemical shift. Carbons bonded to oxygen or nitrogen atoms that act as hydrogen bond acceptors experience a net decrease in electronic charge, which results in deshielding of the nucleus. Deshielding causes an increase to higher ppm values for these carbons. This sensitivity to electronic environment can be particularly useful for detecting differences between conformational and packing arrangements between the different polymorphs of a molecule. Additionally, differences between the free acid or base and the salt forms of a compound may be detected. Finally, hydrogen-bonding interactions with excipients may also be detected by monitoring changes in the chemical shift values of the API, the excipient, or both. For example, Aso et al. attributed peak shifts observed in the ^{13}C SSNMR spectra of amorphous solid dispersions of nifedipine:PVP and

phenobarbital:PVP systems to hydrogen-bonding interactions between the PVP carbonyl group and the NH groups present in each API.[17]

2.4.2 Detection and identification of solid form

Through acquisition and comparison of ^{13}C SSNMR spectra it is possible to characterize transitions between different solid forms. As shown in Figure 2.4, ^{13}C SSNMR spectroscopy is very useful for looking at polymorphism. Detection of polymorphism by SSNMR spectroscopy has been extensively reviewed.[9-13] However, the acquisition and analysis of high-resolution SSNMR spectra do not require a sample to be crystalline. Therefore, important structural information on API and excipients in the amorphous state can still be obtained. This is a significant advantage of SSNMR spectroscopy over diffraction techniques.

The ^{13}C SSNMR spectra of amorphous forms usually display characteristic broad peaks, due to the lack of long-range order that makes the nuclei experience a number of different environments and situations. This results in a broad distribution of the isotropic chemical shift values and detectable differences when compared to the SSNMR spectrum of the corresponding crystalline forms in which the nuclei have a more defined environment. For example, Li et al. were able to use ^{13}C SSNMR spectroscopy to detect changes in the physical state of sucrose and mannitol after formulation and storage at various conditions.[18] The authors determined that the formulation process had resulted in the formation of amorphous sucrose, as evidenced by the broad peaks in the ^{13}C SSNMR spectrum compared to the narrow lines observed in the spectrum of the crystalline form, as

shown in Figure 2.5. In general, the SSNMR linewidths for API and excipients in the crystalline state are on the order of tens of Hz and on the order of hundreds of Hz in the amorphous state.

2.4.4 Molecular dynamics

SSNMR relaxation times reflect the different processes through which equilibrium of the nuclear spins is restored after perturbation by applied RF pulses, as described in section 2.2. The excited nuclei lose energy via interactions between the spins of adjacent nuclei (spin-spin) and with the surroundings (spin-lattice). Of the different relaxation processes, the two most relevant to the work presented in this dissertation are the proton spin-lattice relaxation times referred to as ^{1}H T_1 and $T_{1\rho}$. The possibility of measuring these different types of relaxation times allows the dynamics of the solid to be investigated over a broad frequency range, as T_1 is more sensitive to motions in the MHz regime, whereas $T_{1\rho}$ is more sensitive to motions in the kHz regime. It is important to note that the spin-lattice relaxation of protons contains dynamic "global" information, which is due to the spin diffusion that occurs in the sample. The relaxation times for ^{13}C provide information about "local" mobility, since they are unaffected by spin diffusion. However, ^{13}C relaxation times can be very long (on the order of minutes), which results in extremely long experimental times, making the acquisition of ^{1}H spin-lattice relaxation times more common. The measurement of ^{1}H T_1 and $T_{1\rho}$ gives valuable insights into the dynamic

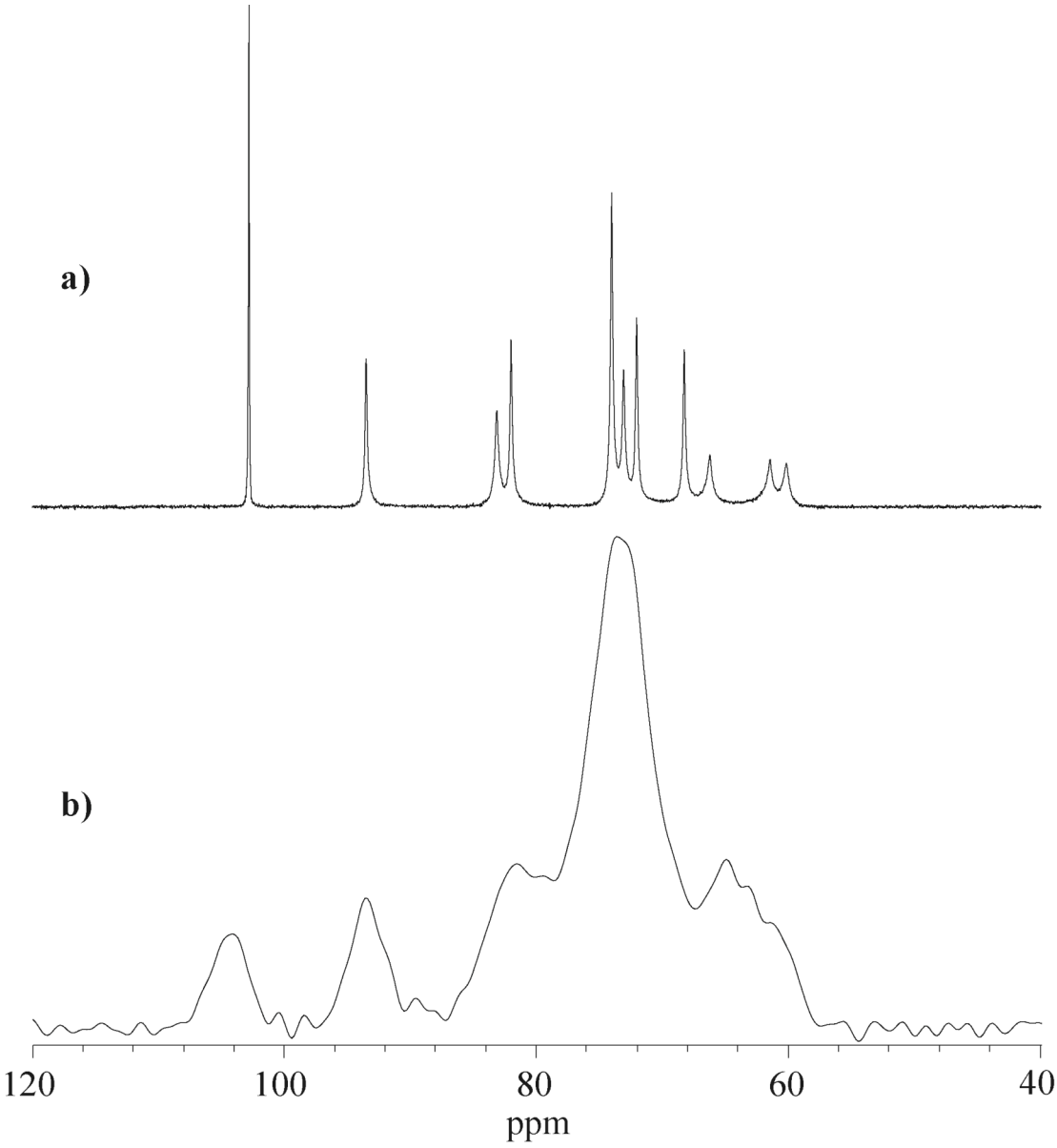

Figure 2.5. ^{13}C SSNMR spectra of sucrose in (a) the crystalline state and (b) the amorphous state. (Adapted from Reference 18).

properties of the solid sample. Due to a higher degree of disorder, amorphous forms have higher mobility and shorter ^{1}H spin-lattice relaxation times than their crystalline counterparts. For example, Lubach and co-workers used ^{13}C SSNMR spectral analysis and ^{1}H T_1 measurements to investigate the effects of processing on the crystalline forms of lactose.[19] Crystalline α-lactose monohydrate had a ^{1}H T_1 value of 243 s. Cryogrinding for 2 min, 10 min, 30 min, and 60 min resulted in ^{1}H T_1 values of 23, 5.1, 2.9, and 2.0 s, respectively. The authors also observed line broadening indicative of the formation of amorphous material. Thus, the decrease in relaxation time was attributed to the formation of crystal defects and amorphous material, which increased with increased grinding time.

^{1}H T_1 relaxation values can also be used to probe the molecular mobility of the amorphous state as a function of temperature. For example, Forster et al. measured the ^{1}H $T_{1\rho}$ values for melt-quenched amorphous forms of nifedipine and indomethacin alone and with PVP at various temperatures.[20] The authors observed a large decrease in ^{1}H $T_{1\rho}$ for nifedipine before the T_g was reached, indicating that the amorphous nifedipine was mobile, even in the glassy state. On the other hand, decreases in ^{1}H $T_{1\rho}$ values (increased mobility) for indomethacin corresponded with the T_g. This study highlights the valuable addition of SSNMR relaxation measurements as a tool to complement thermal methods traditionally used to measure mobility and physical stability of amorphous solids.

The degree of mixing of two components in a pharmaceutical formulation can be determined using ^{1}H T_1 and $T_{1\rho}$ relaxation measurements. As described in Chapter 1, maximum stability of an amorphous solid dispersion will be achieved only when a single

miscible phase is formed. Miscibility of the API in the polymer is typically measured using DSC. The observation of a single T_g that falls between the T_g of the drug and the polymer is indicative of a single phase within the detection limits of DSC, as outlined in Table 2.1a. In DSC, the detection limit is a domain size of 30 nm. Therefore, if separated phases with domain sizes less than 30 nm exist, they will not be detected using DSC.[21]

By SSNMR spectroscopy, one common relaxation value indicates that a mixture of API and excipients is well dispersed. Domains that exhibit different relaxation dynamics are an indication of phase separation. As with DSC, the limit of detection must be considered. If more than one phase exists, the observation of more than one ^1H T_1 and ^1H $T_{1\rho}$ value will depend on the domain size of the phases. The three possible cases are outlined in Table 2.1b. As can be seen, ^1H $T_{1\rho}$ measurements are able to determine phase separation for domain sizes less than 30 nm, which is an advantage over DSC. Aso et al. analyzed the miscibility of nifedipine with various polymers using both DSC and SSNMR spectroscopy.[22] The authors found that for nifedipine and HPMC dispersions, miscibility could not be determined using DSC. On the contrary, a common ^1H $T_{1\rho}$ value was observed for this system, suggesting that SSNMR spectroscopy can be very useful for assessing the miscibility of API and polymer in a solid dispersion, especially when T_g is not clearly detected by DSC.

Although most of the SSNMR spectra presented in this dissertation were collected using CP, some spectra were also acquired without CP. These types of experiments are

Table 2.1. Determination of number of solid phases using (a) thermal analysis and (b) SSNMR spectroscopy.

a)

Number of T_g Values	Location of T_g	Number of Phases
1	Between those of individual components	1 completely miscible
2	Between those of individual components	2 partially miscible
2	Equal to those of individual components	2 immiscible

b)

Number of ^1H T_1 Values	Number of ^1H $T_{1\rho}$ Values	Number of Phases
1	1	1 (domain size > 5 nm)
1	2	2 (domain size between 5-50 nm)
2	2	2 (domain size > 50 nm)

known as single-pulse experiments. Cross polarization and single-pulse experiments are complementary techniques. In CP, the rigid components are detected, while single-pulse experiments detect the mobile components. This makes a combination of CP and single-pulse experiments very useful for looking at the mobility of amorphous solids and amorphous solid dispersions in the rigid, glassy state versus the rubbery state.

2.4.3 Quantitation

While qualitative analysis of SSNMR spectra can provide a wealth of information, quantitative analyses are also possible and provide even more valuable information about the solid forms present in a sample. NMR is inherently quantitative because the observed signal corresponds to the relative number of like nuclei in the sample. This makes SSNMR spectroscopy a useful technique for determining the amounts of crystalline and amorphous material present in a sample, the amounts of different monomers or residues present in an amorphous excipient, and the amounts of the different solid forms present within a formulation.

Some general aspects must be carefully considered when attempting to obtain quantitative ^{13}C SSNMR spectra. As stated in earlier sections, CP is a technique used to increase the sensitivity of ^{13}C SSNMR spectroscopy, and the increase is achieved through transfer of the bulk magnetization from the abundant ^{1}H spins to the dilute ^{13}C spins. The efficiency of this transfer, and therefore the intensity of the SSNMR signals, is a function of the contact time, which is dependent on factors such as the relaxation time $T_{1\rho}$ and the cross polarization time T_{CH}. In amorphous samples, high mobility leads to minimal

differences in CP dynamics for most of the carbons as a function of contact time. However, in crystalline systems, different carbons may experience very different relaxation times. Careful optimization of the experimental conditions and use of calibration curves allows for quantitative spectra to be acquired. For example, Offerdahl et al. have used ^{13}C SSNMR to quantitate the different polymorphic forms of neotame in physical mixtures.[20] Once appropriate experimental conditions are identified, integration of peak areas can be used for quantitation. In cases where peak overlap is strong, spectral deconvolution must be used for accurate integration.

2.5 Limitations of SSNMR Spectroscopy

The adoption of SSNMR spectroscopy as a frequently used technique in the pharmaceutical industry has been hampered by the following factors: long analysis times, low sensitivity, cost of instrumentation, and the level of expertise required for collecting and interpreting data. The inherent lack of sensitivity of the ^{13}C nucleus and long relaxation times requires large amounts of sample, extensive signal averaging, and lengthy (in some cases hours to days) data acquisition times. These drawbacks have hindered the routine use of SSNMR spectroscopy for the analysis of API and excipients at the preformulation and formulation development stages, where the technique would likely be extremely beneficial. The design and construction of a multiple-sample SSNMR probe to

alleviate some of these problems is currently underway in our laboratory.[24] Development of this instrumentation would greatly increase sample throughout and sensitivity.

2.6 Conclusions

Despite the inherent difficulties in obtaining high quality SSNMR spectra, SSNMR spectroscopy offers many advantages. Its non-destructive and selective nature enables analysis of pharmaceutical solids without any sample alteration or separation of components, including intact formulations such as tablets. Structural changes in APIs and excipients can be detected, even in amorphous forms, where the lack of long-range order limits the use of X-ray diffraction techniques. SSNMR spectroscopy can be used to identify and quantify the different solid forms in which APIs and excipients can exist. Spin-lattice relaxation measurements can also provide valuable insight into the mobility of amorphous forms and miscibility of the API and polymer used in an amorphous solid dispersion. Thus, whenever possible, SSNMR spectroscopy should be used in conjunction with other classical solid-state characterization techniques in order to gain a full understanding of the sample under investigation.

2.7 References

1. Harris R. 1986. Nuclear Magnetic Resonance Spectroscopy: A Physicochemical View. 1st ed., New York: Longman Scientific and Technical. p 260.

2. Fyfe C. 1983. Solid State NMR for Chemists. ed., Guelph, Ontario C.F.C. Press. p 593.

3. Andrew ER, Bradbury A, Eades RG. 1959. Removal of dipolar broadening of nuclear magnetic resonance spectra of solids by specimen rotation. Nature 183:1802-1803.

4. Andrew ER. 1971. Narrowing of NMR spectra of solids by high-speed specimen rotation and the resolution of chemical shift and spin multiplet structures for solids. Prog Nucl Mag Res Sp 8:1-39.

5. Dixon WT, Schaefer J, Sefcik MD. 1982. Total suppression of sidebands in CPMAS carbon-13 NMR. J Magn Reson 49(2):341-345.

6. Fung BM, Khitrin AK, Ermolaev K. 2000. An improved broadband decoupling sequence for liquid crystals and solids. J Magn Reson 142:97-101.

7. Pines A, Gibby MG, Waugh JS. 1972. Proton-enhanced nuclear induction spectroscopy. Method for hig-resolution NMR of dilute spins in solids. J Chem Phys 59:569-590.

8. Pines A, Gibby MG, Waugh JS. 1973. Proton-enhanced NMR of dilute spins in solids. J Chem Phys 56:1776-1777.

9. Geppi M, Mollica G, Borsacchi S, Vericini CA. 2008. Solid state NMR studies of pharmaceutical systems. Applied Spectroscopy Reviews 43(3):202-302.

10. Brittain HG, Bogdanowich SJ, Bugay DE, DeVincentis J, Lewen G, Newman AW. 1991. Physical characterization of pharmaceutical solids. Pharm Res 8:963-973.

11. Bugay DE. 1993. Solid-state nuclear magnetic resonance spectroscopy: Theory and pharmaceutical applications. Pharm Res 10:317-327.

12. Tishmack PA, Bugay DE, Byrn SR. 2003. Solid-state nuclear magnetic resonance spectroscopy-pharmaceutical applications. J Pharm Sci 92:441-474.

13. Berendt RT, Sperger DM, Isbester PK, Munson EJ. 2007. Solid-state NMR spectroscopy in pharmaceutical research and analysis. Trends in Analytical Chemistry 25:977-984.

14. Kistenmacher TJ, Marsh RE. 1972. Crystal and molecular structure of an antiinflammatory agent, indomethacin, 1-(p-chlorobenzoyl)-5-methoxy-2-methlyindole-3-acetic acid. J Am Chem Soc 23:1340-1345.

15. Chen X, Morris KR, Griesser UJ, Byrn SR, Stowell JG. 2002. Reactivity of different indomethacin solid forms with ammonia gas. J Am Chem Soc 124:15012-15019.

16. Apperley DC, Forster AH, Fournier R, Harris RK, Hodgkinson P, Lancaster RW, Rades T. 2005. Characterisation of indomethacin and nifedipine using variable-temperature solid-state NMR. Magn Reson Chem 43:881-892.

17. Aso Y, Yoshioka S. 2006. Molecular mobility of nifedipine-PVP and phenobarbital-PVP solid dispersions as measured by ^{13}C-NMR spin-lattice relaxation time. J Pharm Sci 95:318-325.

18. Li B, O'Meara MH, Lubach JW, Schowen RL, Topp EM, Munson EJ, Borchardt RT. 2005. Effects of sucrose and mannitol on asparagine deamidation rates in solution and in the solid state. J Pharm Sci 94(8):1723-1735.

19. Lubach JW, Dawie X, Segmuller BE, Munson EJ. 2007. Investigation of the effects of pharmaceutical processing upon solid-state NMR relaxation times and implications to solid-state formulation stability. J Pharm Sci 96:777-787.

20. Forster AH, Apperley DC, Hempenstall J, Lancaster RW, Rades T. 2003. Investigation of the physical stability of amorphous drug and drug/polymer melts using variable-temperature solid-state NMR. Pharmazie 58:761-762.

21. Newman A, Engers D, Bates S, Ivanisevic I, Kelly RC, Zografi G. 2008. Characterization of amorphous API:polymer mixtures using X-ray powder diffraction. J Pharm Sci 97(11):4840-4856.

22. Aso Y, Yoshioka S, Miyazaki T, Kawanishi T, Tanaka K, Kitamura S. 2007. Miscibility of nifedipine and hydrophilic polymers as measured by ^{1}H-NMR spin-lattice relaxation. Chem Pharm Bull 55(8):1227-1231.

23. Offerdahl TJ, Salsbury JS, Dong Z, Grant DJW, Schroeder SA, Prakash I, Gorman EM, Barich DH, Munson EJ. 2005. Quantitation of crystalline and amorphous forms of anhydrous neotame using ^{13}C CPMAS NMR spectroscopy. J Pharm Sci 94(12):2591-2560.

24. Nelson BN, Schieber LJ, Barich DH, Lubach JW, Offerdahl TJ, Lewis DH, Heinrich JP, Munson EJ. 2006. Multiple-sample probe for solid-state NMR studies of pharmaceuticals. Solid State Nucl Magn Reson. 29: 204-213.

Chapter 3

Structural Characterization of Polymeric Excipients

3.1 Introduction

The overall objective of this work is to identify the SSNMR parameters that can be used to detect differences in structural properties and functionally related characteristics among some common polysaccharide-based excipients. As described in Chapter 1, the majority of oral dosage forms are marketed in the solid state, with excipients constituting the largest component of most formulations. Many of these excipients are polysaccharides and are derived from natural products. Multiple companies manufacture these excipients on large scales, using various processes, in numerous locations, and at different times of the year. Thus, variability among naturally derived excipients from different suppliers is inevitable. Similarly, changes or updates to a company's manufacturing process or source of raw materials can result in lot-to-lot variability. This variability may significantly impact the physicochemical properties and hence functionality of the excipient in the final dosage form. Therefore, it is important to have analytical methods in place for accurately assessing and identifying differences in these materials.[1]

SSNMR spectroscopy is a valuable tool for the structural analysis of polysaccharide-based excipients, as the amorphous or semi-crystalline nature of these materials limits the capability of more commonly used solid-state techniques such as differential scanning calorimetry (DSC) and powder X-ray diffraction (PXRD).[2] A major advantage of SSNMR spectroscopy is that it is a non-destructive and selective technique that allows characterization of the excipient directly in the physical state in which it is to be administered, even when in the presence of other excipients and the active pharmaceutical

ingredient (API).[3] Additionally, SSNMR spectroscopy can provide unique insight into the molecular dynamics of pharmaceutical solids such as excipients through the use of relaxation measurements.[4]

In this chapter, the SSNMR parameters that can be used to detect differences in structural properties among some common polysaccharide-based excipients will be discussed. Excipients for analysis include alginic acid and alginate, carrageenans, starch and derivatives, and cellulose-based excipients such as microcrystalline cellulose, carboxymethylcellulose sodium, hydroxyethylcellulose (HEC), hydroxypropylcellulose (HPC), and hydroxypropylmethylcellulose (HPMC). Parameters that were assessed via SSNMR spectroscopy include chemical shift (peak position), relative signal areas and intensities, and proton relaxation times (^{1}H T_1 and $^1T_{1\rho}$).

3.2 Experimental

3.2.1 Samples

Excipients studied are listed in Table 3.1. Cases in which different forms, grades/types, or lots were analyzed are also specified. Excipients were stored at ambient temperatures with desiccant and analyzed as received without further modification.

3.2.2 Water content

Thermogravimetric Analysis (TGA) using a TA Q50 Thermogravimetric Analyzer

Table 3.1. Excipient samples used in this study.

Excipient	Supplier (Grade)	# of Lots	Function*
Alginic acid	FMC Biopolymer (120 NM) Sigma; Spectrum	1 1; 1	stabilizing agent; suspending agent; tablet binder; disintegrant; viscosity-increasing agent
Sodium Alginate	FMC Biopolymer (LF 10/60LS) Aldrich; Spectrum	1 1; 1	
ι-Carrageenan	FMC Biopolymer; Sigma; Fluka	2; 2; 1	emulsifying agent; stabilizing agent; sustained release matrix; viscosity-increasing agent
κ-Carrageenan	FMC Biopolymer; Fluka	2; 1	
λ-Carrageenan	FMC Biopolymer; Fluka	2; 1	
Carrageenan	Sigma; Spectrum	1; 2	
Starch (corn)	Grain Processing (B880, B700) Sigma	1 of each 1	glidant; tablet diluent and binder; disintegrant
Starch (potato)	Sigma	1	
Starch (wheat)	Sigma	1	
Maltodextrin	Aldrich (419672, 419680, 419699)	1 of each	coating agent; tablet diluent and binder
Corn Syrup Solids	Grain Processing (M200, M250) Globe (42DE)	1 of each 1	
Avicel	FMC Biopolymer (PH101, 102) FMC Biopolymer (PH105, 112, 113)	2 of each 1 of each	tablet diluent,/binder
HEC	Spectrum; Aldrich	2; 1	Coating agent; sustained release agent; tablet binder; viscosity-increasing
HPC	Spectrum; Aldrich	3; 1	
HPMC	Spectrum 2208; Spectrum 2910 Sigma (type 2910)	2; 1 1	
Carboxymethyl -cellulose sodium	Fluka; Acros Organics	1; 3	tablet binder/disintegrant; viscosity increasing agent

* From Reference 5

(TA Instruments, New Castle, DE) was used to determine the water content of some of the excipients as received. Approximately 10-15 mg of each sample was heated to 105 °C at a heating rate of 20 °C/min and held isothermally for 180 min. Total weight loss was attributed to water content of the sample.

3.2.3 Solid-state NMR spectroscopy

Solid-state ^{13}C NMR spectra were acquired using a Chemagnetics CMX-300 spectrometer (Varian, Inc., Palo Alto, CA) operating at approximately 75 MHz for ^{13}C. Chemagnetics double-resonance probes equipped with either PENCIL™ 7.5-mm spinning modules or Revolution NMR 7-mm spinning modules (Revolution NMR, LLC, Fort Collins, CO) were used to acquire all spectra. Samples were packed into zirconia rotors and sealed with either Kel-F or Teflon end caps. Spectra were acquired using variable-amplitude or ramped-amplitude cross polarization (CP)[6], magic-angle spinning (MAS)[7] at 4.0 kHz, contact times of 1-2 ms, and high-power ^{1}H-decoupling fields of approximately 60-70 kHz. Total sideband suppression (TOSS)[8] and SPINAL64 decoupling[9] were used when possible. 3-methylglutaric acid (MGA) was used to optimize the spectrometer settings and set the reference frequency.[10] The recycle delays varied based upon ^{1}H T_1 values for each excipient, which were measured using saturation recovery experiments. Using KaliedaGraph (Synergy, version 4.01), plots of integrated signal areas versus saturation recovery times were fit to the equation $y = amp(1 - e^{-\tau/T_1})$ where y is the integrated signal area, amp is the amplitude constant, τ is the saturation recovery time,

and T_1 is the spin-lattice relaxation time. A recycle delay equal to at least 1.5 times the ^1H T_1 value of each sample was used to acquire each spectrum. To determine ^1H $T_{1\rho}$ values, multiple-contact time experiments were performed and the rate of magnetization decay was calculated using Chemagnetics Spinsight software. When necessary, deconvolution of signals to aid in calculation of peak areas and intensities was achieved using Chemagnetics Spinsight software.

3.3 Results and Discussion

3.3.1 Alginic acid and sodium alginate

Alginic acid and sodium alginate are linear unbranched polysaccharides extracted from certain seaweed species. Both contain various proportions of β-D-mannuronic acid (M) and α-L-guluronic acid (G) residues, with the only chemical difference between them being the protonation or deprotonation of the carboxylic acid group (Figure 3.1).[11] Representative ^{13}C SSNMR spectra of alginic acid and sodium alginate are shown in Figure 3.2. While there are some differences in relative peak intensities in the region 60-110 ppm, too much overlap exists in this part of the spectrum to be able to use it to distinguish between the two forms. However, the chemical shift of the peak to the far left in each spectrum, corresponding to the carbonyl carbon, is significantly different depending on which alginate form (acid or sodium salt) is present. As shown in Table 3.2,

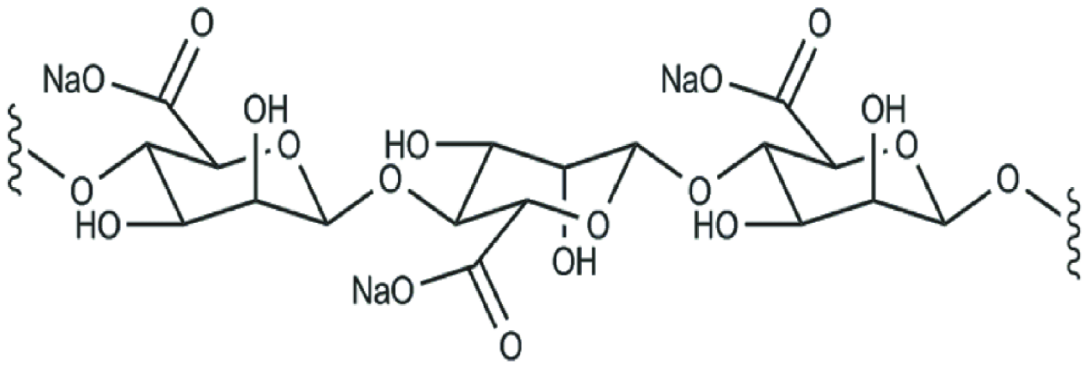

Figure 3.1. Structure of sodium alginate. The structure of alginic acid is identical except for the presence of a proton in place of the sodium ion.

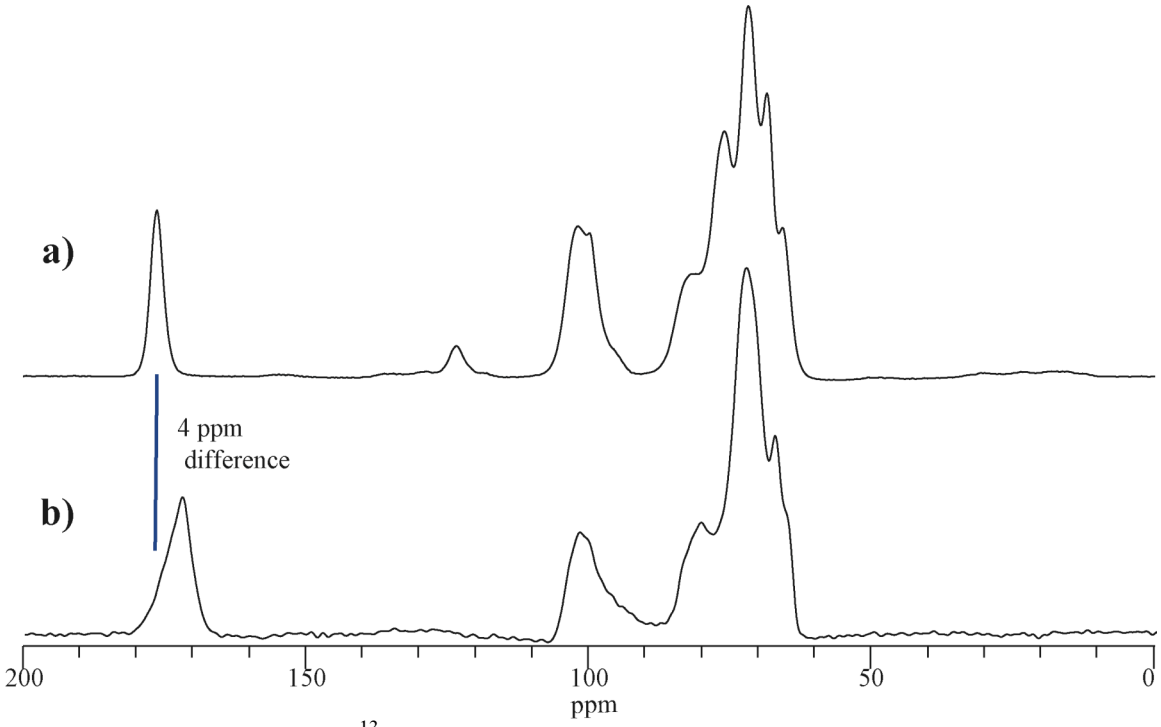

Figure 3.2. Representative ^{13}C SSNMR spectra of (a) sodium alginate and (b) alginic acid.

Table 3.2. Differences in carbonyl chemical shift values for alginic acid and sodium alginate samples.

Carbonyl Chemical Shift Values			
Alginic Acid		Sodium Alginate	
Supplier	Peak position (ppm)	Supplier	Peak position (ppm)
FMC Biopolymer	172.1	FMC Biopolymer	176.5
Sigma	172.3	Aldrich	176.4
Spectrum	171.9	Spectrum	176.7

the carbonyl peak position consistently occurs at ~172 ppm in all alginic acid samples and at ~176 ppm in all sodium alginate samples. Thus, although alginic acid and sodium alginate are very structurally similar, they can be identified and distinguished based on the carbonyl peak position in the SSNMR spectra.

The differences in relative peak intensities in the region 60-90 ppm noted in Figure 3.2 are further illustrated in Figure 3.3; the ^{13}C SSNMR spectra of three sodium alginate samples obtained from different suppliers are shown. While these differences are not useful for distinguishing between the acid and sodium salt forms of alginate, variations in this region do reflect differences in monomer composition. As shown in Figure 3.3, signals in this area of the spectrum can be assigned as either G or M residues, based on solution-state NMR values[12] and a previous study of sodium alginate by SSNMR spectroscopy.[13] Upon examination of Figure 3.3, it can be clearly seen that the sample from FMC Biopolymer contains more G monomer than those from Spectrum and Aldrich, as the signals corresponding to the G monomer are dominant in the FMC Biopolymer spectrum and less intense in the spectra of the other two samples. The relative intensities between G and M peaks in the SSNMR spectra of the sodium alginate samples from Spectrum and Aldrich are very similar, suggesting that these two materials contain comparable amounts of each monomer. Although outside the scope of this chapter, quantitation of the G and M residues by SSNMR spectroscopy with the aid of spectral deconvolution is possible and has been demonstrated in a few cases.[13-14] However, for various reasons, the values obtained do not always agree with those obtained via solution-state NMR analysis. This issue will be further addressed in Chapter 4.

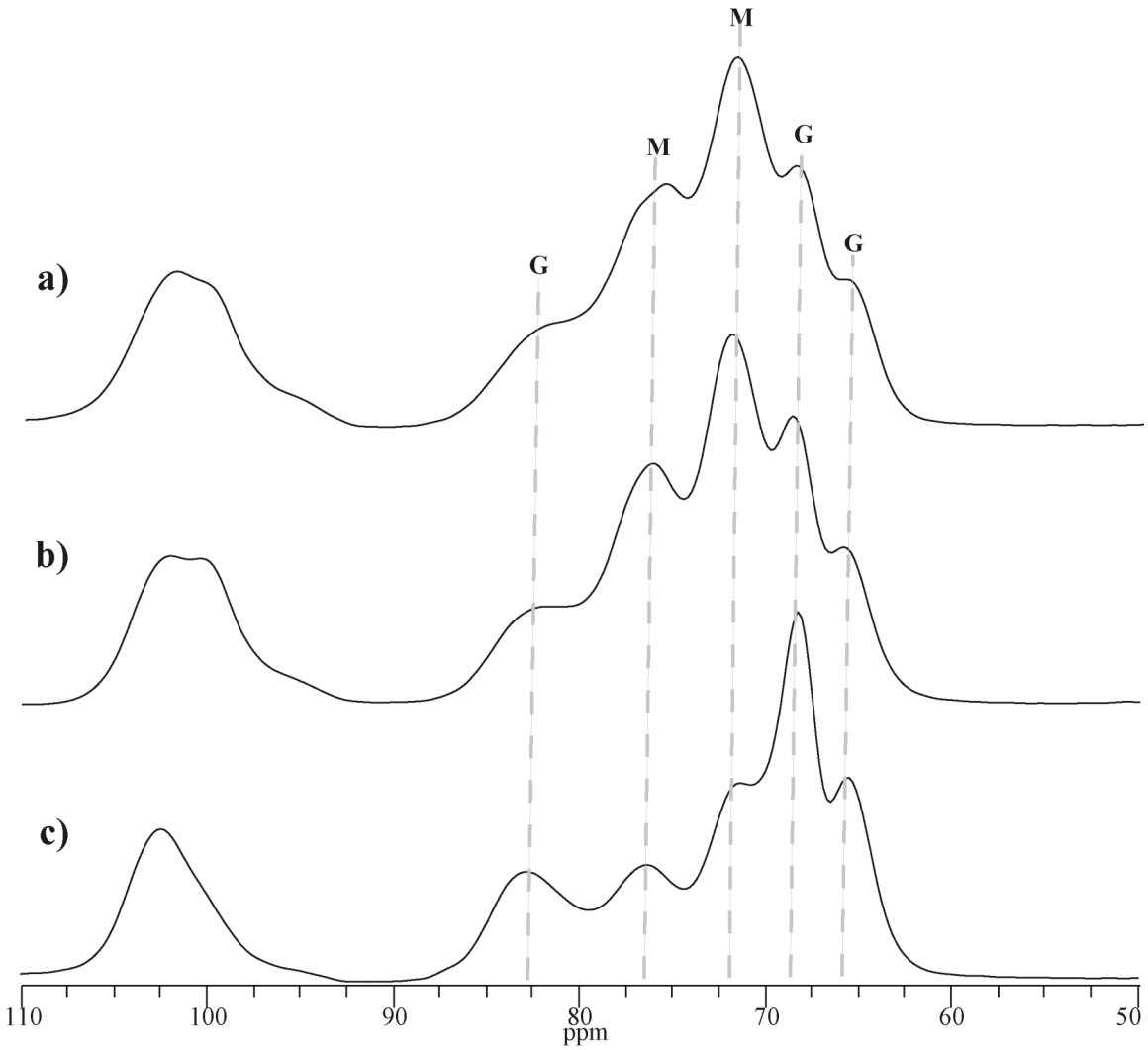

Figure 3.3. ^{13}C SSNMR spectra of sodium alginate samples from (a) Aldrich, (b) Spectrum, and (c) FMC Biopolymer. Peaks labeled G and M correspond to ring carbons of the guluronic and mannuronic acid residues, respectively.

3.3.2 Carrageenans

Like alginates, carrageenans are found in the cell walls of some species of seaweed. Carrageenan is primarily composed of a polysaccharide chain of alternating 1,3-linked β-D- and 1,4-linked α-D-galactopyranose residues, with sulfate groups located in various positions (Figure 3.4).[15] The iota (ι), kappa (κ), and lambda (λ) forms of carrageenan are structurally different due to the varied presence and number of 3,6-anhydro-bridge and sulfate groups, which results in vast differences in gelling properties among the three forms. As shown in Table 3.1, carrageenans are available as pure forms identified by the supplier, which will be referred to as "known" samples, and also as forms or mixtures of forms not completely identified by the supplier, which will be referred to as "unknown" samples throughout the remainder of this chapter.

The ^{13}C SSNMR spectra of the "known" samples identified as ι, κ, and λ are shown in Figures 3.5a, 3.5b, and 3.5c, respectively. The first thing to note is the number of signals present in the SSNMR spectrum of each form. Discounting the slight shoulders that appear on some peaks, the spectra of all the ι-samples are resolved into seven distinct signals, those of the κ-samples into six distinct signals, and those of the λ-samples into just five signals. This data agrees with previous studies,[16] although we believe that this is the first report of seven distinct signals being observed for the ι-form. An earlier study compared only one sample each of ι- and κ-carrageenan, and reported six chemical shifts for both forms.[16] Advancements in SSNMR decoupling methods since the previous study are the likely reasons for this improved ability to resolve a seventh signal in the ι-form.

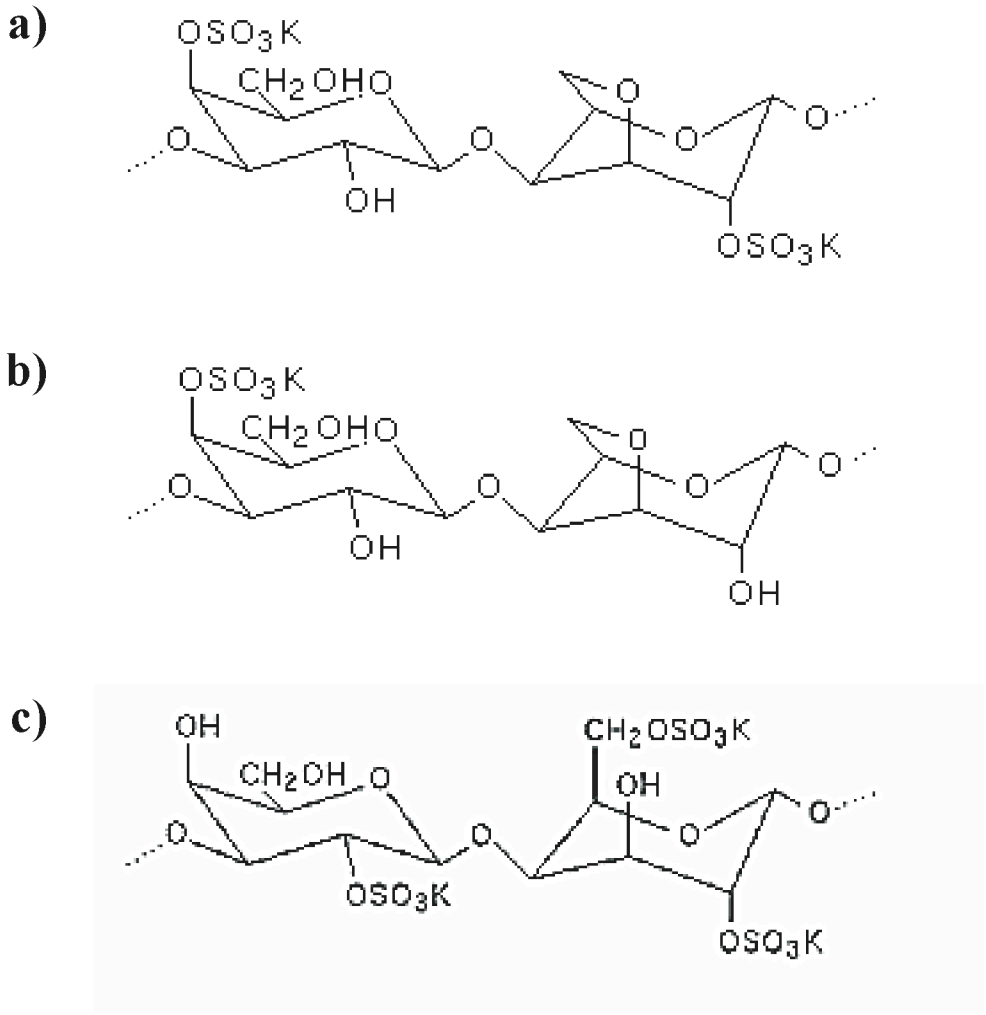

Figure 3.4. Structures of the three different carrageenan forms: (a) iota (ι), (b) kappa (κ), and (c) lambda (λ).

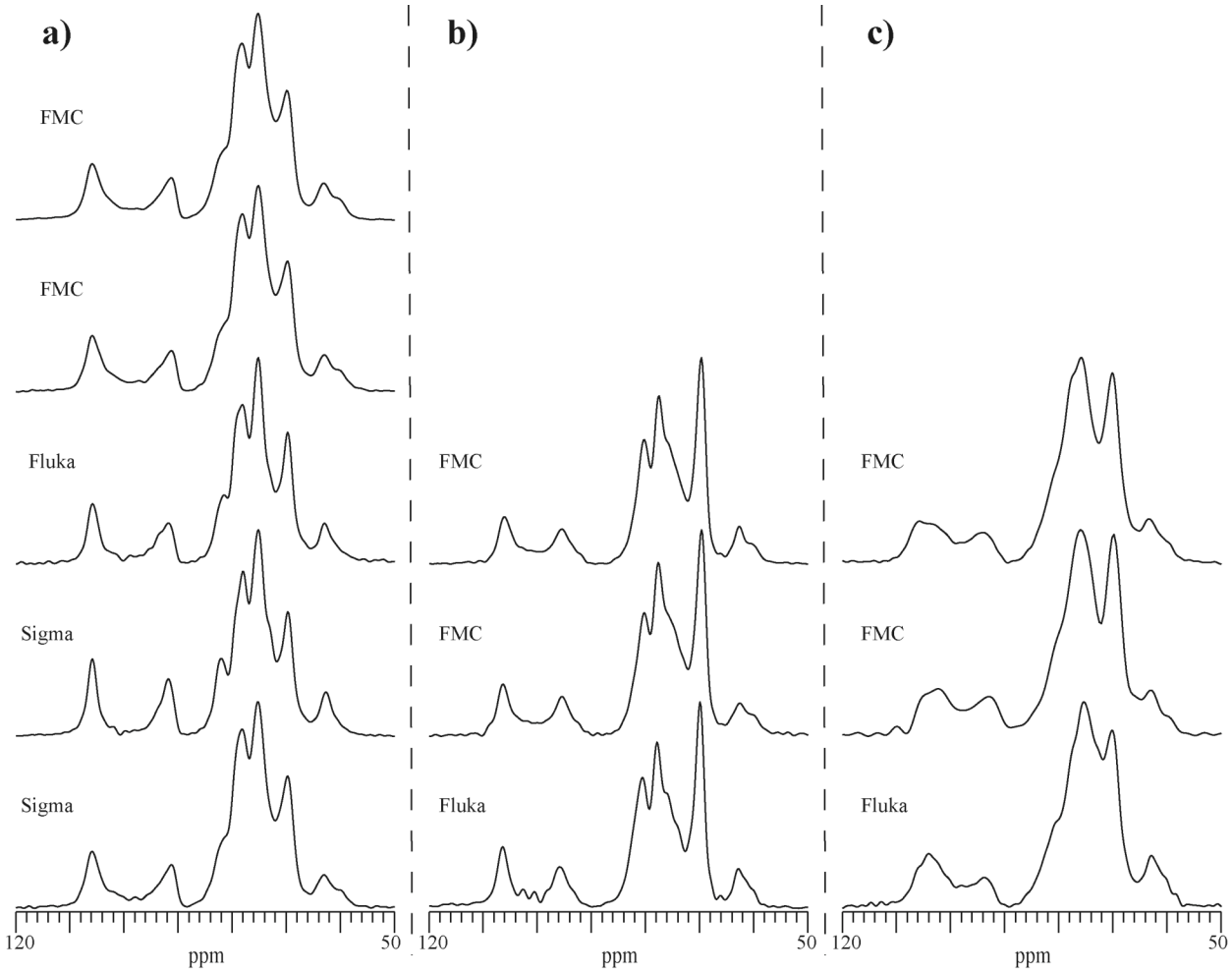

Figure 3.5. ^{13}C SSNMR spectra of carrageenan samples: (a) ι-forms, (b) κ-forms, and (c) λ-forms.

As shown in Figure 3.5, the number of resolved peaks is consistent across all samples, regardless of supplier. However, slight differences between the spectra of samples from different suppliers can be observed. For instance, in the ι-forms (Fig.3.5a), the SSNMR spectra of the two samples received from FMC Biopolymer are essentially identical. The SSNMR spectrum of one of the Sigma samples strongly resembles that of the FMC Biopolymer samples, but the spectra of the other Sigma sample and of the Fluka sample show sharper resolution between peaks and lack of the shoulder on the peak at ~60 ppm. It is likely that these two samples were obtained from different materials and/or by a different process. Differences between the FMC Biopolymer samples and Fluka sample of the λ-form are also observed (Fig.3.5c). The SSNMR spectra of the κ-samples (Fig.3.5b) are very similar, suggesting that the processes used to produce the κ-sample from Fluka and the κ-sample from FMC Biopolymer resulted in the same product and/or samples that produce the same SSNMR spectrum.

To better highlight the spectral differences between the three forms, an overlay of representative ^{13}C SSNMR spectra of the ι, κ, and λ-samples is shown in Figure 3.6a. While there are differences in the peak shapes and positions of signals 1 and 2, the major distinction between forms occurs in the region 60-90 ppm. The changes seen in the number of peaks and relative intensities observed in this region are due to differences in the degree of sulfation between the three forms.[16] In Figure 3.6b, the ^{13}C SSNMR spectra of the "unknown" samples (Table 3.1) are shown. It is clear upon visual examination that the spectra of the two Spectrum samples are dissimilar. The SSNMR spectrum of one lot

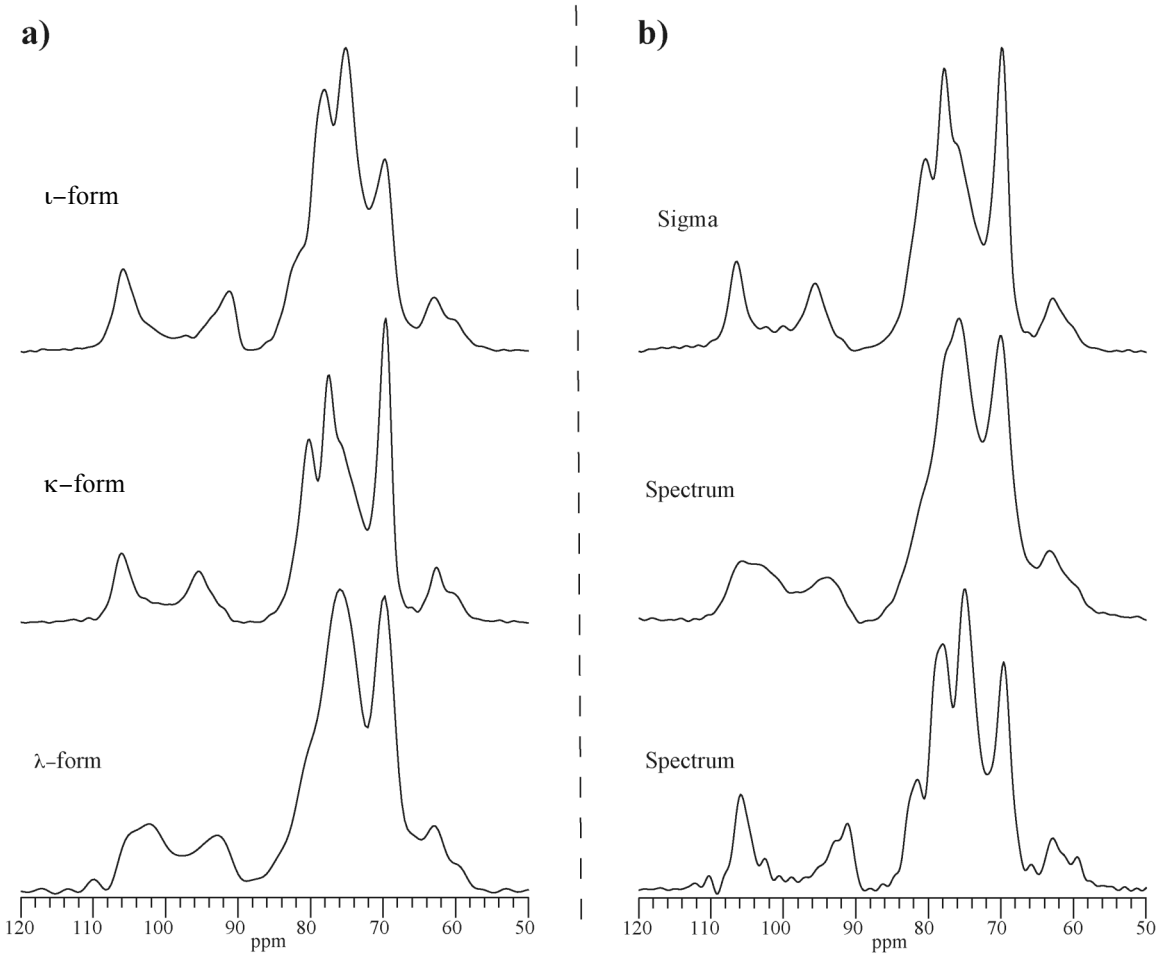

Figure 3.6. ^{13}C SSNMR spectra of carrageenan samples: (a) "known" forms, and (b) "unknown" forms.

is similar to that of the ι-form while the SSNMR spectrum of the other lot matches that of the λ-form. The Sigma sample appears to consist primarily of κ-carrageenan.

Table 3.3 outlines the range of chemical shifts and normalized relative intensity values for all of the "known" and "unknown" samples. The Sigma "unknown" sample has chemical shifts and normalized relative intensities that fall within the range of all "known" κ-forms that were analyzed. Similarly, Spectrum lot #2 can be identified as λ-carrageenan, as its peak positions and relative intensities fall within the range for all "known" λ-forms that were analyzed. The chemical shift values and intensities for Spectrum lot #1 appear to match up well with the values for "known" ι-forms, with one exception. As can be seen in Table 3.3, the relative intensity of peak #6 for Spectrum lot #1 falls above the range for the "known" ι-forms. Considering this peak corresponds to the most intense signal (peak #5) in the κ-forms, it can be concluded that Spectrum lot #1 consists of primarily ι-form with some κ-form impurity.

3.3.3 Starch and derivatives

Starch is one of the most abundant polymers in nature and contains two distinct polysaccharides, the linear amylose and the highly branched amylopectin (Figure 3.7).[17] The structure of starch consists of crystalline amylopectin clusters separated by disordered zones composed of amorphous material and/or amylose-lipid inclusion complexes.[17-21] X-ray diffraction studies have shown that there are three types of crystalline polymorphs, referred to as A, B, and C.[18] A- and B-type starch polymorphs are most common and

Table 3.3. Summary of differences in relative peak intensities for "known" and "unknown" carrageenan samples.

Knowns						
	ι-form		**κ-form**		**λ-form**	
Peak	Chemical shift (ppm)	Relative intensity (normalized)	Chemical shift (ppm)	Relative intensity (normalized)	Chemical shift (ppm)	Relative intensity (normalized)
1	105.8 - 106	0.27 - 0.38	106.1- 106.5	0.19 - 0.29	102.5 - 104.8	0.18 - 0.25
2	91.2 - 91.9	0.20 - 0.28	95.3 - 95.8	0.16 - 0.21	93.0 - 93.9	0.13 - 0.19
3	81.3 - 82.2	0.34 - 0.38	80.4	0.62 - 0.66	75.4 - 76.1	1.00
4	78.1 - 78.2	0.78 - 0.88	77.7 - 77.8	0.85 - 0.94	70.0 - 70.1	0.84 - 0.97
5	75.2 - 75.4	1.00	69.8 - 69.9	1.00	62.8 - 63.3	0.21 - 0.23
6	69.7 - 69.8	0.61 - 0.64	62.7 - 62.9	0.15 - 0.16	-	-
7	62.8 - 63.1	0.16 - 0.22	-	-	-	-
Unknowns/Mixtures						
			Sigma		**Spectrum (lot 2)**	
Peak	Chemical Shift (ppm)	Relative intensity (normalized)	Chemical Shift (ppm)	Relative intensity (normalized)	Chemical Shift (ppm)	Relative intensity (normalized)
1	105.4	0.27	106.5	0.30	103.6	0.18
2	91.5	0.23	95.7	0.22	93.9	0.14
3	82	0.36	80.4	0.66	75.8	1.00
4	78.4	0.86	77.8	0.95	70.0	0.93
5	74.8	1.00	69.8	1.00	63.3	0.21
6	69.8	0.73	62.6	0.15	-	-
7	62.6	0.19	-	-	-	-

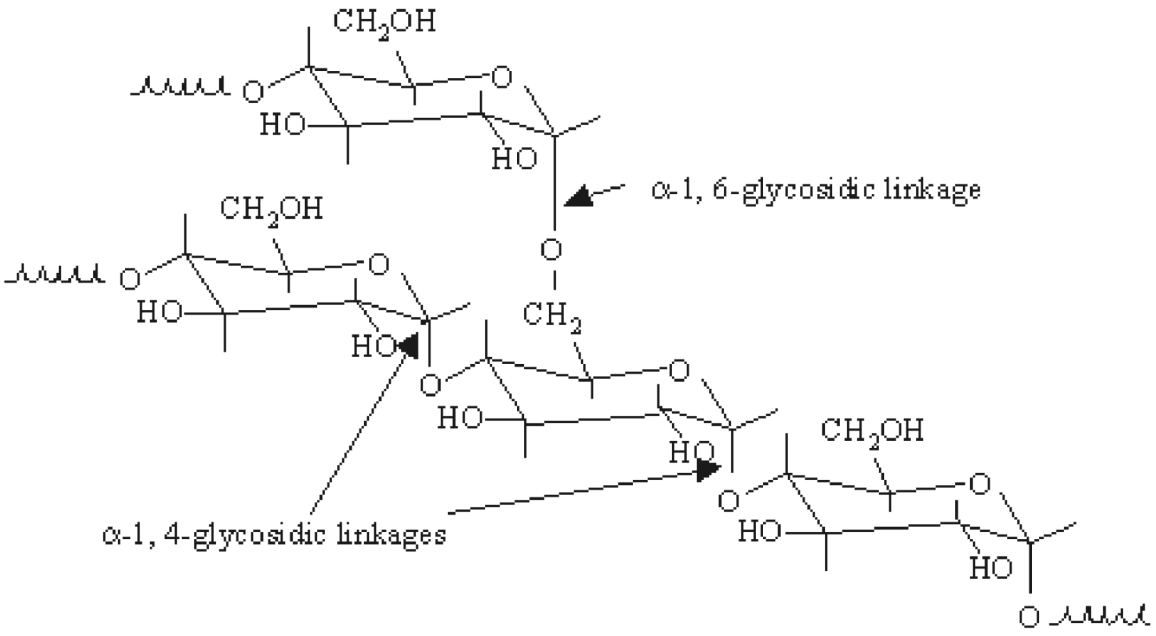

Figure 3.7. Structure of starch.

consist of ordered arrays of double helices with similar conformations but different packing arrangements.[17-19] The amylose-lipid inclusion complex is referred to as the V-type, which, unlike A- and B-type crystalline forms, consists solely of a single helix.[17-21] Common sources of starch such as corn and wheat are classified as A-type, while starch from potato is classified as B-type.

The ^{13}C SSNMR spectra of the corn, wheat, and potato starch samples received from Sigma are shown in Figures 3.8a, 3.8b, and 3.8c, respectively. Distinct differences in the C-1 region (90-110 ppm) are highlighted. It is well established that the C-1 resonance for A-type starches is split into three distinct SSNMR signals and for B-type starches into two distinct SSNMR signals.[19-21] While a cluster of three peaks at approximately 101.5, 100.4, and 99.4 ppm is seen in both the corn and wheat A-type starches, there is also a broad peak present downfield at ~103 ppm in these samples. It has been reported that this peak is made up of signals from amorphous material and the V-type amylose-lipid complex.[21-22] This peak is very large in the potato starch sample from Sigma (Fig.3.8c). The large amount of amorphous or amylose content in this material could explain the difficulties in differentiating the two distinct peaks in the C-1 signal for this B-type starch.

An overlay of the ^{13}C SSNMR spectra of three corn starch samples is shown in Figure 3.9. The three C-1 signals typical of crystalline A-type starches are clearly observed in all samples. However, a fourth peak is also present in this region for all three samples. Deconvolution of this cluster of four peaks allows for integration of areas and calculation of the amount of crystalline A-type versus amorphous and V-type content present in each sample. The amount of crystalline content in the Sigma, Grain Processing

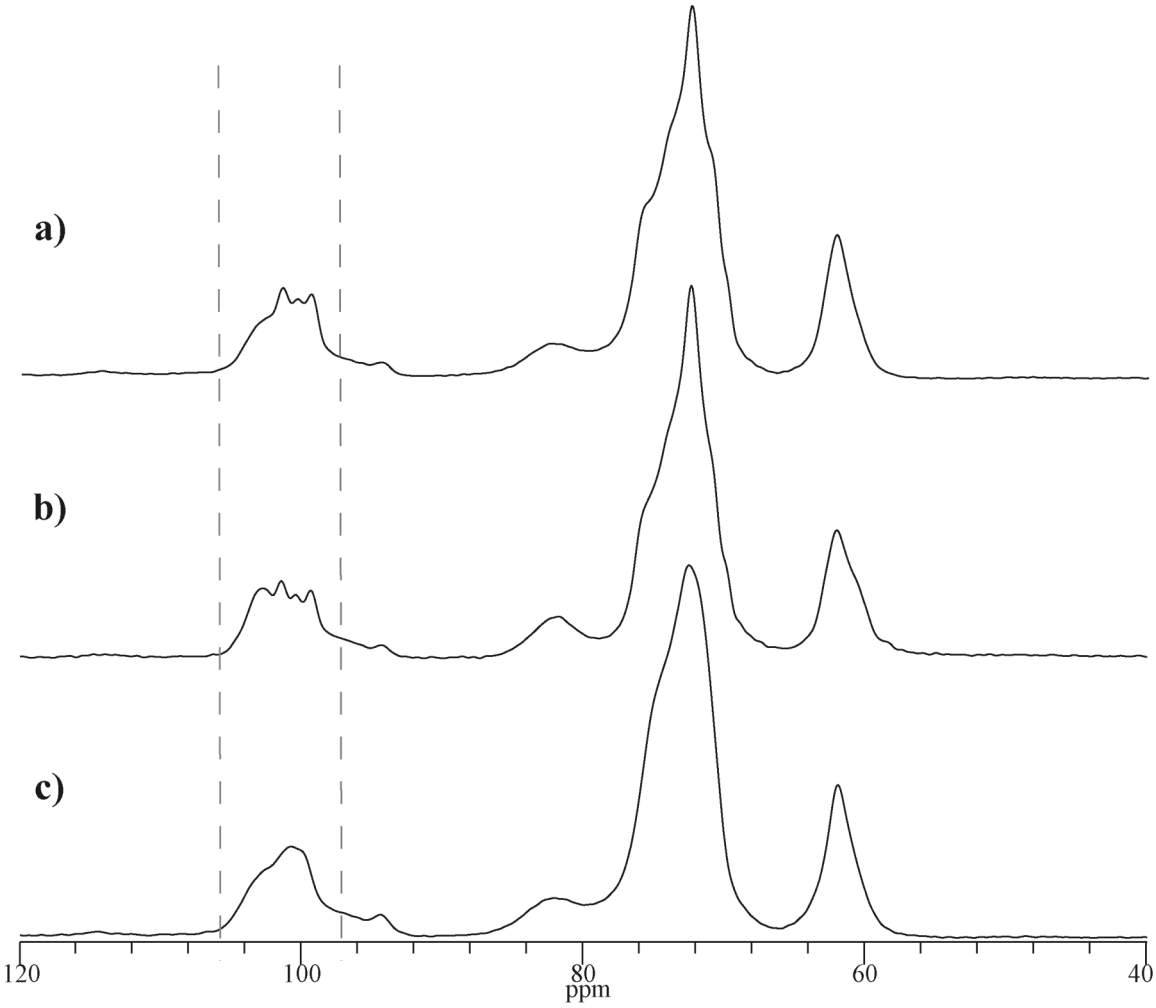

Figure 3.8. Representative ^{13}C SSNMR spectra of (a) corn starch, (b) wheat starch, and (c) potato starch. Differences in the C-1 region of the spectrum are highlighted.

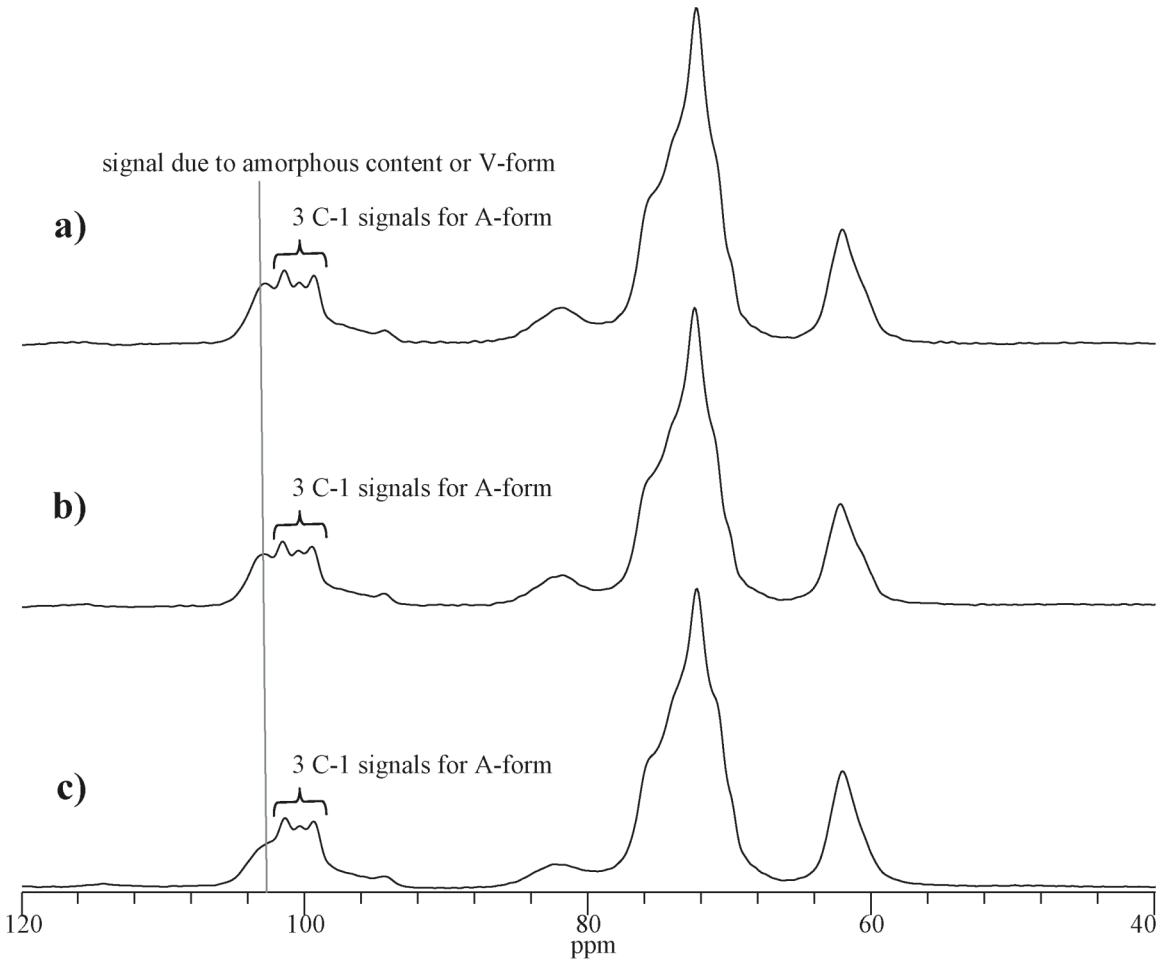

Figure 3.9. ^{13}C SSNMR spectra of corn starch: (a) Grain Processing B880, (b) Grain Processing B700, and (c) Sigma. Variations in crystalline versus amorphous and/or amylose content are highlighted.

B700, and Grain Processing B880 samples was calculated and found to be similar, with values of 61.1%, 59.6%, and 58.0%, respectively.

Maltodextrins and corn syrup solids are produced from either acid or enzymatic hydrolysis of starch.[23] The degree of hydrolytic conversion of starch to these products is analytically referred to as the dextrose equivalent (DE), which is a measure of the total reducing power of the sugar relative to dextrose.[23] Maltodextrins have DE values <20 while corn syrup solids are more extensively hydrolyzed products with DE values >20.

^{13}C SSNMR spectra of several maltodextrin and corn syrup solids samples are shown in Figure 3.10. Two peaks at ~93 and 97 ppm grow as the DE value (provided by the supplier) of the material increases. As the starch is hydrolyzed, species with lower molecular weights and shorter chains are being formed, which results in more end groups being produced. The carbons in these end groups are responsible for the new signals seen between 90 and 100 ppm in the SSNMR spectra. In addition, the ^{1}H T_1 values range from as low as 1.94 s to as high as 4.15 s and appear to increase as the DE value of the material increases. These values are higher than the ^{1}H T_1 values for the starch samples, which were between 0.8 and 0.9 s. This suggests a relationship between degree of hydrolysis and SSNMR proton relaxation time seems to exist. To better examine this relationship, a plot of the peak area of the signals between 90 and 100 ppm versus ^{1}H T_1 value was made and is shown in Figure 3.11. The areas of the peaks at ~93 and 97 ppm were normalized to the area of the peak denoted as 1 in Figure 3.10 and then the normalized area percentage of these peaks was calculated. As illustrated in Figure 3.11, a direct correlation between the area of these peaks and the relaxation time of the sample is observed. The DE value range

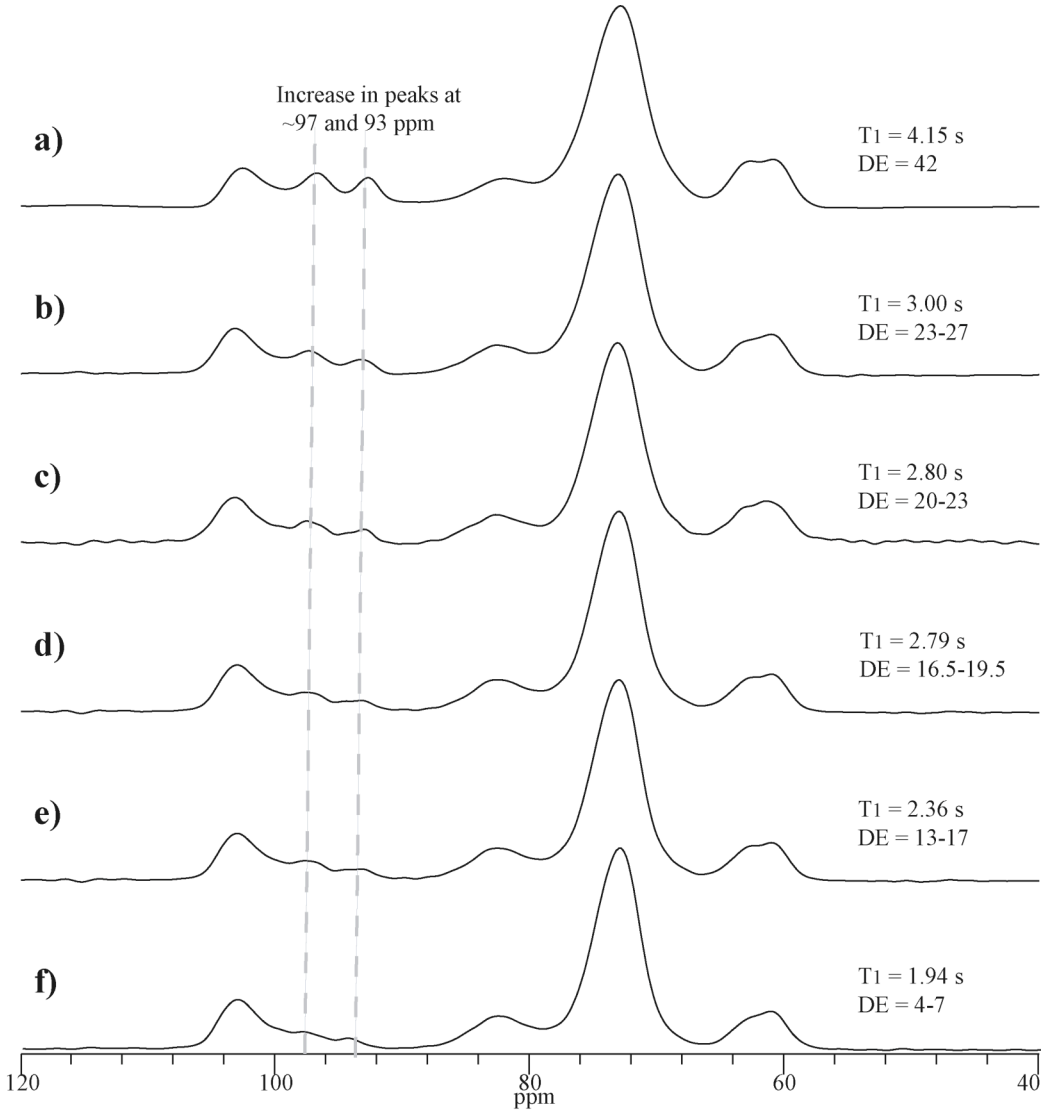

Figure 3.10. ^{13}C SSNMR spectra of corn syrup solids: (a) Globe, (b) Grain Processing M250, (c) Grain Processing M200, and maltodextrins: (d) Aldrich 419699, (e) Aldrich 419680, and (f) Aldrich 419672. Growth of two new peaks between 90 and 100 pm is highlighted. Relaxation times and dextrose equivalent values are also shown.

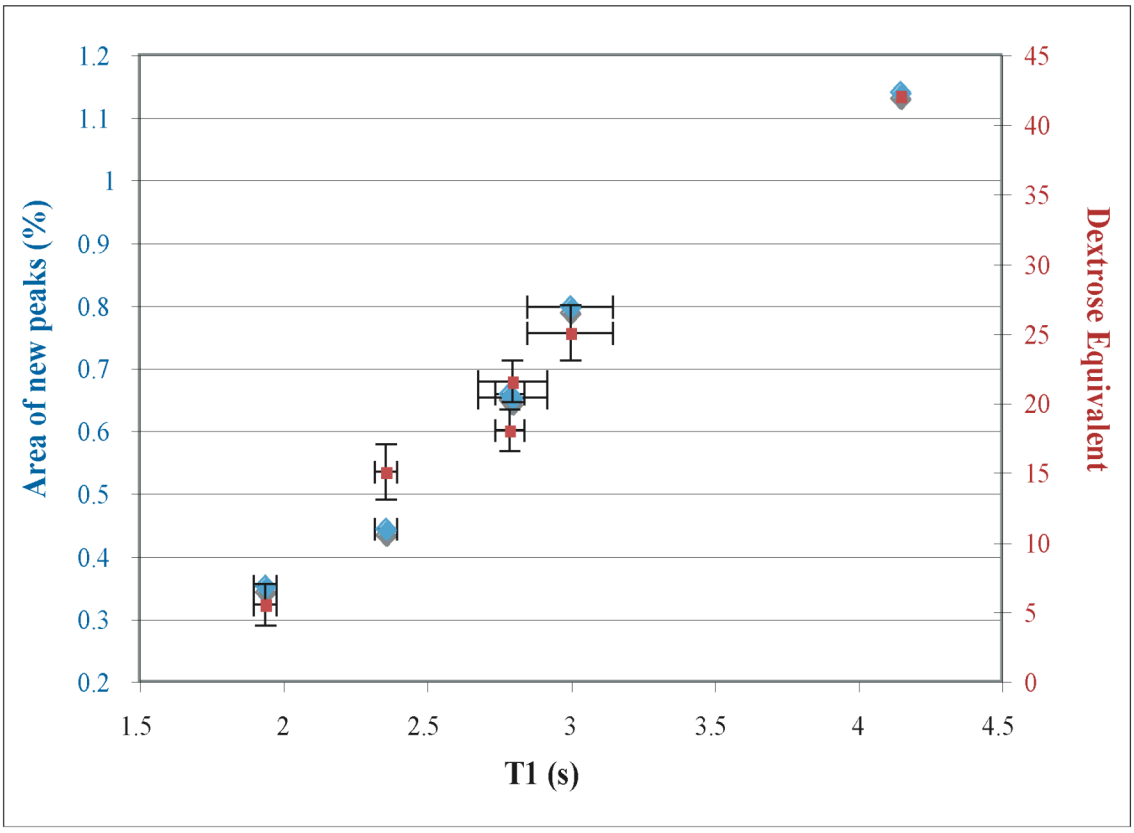

Figure 3.11. Relationship between relaxation times, growth of new peaks in maltodextrin and corn syrup solid samples, and dextrose equivalent.

provided by the supplier is also plotted for comparison. The overlap between the blue data points (peak area) and red data points (DE) is strong and suggests that SSNMR data can be used to determine differences in the degree of hydrolysis between starch derivatives.

3.3.4 Microcrystalline cellulose and cellulose derivatives

Microcrystalline cellulose is one of the most commonly used pharmaceutical excipients for direct tableting. Differences in flow properties and tableting characteristics can be attributed to differences in moisture content and particle size distribution,[24] and microcrystalline cellulose is typically available as grades that are classified according to these parameters. Multiple grades of microcrystalline cellulose varying in mean particle size and water content were received from FMC Biopolymers, as shown in Table 3.1. The SSNMR spectra and corresponding ^{1}H T_1 values of all of the samples analyzed are shown in Figure 3.12. There are no significant differences observed between the spectra of different grades or between lots of the same grade. However, there are noticeable differences in relaxation times. The ^{1}H T_1 values of grades PH-112 and PH-113 appear to be higher than those of grades PH-101, PH-102, and PH-105. This can be explained by differences in water content. According to the specifications provided by the manufacturer, grades PH-112 and PH-113 contain lower amounts of water than the others, and was confirmed using TGA. The PH-112 and PH-113 grades had water contents between 2.0 and 2.5%, while the PH-101, PH-102, and PH-105 grades all had water contents between 3.5 and 4.0%. Thus, the higher relaxation times of PH-112 and PH-113 are likely caused by the reduced mobility of these

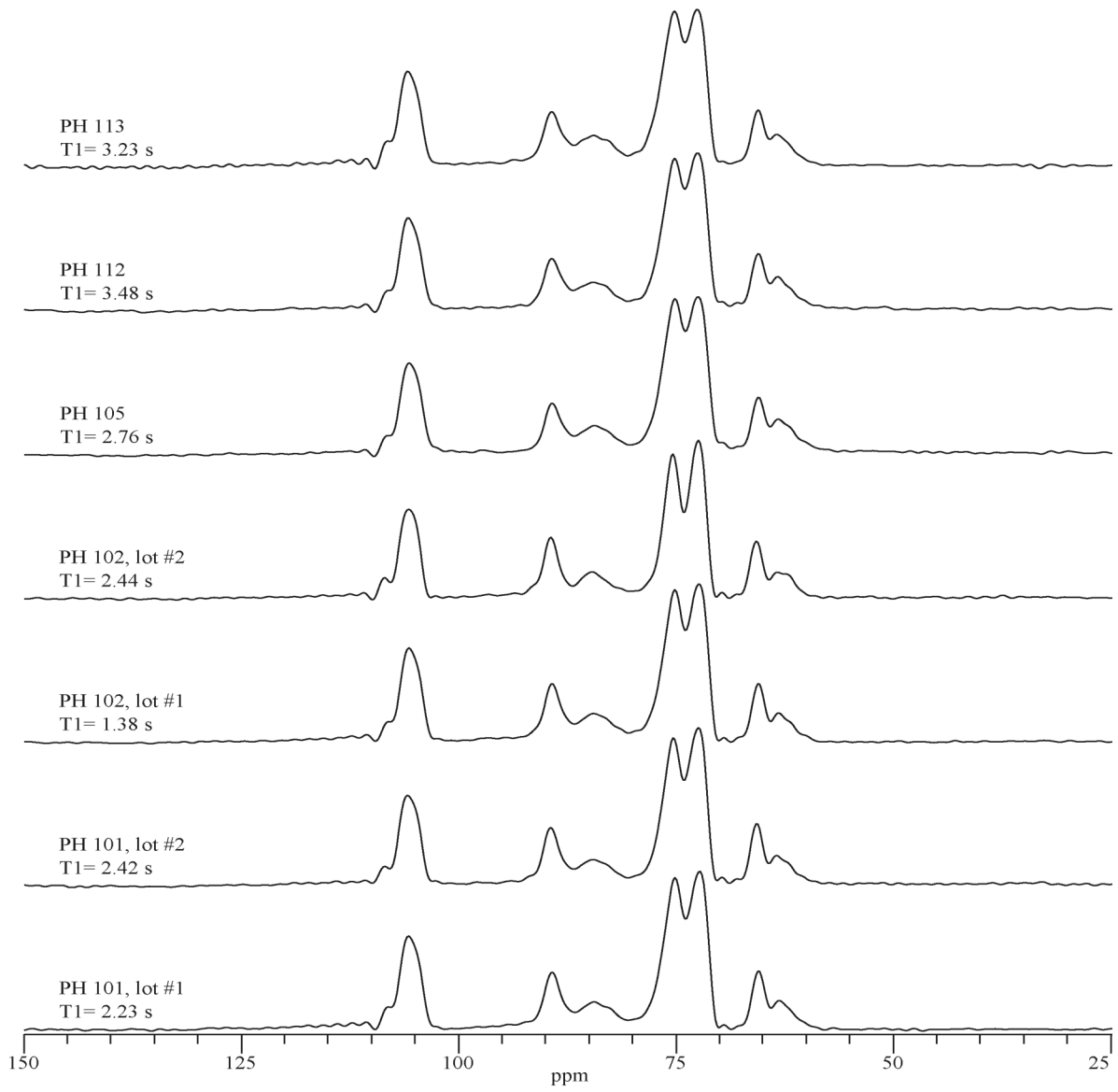

Figure 3.12. ^{13}C SSNMR spectra and relaxation times of Avicel (FMC Biopolymer's brand name for microcrystalline cellulose) samples.

samples compared to the others in which more water is present. Additionally, lot-to-lot variations in the ^{1}H T_1 values for grade PH-102 were observed. The first lot of PH-102 had a relaxation time much lower than that of the second lot of this grade. TGA was performed on these samples in order to detect differences in water content that could potentially explain the observed differences in relaxation times between lots. The first lot of PH-102 had a water content of 4.1% by TGA, while the water content of the second lot was measured as 3.8%. This slight difference in water content does not appear to explain the decrease in ^{1}H T_1 for the first lot. Other factors such as impurities or MW differences could possibly explain the difference, but the samples would have to be examined through further experimentation in order to confirm or deny these possible explanations.

The second cellulose-based excipient that was examined was carboxymethylcellulose sodium. This excipient is primarily used for its viscosity-increasing properties and is therefore available in a wide range of molecular weights.[5] Three samples from Acros Organics, differing in molecular weight, were analyzed, along with one medium-viscosity grade sample from Fluka. The SSNMR spectra of these four samples are shown in Figure 3.13. All three spectra of samples from Acros (Fig.3.13a-c) look practically identical, while the spectrum of the sample from Fluka (Fig.3.13d) appears slightly different, displaying better resolution of peaks in the 50-90 ppm region. All of the samples had ^{1}H T_1 values of ~2 s, except for one Acros sample that had a ^{1}H T_1 value of 4.6 s. This difference in relaxation time did not appear to correlate with molecular weight and viscosity. However, TGA analysis results showed that all samples except for the one Acros lot exhibiting a long relaxation time had water contents between 9.5 and 10%. The

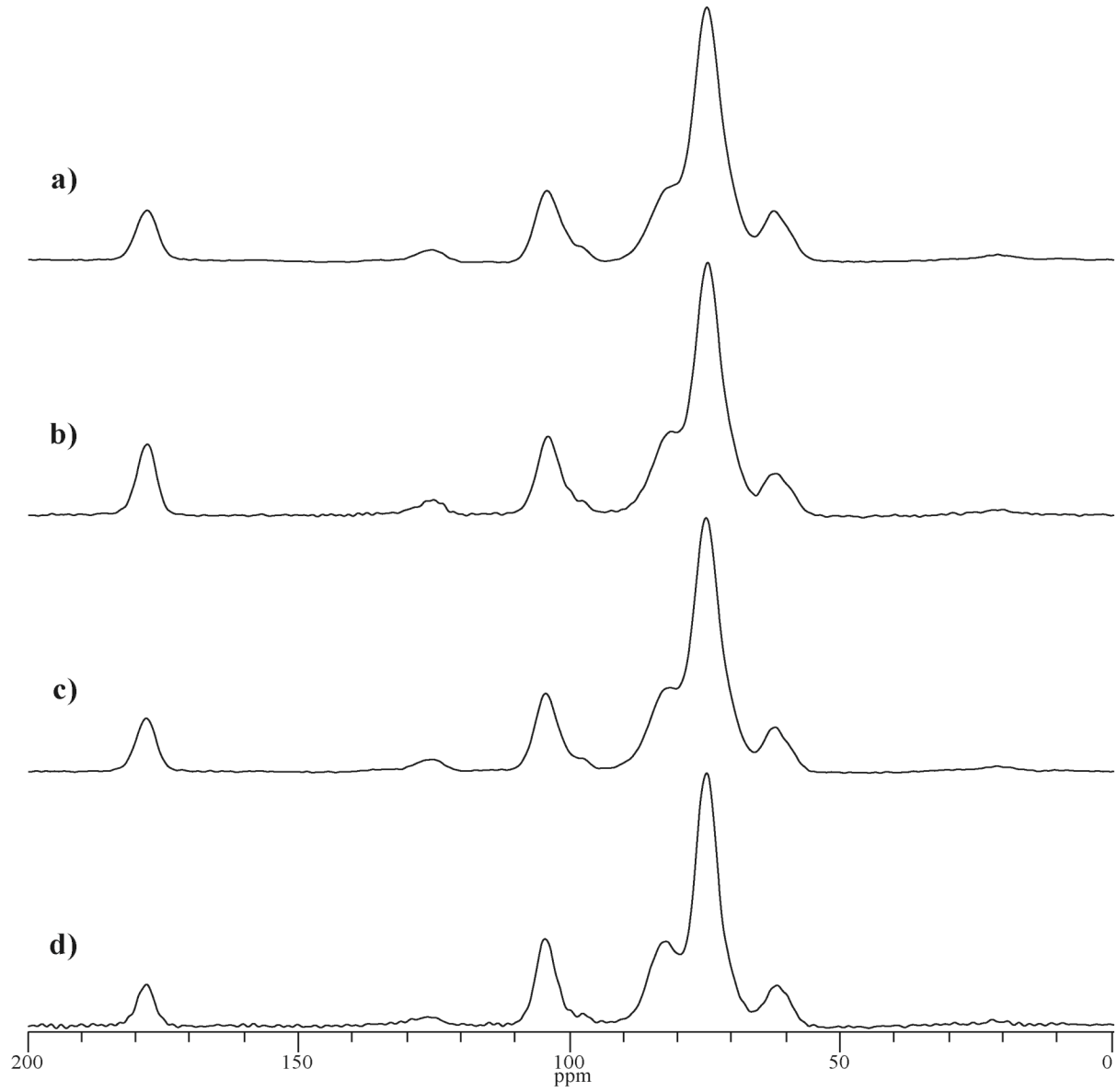

Figure 3.13. ^{13}C SSNMR spectra of carboxymethylcellulose samples received from Acros Organics (a-c) and FMC Biopolymer (d).

Acros sample with a ^{1}H T_1 value of 4.6 s had a water content of only 6.1%. Therefore, the reduced mobility observed in this sample might be attributed to a much lower water content compared to the others.

Cellulose derivatives such as hydroxyethylcellulose (HEC), hydroxypropylcellulose (HPC), and hydroxypropylmethylcellulose (HPMC) were also analyzed. These excipients are partially substituted derivatives of cellulose, and are available as several grades that vary in viscosity and the extent of substitution (Figure 3.14).[5] HPMC grades are also further designated according to the relative percentage of methoxy and hydroxypropoxy groups present. These parameters are key properties known to be important to the performance of these excipients in pharmaceutical formulations.[25] Representative SSNMR spectra for each of these substituted cellulose derivatives are shown in Figure 3.15. Differences between the spectra are highlighted and are due to the varying number and types of CH-, CH_2-, and CH_3 groups present in each sample. Specifically, the peak below 25 ppm corresponds to a methyl group that is not directly attached to an oxygen atom. HPC contains the greatest amount of these types of methyl groups, followed by HPMC. The HEC samples do not contain these groups, and therefore, the SSNMR spectra of these samples do not contain any peaks below 50 ppm. Distinct differences between HEC, HPC, and HPMC in the 55-70 ppm region of the SSNMR spectra are also observed. There were no noticeable differences between spectra and relaxation times for all of the HEC and HPC samples that were studied. However, HPMC type 2208 and 2910, which differ in the number of methoxy and hydroxypropoxy groups, showed distinct differences in their SSNMR spectral details. As shown in Figure 3.16, the

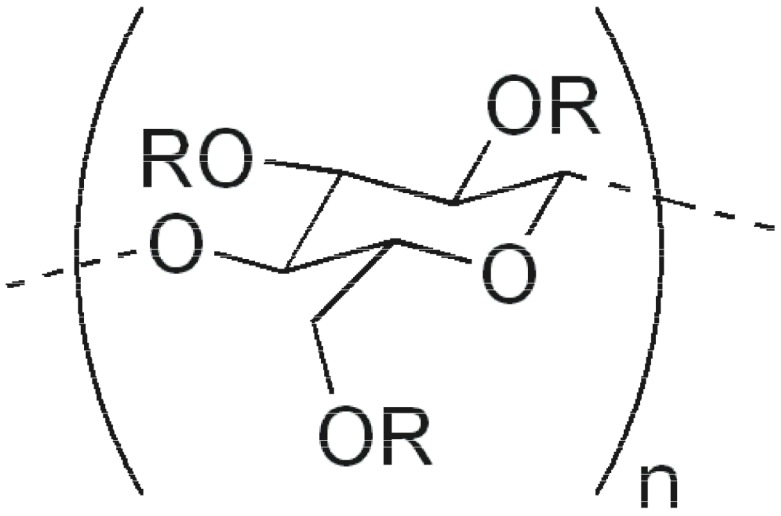

R = H for cellulose
R = H or CH_2CO_2Na for carboxymethylcellulose
R = H or CH_2CH_2OH for hydroxyethylcellulose
R = H or $CH_2CH(OH)CH_3$ for hydroxypropylcellulose
R = H or CH_3 or $CH_2CH(OH)CH_3$ for hydroxypropylmethylcellulose

Figure 3.14. Basic structure of cellulose and possible substitution groups.

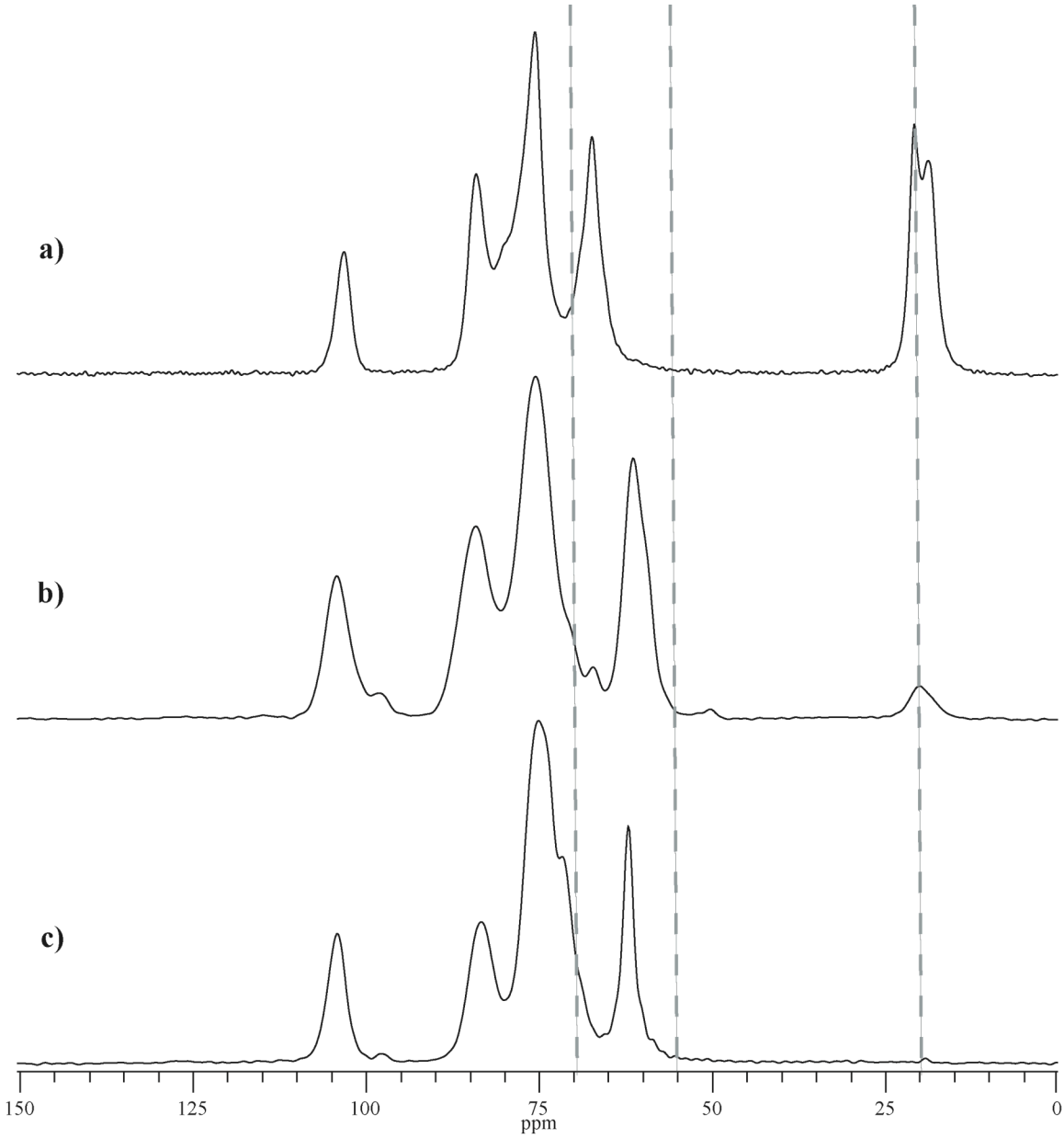

Figure 3.15. Representative ^{13}C SSNMR spectra of (a) hydroxypropylcellulose, (b) hydroxypropylmethylcellulose, and (c) hydroxyethylcellulose. Key differences in the spectra are highlighted.

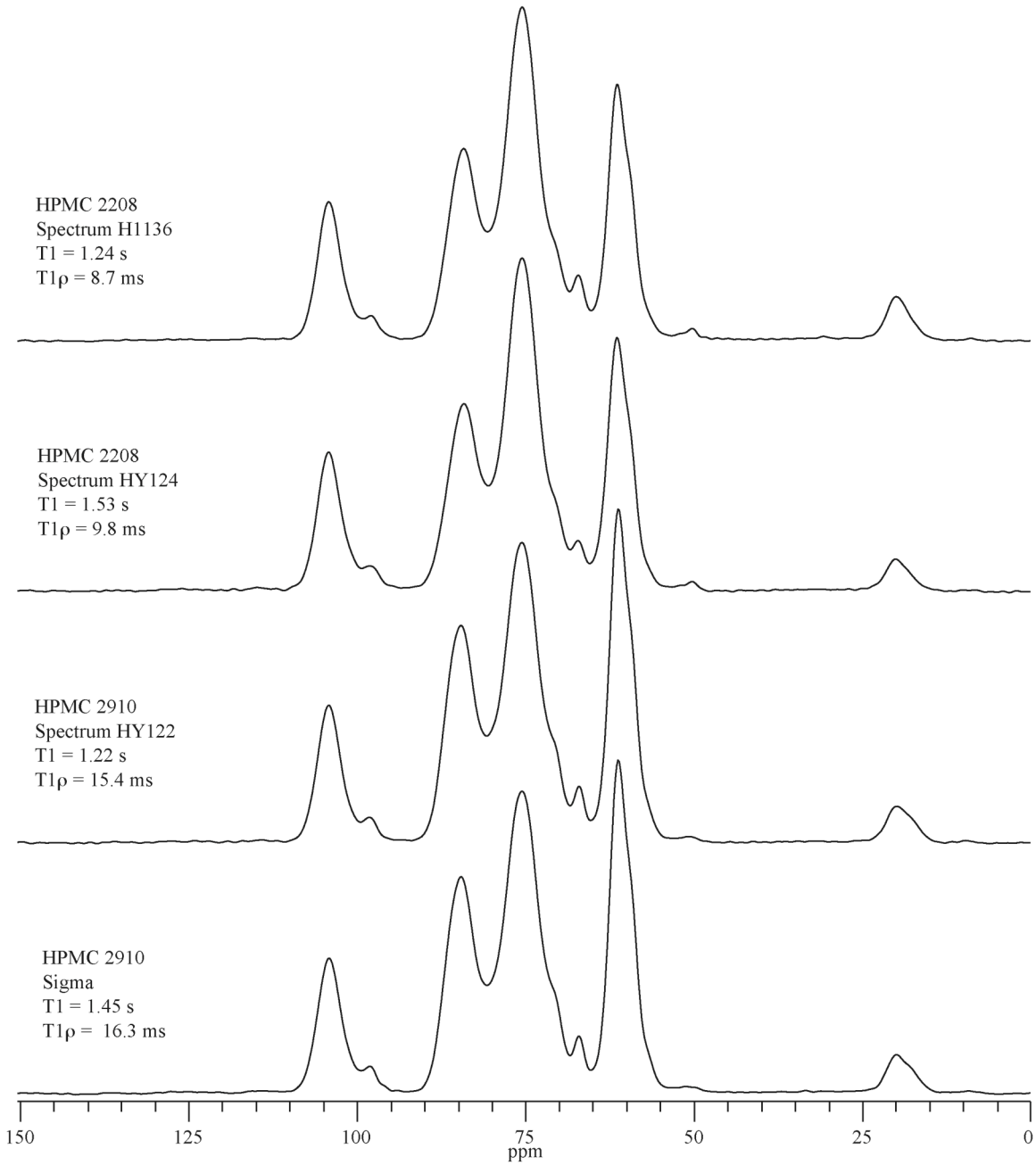

Figure 3.16. ^{13}C SSNMR spectra of type 2208 and type 2910 hydroxypropylmethylcellulose samples. Differences in peak intensity at ~60 ppm are due to differences in methoxy content. ^{1}H $T_{1\rho}$ values differ for these two types.

peak located at ~60 ppm is more intense in type 2910 samples than in the 2208 samples. This is due to the greater methoxy content present in the 2910 samples. Type 2910 HPMC contains 28-30% methoxy, while type 2208 contains 19-24%. The observed differences in the SSNMR spectra allow these two types of HPMC to be clearly distinguished from each other. Another very interesting observation is the difference in ^{1}H $T_{1\rho}$ values between the two types of HPMC. Although all samples had similar ^{1}H T_1 values (1.2-1.5 s), the type 2910 samples showed a ^{1}H $T_{1\rho}$ value equal to almost double that of the type 2208 samples. The greater methoxy content restricts the mobility of type 2910 samples in comparison to type 2208 samples, which have higher hydroxypropoxy groups, longer chains, and hence more flexibility. Thus, ^{1}H $T_{1\rho}$ is another SSNMR parameter that can potentially be used to distinguish between these two types of HPMC.

3.4 Conclusions

Important characteristics of naturally derived excipients such as form identification, structural differences, variations in crystalline and amorphous content, and water content can be detected using SSNMR spectroscopy.

Alginic acid and sodium alginate can be differentiated based on carbonyl peak position. While this can be achieved using other techniques, SSNMR spectroscopy offers the advantage of non-destructive sample preparation and selectivity that enables form

identification in the presence of other materials. The resolution of signals in the SSNMR spectra of the three forms of carrageenan allows for positive identification of the major form present based on number of peaks. Analysis of relative peak intensities provides insight into the purity of a carrageenan sample compared to known standards. However, the high degree of peak overlap makes it difficult to accurately detect and quantitate low levels of other forms that may be present as impurities. The SSNMR spectrum of starch can be used to identify the source (corn, wheat, potato) as well as to determine the amounts of amorphous and crystalline material. Interestingly, relaxation values and peak areas of starch derivatives such as maltodextrin and corn syrup solids can be related to the degree of hydrolysis, making SSNMR spectroscopy an attractive alternative for determining differences in DE values among various samples. SSNMR spectral features of microcrystalline cellulose and carboxymethylcellulose do not change between grades or suppliers, suggesting there is little information to be gained via comparison of SSNMR spectra of these excipients. However, SSNMR relaxation times of these cellulose-based excipients seem to provide insight into water content variations. A correlation of SSNMR relaxation values to viscosity was not found for cellulose derivatives such as HEC, HPC, and HPMC. While no noticeable differences between the SSNMR spectra of HEC and HPC samples were observed, differences in peak intensities and ^{1}H $T_{1\rho}$ values of HPMC samples can be correlated to the amount of methoxy subsituent groups.

SSNMR spectroscopy offers the unique advantages of 1) non-destructive sample preparation, and 2) selectivity. Therefore, SSNMR spectroscopy can potentially be used to monitor changes in excipients present in a solid dosage form without any alteration to the

sample. This could potentially be very useful during preformulation and formulation stages, particularly when the source of an excipient changes, or when manufacturing and/or storage conditions could potentially alter the excipient.

3.5 References

1. Moreton C. Functionality and performance of excipients in quality-by-design world part 4: obtaining information on excipient variability for formulation design space. American Pharmaceutical Review. 2009;12:28-32.

2. Vogt F. A multi-disclipinary approach to the solid-state analysis of pharmaceuticals. American Pharmaceutical Review. 2008;11:50-7.

3. Berendt R, Sperger D, Isbester P, Munson E. Solid-state NMR spectroscopy in pharmaceutical research and analysis. Trends in Analytical Chemistry 2006;25:977-84.

4. Lubach J, Dawie X, Segmuller B, Munson E. Investigation of the effects of pharmaceutical processing upon solid-state NMR relaxation times and implications to solid-state formulation stability. J Pharm Sci. 2007;96:777-87.

5. Rowe R, Sheskey P, Owen S. Handbook of pharmaceutical excipients. 5th ed. Pharmaceutical Press and the American Pharmacists Association; 2006.

6. Pines A, Gibby M, Waugh J. Proton-enhanced NMR of dilute spins in solids. J Chem Phys. 1973;59:569-90.

7. Andrew E. Narrowing of NMR spectra of solids by high-speed specimen rotation and the resolution of chemical shift and spin multiplet structures for solids. Prog Nucl Mag Res. 1971;8:1-39.

8. Dixon W, Schaefer J, Sefcik M, Stejskal E, McKay R. Total suppression of sidebands in CPMAS carbon-13 NMR. J Magn Reson. 1982;49:341-5.

9. Fung B, Khitrin A, Ermolaev K. An improved broadband decoupling sequence for liquid crystals and solids. J Magn Reson. 2000;142:97-101.

10. Barich D, Gorman E, Zell M, Munson E. 3-methylglutaric acid as a ^{13}C solid-state NMR standard. Nucl Magn Reson. 2006;30:125-9.

11. Haug A, Larsen B, Smidsrod O. A study of the constitution of alginic acid by partial acid hydrolysis. Acta Chem Scand. 1966;20:183-90.

12. Grasdalen H, Larsen B, Smidsrod O. A P.M.R. study of the composition and sequence of uronate residues in alginate. Carbohydr Res. 1979;68:23-31.

13. Llanes F, Sauriol F, Morin G, Perlin A. An examination of sodium alginate from sargassum by NMR spectroscopy. Can J Chem. 1997;75:585-90.

14. Salomonsen T, Jensen H, Larsen F, Steuernagel S, Engelsen S. Direct quantification of M/G ratio from ^{13}C CP-MAS NMR spectra of alginate powders by multivariate curve resolution. Carbohydr Res. 2009;344:2014-22.

15. Anderson N, Dolan T, Rees D. Evidence for a common structural pattern in the polysaccharide sulphates of the rhodophyceae. Nature. 1965;205:1060-2.

16. Rochas C, Lahaye M. Solid state ^{13}C-NMR spectroscopy of red seaweeds, agars and carrageenans. Carbohydr Polym. 1989;10:189-204.

17. Imberty A, Buleon A, Tran V, Perez S. Recent advances in knowledge of starch structure. Starch. 1991;43:375-84.

18. Sarko A, Wu H. The crystal structures of A-, B- and C-polymorphs of amylose and starch. Starch. 2006;30:73-8.

19. Gidley M, Block S. Molecular organizations in starches: a ^{13}C CP/MAS NMR study. J Am Chem Soc. 1985;107:7040-4.

20. Veregin R, Fyfe C. Characterization of the crystalline A and B starch polymorphs and investigation of starch crystallization by high-resolution ^{13}C CP/MAS. Macromolecules. 1986;19:1030-4.

21. Morgan K, Furneaux R, Larsen N. Solid-state NMR studies on the structure of starch granules. Carbohydr Res. 1995;276:387-99.

22. Gidley M, Bociek S. ^{13}C CP/MAS NMR studies of amylose inclusion complexes, cyclodextrins, and the amorphous phase of starch granules: relationships between glycosidic linkage conformation and solid-state ^{13}C chemical shift. J Am Chem Soc. 1988;110:3820-9.

23. Dokic L, Jakovljevic J, Dokic P. Relation between viscous characteristics and dextrose equivalent of maltodextrins. Starch. 2004;56:520-5.

24. Doelker E, Mordier D, Iten H, Humbert-Droz P. Comparative tableting properties of sixteen microcrystalline celluloses. Drug Dev Ind Pharm. 1987:13:1847-1875.

25. Mitchell S, Balwinski K. A framework to investigate drug release variability arising from hypromellose viscosity specifications in controlled release matrix tablets. J Pharm Sci. 2008:97:2277-2285.

Chapter 4

Correlation of SSNMR Parameters to Excipient Properties that Affect Functionality: Sodium Alginate

4.1 Introduction

As evidenced by the data presented in Chapter 3, solid-state NMR spectroscopy can provide a wealth of information for a wide variety of pharmaceutical excipients. Certain excipient properties can be related to functionality, and the selection of a specific type and/or grade of an excipient can therefore affect the performance of the formulated product.[1,2] The purpose of the work presented in this chapter is to explore the potential for SSNMR parameters to be correlated to important functionally related characteristics of sodium alginate, an excipient introduced in Chapter 3.

Sodium alginate has traditionally been used in the food industry as a thickening agent.[3] Pharmaceutically, it serves as a suspending agent, a disintegrant, a tablet binder, and a viscosity-increasing agent. It has also been investigated for use in controlled-release delivery systems[4,5] and as a highly elastic deforming excipient in soft tableting.[6] Alginates are linear unbranched polysaccharides containing various proportions of β-D-mannuronic acid (M) and α-L-guluronic acid (G) residues, arranged in a block-wise fashion along the polymer chain. The M and G monomers are linked by 1→4 glycosidic bonds, forming either homogeneous or heterogeneous sequences (Figure 4.1).[7]

Sodium alginate is extracted from various types of marine algae. The seaweed species, harvesting region, season, sea current, water temperature, and processing method can all impact important structural features of the alginate, such as the G/M ratio and

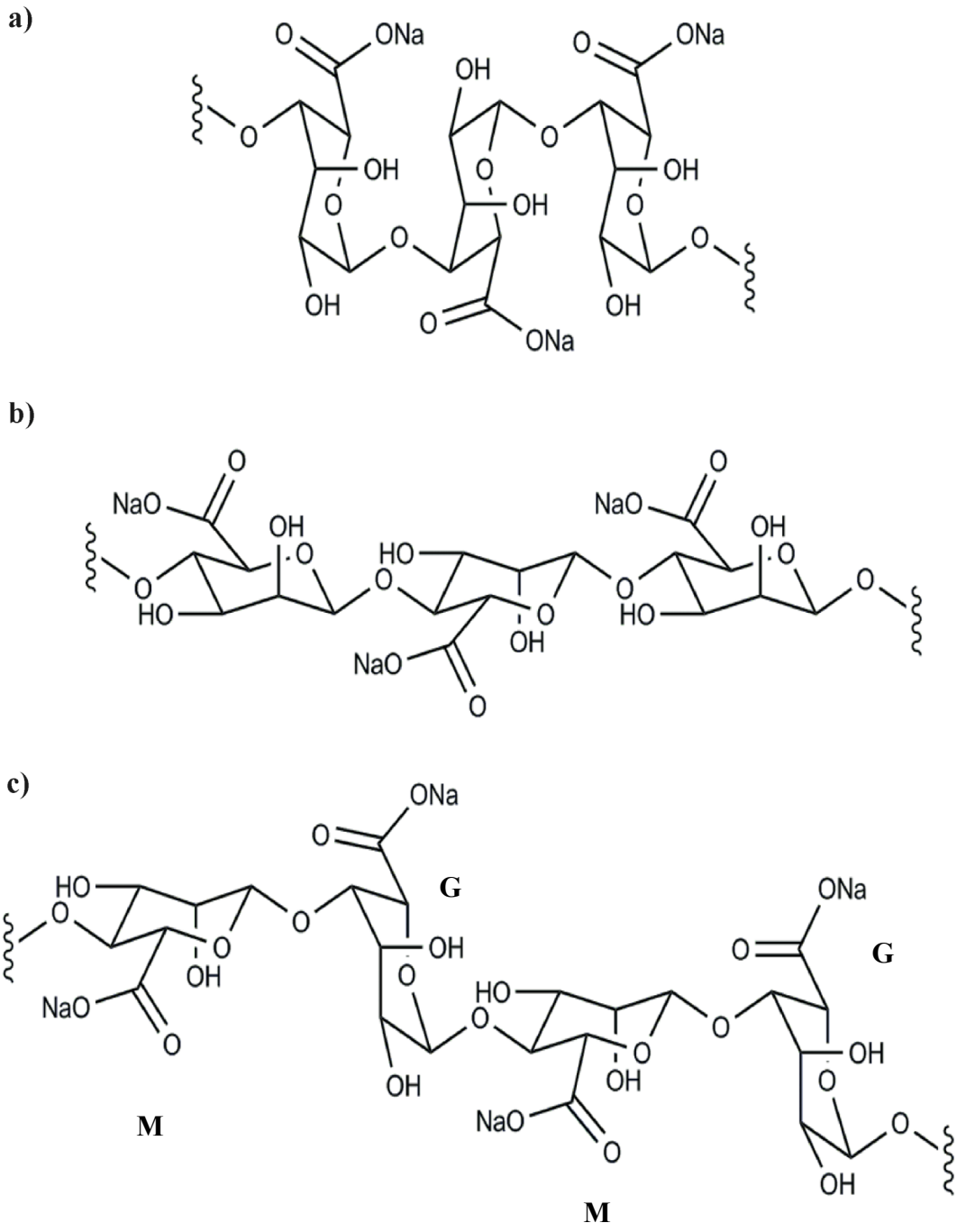

Figure 4.1. Possible arrangements of the M and G monomers in sodium alginate: (a) homogeneous G-G sequence, (b) homogeneous M-M sequence, and (c) heterogeneous M-G sequence.

molecular weight.[8] It is estimated that over 200 different grades of sodium alginate are commercially available from manufacturers.[5] With this abundance of options, it is extremely important to be aware of how variability in alginates can affect the performance characteristics of pharmaceutical formulations.

The chemical composition of sodium alginate can affect its behavior in pharmaceutical formulations. For example, the strength of the gel formed from alginate in the presence of divalent metal ions depends on the G/M ratio, as the G residues exhibit a greater affinity for the ions than the M residues.[9,10] Sugawara et al.[11] observed rapid swelling and erosion of gel beads prepared from alginates with a low G/M ratio at neutral pH, while beads prepared from a high G/M ratio alginate did not erode under the same conditions. Liew et al.[3] studied the effect of monomer content on the release of chlorpheniramine maleate from alginate-based matrix tablets, and showed that M-rich alginates gave higher drug release rates in phosphate buffer while G-rich alginates gave higher drug release rates in acidic media. Sriamornsak et al.[12] observed similar results upon examination of metronidazole release from alginate-based matrix tablets. The tableting behavior of sodium alginates has also been found to depend on chemical composition.[6]

Another property that affects the pharmaceutical functionality of sodium alginate is the molecular weight and viscosity. Imai et al.[13] found that the release rate from gel beads prepared from three sodium alginate samples with similar G/M ratios but different viscosities was the same in acidic conditions but drastically different at neutral pH. Efentakis et al.[14] studied the release of furosemide from formulations containing different

viscosity grades of sodium alginate. Formulations prepared with the low viscosity grade showed the fastest release rate, those prepared with a medium viscosity grade exhibited an intermediate release rate, and those prepared with the high viscosity grade showed the slowest release rate. In a similar study, Efentakis et al.[15] studied the extent of dissolution of theophylline from low and high viscosity sodium alginate matrices, and measured a faster dissolution rate of theophylline from the low viscosity matrix in water, while the opposite result was observed in acid.

Although these examples illustrate how differences in the chemical composition and molecular weight distribution of sodium alginate can affect its functionality, pharmacopoeial standards do not currently include specifications and tests for analyzing these variations. Early methods for the determination of monomer content involved total acid hydrolysis of the glycosidic bonds followed by separation techniques such as paper chromatography, thin-layer chromatography (TLC), anion-exchange liquid chromatography, and gas-liquid chromatography (GLC).[16] Today, the most common method currently used for the structural analysis of sodium alginates is ^{1}H and ^{13}C solution-state nuclear magnetic resonance spectroscopy (NMR).[17-22] Unfortunately, solution-state NMR of alginates requires partial acid hydrolysis, which results in lengthy sample preparation and the potential for some insoluble material to be underrepresented. These drawbacks have recently motivated some researchers to investigate the potential use of solid-state NMR (SSNMR) spectroscopy as an alternative tool for characterization of intact sodium alginate powders.[23,24]

As described in Chapter 2, SSNMR spectroscopy has become more prevalent in the

pharmaceutical industry due to its non-destructive and non-invasive sample preparation, selective nature, ability to quantify solid forms, and the structural information it can provide.[25,26] In particular, SSNMR spectroscopy is a valuable tool for the structural analysis of excipients, as the amorphous or semi-crystalline nature of these materials limits the capability of more commonly used solid-state techniques such as differential scanning calorimetry (DSC) and powder X-ray diffraction (PXRD).[27] Another unique quality of SSNMR spectroscopy is its ability to provide insight into the molecular motions of solids.

Schaefer et al.[28] demonstrated how the ^{13}C SSNMR relaxation parameters describing the motions of polymers could be related to macroscopic properties such as mechanical impact strength. More recently, Lubach et al.[29] used SSNMR to study differences in proton spin-lattice relaxation times (^{1}H T_1) of processed lactose samples, and demonstrated the potential for the relative stability of solid-state formulations to be predicted by SSNMR relaxation measurements. Thus, it is of interest to determine if these insights into molecular motion can also be correlated to the viscosity of a polymeric excipient. Similarly, variations in the water content of an amorphous polymer might also be reflected by changes in the SSNMR relaxation times.

The data in this chapter will demonstrate the ability of ^{13}C SSNMR spectroscopy to detect variations in the chemical composition, molecular weight, and water content of sodium alginate samples. Salomensen et al.[24] recently evaluated SSNMR as a tool for calculating the G/M ratio of alginate samples and concluded that estimation of the G/M ratio from spectral deconvolution is relatively accurate but difficult due to the highly overlapping signals. These concerns are addressed through the comparison of different

spectral deconvolution methods, and improved resolution of signals upon hydration of the alginate is also shown. Furthermore, the differences in SSNMR relaxation times among sodium alginate samples will be investigated and the potential to correlate ^{1}H T_1 relaxation values to the intrinsic viscosity and hence molecular weight of these samples will be evaluated. Currently, there is not one single analytical technique that can be used to detect variations in the chemical composition, molecular weight, and water content of sodium alginate samples. Thus, the overall objective of this chapter is to evaluate SSNMR spectroscopy as an accurate, non-destructive, and relatively rapid analytical technique for the detection of differences in these important characteristics of sodium alginate.

.

4.2 Experimental

4.2.1 Samples

Seven pharmaceutical grades of sodium alginate were kindly provided by FMC Biopolymers (Drammen, Norway). The grades obtained represented a wide range of monomer compositions and viscosities, and in some cases, multiple lots of a specific grade were evaluated (Table 4.1). Polymannuronic acid and polyguluronic acid were isolated from sodium alginate using an acid hydrolysis method similar to one previously reported and outlined in Figure 4.2.[30] Oxalic acid and sodium chloride (ACS grade) were purchased from Sigma Aldrich (St. Louis, MO). Excipients used to make formulations

Table 4.1. Sodium alginate grades and specifications provided by FMC Biopolymers.

Grade designation in this study	**FMC Product Name**	**G/M (%)**	**Viscosity range (mPas) (1% sol., 20°C)**
1	Protonal LFR 5/60	65-75/25-35	<10
2	Protonal LF 200 DL	55-65/35-45	200-400
3	Protanal HF 120 RBS	45-55/45-55	600-800
4*	Protonal LF 10/60 LS	35-45/55-65	20-70
5*	Protonal LF 120 M	35-45/55-65	70-150
6*	Protonal LF 200 M	35-45/55-65	200-400
7	Protonal LF 240 D	30-35/65-70	70-150

* Indicates multiple lots were evaluated.

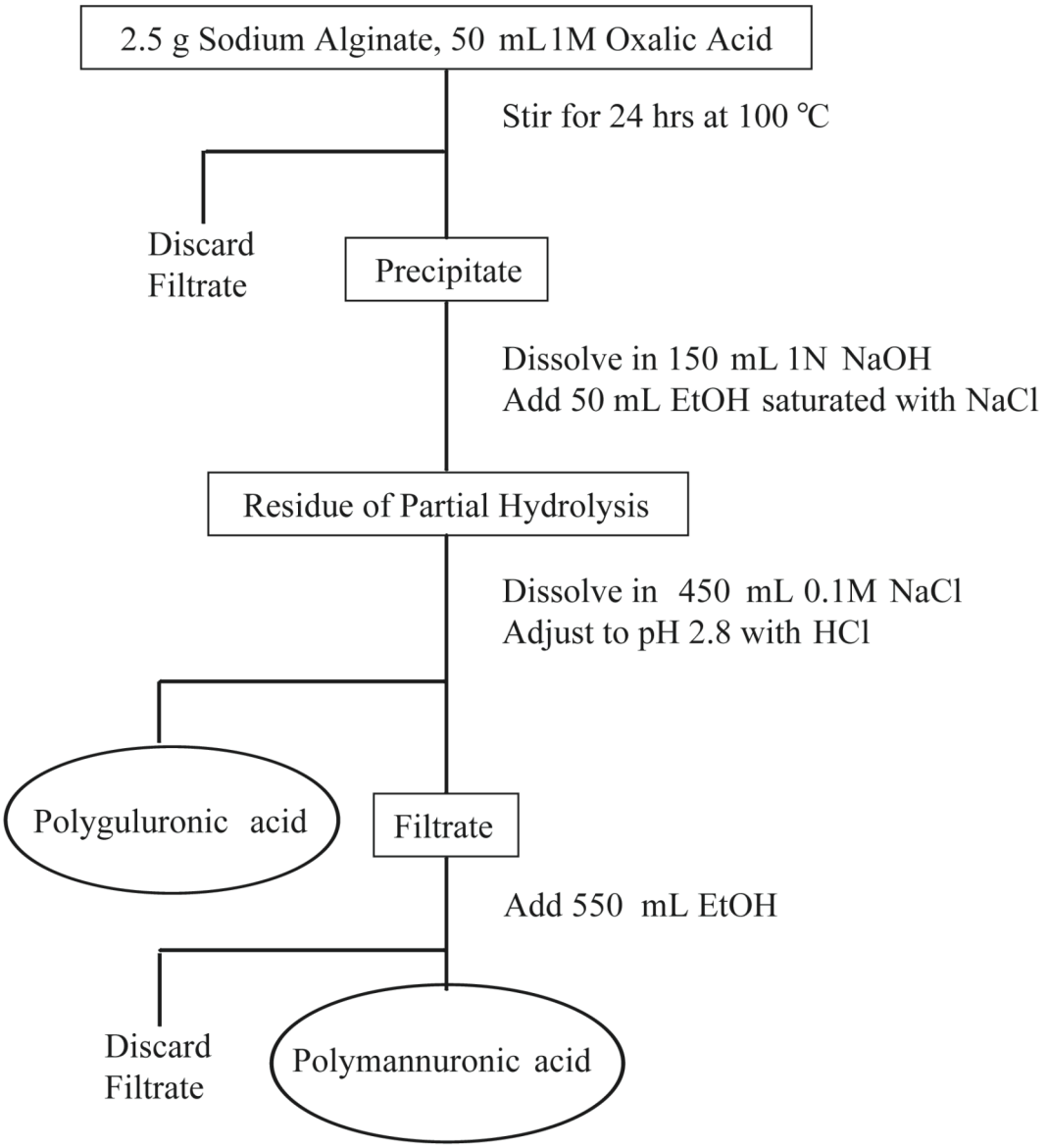

Figure 4.2. Procedure used for the separation and isolation of guluronic and mannuronic acid residues from intact sodium alginate powders.

with sodium alginate included lactose monohydrate (Foremost Farms, Baraboo, WI) and hydroxypropylmethylcellulose (Sigma Aldrich, St. Louis, MO).

4.2.2 Calcium and water content

The calcium and water content of the samples as received from FMC Biopolymers was measured. For calcium determination, 0.1% w/v sodium alginate solutions were prepared and the calcium content then measured using a Model 1100 Atomic Absorption Spectrophotometer (Perkin-Elmer, Waltham, MA). This analysis was performed by Shao Fu, a graduate student in the laboratory of Dr. Lawrence Block, our collaborator at Duquesne University. Water content by Thermogravimetric analysis (TGA) was performed using a TA Q50 Thermogravimetric Analyzer (TA Instruments, New Castle, DE). Samples were heated to 105 °C and held isothermally until the weight change was less than 0.01% per minute. Total percentage of weight loss was attributed to the amount of water in the sample.

4.2.3 Intrinsic viscosity determination

Our collaborators at Duquesne University also performed the intrinsic viscosity measurements. The apparent viscosities of aqueous solutions of sodium alginate containing sodium chloride (0.1 M) and of the solvent, $\eta_{solution}$ and $\eta_{solvent}$, respectively, were evaluated at 25 °C using an Ubbelohde viscometer (Cannon Instruments, State College, PA). All alginate concentrations were corrected for moisture content as

determined by TGA. Intrinsic viscosities [η] were determined from the concentration dependence of the reduced specific viscosity $\frac{\eta_{sp}}{C}$ in accordance with the Huggins equation,

$$\frac{n_{sp}}{C} = [n] + k' \cdot [n]^2 \cdot C,$$

where C is concentration in g/dL, k′ is a constant, and η_{sp} is specific viscosity, defined as

$$\eta_{sp} = \frac{\eta_{solution}}{\eta_{solvent}} - 1.$$

The molecular weight (M_w) in kDa was then calculated according to the following equation:[31]

$$[\eta] = 0.023 \bullet M_w^{0.984} \Rightarrow M_w = \left(\frac{[\eta]}{0.023}\right)^{\frac{1}{0.984}}$$

4.2.4 Solid-state NMR spectroscopy

Solid-state ^{13}C NMR spectra were acquired using a Chemagnetics CMX-300 spectrometer (Varian, Inc., Palo Alto, CA) operating at approximately 75 MHz for ^{13}C. Chemagnetics double-resonance probes equipped with either a Chemagnetics 7.5 mm PENCIL spinning module or a Revolution NMR 7-mm spinning modules (Revolution NMR, LLC, Fort Collins, CO) were used to acquire all spectra. Samples were packed into zirconia rotors and sealed with either Teflon or Kel-F end caps. Spectra were acquired using ramped-amplitude cross polarization (CP),[32,33] magic-angle spinning (MAS)[34,35] with

total sideband suppression (TOSS),[36] and SPINAL64 decoupling.[37] 3-methylglutaric acid (MGA) was used to optimize the spectrometer settings and set the reference frequency.[38] A contact time of 1 ms, MAS frequency of 4.0 kHz, and a ^{1}H decoupling field of approximately 80 kHz was used to acquire all spectra. The recycle delays varied based upon ^{1}H T_1 values for each sample, which were measured using saturation recovery experiments. Using Chemagnetics Spinsight software, plots of integrated signal intensity versus saturation recovery times were fit to the equation $y = amp(1 - e^{-\tau/T_1})$ where y is the integrated signal intensity, *amp* is the amplitude constant, τ is the saturation recovery time, and T_1 is the spin-lattice relaxation time. Saturation recovery times were arrayed from 0.01 to 20 s, depending on the nature of the sample. Monoexponential curve fitting provided an accurate fit for all data sets. A recycle delay equal to 5 times the ^{1}H T_1 value of each sample was used to acquire each spectrum. 5120 transients were acquired in order to achieve a high signal-to-noise ratio (SNR). Deconvolution of peaks in the region 60-90 ppm was achieved using Chemagnetics Spinsight software, and fitted peak areas and intensities were then used to calculate the amount of guluronic and mannuronic acid present in each sample. All samples were analyzed as received, and some were also analyzed after drying under vacuum and after exposure to high relative humidity in order to investigate the effects of water content on the SSNMR spectra and relaxation times.

4.2.5 Tableting

Effects of tableting on the relaxation behavior of sodium alginate alone and in the presence of other excipients were also assessed. Tablets of pure alginate and alginate mixed with either lactose monohydrate or hydroxypropylmethylcellulose were prepared in the laboratory of Dr. John Haslam using a model F Stokes single punch press with standard concave ¼" punch and dye. Compression forces on the order of 2-3 tons were used to make all tablets, which ranged from 120-150 mg in weight.

4.3 Results and Discussion

4.3.1 Determination of calcium and water content

The calcium content of the sodium alginate samples ranged from 0.08% to 0.74% w/w, corresponding to calcium:alginate molar ratios of 0.004 to 0.04. No calcium could be detected in grade 1. These low amounts of calcium were not expected to impact the viscosity measurements, as it has previously been reported that calcium:alginate molar ratios below 0.05 have little or no effect on the rheological properties of aqueous alginate solutions.[39] The water content of the as received sodium alginate samples varied from approximately 7.5% to 12.5% w/w.

4.3.2 Analysis of SSNMR spectra

Representative ^{13}C CP-MAS NMR spectra of the seven different sodium alginate grades are shown in Figure 4.3. The peak between 170-180 ppm corresponds to the carboxyl carbon atom and occurs at the same chemical shift for all grades. The anomeric carbons give rise to the signals located between 90-110 ppm. Slight differences in this region can be observed between the seven grades. However, the most obvious differences in the spectra are seen in the signals from the pyranose ring carbons, which are located in the region 60-90 ppm and are labeled A-E in Figure 4.3. Grasdalen et al.[19, 21] first reported the ^{13}C NMR chemical shift values for these ring carbons in solution. The authors observed eight distinct signals that could be assigned to a specific ring carbon of either the G or M residue. In the SSNMR spectra (Fig.4.3), only five distinct peaks for these carbons can be observed, due to the broad, overlapping signals typical of amorphous materials. This makes specific peak assignment in the SSNMR spectra very difficult compared to solution-state spectra. However, based on the monomer composition determined using ^{1}H solution-state NMR (provided by the manufacturer), the amount of G residue present in each grade is known to decrease in the following order: 1 > 2 > 3 > 4=5=6 > 7. Therefore, those signals in the SSNMR spectra that decrease in intensity as the G(%) decreases (peaks A, D and E in Fig.4.3) can be related to G residues, while those that increase in intensity (peaks B and C in Fig.4.3) can be related to M residues. Similar variations in these peaks were observed in other SSNMR investigations of sodium alginate.[24,40] The peaks labeled A-E in Figure 4.3 were assigned based on these observations and the ^{13}C solution-state

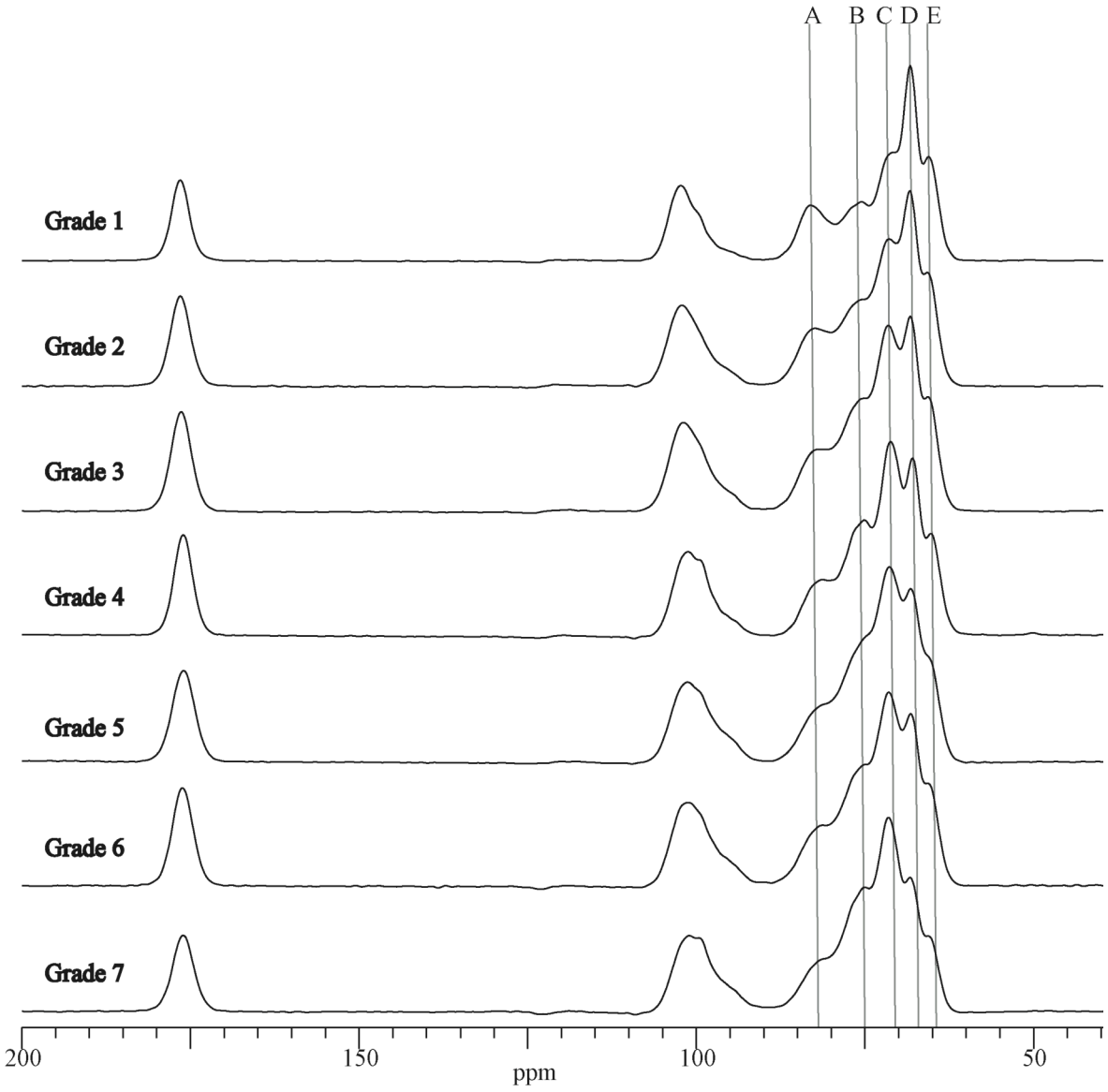

Figure 4.3. Representative ^{13}C SSNMR spectra of the seven different sodium alginate grades examined in this study. Peaks labeled A, D, and E correspond to ring carbons of the G monomer. Peaks labeled B and C correspond to ring carbons of the M monomer.

NMR spectral assignments made by Grasdalen et al.[21] The peak positions and assignments are outlined in Table 4.2.

A comparison of the ^{13}C CP-MAS NMR spectra of the pure G and M residues would help verify these assignments; however, no such comparison has been reported. Salomensen et al.[24] collected the ^{13}C CP-MAS spectrum of a bacterial alginate containing 100% mannuronate and used this to support their peak assignments. However, the authors did not analyze a 100% guluronate sample for comparison. For this reason, we attempted to prepare pure standards of each residue. The G and M acid residues were separated and isolated from the pharmaceutical grade sodium alginates received from FMC Biopolymers. The procedure was repeated twice, once using a high G(%) sodium alginate (grade 1) as the starting material and once using a high M(%) sodium alginate (grade 7) as the starting material, in order to get the highest possible yield of each fraction.

The ^{13}C CP-MAS NMR spectra of the collected fractions and the starting material are shown in Figure 4.4. These spectra allow for several conclusions to be drawn about the relative contributions of the M and G residues to the peaks in the spectra. First, the signals in the spectrum of the M fraction (Fig.4.4b) do not significantly contribute to the peaks designated A, D, and E, which supports the assignment of these three peaks as ring carbons of the G monomer. Due to partial recrystallization of the G fraction (Fig.4.4c) during the isolation process, the signals are sharper and more resolved than in the M fraction. One of the signals in the G fraction actually overlaps with the taller peak of the M fraction (peak C). This overlap could simply be a result of the crystalline nature of the G fraction, which

Table 4.2. Peak assignments of the ^{13}C resonances designated A-E in Figure 4.3.

	Peak Designation in Figure 4.3				
	A	B	C	D	E
Chemical shift (ppm)	82.7	76.1	71.5	68.4	65.7
Residue assignment	G	M	M	G	G
Carbon atom	4	4,5	2,3	3,5	2

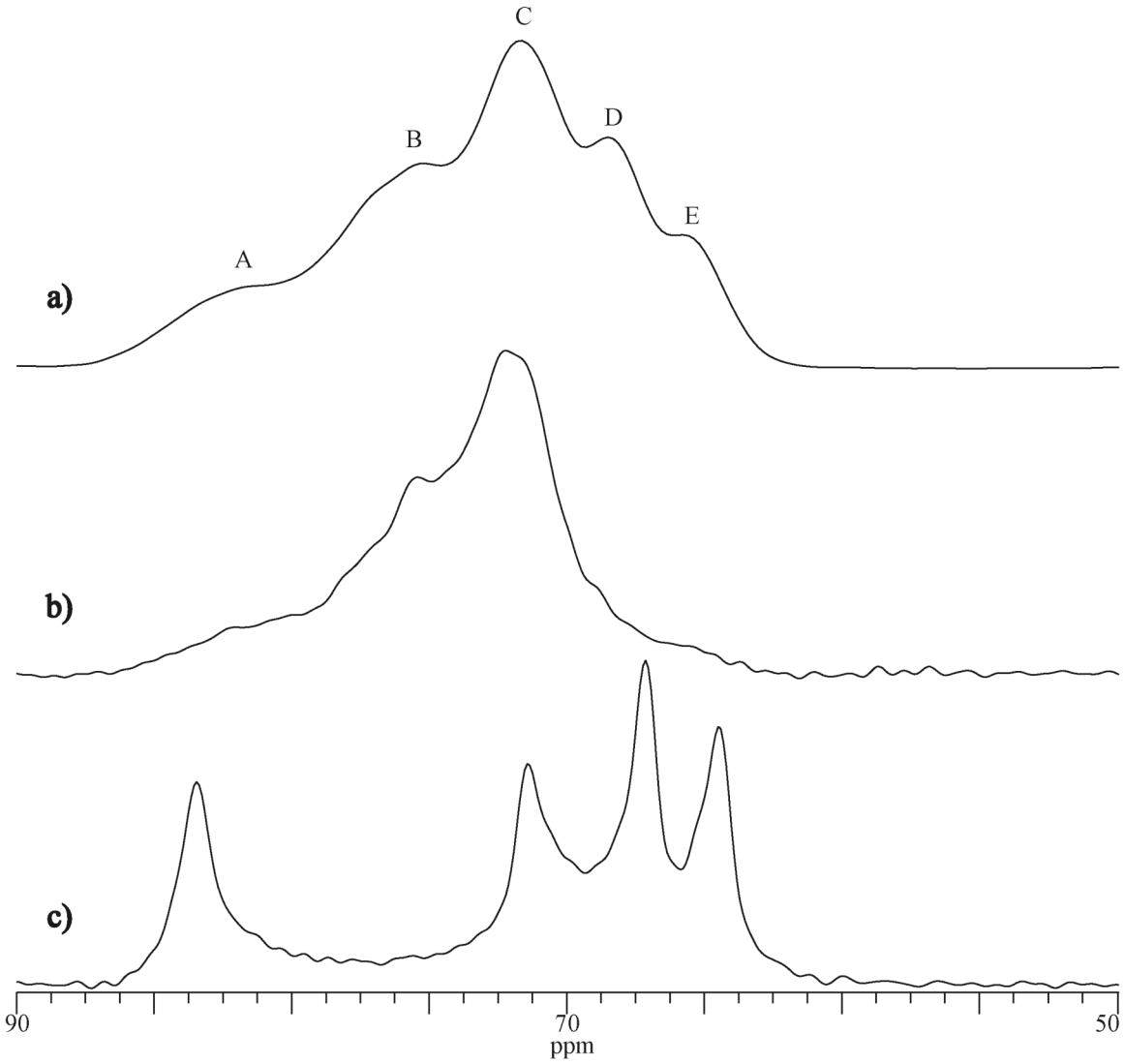

Figure 4.4. ^{13}C SSNMR spectra of the fractions collected using the acid hydrolysis method outline in Figure 2: (a) starting material, (b) mannuronic acid fraction, and (c) guluronic acid fraction.

results in the resolution of peak D into two distinct signals for G ring carbons 3 and 5, with chemical shifts different than the average chemical shift observed in the amorphous material. However, since attempts to make the G fraction amorphous were unsuccessful, this could not be confirmed or denied. Therefore, although the two broad peaks observed in the spectrum of the M fraction (Fig.4.4b) overlap with the peaks designated B and C in the starting material (Fig.4.4a), possible contribution to these signals from the G ring carbons cannot be completely ruled out. This contribution must be considered when using the signals in this region to calculate the relative amounts of each residue present in sodium alginate samples. In addition, these signals correspond to "pure" M and G, and may be different for more random copolymers, where M and G monomers may be adjacent.

4.3.3 Calculation of monomer content via SSNMR

SSNMR is a quantitative technique by nature, as the observed signal directly corresponds to the relative number of like nuclei present in the sample. In order to perform quantitative analysis, the signals must have sufficient resolution either to integrate the peak areas or perform deconvolution to calculate peak areas. In the SSNMR spectrum of sodium alginate (Fig.4.3), the signals labeled A-E are more resolved than peaks in other regions of the spectrum, but enough overlap exists to make accurate integration without deconvolution difficult. An example of spectral deconvolution of the five peaks in the pyranose region (60-90 ppm) is shown in Figure 4.5. Lineshapes that were 90% Gaussian and 10% Lorentzian resulted in the best fits and least amount of residual noise. The

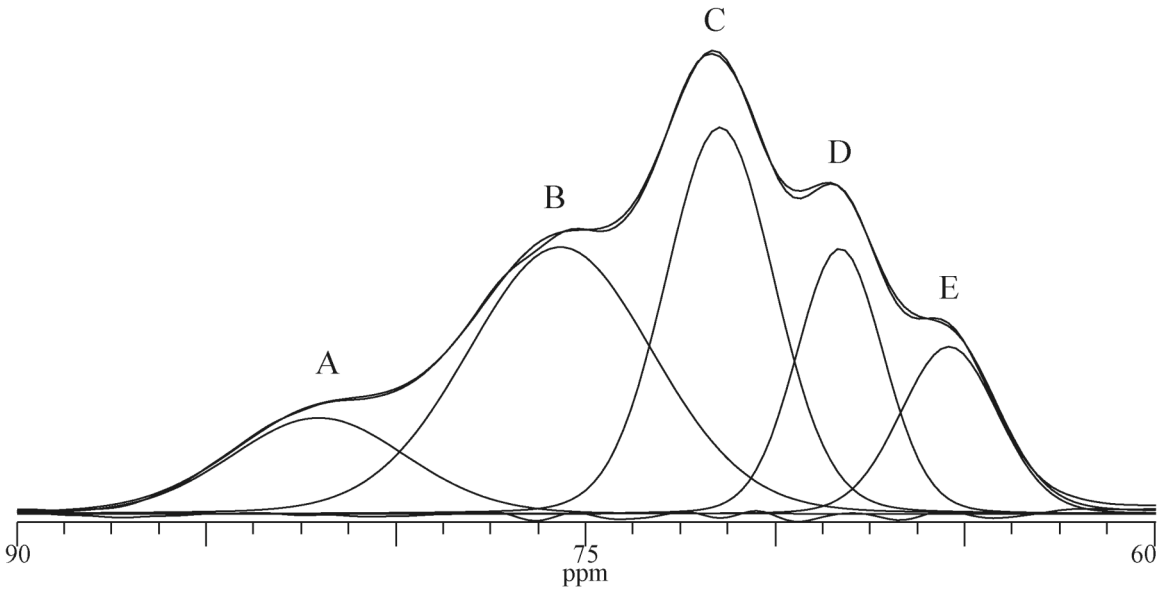

Figure 4.5. An example of spectral deconvolution of the signals corresponding to G and M monomers in sodium alginate. Without spectral deconvolution, accurate integration and quantitation of the relative amounts of G and M monomer present in sodium alginate powders would not be possible.

amounts of each residue were calculated from these deconvoluted signals in various ways, as described below.

In the first method, there were no constraints placed on the widths of the fitted functions. The amount of G(%) was calculated by dividing the peak areas of deconvoluted signals A, D, and E by the total area of all peaks. Each sample was analyzed twice and the range of measured values is reported in Table 4.3. The G(%) range provided by the manufacturer is also reported in Table 4.3. It can be seen that for samples with an average G content below 50% (grades 4-7), this method results in values that fall within the range provided by the manufacturer. However, for samples with higher G contents (grades 1-3), the calculated values fall below the reported range. Salomensen et al.[24] also found that comparing the areas of the deconvoluted signals resulted in poor agreement with solution-state NMR values for grades with higher G contents. These observations and the overlap observed in the spectra of the two isolated residues (Fig.4.4) support the suggestion that the G monomer is contributing to the area of the signals assigned to the M monomer, resulting in an overestimation of M(%) and corresponding underestimation of G(%) by SSNMR.

In the second method, in order to investigate the effects of constraints, the width of M signals was restricted to those of grade 7, as this grade should have the least amount of G contribution to the M signals. The amount of G(%) was again calculated by dividing the peak areas of deconvoluted signals A, D, and E by the total area of all peaks. Each sample was analyzed twice and the range of measured values is also reported in Table 4.3. It can be seen that this second method results in values that are closer to the range obtained with

Table 4.3. Comparison of the G(%) values calculated from the ^{13}C CP-MAS spectra using three different methods. The manufacturer's reported G(%) ranges for each grade are also included.

Grade	**G(%) Determination**			
	Manufacturer	Areas, no constraints $\left[\frac{(A+D+E)}{(A+B+C+D+E)}\right]*100\%$	Areas, with constraints $\left[\frac{(A+D+E)}{(A+B+C+D+E)}\right]*100\%$	Intensities $\left[\frac{(D)}{(C+D)}\right]*100\%$
1	65-75	57	57-59	65
2	55-65	47-48	51-53	57
3	45-55	42-44	45-47	51-52
4	35-45	42	38-40	47-48
5	35-45	38-40	41-42	47
6	35-45	39-41	42-43	47-48
7	30-35	34-36	34-36	42

solution-state NMR, suggesting that there is indeed contribution to the signals assigned as M residues in the SSNMR spectra as the G content increases.

In the third method, the intensities of deconvoluted signals C and D were compared. The amount of G(%) was calculated by dividing the intensity of signal D by the total intensity of signals C and D and can be seen in Table 4.3. Salomensen et al.[24] reported the highest correlation with solution-state NMR values using a similar method. However, as seen in Table 4.3, while this method displayed good agreement with solution-state NMR values for grades 1-3, the calculated values for the amount of G monomer for grades 4-7 were above the reported ranges. This suggests that the use of intensities of deconvoluted signals results in overestimation for grades with less than 50% G content. Therefore, using areas of the deconvoluted signals with some restraints on width appears to be the best way of obtaining accurate G(%) values with SSNMR. The complete range of G(%) values obtained using all three methods is reported in Table 4.4.

4.3.4 SSNMR relaxation times and molecular weight

The intrinsic viscosity values and average molecular weights (MW) were calculated as described above and are reported in Table 4.4. The intrinsic viscosity and MW of the grades increases in the following order: 1 < 4=7 < 5 < 2 < 6 < 3. Table 4.4 also displays ^{1}H T_1 relaxation times for each sample. Relaxation measurements were performed on each of the as received samples at least twice over the course of several weeks. The ^{1}H T_1 value reported in Table 4.4 is the average of these measurements, and the range given is the difference between the longest and shortest time measured. At first glance, there does not

Table 4.4. Summary of G(%), intrinsic viscosity, molecular weight, and ^{1}H T^{1} relaxation measurements for all grades and lots of sodium alginate used in this study.

Grade	G (%) Range by SSNMR	Intrinsic Viscosity (dL/g)	Average MW (kDa)	Average ^{1}H T_1 (range) (s)
1	57-65	1.35	63	0.18 (0.01)
2	47-57	8.54+/-0.12	409	0.49 (0.02)
3	42-52	11.26+/-1.21	541	0.47 (0.06)
4a	38-48	5.53+/-0.15	263	0.35 (0.05)
4b	38-47	6.16+/-0.08	293	0.30 (0.02)
5a	38-47	6.43+/-0.06	306	0.56 (0.06)
5b	35-46	6.53+/-0.39	311	0.64 (0.09)
5c	36-44	6.67+/-0.12	318	0.45 (0.05)
5d	37-47	6.87+/-0.27	328	0.49 (0.09)
5e	34-47	6.91+/-0.29	330	0.56 (0.03)
5f	36-44	7.14+/-0.07	341	0.64 (0)
5g	35-47	7.16+/-0.09	342	0.70 (0.03)
5h	36-46	7.32+/-0.18	350	0.48 (0.05)
5i	33-47	7.33+/-0.19	350	0.72 (0.03)
5j	35-47	7.48+/-0.11	357	0.64 (0.06)
6a	39-48	8.73+/-0.24	418	0.89 (0.06)
6b	40-47	10.24+/-0.65	492	0.72 (0.03)
7	34-42	6.04+/-0.09	287	0.62 (0.05)

seem to be a direct correlation between intrinsic viscosity and ^1H T_1 relaxation time. However, there does appear to be a relationship between intrinsic viscosity and relaxation time for samples with similar chemical content. Grades 4, 5, and 6 have comparable ranges of G(%) by both solution- and solid-state NMR. These three grades can be ranked in terms of intrinsic viscosity and MW as follows: $4 < 5 < 6$. Similarly, their relaxation values seem to follow the same order. Therefore, when chemical composition is the same, it should be feasible to determine intrinsic viscosity and MW differences between samples based on ^1H T_1 relaxation times.

In order to illustrate this relationship, the intrinsic viscosity values for multiple lots of grades 4, 5, and 6 were plotted as a function of each sample's ^1H T_1 relaxation time. This graph can be seen in Figure 4.6a. The blue data points correspond to the two lots of grade 4 that were evaluated, the red data points correspond to the ten lots of grade 5 that were evaluated, and the green data points correspond to the two lots of grade 6 that were evaluated. Grade 4 lots have the lowest MWs and relaxation times. Grade 5 lots have intermediate MWs and relaxation times. One lot of grade 6 (a) has the highest MW and relaxation time, but the other lot (6b) has a lower relaxation time than expected based on its MW. Thus, while there does appear to be a linear relationship between the intrinsic viscosity and relaxation time for most of the samples, grade 6b is an outlier that deviates from this relationship.

Variations in water content were hypothesized as one reason for this observed deviation. As stated earlier, the water content of all of the samples received from FMC Biopolymers ranged from 7.5% to 12.5% w/w. These differences could account for the

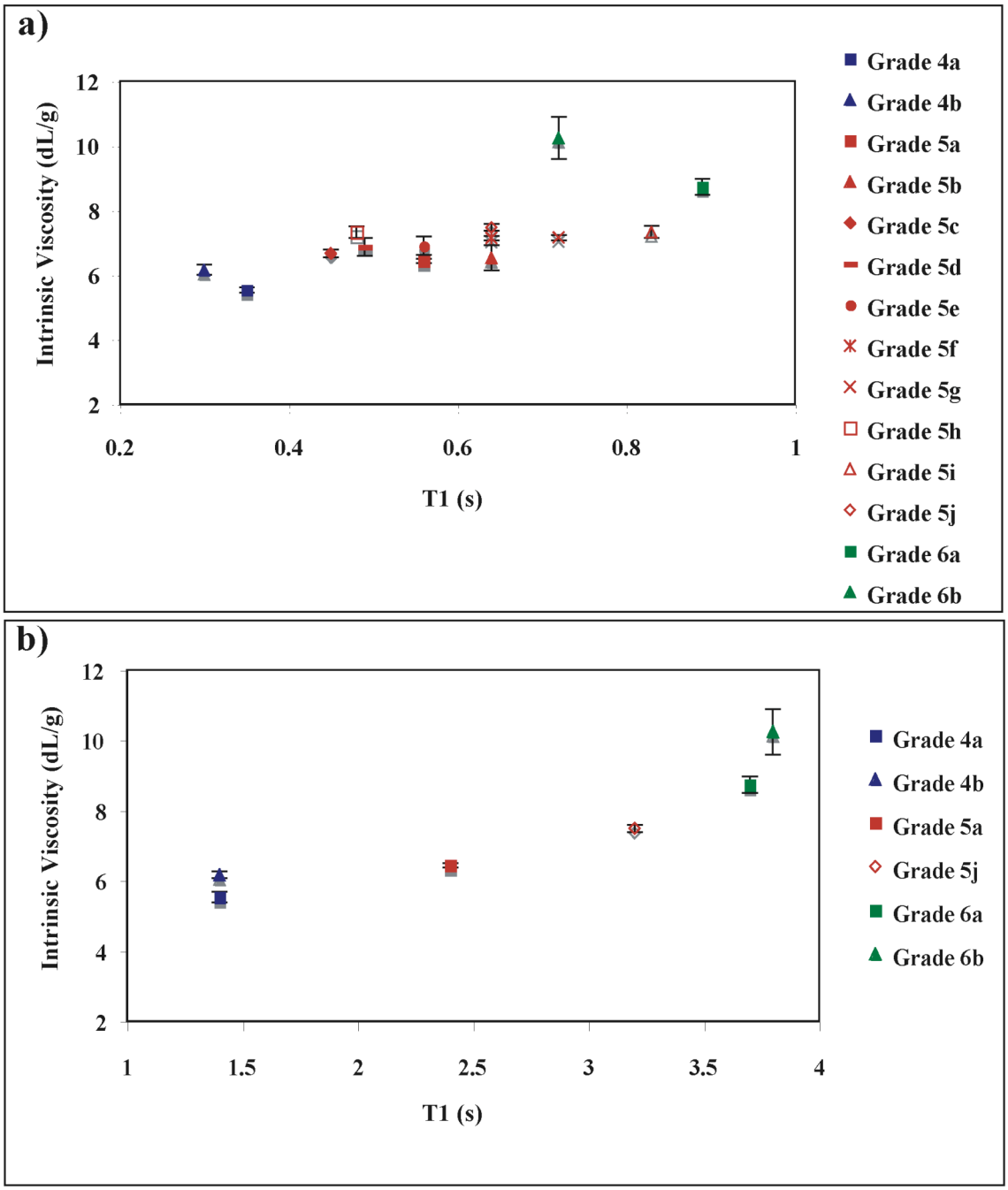

Figure 4.6. Plots of intrinsic viscosity versus relaxation time for (a) as received sodium alginate samples, grades 4-6, and (b) sodium alginate samples, grades 4-6, after drying under vacuum at 105 °C for one hour.

variations in relaxation times for samples with similar chemical content and MW, as the presence of water could potentially increase the mobility of the sample and allow it to relax faster than if it had less water associated with it. To test this hypothesis, both lots of grades 4 and 6, along with two lots of grade 5, were dried at 105 °C under vacuum for one hour. This resulted in water contents between 1.0 and 1.5% w/w for all samples. The ^{1}H T_1 relaxation times of these dried samples were measured and used to create a new plot of intrinsic viscosity versus relaxation time (Fig.4.6b). As can be seen, drying resulted in longer relaxation times due to a decrease in mobility once water was removed. The deviation of grade 6b that was observed for the as received sample (Fig.4.6a) is not seen with the dried sample (Fig.4.6b). Drying the samples to the same water content resulted in much better agreement between intrinsic viscosity and relaxation times, which is not surprising since the intrinsic viscosity measurements were corrected for water content. Thus, it is concluded that SSNMR ^{1}H T_1 relaxation times can be correlated to intrinsic viscosity and hence MW variations for sodium alginate samples of similar chemical composition and water content.

4.3.5 Effects of water content on SSNMR relaxation times

As stated above**,** the alginate's water content had a drastic effect on the ^{1}H T_1 relaxation time. Thus, it was of interest to see if the ^{1}H T_1 values could be used to determine the amount of water present in amorphous polymeric excipients such as sodium alginate, as changes in water content during processing or storage could potentially affect

the stability or performance of a formulation. Four samples of sodium alginate (grades 1, 4b, 5a, and 6b) were analyzed as received, after drying, and after being exposed to high relative humidity. Water content of the samples ranged from <1% to ~20%. The relationship between water content and ^{1}H T_1 relaxation times for all four samples is shown in Figure 4.7a. The largest difference in relaxation times among the four grades is observed at the lowest water content analyzed while the smallest difference in relaxation times is observed at the highest water content analyzed. All four samples show an exponential rather than linear decrease in ^{1}H T_1 relaxation times as water content increases. In order to more easily assess this relationship, the log of each ^{1}H T_1 value was plotted versus water content, as shown in Figure 4.7b. The data was fit to an equation of the form log (y) = -mx + b, where y is the ^{1}H T_1 value, x is the % H_2O, m is the slope, and b is the y-intercept, which is equivalent to the log of the ^{1}H T_1 value when no water is present. The theoretical ^{1}H T_1 values in the absence of water were found to be 3.98, 1.95, 1.03, and 0.90 s for grades 6b, 5a, 4b, and 1, respectively. The slope of the lines fit to the data shown in Figure 4.7b ranged from -0.045 to -0.057 and R^2 values were between 0.93 and 0.98.

While these results show that ^{1}H T_1 values can be used to determine water content in bulk sodium alginate powders, assessing water content changes in actual formulations would be of even greater value. Most formulations typically contain more than one excipient, which can make it difficult to monitor changes in individual components. SSNMR spectroscopy is a selective technique in that there is typically at least one region of the spectrum where no overlap between the peaks of the different components occurs.

a)

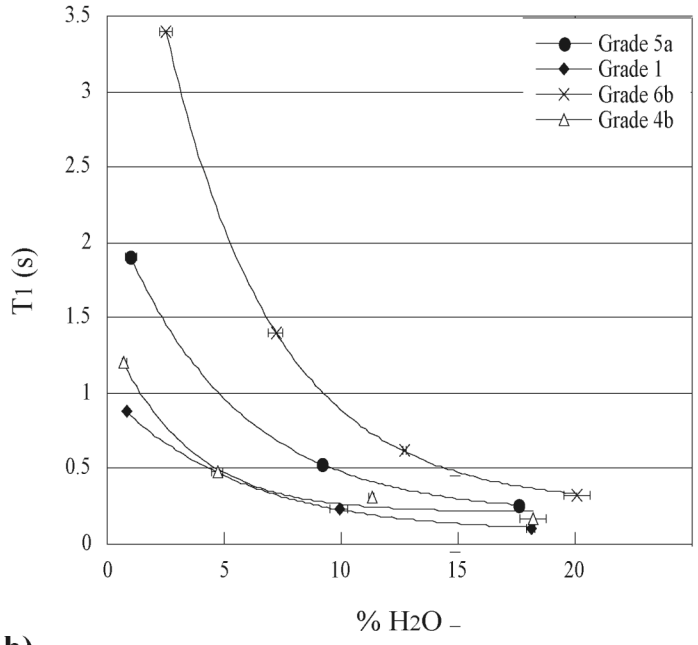

b)

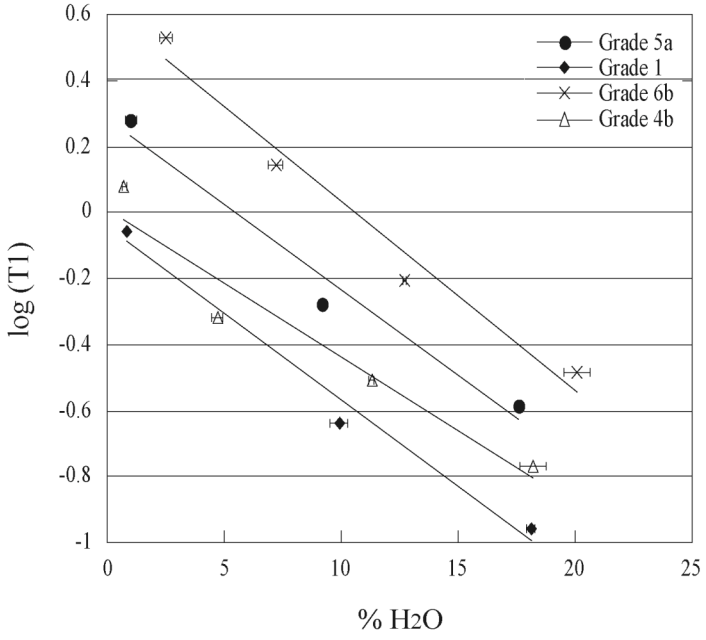

Figure 4.7. The dependence of alginate relaxation time on water content plotted (a) as an exponential relationship and (b) as a linear relationship.

To determine if the relaxation time changes that occur with water uptake and loss could be detected in alginates while in the presence of other excipients, one sample (grade 6b) was mixed with lactose monohydrate and HPMC, common excipients used for making tablets. Physical mixtures and tablets with each of these excipients were prepared using the as received grade 6b material analyzed at ambient conditions, after drying at 105 °C under vacuum for 20 minutes, and after 12 hours stored at 25 °C/75% RH. Results are shown in Table 4.5. The results for grade 6b bulk alginate powder in the absence of other excipients are also included for comparison. The first thing to note in Table 4.5 is that tableting of the alginate powder does not cause a change in the relaxation time, as both the powder and the tablet have a ^{1}H T_1 value of 0.61 s. Therefore, any changes in relaxation times are assumed to be due to changes in water content. The bulk alginate powder and the tablet both show an increase in relaxation time after drying and a decrease in relaxation time after hydration, which agrees with the results shown in Figure 4.7. The changes in relaxation times of the tablet due to water uptake or loss after storage are not as great as in the bulk powder, which is expected due to the smaller surface area of the tablet. When grade 6b is mixed with another excipient in a 1:1 w/w ratio, the ^{1}H T_1 values seem to decrease slightly from the 0.61 s value measured for the bulk powder. This could be due to the water that is present in the lactose monohydrate and the HPMC being adsorbed by the alginate and affecting its mobility. Tableting of the alginate:excipient mixtures does not cause a significant change in the alginate's ^{1}H T_1 value. After drying, all of the alginate relaxation times increase in both the powder mixtures and in the tablets; conversely, the relaxation times all decrease after exposure to 75% RH. These results demonstrate the

Table 4.5. Summary of ^{1}H T_1 relaxation times as a function of storage condition for grade 6b sodium alginate powder and tablets.

^{1}H T_1 (s)	**Storage Condition**		
	105 °C Vacuum	**Ambient**	**25 °C/75% RH**
alginate powder	3.4	0.61	0.33
alginate tablet	3.0	0.61	0.40
alginate/lactose powder	2.5	0.51	0.37
alginate/lactose tablet	2.0	0.52	0.44
alginate/HPMC powder	1.9	0.58	0.35
alginate/HPMC tablet	1.8	0.53	0.31

ability of SSNMR relaxation times to be used for monitoring changes in water content of alginate bulk powder, an alginate tablet, alginate mixed with another excipient, and in alginate that has been tableted with another excipient.

4.3.6 Effects of water content on SSNMR spectra

Variations in water content not only resulted in relaxation time changes, but also drastically affected the resolution of signals in the SSNMR spectra. These changes are highlighted in Figure 4.8, which shows SSNMR spectra of grade 1 as received (Fig.4.8a), after exposure to 75% RH (Fig.4.8b), and after drying at 105 °C under vacuum (Fig.4.8c). The resolution of the signals between 60-90 ppm, which are used for calculating the amounts of each monomer, is greatly enhanced when the alginate takes up water. On the contrary, the resolution between these peaks worsens when the alginate is dried. This suggests that spectral deconvolution and corresponding calculation of peak areas of alginate after exposure to high humidity should result in more accurate values for the amount of G(%), as overlap between signals from each monomer should be diminished with an increase in resolution. For example, the amount of G monomer calculated from the spectra of grade 1 after hydration (Fig.4.8b) is 60%, compared to the value of 57% (Table 4.3) that was obtained from the SSNMR spectrum of the as received material (Fig.4.8a). The value of 60% is closer to the range obtained via solution-state NMR (Table 4.3). Thus, it can be concluded that simply hydrating the alginate can increase resolution of the SSNMR signals and may give values of G(%) that are closer to those obtained via solution-state NMR.

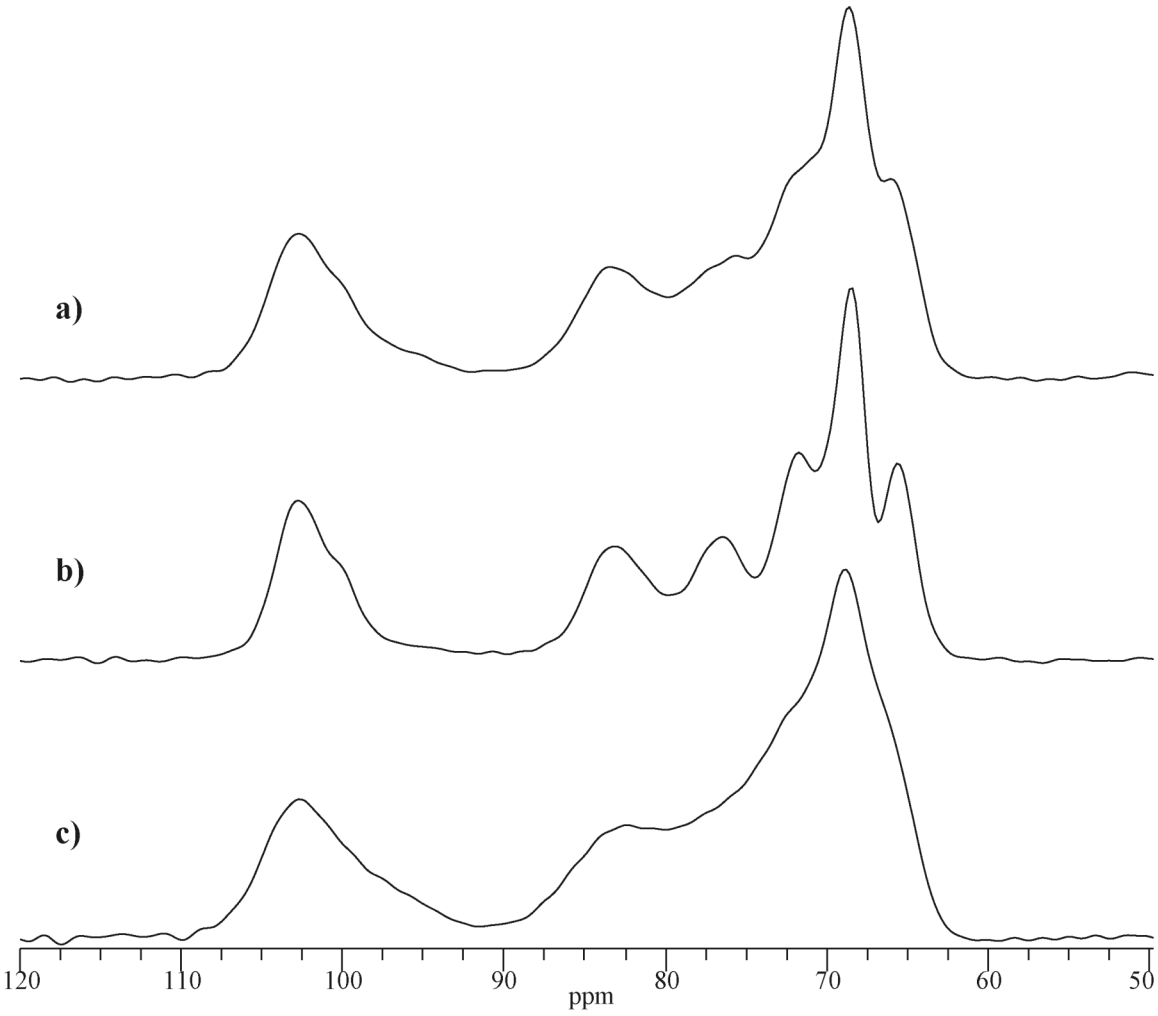

Figure 4.8. ^{13}C SSNMR spectra showing the effect of water content on the resolution of signals: (a) grade 1 as received, (b) grade 1 after exposure to 75% RH, and (c) grade 1 after drying under vacuum at 105 °C for one hour.

4.4 Conclusions

The ability of SSNMR spectroscopy to determine the variations in monomer content among different grades of sodium alginate has been demonstrated. Although signal overlap can make spectral deconvolution difficult, hydration appears to be a fast and simple way to increase the resolution of signals in the SSNMR spectra of sodium alginate. Once the amount of each monomer is determined, differences in intrinsic viscosity and MW of samples with similar monomer content can be correlated to SSNMR relaxation times. Variations in water content of sodium alginate samples can also be detected using SSNMR relaxation times. The technique is sensitive and selective enough to detect changes in the relaxation time of alginate that has been diluted with another excipient and compressed into a tablet.

4.5 References

1. Moreton RC. 2004. Excipient functionality. Pharmaceutical Technology 28:98-99+.

2. Moreton C. 2009. Functionality and performance of excipients in quality-by-design world part 4: obtaining information on excipient variability for formulation design space. American Pharmaceutical Review 12:28-32.

3. Liew CV, Chan LW, Ching AL, Heng PWS. 2006. Evaluation of sodium alginate as drug release modifier in matrix tablets. Int J Pharm 309:25-37.

4. Cable CG. 2006. Sodium alginate. In Rowe RC, Sheskey PJ, Owen SC, editors. Handbook of pharmaceutical excipients 5th ed., Washington DC: American Pharmacists Association. p 656-658.

5. Tonnesen HH, Karlsen J. 2002. Alginate in drug delivery systems. Drug Dev Ind Pharm 28:621-630.

6. Schmid W, Picker-Freyer KM. 2009. Tableting and tablet properties of alginates: characterization and potential for soft tableting. Eur J Pharm Biopharm 72:165-172.

7. Haug A, Larsen B, Smidsrod O. 1966. A study of the constitution of alginic acid by partial acid hydrolysis. Acta Chem Scand 20:183-190.

8. Rioux LE, Turgeon SL, Beaulieu M. 2007. Characterization of polysaccharides extracted from brown seaweeds. Carbohydr Polym 69:530-537.

9. Haug A, Larsen B, Smidsrod O. 1974. Uronic acid sequence in alginate from different sources. Carbohydr Res 32:217-225.

10. Draget KI, Strand B, Hartmann M, Valla S, Smidsrod O, Skjak-Braek G. 2000. Ionic and acid gel formation of epimerised alginates; the effect of AlgE4. Int J Biol Macromol 27:117-122.

11. Sugawara S, IMai T, Otagiri M. 1994. The controlled release of prednisolone using alginate gel. Pharm Res 11:272-277.

12. Sriamornsak P, Thirawong N, Korkerd K. 2007. Swelling, erosion and release behavior of alginate-based matrix tablets. Eur J Pharm Biopharm 66:435-450.

13. Imai T, Kawasaki C, Nishiyama T, Otagiri M. 2000. Comparison of the pharmaceutical properties of sustained-release gel beads prepared by alginate having different molecular size with commercial sustained-release tablet. Pharmazie 55:218-222.

14. Efentakis M, Koutlis A. 2001. Release of furosemide from multiple-unit and single-unit preparations containing different viscosity grades of sodium alginate. Pharm Dev Technol 6:91-98.

15. Efentakis M, Buckton G. 2002. The effect of erosion and swelling on the dissolution of theophylline from low and high viscosity sodium alginate matrices. Pharm Dev Technol 7:69-77.

16. Usov AI. 1999. Alginic acids and alginates: analytical methods used for their estimation and characterisation of composition and primary structure. Russ Chem Rev 68:957-966.

17. Salomonsen T, Jensen HM, Stenbaek D, Engelsen SB. 2008. Chemometric prediction of alginate monomer composition: a comparative spectroscopic study using IR, Raman, NIR and NMR. Carbohydr Polym 72:730-739.

18. Penman A, Sanderson GK. 1972. A method for the determination of uronic acid sequence in alginates. Carbohydr Res 25:273-282.

19. Grasdalen H. 1983. High-field, ^{1}H-n.m.r. spectroscopy of alginate: sequential structure and linkage conformations. Carbohydr Res 118:255-260.

20. Grasdalen H, Larsen B, Smidsrod O. 1977. ^{13}C-N.m.r. studies of alginate. Carbohydr Res 56:C11-C15.

21. Grasdalen H, Larsen B, Smidsrod O. 1979. A P.M.R. study of the composition and sequence of uronate residues in alginates. Carbohydr Res 68:23-31.

22. Grasdalen H, Larsen B, Smidsrod O. 1981. ^{13}C-N.M.R studies of monomeric composition and sequence in alginate. Carbohydr Res 89:179-191.

23. Salomonsen T, Jensen HM, Larsen FH, Steuernagel S, Engelsen SB. 2009. Alginate monomer composition studied by solution- and solid-state NMR- a comparative chemometric study. Food Hydrocolloids 23:1579-1586.

24. Salomonsen T, Jensen HM, Larsen FH, Steuernagel S, Engelsen SB. 2009. Direct quantification of M/G ratio from ^{13}C CP-MAS NMR spectra of alginate powders by multivariate curve resolution. Carbohydr Res 344:2014-2022.

25. Tishmack PA, Bugay DE, Byrn SR. 2003. Solid-state nuclear magnetic resonance spectroscopy-pharmaceutical applications. J Pharm Sci 92:441-474.

26. Berendt RT, Sperger DM, Isbester PK, Munson EJ. 2006. Solid-state NMR spectroscopy in pharmaceutical research and analysis. Trends Anal Chem 25:977-984.

27. Vogt FG. 2008. A multi-disciplinary approach to the solid-state analysis of pharmaceuticals. American Pharmaceutical Review 11:50-57.

28. Schaefer J, Stejskal EO, Buchdahl R. 1977. Magic-angle ^{13}C NMR analysis of motion in solid glassy polymers. Macromolecules 10:384-405.

29. Lubach JW, Dawie X, Segmuller BE, Munson EJ. 2007. Investigation of the effects of pharmaceutical processing upon solid-state NMR relaxation times and implications to solid-state formulation stability. J Pharm Sci 96:777-787.

30. Sakugawa K, Ikeda A, Takemura A, Ono H. 2004. Simplified method for estimation of composition of alginates by FTIR. J Appl Polym Sci 93:1372-1377.

31. Clementi F, Mancini M, Moresi M. 1998. Rheology of alginate from Azotobacter vinelandii in aqueous dispersions. J Food Eng 36:51-62.

32. Pines A, Gibby MG, Waugh JS. 1972. Proton-enhanced nuclear induction spectroscopy: method for high-resolution NMR of dilute spins in solids. J Chem Phys 56:1776-1777.

33. Pines A, Gibby MG, Waugh JS. 1973. Proton-enhanced NMR of dilute spins in solids. J Chem Phys 59:569-590.

34. Andrew ER. 1971. Narrowing of NMR spectra of solids by high-speed specimen rotation and the resolution of chemical shift and spin multiplet structures for solids. Prog Nucl Mag Res 8:1-39.

35. Andrew ER, Bradbury A, Eades RG. 1959. Removal of dipolar broadening of nuclear magnetic resonance spectra of solids by specimen rotation. Nature 183:1802-1803.

36. Dixon WT, Schaefer J, Sefcik MD, Stejskal EO, McKay RA. 1982. Total suppression of sidebands in CPMAS carbon-13 NMR. J Magn Reson 49:341-345.

37. Fung BM, Khitrin AK, Ermolaev K. 2000. An improved broadband decoupling sequence for liquid crystals and solids. J Magn Reson 142:97-101.

38. Barich DH, Gorman EM, Zell MT, Munson EJ. 2006. 3-methylglutaric acid as a ^{13}C solid-state NMR standard. Solid State Nucl Magn Reson 30:125-129.

39. Smidsroed O, Haug A. 1965. Effect of the properties of divalent metals on the properties of alginate solutions. I. Calcium ions. Acta Chem Scand 19:329-340.

40. Llanes F, Sauriol F, Morin FG, Perlin AS. 1997. An examination of sodium alginate from Sargassum by NMR spectroscopy. Can J Chem 75:585-590.

Chapter 5

Analysis of Amorphous Structure and Drug-Excipient Interactions in Indomethacin Solid Dispersions using SSNMR Spectroscopy

5.1 Introduction

While Chapters 3 and 4 focused on the structural analysis of amorphous excipients using ^{13}C SSNMR spectroscopy, Chapters 5 and 6 will examine the application of ^{13}C SSNMR spectroscopy to the analysis of the structure and mobility of amorphous API and amorphous solid dispersions. Specifically, the poorly water-soluble drug indomethacin in the amorphous state and in amorphous solid dispersions will be examined. The major objective of this chapter is to determine the structure of indomethacin in the amorphous state and to identify any structural changes that occur upon formulation in amorphous solid dispersions with polyvinylpyrollidone (PVP) and hydroxypropylmethylcellulose (HPMC).

As described in Chapter 1, the solubility of a compound in the amorphous form is higher than the more stable crystalline form.[1] However, because the crystalline state is thermodynamically more stable, crystallization of the higher energy amorphous form will occur over time, and all benefits of increased dissolution rate and solubility will be lost. One strategy for stabilizing the amorphous form is through the creation of an amorphous solid dispersion, which involves dispersion of the API in an amorphous hydrophilic polymer. The polymer can stabilize the amorphous API through hydrogen-bonding interactions, increasing the glass transition temperature (T_g) of the material through reduction of molecular mobility, or by a combination of these factors.[2] Because of their potential to increase the oral bioavailability of poorly soluble drugs, amorphous solid dispersions have been intensely studied over the past two decades. The limited number of

amorphous solid dispersions on the market indicates that despite this large amount of research, significant gaps in the understanding of the properties of these systems exist.

The non-steroidal, anti-inflammatory drug indomethacin was one of the first small molecule pharmaceuticals shown to exhibit crystallization even when stored at temperatures below its T_g and has, therefore, proven to be a useful model compound for studying various properties influenced by amorphous structure. As shown in Figure 5.1, its structure includes both hydrogen bond acceptors and donors, allowing it to form stabilizing interactions with polymers that also have hydrogen-bonding capabilities, such as PVP and HPMC (Figure 5.1). The properties of indomethacin:PVP amorphous solid dispersions have been extensively examined.[3-6] However, there are only a limited number of reports on the study of indomethacin:HPMC amorphous solid dispersions. Additionally, very few studies have examined the effect of preparation method on these amorphous mixtures. While FT-IR and Raman spectroscopy are commonly used to detect drug-excipient interactions such as hydrogen bonding, reports on the use of ^{13}C SSNMR spectroscopy for the detection of these structural features of amorphous solid dispersions are limited. Thus, the overall purpose of the work presented in this chapter is to detect any changes in hydrogen-bonding interactions that occur between amorphous indomethacin and amorphous solid dispersions of indomethacin:PVP and indomethacin:HPMC as a function of preparation method and API:polymer weight ratio using ^{13}C SSNMR spectroscopy.

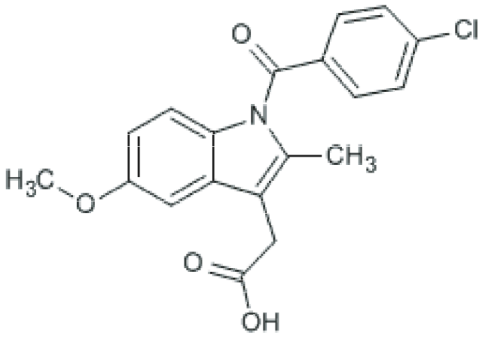

Indomethacin
H-bond donors and acceptors

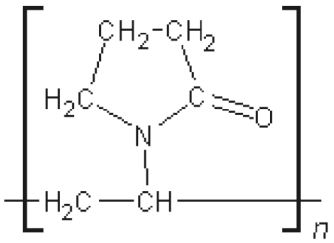

PVP
H-bond acceptors

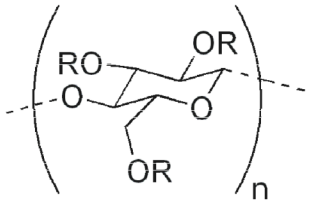

R = H or CH_3 or $CH_2CH(OH)CH_3$

HPMC
H-bond donors

Figure 5.1. Structures of indomethacin, PVP, and HPMC.

5.2 Experimental

5.2.1 Materials

Crystalline indomethacin (γ form) was purchased from Sigma (St. Louis, Missouri) and used as received. PVP (Kollidon 25, MW 28,000-34,000) was obtained from the BASF Corporation and HPMC was purchased from Sigma. PVP and HPMC were dried for 12 hours at 105 °C before use. The crystalline α form of indomethacin was prepared from the γ form as previously described.[7] Approximately 6 g of the γ form was dissolved in 6 mL of ethanol heated to 80 °C. Once the indomethacin dissolved, 10 mL of deionized water at room temperature was added. The precipitate was collected and dried at 30 °C under vacuum for 12 hours. The resulting crystalline material was then analyzed by differential scanning calorimetry (DSC), powder X-Ray diffraction (PXRD), and ^{13}C SSNMR spectroscopy to ensure the α form had been obtained. Amorphous indomethacin was prepared using the melt-quench method. Crystalline indomethacin (γ form) was held above its melting point at 170 °C for 10 minutes, and then liquid N_2 was poured directly onto the melt to form the amorphous material. Formation of amorphous material was confirmed using DSC, PXRD, and SSNMR spectroscopy. The density of each amorphous material was measured using a Micromeritics AccuPyc 1330 helium pycnometer (Micromeritics Instrument Corporation, Norcross, GA) and was found to be 1.34, 1.21, and 1.28 g/cm^3 for melt-quenched indomethacin, PVP, and HPMC, respectively.

5.2.2 Cryogrinding

Cryogrinding was performed using a SPEX CertiPrep 6750 Freezer/Mill (SPEX CertiPrep, Inc., Metuchen, NJ). Approximately 1-2 g of crystalline γ form indomethacin was loaded into the cryogrinding vial. The mill was first filled with liquid nitrogen and allowed to cool before the sample was introduced. Once the sample was inserted, it was allowed to pre-cool for 10 minutes. Each grinding cycle thereafter consisted of a 2-minute grinding period followed by a 2-minute cooling period, with a grinding rate of 10 impacts per second. The number of cycles was modified in order to obtain samples that were ground for different lengths of time. For instance, a 15-cycle experiment had a total of 30 minutes of grinding time. Samples were ground for either 15, 30, or 60 cycles in order to achieve grinding times of 30, 60, and 120 minutes, respectively.

5.2.3 Preparation of physical mixtures

Physical mixtures of melt-quenched amorphous indomethacin and each excipient were prepared. For indomethacin:PVP mixtures, ratios of 4:1, 1:1, and 1:3 w/w were prepared. For indomethacin:HPMC mixtures, ratios of 1:1 and 1:3 w/w were prepared. In all cases, the two materials were lightly ground together in a mortar and pestle to ensure thorough mixing. These mixtures were analyzed using DSC and ^{13}C SSNMR spectroscopy.

5.2.4 Preparation of amorphous solid dispersions

Amorphous solid dispersions of indomethacin:PVP and indomethacin:HPMC were prepared using the melt-quench method. Physical mixtures of indomethacin and each polymer were heated to 170 °C and held for 10 minutes before being quenched with liquid N_2, as described in section 5.3.1. Indomethacin:PVP amorphous dispersions were also prepared using the solvent evaporation method. Physical mixtures were dissolved in anhydrous methanol heated to 65 °C. The solvent was removed under vacuum at 50 °C using a Buchi Rotovapor R-215 (Buchi Laboratory Equipment, Switzerland). The recovered products were then dried at 30 °C and under vacuum for 12 hours to ensure complete solvent removal. All of the amorphous solid dispersions were analyzed using DSC and ^{13}C SSNMR spectroscopy.

5.2.5 Thermal analysis

DSC analysis using a TA Q1000 (TA Instruments, New Castle, DE) was performed on all samples in order to detect T_g, crystallization, and melting events. To overcome the complication caused by the overlapping of thermal events, modulated DSC (MDSC) was used. MDSC separates the total heat flow into its reversible and nonreversible components. The reversible component contains information on thermodynamic events such as the T_g, while the nonreversible component detects kinetic events such as crystallization. Melting events are observed in both components. Samples of approximately 5-10 mg were weighed into aluminum DSC pans and hermetically sealed.

Three pinholes were put in the lid to allow water to escape. Samples were equilibrated at 20 °C and then heated to 200 °C at a rate of 2 °C/min while using a temperature modulation of ±0.5 °C every 60 seconds.

5.2.6 Powder X-ray diffraction

The crystalline and amorphous indomethacin samples were analyzed using a Scintag X2 Powder X-ray Diffractometer (Scintag Inc., Cupertino, CA). Samples were packed into stainless steel sample holders that were spun during data collection. Analysis was performed from 2.0 to 42.0 deg 2-theta using a scan rate of 0.02 deg 2-theta per minute and a dwell time of 2 sec.

5.2.7 Solid-state NMR spectroscopy

Solid-state ^{13}C NMR spectra were acquired using a Chemagnetics CMX-300 spectrometer (Varian, Inc., Palo Alto, CA) operating at approximately 75 MHz for ^{13}C. Chemagnetics double-resonance probes equipped with either a Chemagnetics 7.5 mm PENCIL spinning module or a Revolution NMR 7-mm spinning modules (Revolution NMR, LLC, Fort Collins, CO) were used to acquire all spectra. Samples were packed into zirconia rotors and sealed with either Teflon or Kel-F end caps. Spectra were acquired using ramped-amplitude cross polarization (CP)[8], magic-angle spinning (MAS)[9] with total sideband suppression (TOSS)[10], and SPINAL64[11] decoupling. 3-methylglutaric acid (MGA) was used to optimize the spectrometer settings and set the reference frequency.[12] A contact time of 2 ms, MAS frequency of 3.0-4.0 kHz, and a ^{1}H-decoupling field of

approximately 60-70 kHz was used to acquire all spectra. The recycle delay was based upon the ^{1}H T_1 values for crystalline indomethacin, which were measured using saturation recovery experiments. Using Chemagnetics Spinsight software, plots of integrated signal intensity versus saturation recovery times were fit to the equation $y = amp(1 - e^{-\tau/T_1})$ where y is the integrated signal intensity, amp is the amplitude constant, τ is the saturation recovery time, and T_1 is the spin-lattice relaxation time. Monoexponential curve fitting resulted in a ^{1}H T_1 value of ~ 5 s for both indomethacin polymorphs. A recycle delay equal to 1.5 times this value (~8 s) was used to acquire each spectrum so that any crystalline component could be detected.

5.2 Results

5.3.1 Characterization of indomethacin forms

Crystallization of amorphous indomethacin to either the γ or α forms is known to occur.[13] Thus, it is important to characterize all of the indomethacin forms that may be present in the samples. The DSC thermograms of the as-received γ form and the prepared α form are shown in Figure 5.2. The γ form is thermodynamically most stable, and it melts at ~159 °C. The melting point of the prepared α form was ~154 °C, which agrees with the reported literature value.[14] The results of MDSC analysis of amorphous indomethacin are shown in Figure 5.3. The top trace shows the total heat flow while the

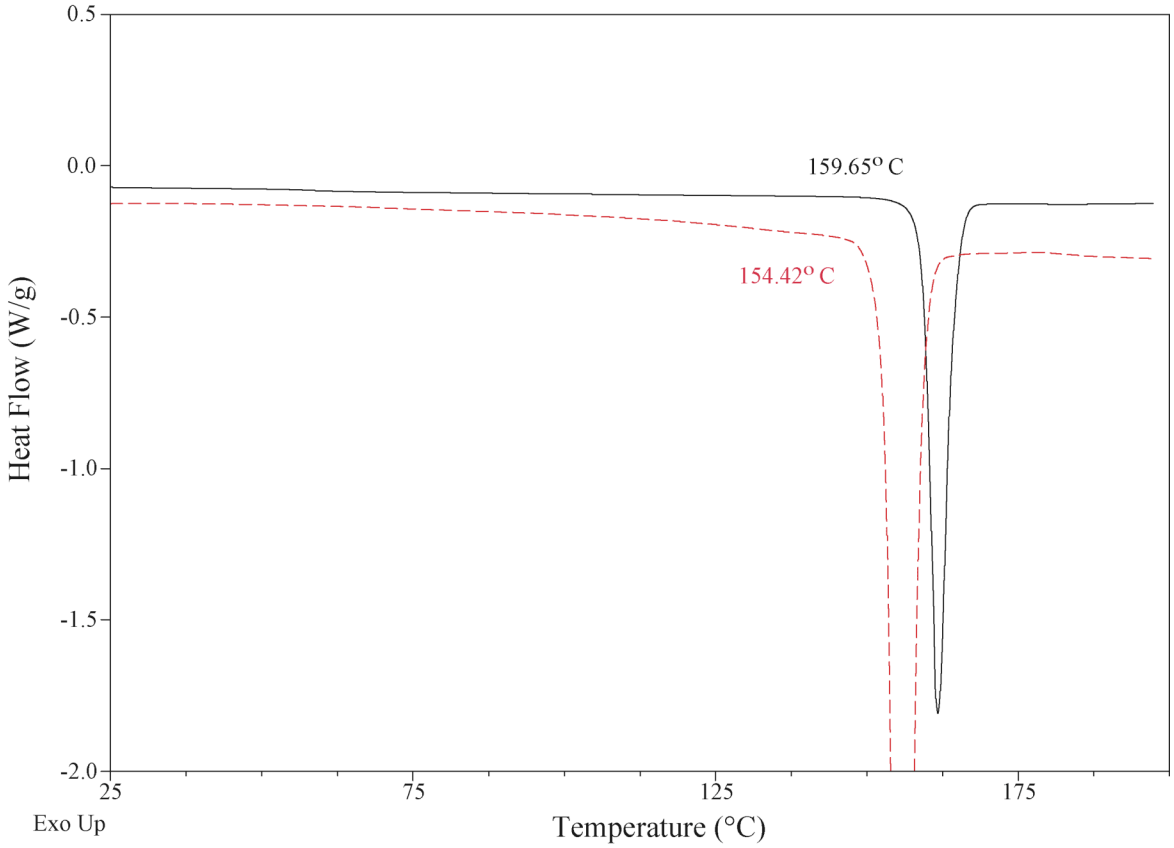

Figure 5.2. DSC analysis showing melting of indomethacin polymorphs. Solid black line corresponds to the γ form and dashed red line corresponds to the α form.

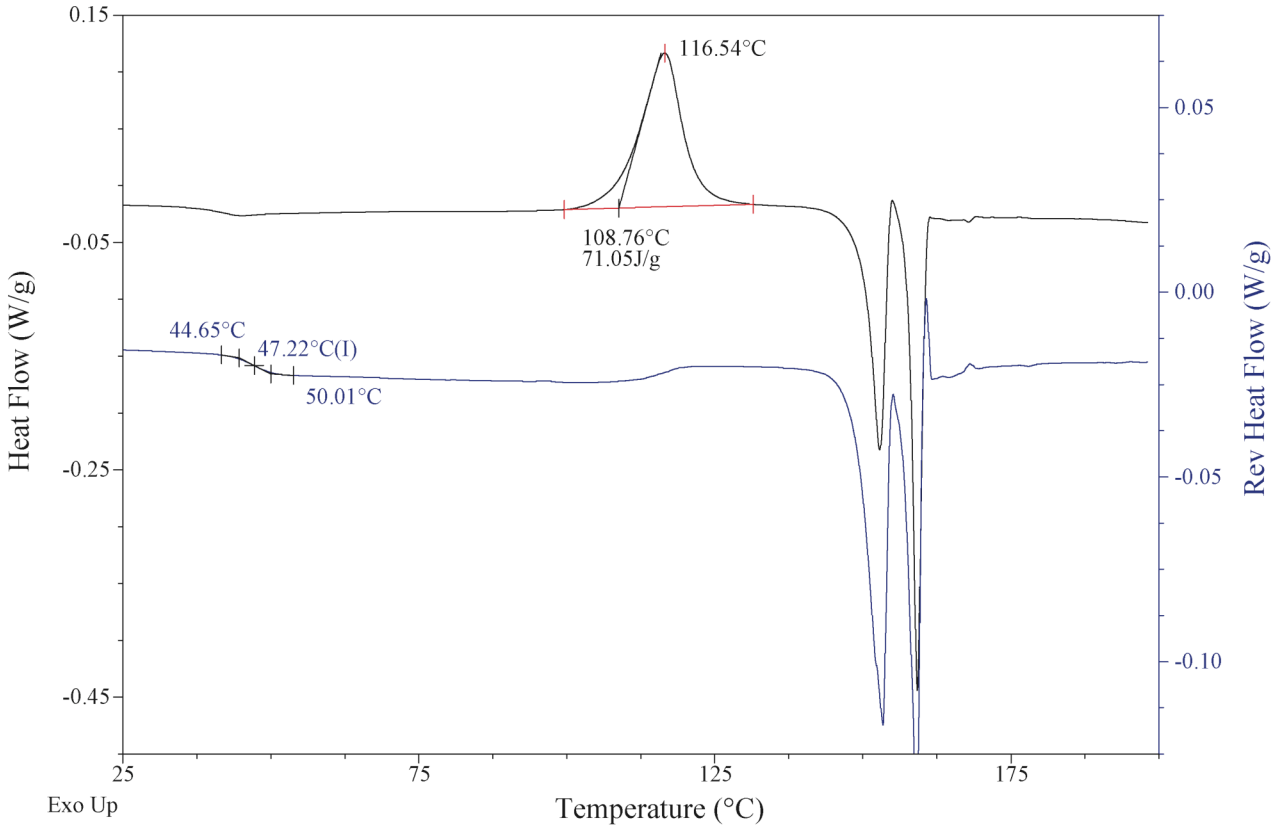

Figure 5.3. MDSC analysis of melt-quenched amorphous indomethacin. The black line represents the total heat flow and the blue line corresponds to the reversible component of the total heat flow.

bottom trace shows the reversible heat flow. The T_g can be clearly seen as a change in the baseline of the reversible component and occurs at ~47 °C. The exothermic crystallization event is not detected in the reversible heat flow, but it is observed in the total heat flow and has an onset temperature of ~108 °C. Finally, the melting events are observed in both components. The two endothermic peaks correspond to melting of the α and γ forms. The melt-quenched amorphous indomethacin first crystallizes to the α form, which melts and recrystallizes to the more stable γ form, which then melts. PXRD and ^{13}C SSNMR spectroscopic analyses were also performed in order to further confirm the formation of pure α form and amorphous material. The PXRD results are shown in Figure 5.4. The diffraction pattern shown in green is that of the γ form. The differences observed between this pattern and that of the α form (black diffraction pattern) support the conclusion that the α polymorph was formed. Both of these diffraction patterns show sharp peaks typical of crystalline materials, while that of the amorphous material (red) only shows a broad halo. The presence of this halo and lack of diffraction supports the formation of amorphous indomethacin. The ^{13}C SSNMR spectra of the γ, α, and melt-quenched amorphous forms are shown in Figures 5.5a, 5.5b, and 5.5c, respectively. As explained in Chapter 2, SSNMR spectroscopy is an excellent tool for distinguishing between polymorphs. The differences observed between the SSNMR spectra of the γ and α forms are due to different packing arrangements and differences in the number of crystallographically inequivalent molecules per unit cell for each form. The SSNMR

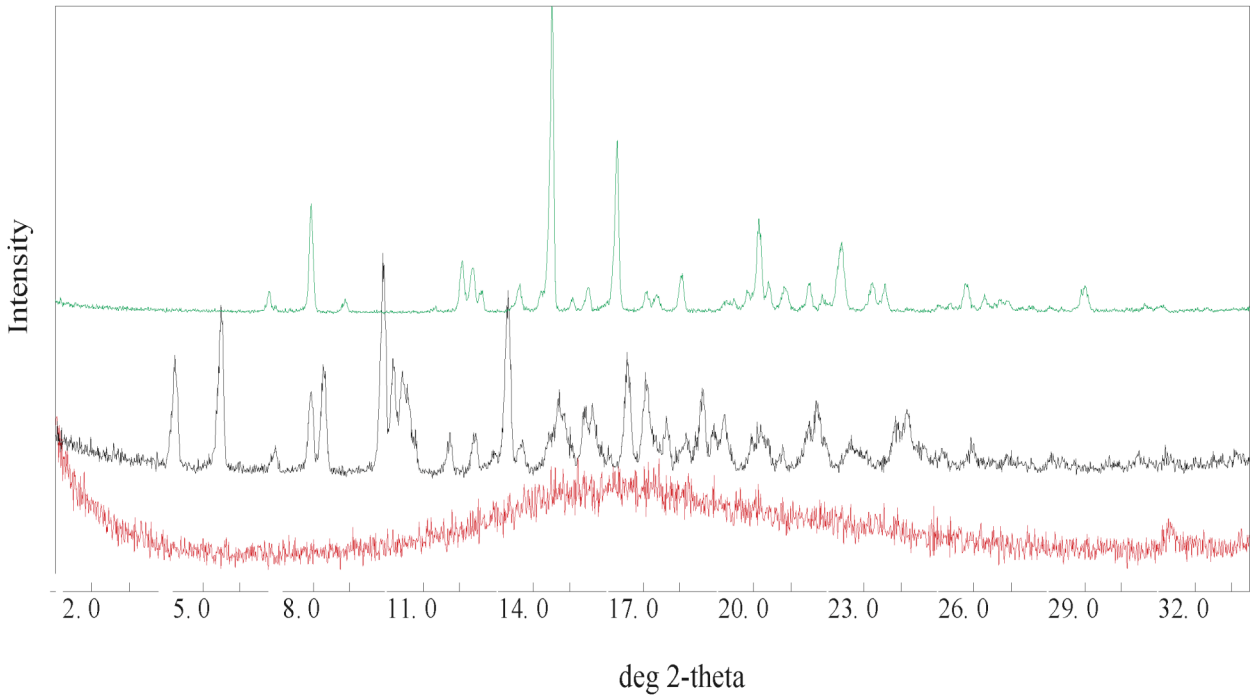

Figure 5.4. PXRD analysis of indomethacin forms. (Green = γ form, black = α form, and red = melt-quenched amorphous).

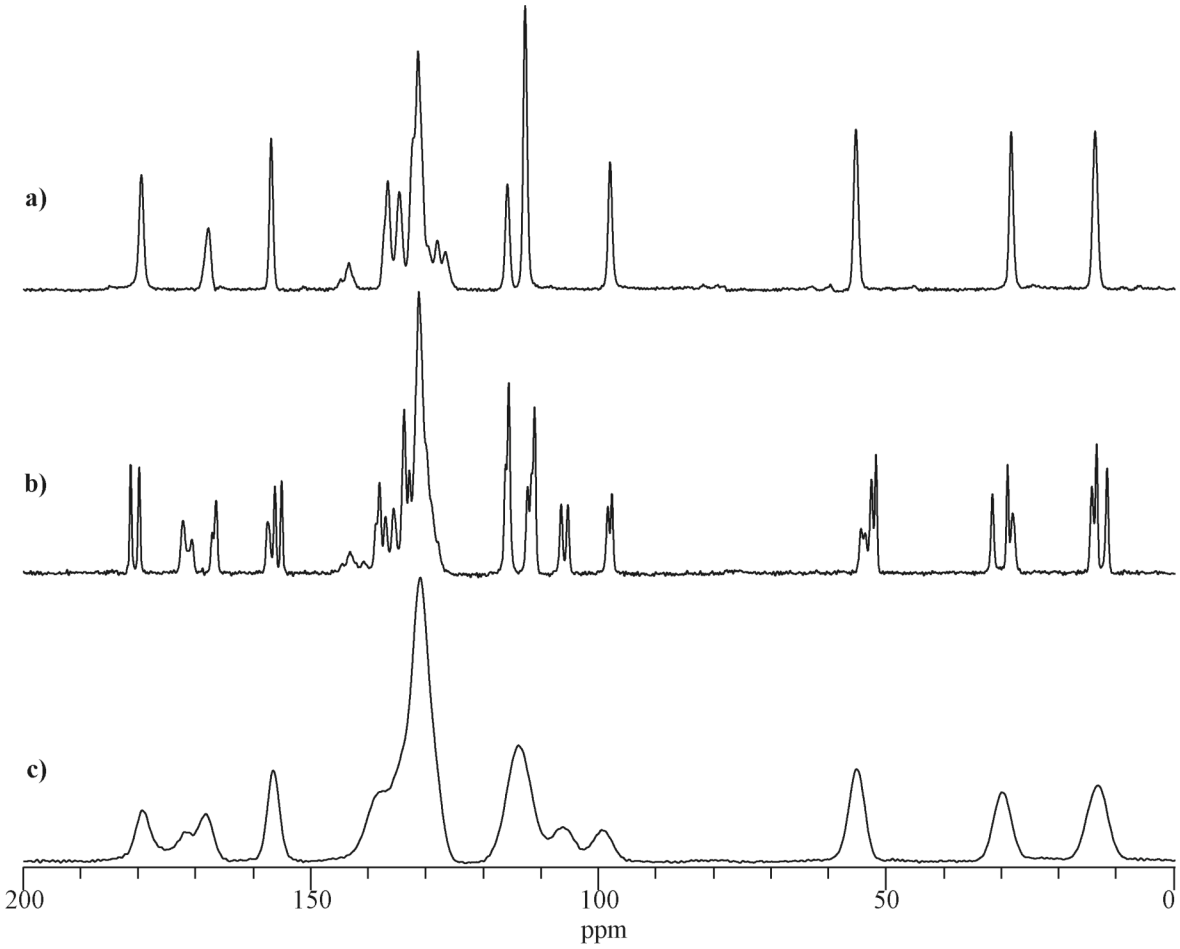

Figure 5.5. ^{13}C SSNMR spectra of indomethacin forms: (a) γ form, (b) α form, and (c) melt-quenched amorphous form.

spectrum of the melt-quenched sample consists of broad peaks and lacks the sharp narrow signals seen in either crystalline material, which is typical of amorphous materials.

5.3.2 Hydrogen bonding in indomethacin forms

In order to examine the hydrogen-bonding interactions occurring in amorphous solid dispersions of indomethacin with PVP and HPMC, it is necessary to start with an understanding of the hydrogen bonding that occurs in each indomethacin solid form and how this is reflected in the ^{13}C SSNMR spectra. Figures 5.6a and 5.6b show the known crystal structures of the γ and α form, respectively. As shown in Figure 5.6a, the γ form is known to consist of cyclic dimers stabilized by hydrogen bonds between the carboxylic acid groups, with one crystallographically inequivalent molecule per unit cell.[15] The amide group of the γ form is not involved in any hydrogen bonding. The crystal structure of the α form, shown in Figure 5.6b, has three crystallographically inequivalent molecules per unit cell, labeled A, B, and C.[16] Hydrogen bonding between the carboxylic acid groups of molecules A and B, forming a dimer similar to that observed in the γ form, occurs. However, the amide group of molecule B also acts as a proton acceptor and forms a hydrogen bond with the -OH group of the carboxylic acid of molecule C, which acts as a proton donor. These differences in hydrogen-bonding interactions between the two crystal forms are reflected in the 165-185 ppm region of the ^{13}C SSNMR spectrum, which is shown in Figure 5.7. In Figure 5.7a, two peaks are observed for the γ form. The peak at higher ppm is assigned to the carbon of the hydrogen-bonded carboxylic acid group, while

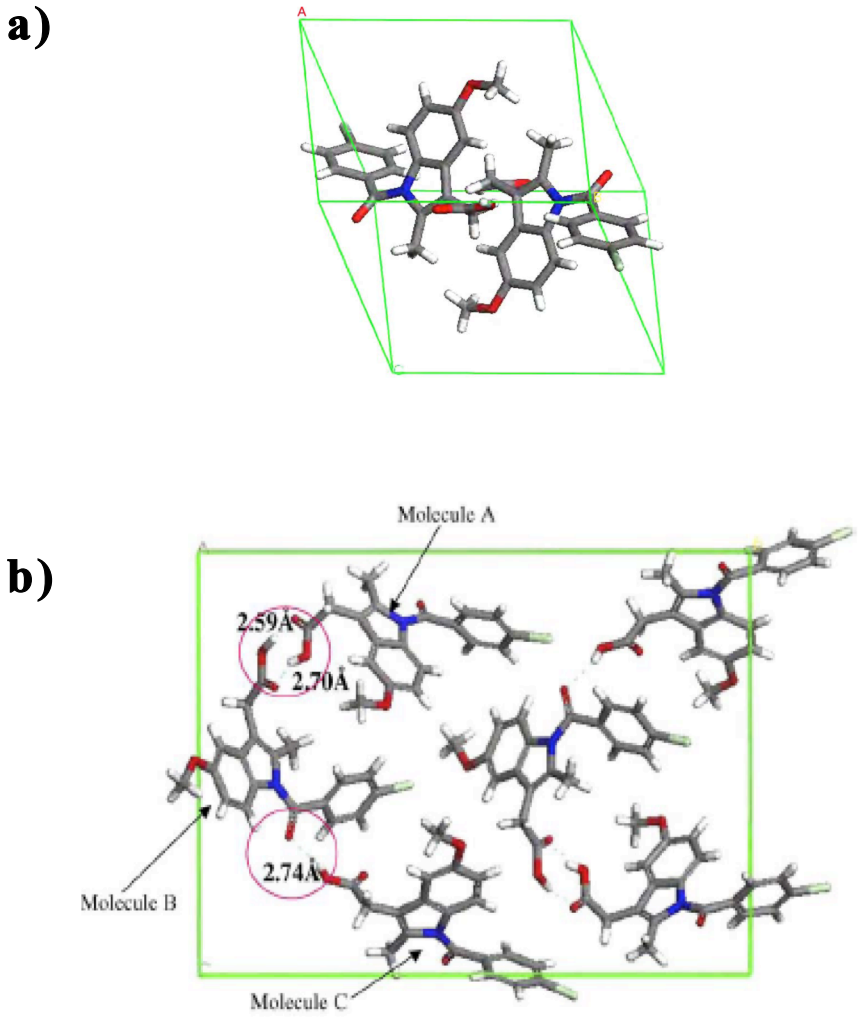

Figure 5.6. Crystal structures of indomethacin: (a) γ form and (b) α form.

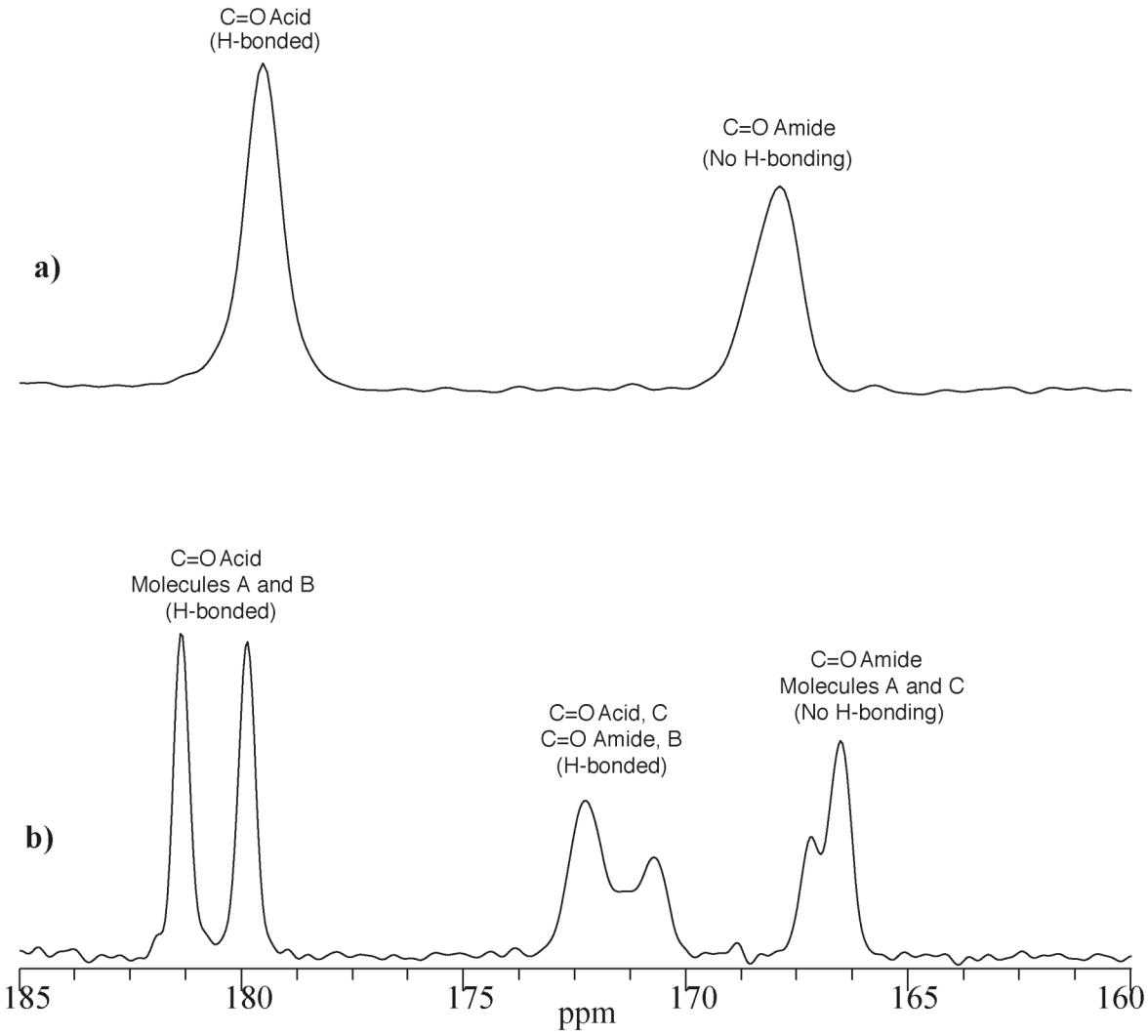

Figure 5.7. ^{13}C SSNMR spectra of the (a) γ form and (b) α form of indomethacin. Differences in hydrogen bonding interactions are highlighted.

the other peak corresponds to the carbon of the amide group, which is not involved in hydrogen bonding. The spectrum of the α form, shown in Figure 5.7b, shows six peaks in this region. This is expected because the three crystallographically inequivalent molecules should differ, resulting in three peaks for the carboxylic acid carbon and three peaks for the amide carbon, for a total of six peaks. The peaks between 179 and 183 ppm correspond to the carbons of the hydrogen-bonded carboxylic acid groups in molecules A and B. The two peaks between 166 and 168 ppm are due to the carbons of the amide groups in molecules A and C. The peaks between 170 and 175 ppm correspond to the carbon of the amide group of molecule B and the carbon of the carboxylic acid group of molecule C, which interact through non-cyclic dimer hydrogen bonds, as shown in Figure 5.6b. This amide-acid hydrogen bonding does not occur in the γ form, which is why no peaks between 170 and 175 ppm are observed in the SSNMR spectrum of this form. The hydrogen bonding that occurs in the amorphous form can be investigated by comparing the SSNMR spectrum of the melt-quenched amorphous indomethacin to that of the crystalline γ and α forms. This comparison is shown in Figure 5.8. Three peaks are observed in this region for the amorphous form (Figure 5.8b). The peak furthest upfield (high ppm) overlaps with that of the hydrogen-bonded cyclic dimer of the γ form (Figure 5.8c). Similar overlap occurs with the peak furthest downfield, which overlaps with the peak for the non-hydrogen-bonded amide carbon of the γ form. There is an additional peak at ~172 ppm in the amorphous form that is not present in the γ form but is present in the α form

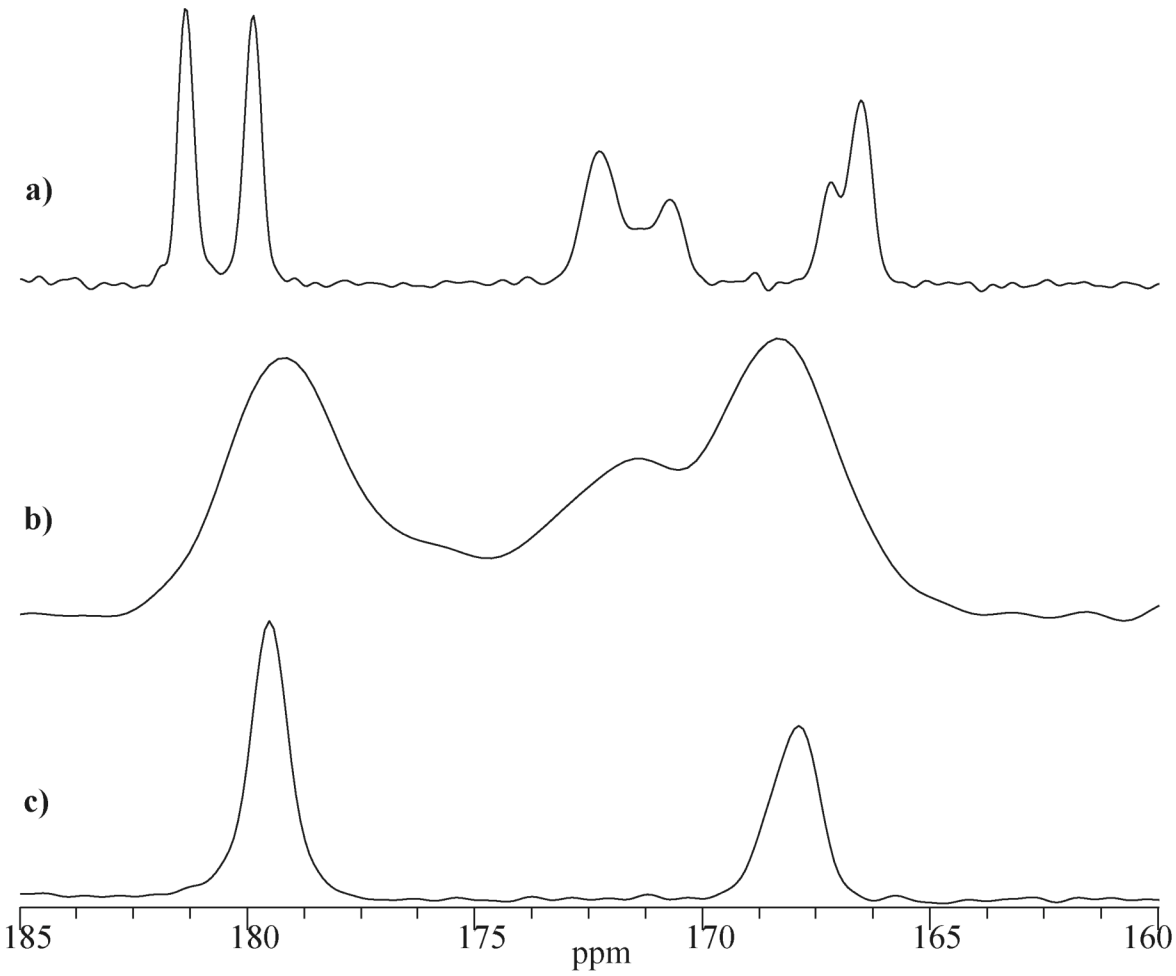

Figure 5.8. Overlay of the 160-185 ppm region of the ^{13}C SSNMR spectra for the (a) α form, (b) melt-quenched amorphous form, and (c) γ form of indomethacin.

(Figure 5.8a). This peak corresponds to non-cyclic dimer hydrogen-bonding interactions that occur in the amorphous form. Therefore, it can be concluded that the amorphous form retains a local structure and hydrogen-bonding network very similar to that of the γ form, but some non-cyclic dimer hydrogen-bonding interactions similar to those seen in the α form also exist.

5.3.3 Cryogrinding as a route to the amorphous state

As described in Chapter 1, mechanical disruption of the crystal lattice is another route to the amorphous state. Formation of the amorphous form via cryogrinding has been the focus of recent studies.[17] Thus, it is of interest to determine if structural differences exist between amorphous indomethacin prepared by cryogrinding and the melt-quench method. The ^{13}C SSNMR spectra of crystalline γ form indomethacin that was cryoground for various amounts of time are shown in Figure 5.9. The spectra of the starting material (Figure 5.9e) and the melt-quenched amorphous material (Figure 5.9a) are also included for comparison. Broadening of the peaks, which indicates formation of amorphous material, increases with grinding time. However, even after 120 min of grinding, there is crystalline material present, as evidenced by the sharpness of some peaks. It is difficult to confirm if this crystalline component is starting material that was not converted to the amorphous state or is due to some recrystallization of amorphous material during the course of the SSNMR experiment, which would be facilitated by residual seed crystals of the γ form starting material. In order to test this, the sample cryoground for 60 min was

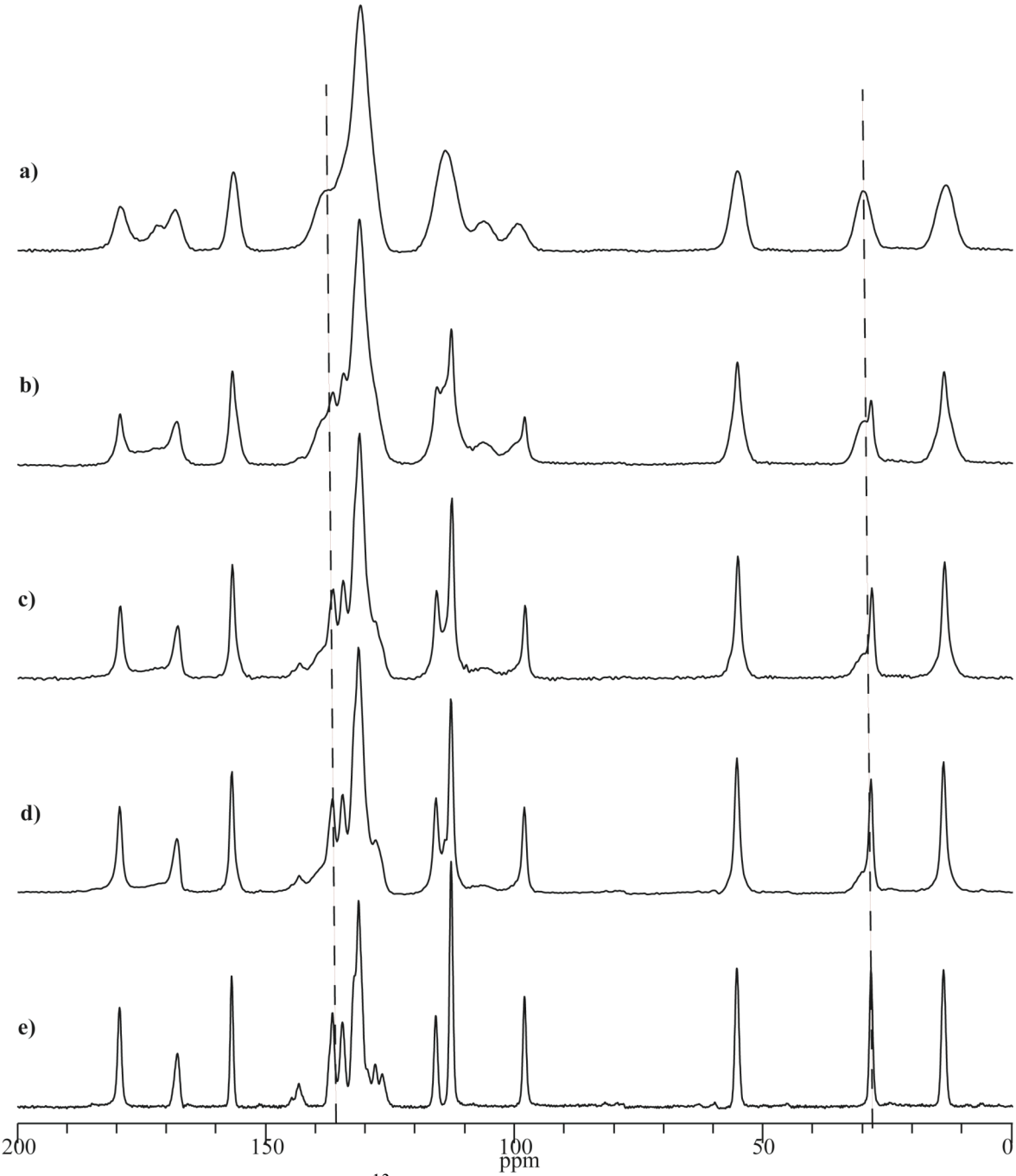

Figure 5.9. Comparison of the ^{13}C SSNMR spectrum of (a) melt-quenched amorphous form to the spectra of samples cryoground for (b) 120 minutes, (c) 60 minutes, and (d) 30 minutes. The spectrum of the starting crystalline material (γ form) is shown in (e).

analyzed by SSNMR at room temperature and -80 °C. The extremely low temperature was selected to inhibit any potential recrystallization from occurring. The SSNMR spectra of these two samples and the melt-quenched sample are shown in Figure 5.10. The spectrum of the 60-min cryoground sample collected at -80 °C (Figure 5.10b) consists of broad peaks that resemble those seen in the melt-quenched amorphous form (Figure 5.10a), with some slight differences. For example, the relative intensities of the peaks in the 165-185 ppm region are different for the melt-quenched and cryoground samples, suggesting that the hydrogen-bonding network between these two samples is not the same. The spectrum of the 60-min cryoground sample analyzed at ambient temperature (Figure 5.10c) shows sharper peaks and the presence of more crystalline material than the 60-min cryoground sample analyzed at -80 °C. It can therefore be concluded that residual seed crystals are present in the cryoground amorphous material and this results in recrystallization during room temperature storage and analysis. This is also supported by results from MDSC analysis of the 60-min cryoground sample, shown in Figure 5.11. A T_g similar to that of melt-quenched amorphous indomethacin at ~47 °C is observed in the reversible heat flow, but the crystallization event observed in the total heat flow occurs at much lower temperatures than for melt-quenched amorphous material (Figure 5.3). Also, there is only one endothermic melting peak corresponding to the crystalline γ form. This supports the conclusion that differences between the two amorphous materials exist, and residual γ-form seed crystals in the cryoground material cause crystallization to occur more readily and only to the γ form. Due to this crystallization behavior and

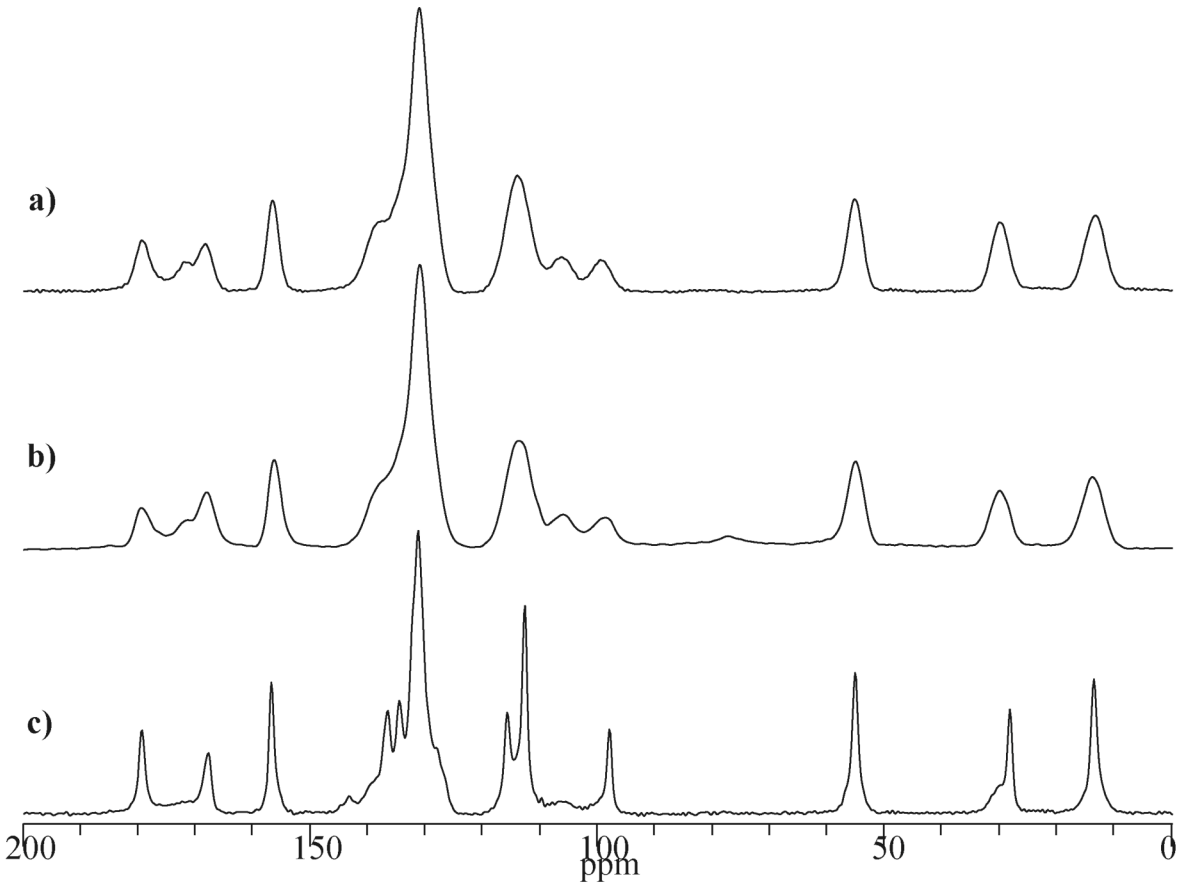

Figure 5.10. ^{13}C SSNMR spectra of (a) melt-quenched amorphous indomethacin, (b) indomethacin cryoground for 60 minutes and analyzed at -80 °C, and (c) same as (b) but analyzed at ambient temperature.

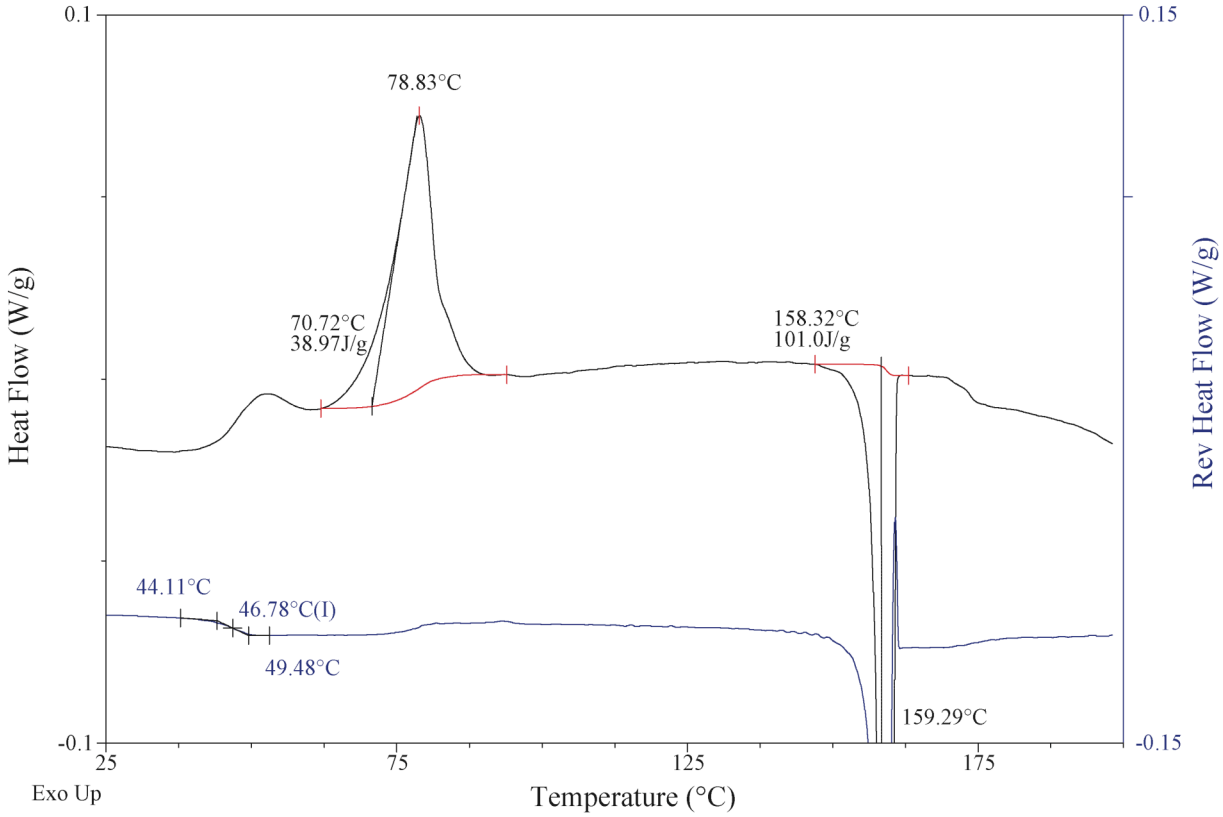

Figure 5.11. MDSC analysis of cryoground indomethacin. The black solid line corresponds to the total heat flow and shows integration of crystallization and melting events. The blue solid line corresponds to the reversible heat flow and contains information about the glass transition.

physical instability at ambient temperatures, cryogrinding was not further pursued as a means of making amorphous material or amorphous solid dispersions.

5.3.4 Analysis of amorphous indomethacin:excipient physical mixtures

The physical mixtures of melt-quenched amorphous indomethacin with PVP and HPMC were analyzed using MDSC and ^{13}C SSNMR spectroscopy. The MDSC results for the 1:1 indomethacin:PVP physical mixture and the 1:1 indomethacin:HPMC physical mixture are shown in Figure 5.12. In both samples, a T_g at ~47 °C occurs, corresponding to the melt-quenched amorphous indomethacin. The material then crystallizes (not shown) and melts between 150 and 160 °C. The broadness of the melting endotherm is due to the presence of the polymer. This behavior was observed in all physical mixtures, suggesting that no interactions between the indomethacin and the excipient exist. It also suggests that the presence of this polymer is not enough to inhibit crystallization.

The ^{13}C SSNMR spectra of the indomethacin:PVP physical mixtures are shown in Figure 5.13. The spectra of the melt-quenched amorphous indomethacin and PVP are also included for comparison. This figure highlights the selectivity of SSNMR spectroscopy, as there are regions in the spectrum where there is no overlap between peaks from the API and peaks from the excipient. For instance, in the region from 60-170 ppm, no peaks from the PVP are found. This allows for changes in the indomethacin peaks in this region to be monitored without any interference. Because the region of 165-185 ppm is

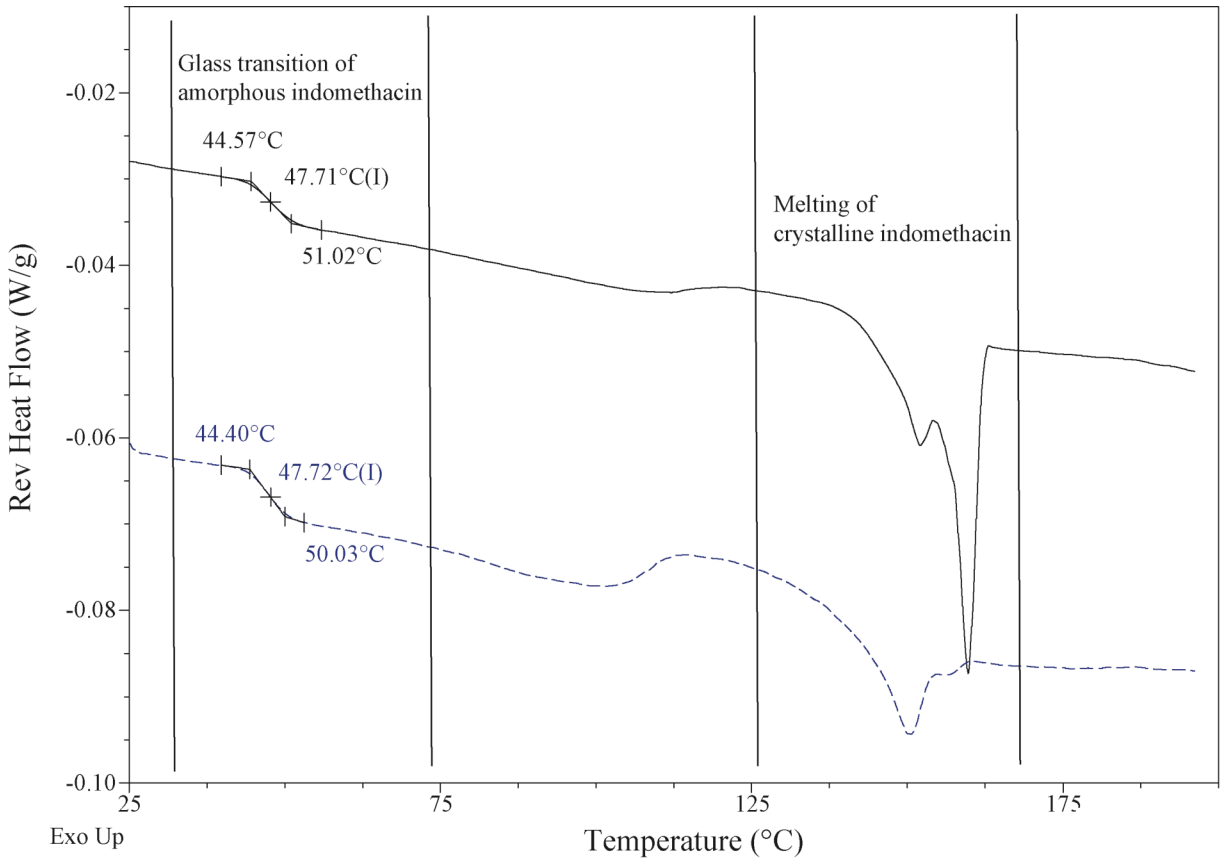

Figure 5.12. MDSC analysis showing the reversible heat flow for indomethacin:excipient physical mixtures. The solid line corresponds to a 1:1 indomethacin:HPMC physical mixture and the dashed line corresponds to a 1:1 indomethacin:PVP physical mixture. Regions where the T_g and melting events occur are highlighted.

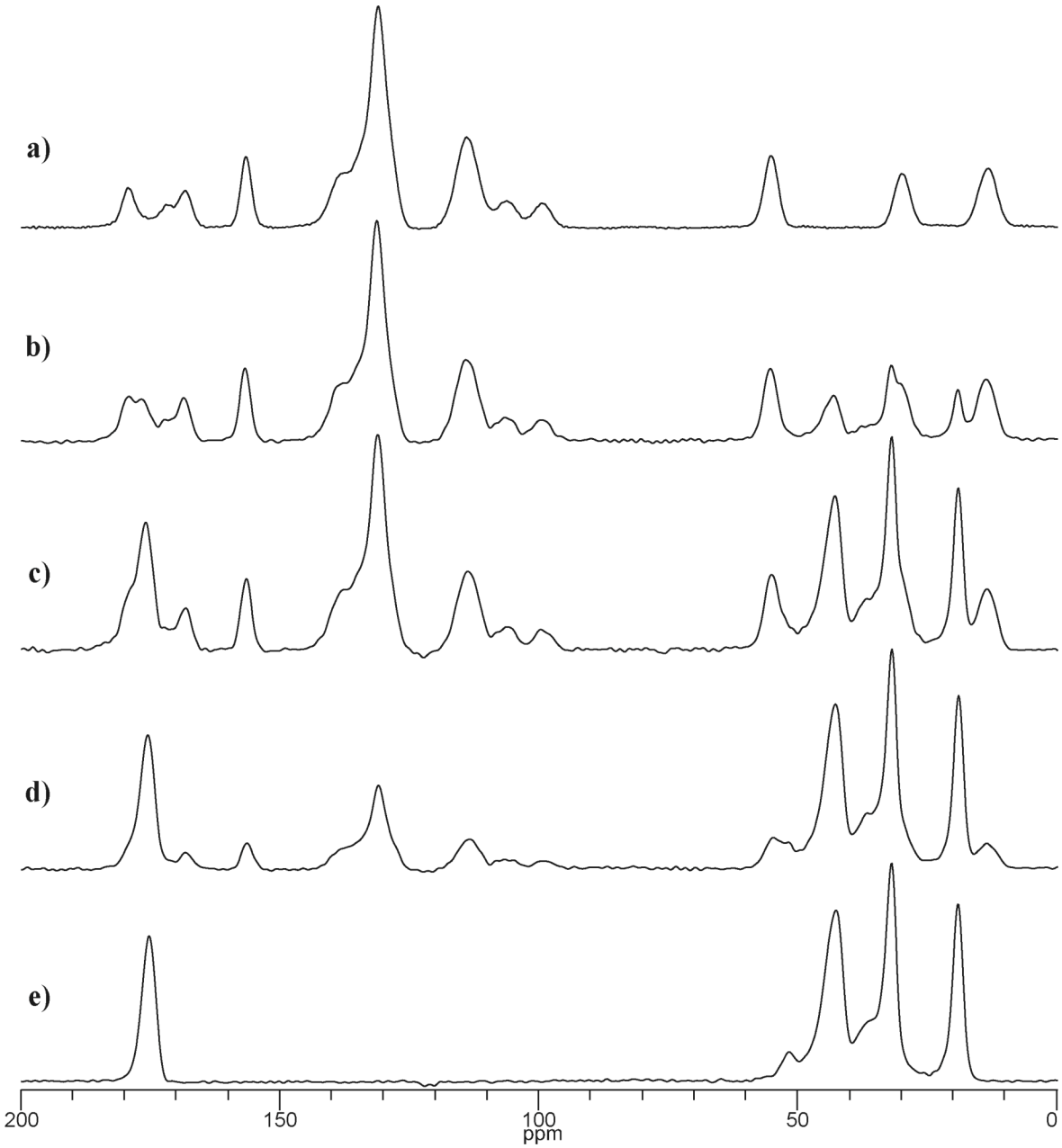

Figure 5.13. ^{13}C SSNMR spectra of indomethacin:PVP physical mixtures: (a) melt-quenched amorphous indomethacin, (b) 4:1 indomethacin:PVP, (c) 1:1 indomethacin:PVP, (d) 1:3 indomethacin:PVP, and (e) PVP.

of most interest due to the information it provides on hydrogen bonding, it is helpful to have spectral resolution between indomethacin and excipient in this region. As shown in Figure 5.13, the peak from the amide carbonyl carbon in PVP occurs at 175.9 ppm, which is very close to the peak corresponding to the hydrogen-bonded cyclic dimer of indomethacin at 178.8 ppm. Although this is not ideal, there is still sufficient resolution to detect each component in the mixtures studied. For example, in Figure 5.13d, the spectrum of a 1:3 indomethacin:PVP mixture is shown. Although the indomethacin is the minor component, its carboxylic acid carbon peak can still be detected as a shoulder on the peak of the PVP amide carbon. The spectra of the physical mixtures (Figure 5.13b-d) are equivalent to the sum of the spectrum of the melt-quenched amorphous indomethacin (Figure 5.13a) and the spectrum of PVP (Figure 5.13e), indicating that no interaction is occurring between the two components in any of the indomethacin:PVP physical mixtures analyzed.

The ^{13}C SSNMR spectra of the indomethacin:HPMC physical mixtures are shown in Figure 5.14. Again, the spectrum of the melt-quenched amorphous indomethacin (Figure 5.14a) and the spectrum of HPMC (Figure 5.14d) are shown for comparison. Unlike with PVP, there is no overlap between the peaks from indomethacin and the peaks from HPMC in the region from 165-185 ppm. This is an advantage of using HPMC, as any difficulties associated with monitoring changes in the hydrogen bonding of the amorphous indomethacin are completely absent. As with the indomethacin:PVP physical mixtures, the SSNMR spectra of the indomethacin:HPMC physical mixtures (Figure

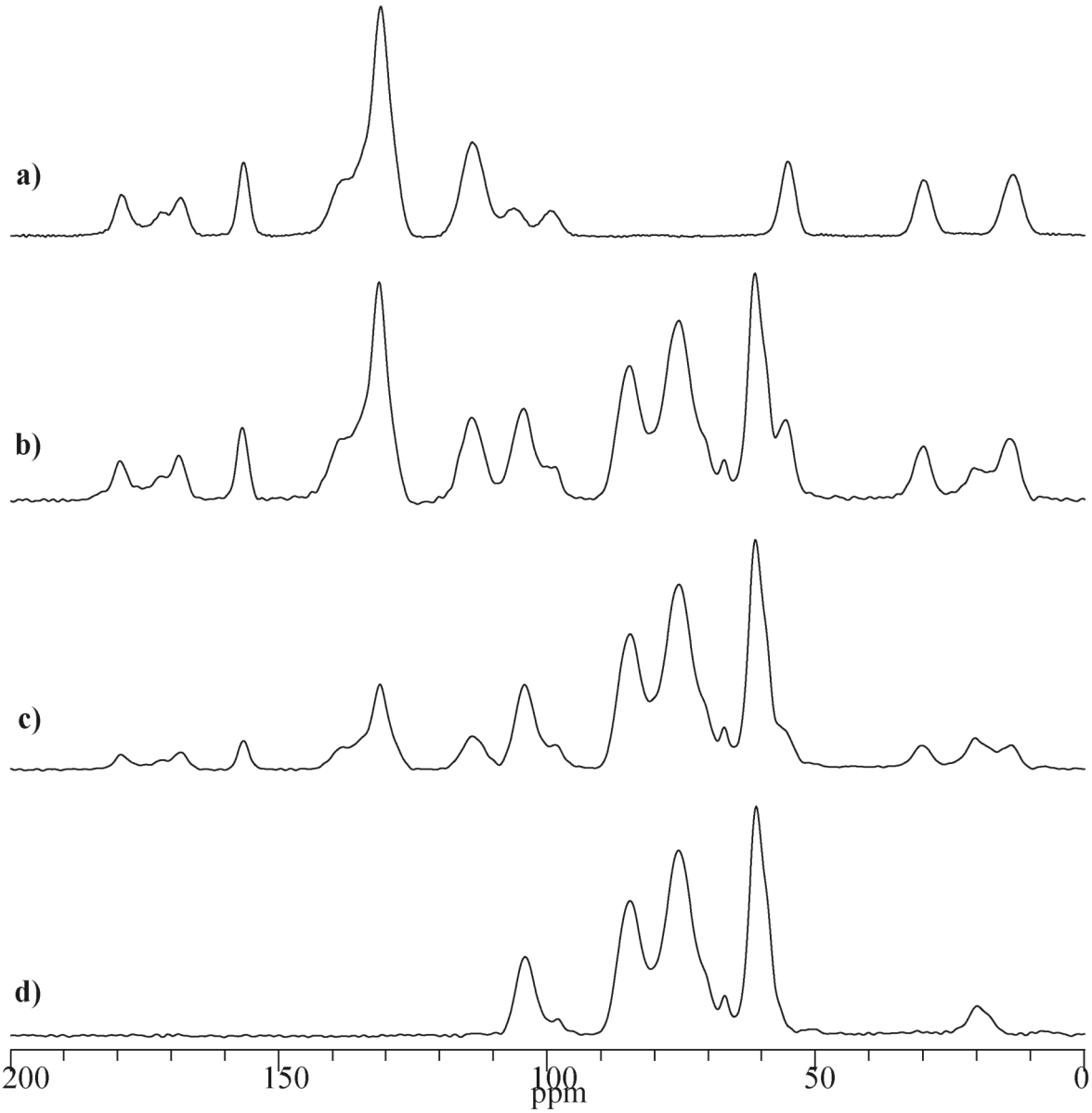

Figure 5.14. ^{13}C SSNMR spectra of indomethacin:HPMC physical mixtures: (a) melt-quenched amorphous indomethacin, (b) 1:1 indomethacin:HPMC, (c) 1:3 indomethacin:HPMC, and (d) HPMC.

5.14b-c) are equivalent to the sum of the spectrum of the melt-quenched amorphous indomethacin (Figure 5.14a) and the spectrum of HPMC (Figure 5.14d), which further supports the MDSC results and confirms the conclusion that there is no interaction between the two components in any of the indomethacin:HPMC physical mixtures studied.

5.3.5 Analysis of indomethacin:excipient amorphous solid dispersions

The amorphous solid dispersions were also analyzed using MDSC and ^{13}C SSNMR spectroscopy. The results from MDSC analysis of the indomethacin:PVP amorphous solid dispersions prepared by the melt-quench method and the solvent-evaporated method are outlined in Tables 5.1a and 5.1b, respectively. In all of these samples, one single T_g that did not correspond to that of amorphous indomethacin or PVP was observed. The value of T_g was found to depend on the indomethacin:PVP weight ratio, which agrees with other reported studies,[4] and supports the formation of an amorphous solid dispersion in which interactions between the indomethacin and the PVP occur. The only sample that showed a crystallization and melting event was the 4:1 indomethacin:PVP melt-quenched mixture. All other samples did not show any evidence of crystallization and subsequent melting by MDSC. Theoretical values for T_g were calculated using the Gordon-Taylor equation, $Tg = (w_1Tg_1 + Kw_2Tg_2)/(w_1 + Kw_2)$, where $K \sim (\rho_1 Tg_1)/(\rho_2 Tg_2)$, w is weight, and ρ is density. These calculated values are also shown in Tables 5.1a and 5.1b. Negative deviation from the theoretical values exists for all samples, regardless of weight ratio or preparation method. This negative deviation has been observed in other studies,[4,18] and

Table 5.1. Comparison of measured and theoretical T_g values for indomethacin:PVP amorphous solid dispersions prepared via (a) melt quenching, and (b) solvent evaporation.

a)

	Melt-quenched Mixtures (Indomethacin:PVP w/w)				
Sample	Indomethacin	4:1	1:1	1:3	PVP
Measured T_g	47 °C	54 °C	78 °C	89 °C	151 °C
Theoretical T_g	-	65 °C	94 °C	119 °C	-

b)

	Solvent-evaporated Mixtures (Indomethacin:PVP w/w)			
Sample	Indomethacin	1:1	1:3	PVP
Measured T_g	47 °C	81 °C	107 °C	151 °C
Theoretical T_g	-	94 °C	119 °C	-

can be attributed to non-ideality of mixing. The fact that the measured T_g for the 1:3 solvent-evaporated mixture is 20 °C higher than the 1:3 melt-quenched mixture, and is therefore much closer to the ideal T_g, suggests that, for this particular weight ratio, better mixing was achieved using the solvent-evaporated method.

The ^{13}C SSNMR spectra of the melt-quenched indomethacin:PVP mixtures are shown in Figure 5.15. Again, the spectrum of melt-quenched amorphous indomethacin and the spectrum of PVP are included for comparative purposes. From 0-165 ppm, the spectra of the melt-quenched amorphous dispersions (Figure 5.15b-d) look like an addition of the spectra of the two individual components. However, this is not the case in the 160-185 ppm region of the SSNMR spectra for these samples. Contrary to what was observed in the spectra of the indomethacin:PVP physical mixtures (Figure 5.13), the peaks in this area do not correspond to a simple addition of the peaks from melt-quenched amorphous indomethacin and PVP. Rather, changes are observed, which are better highlighted in Figure 5.16. Here, the 160-185 ppm region of the SSNMR spectra for physical mixtures and melt-quenched mixtures is shown. In Figure 5.16a, the 4:1 indomethacin:PVP mixtures are compared. In the physical mixture, four distinct peaks are observed. They correspond to the hydrogen-bonded cyclic dimer of indomethacin (178.8 ppm), the PVP amide carbonyl (175.9 ppm), the non-cyclic dimer hydrogen-bonding interactions in indomethacin (172.2 ppm), and the non-hydrogen-bonded amide group of indomethacin (168.5 ppm). In the melt-quenched mixture, only three distinct peaks are

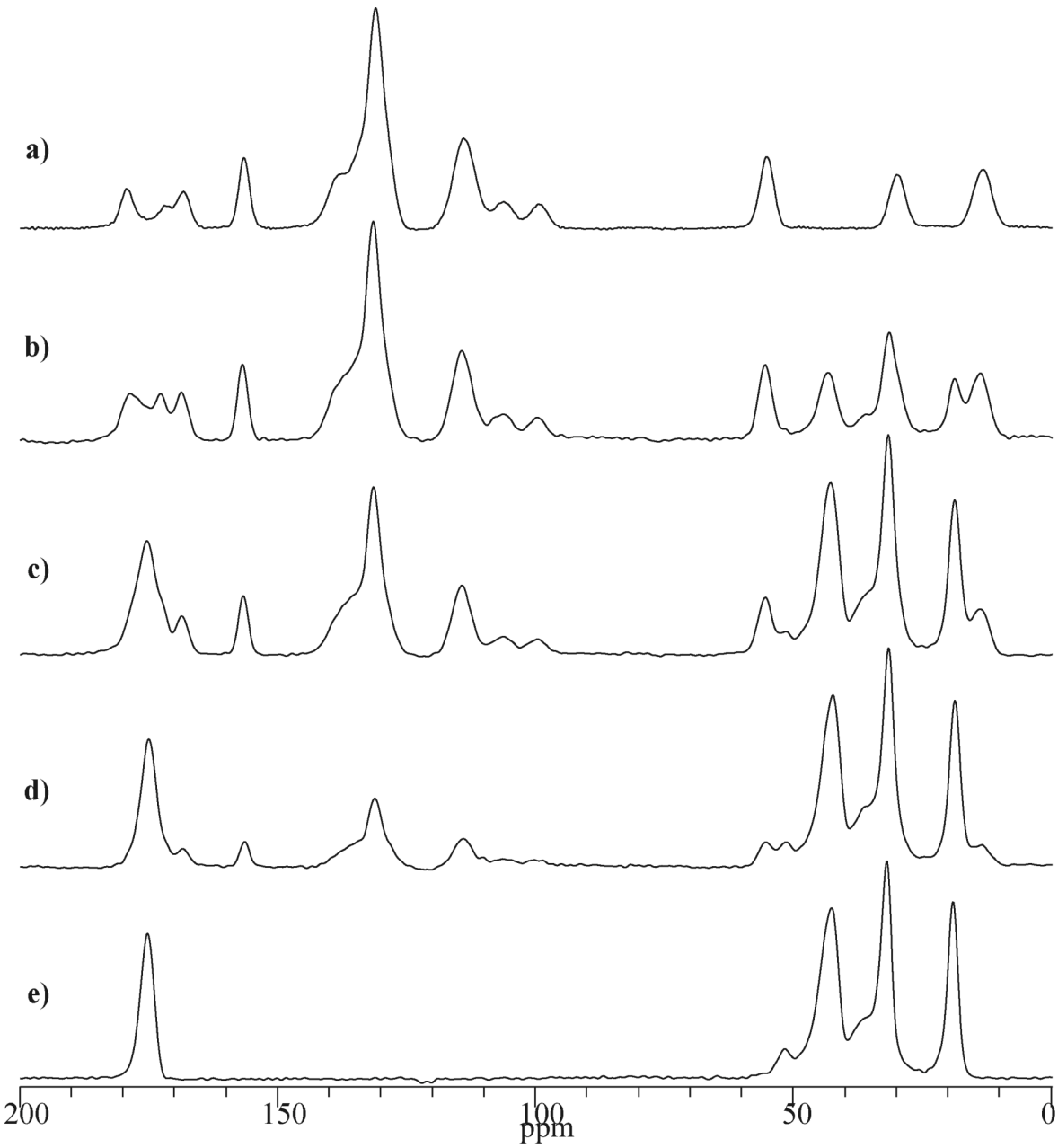

Figure 5.15. ^{13}C SSNMR spectra of indomethacin:PVP melt-quenched mixtures: (a) melt-quenched amorphous indomethacin, (b) 4:1 indomethacin:PVP, (c) 1:1 indomethacin:PVP, (d) 1:3 indomethacin:PVP, and (e) PVP.

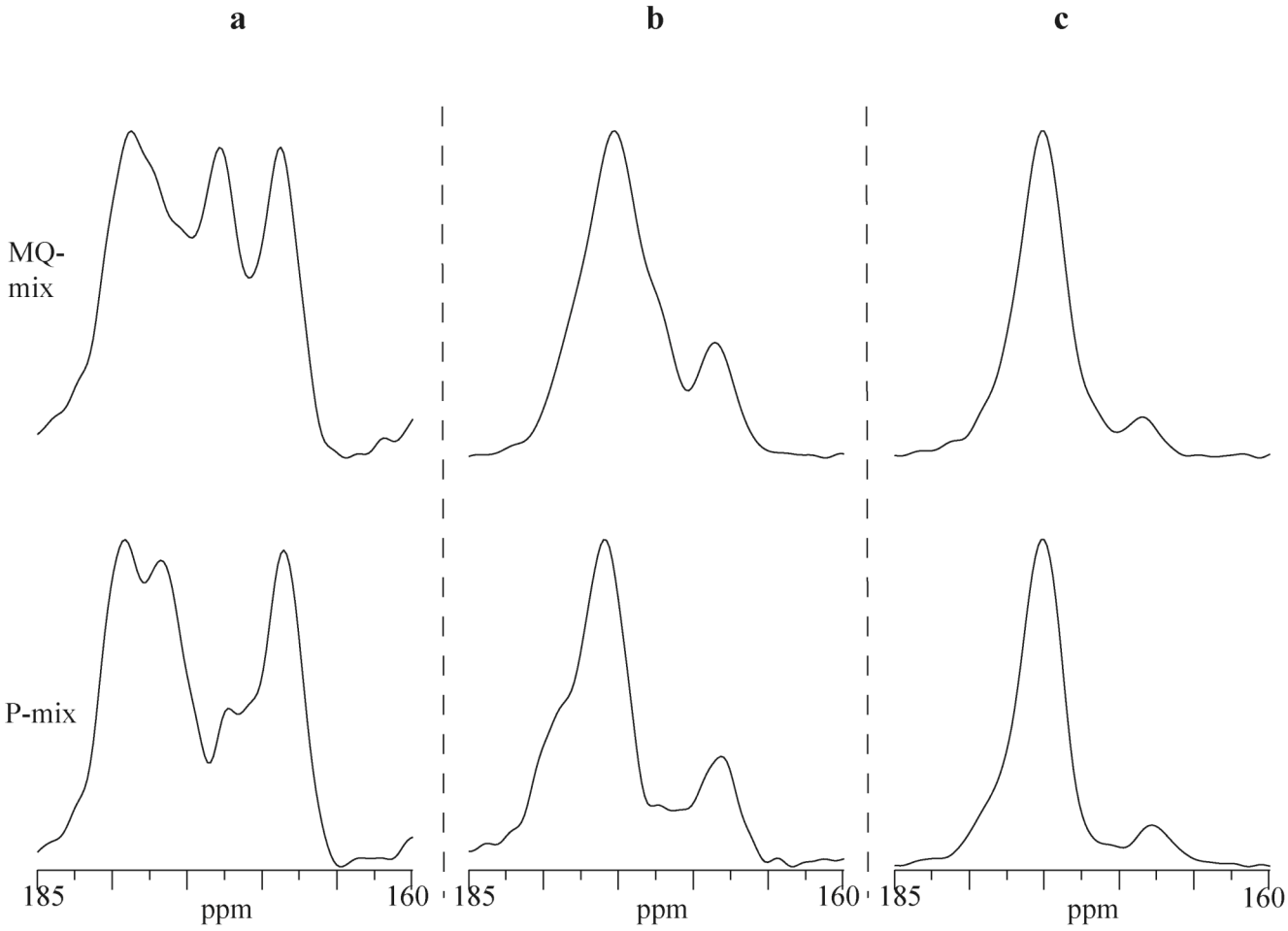

Figure 5.16. Comparison of the ^{13}C SSNMR spectra of indomethacin:PVP melt-quenched mixtures (top row) to the spectra of physical mixtures (bottom row): (a) 4:1 indomethacin:PVP, (b) 1:1 indomethacin:PVP, and (c) 1:3 indomethacin:PVP.

resolved, albeit with the presence of some shoulders. First, the peak at 178.8 ppm is still present, indicating that indomethacin cyclic dimers are still intact. However, the peak of the amide carbon for PVP has shifted upfield to higher ppm so that it can no longer be resolved from the indomethacin peak at 178.8 ppm, suggesting that the amide group of PVP is now involved in hydrogen bonding with indomethacin. A significant difference between the two mixtures is a change in the region corresponding to the non-cyclic dimer hydrogen-bonding interactions in indomethacin. In the physical mixtures, this peak occurs at 172.2 ppm. However, in the melt-quenched mixtures, a peak of larger intensity located at 172.8 ppm is observed. This suggests that the PVP has disrupted the non-cyclic dimer hydrogen-bonding interactions and the indomethacin is now preferentially bonding with the PVP amide group instead of with another indomethacin molecule. This is also supported by the shift in the amide carbon peak of PVP to 177.1 ppm, which, as previously noted, indicates it is now involved in hydrogen bonding. The fact that there does not seem to be enough PVP present to also completely disrupt the hydrogen bonding between the carboxylic acid groups of the indomethacin cyclic dimer could explain why the 4:1 indomethacin:PVP melt-quenched sample readily crystallized during the MDSC experiments. The SSNMR spectra of the 1:1 mixtures are shown in Figure 5.16b. In the melt-quenched 1:1 mixture, the same change in the peak that corresponds to the non-cyclic dimer hydrogen-bonding interactions in indomethacin also occurs, suggesting that there is also a disruption in these hydrogen bonds. Additionally, the peak corresponding to the hydrogen-bonded cyclic dimer at 178.8 ppm is no longer observed, suggesting that at this weight ratio, there is enough PVP present to completely disrupt these interactions. Finally,

in Figure 5.16c, the SSNMR spectra of the 1:3 mixtures are shown. Here, the only difference that can be easily observed is the loss of the shoulder on the PVP peak when going from the physical mixture to the melt-quenched mixture, which corresponds to disruption of the hydrogen bonds of the cyclic dimer in indomethacin. The ^{13}C SSNMR spectra of the solvent-evaporated indomethacin:PVP mixtures are shown in Figure 5.17. Again, the spectrum of melt-quenched amorphous indomethacin and the spectrum of PVP are included for comparative purposes. The same changes that occurred in the melt-quenched mixtures are also observed in the solvent-evaporated mixtures. From 0-165 ppm, the spectra of the solvent-evaporated amorphous dispersions (Figure 5.17b-c) look like an addition of the spectra of the two individual components. However, this does not hold true for the peaks located in the 160-185 ppm region of the SSNMR spectra. Figure 5.18 compares the indomethacin:PVP physical mixtures to the melt-quenched and solvent-evaporated mixtures, and shows that the same changes in hydrogen-bonding interactions that were seen in the melt-quenched amorphous dispersions are also observed in the mixtures that were prepared via solvent evaporation.

The melt-quenched indomethacin:HPMC mixtures were analyzed by MDSC, and the results from the reversible heat flow are presented in Table 5.2. A single T_g not equal to the T_g of either component was observed, indicating that an amorphous dispersion was formed in both cases. The theoretical T_g values determined using the Gordon-Taylor equation described earlier are also shown. It is interesting to find that the T_g

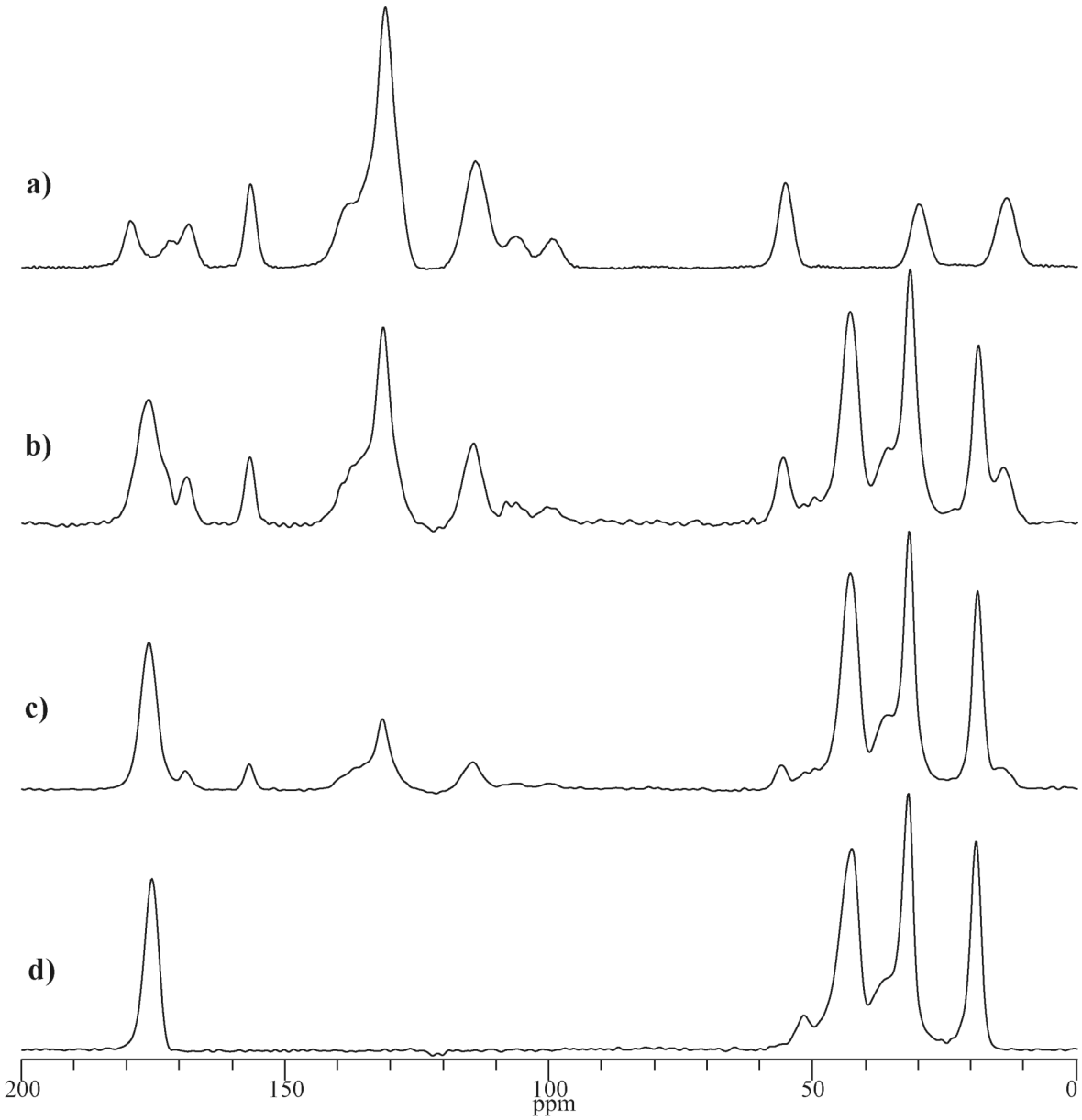

Figure 5.17. ^{13}C SSNMR spectra of indomethacin:PVP solvent-evaporated mixtures: (a) melt-quenched amorphous indomethacin, (b) 1:1 indomethacin:PVP, (c) 1:3 indomethacin:PVP, and (d) PVP.

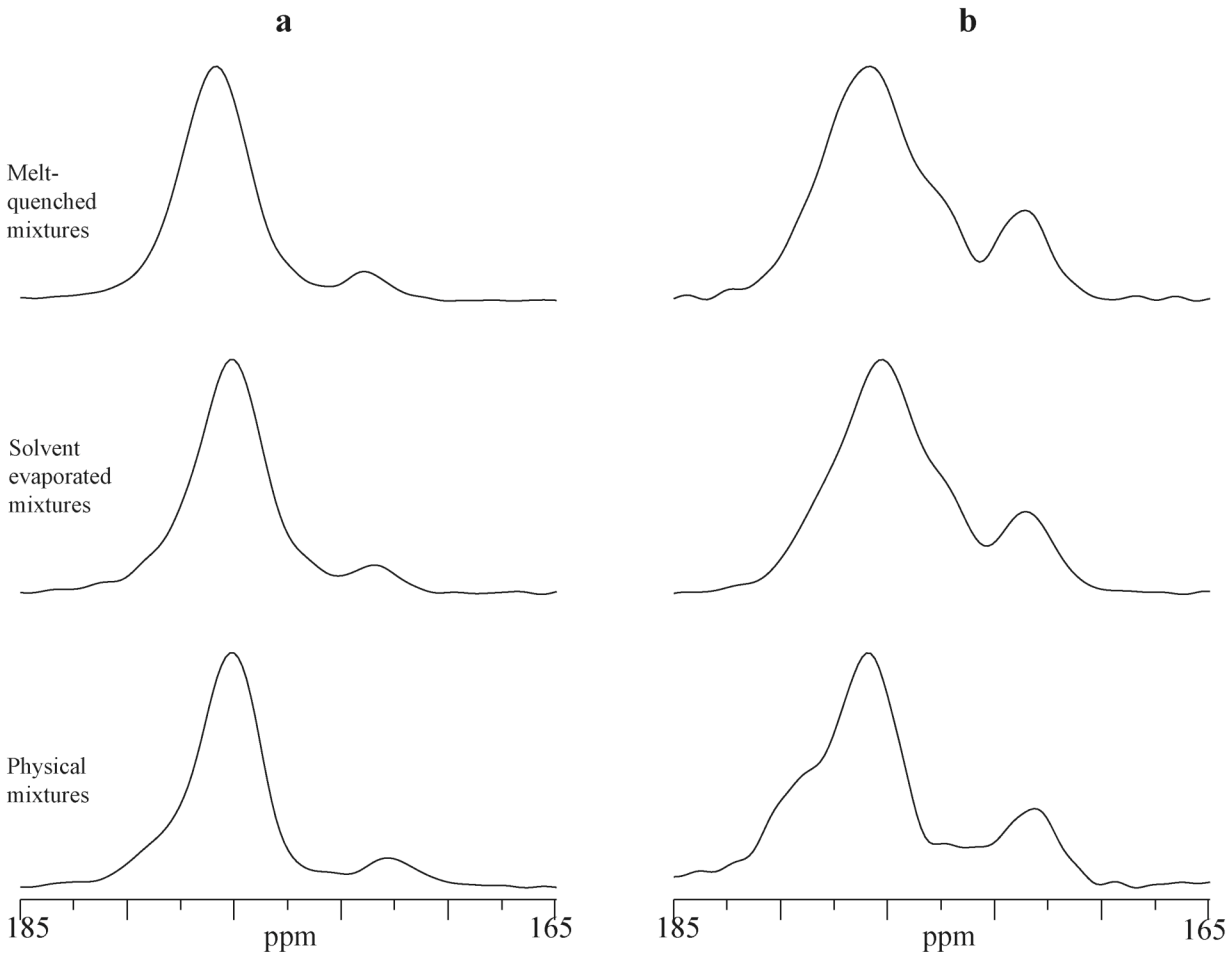

Figure 5.18. Comparison of the ^{13}C SSNMR spectra of indomethacin:PVP melt-quenched mixtures (top row), solvent-evaporated mixtures (middle row) and physical mixtures (bottom row): (a) 1:3 indomethacin:PVP, and (b) 1:1 indomethacin:PVP.

Table 5.2. Comparison of measured and theoretical T_g values for indomethacin:HPMC amorphous solid dispersions prepared via melt quenching.

	Melt-Quenched Mixtures (Indomethacin:HPMC w/w)			
Sample	Indomethacin	1:1	1:3	HPMC
Measured T_g	47 °C	56 °C	58 °C	156 °C
Theoretical T_g	-	123 °C	139 °C	-

values for both melt-quenched mixtures were essentially the same and did not depend on weight ratio. These values are drastically lower than the theoretical values, indicating severe deviation from ideal mixing. The ^{13}C SSNMR spectra of the melt-quenched indomethacin:HPMC mixtures are shown in Figure 5.19. The spectrum of melt-quenched amorphous indomethacin (Figure 5.19a) and the spectrum of HPMC (Figure 5.19d) are also shown. Unlike with the indomethacin:PVP mixtures, it is much easier to detect changes in hydrogen bonding in this system since the HPMC displays no peaks in the 165-185 region of the spectrum. Upon examination of the spectra in Figure 5.18, it can quickly be seen that the peak corresponding to the hydrogen-bonded cyclic dimer of indomethacin completely disappears in the melt-quenched indomethacin:HPMC mixtures, as indicated by the dashed line. This is the case in both the 1:1 mixture (Figure 5.19b) and the 1:3 mixture (Figure 5.19c). In order to more closely examine this region, the peaks from 160-185 ppm in the SSNMR spectra of melt-quenched amorphous indomethacin, the 1:1 indomethacin:HPMC physical mixture, and the 1:1 indomethacin:HPMC melt-quenched mixture were compared and are displayed in Figures 5.20a, 5.20b, and 5.20c, respectively. The spectra of the melt-quenched amorphous indomethacin (Figure 5.20a) and the 1:1 indomethacin:HPMC physical mixture (Figure 5.20b) are very similar. However, in the 1:1 indomethacin:HPMC melt-quenched mixture, the signal between 170 and 175 ppm has grown in intensity and width. This is likely due to the presence of hydrogen-bonding interactions between the ether oxygen groups or the –OH group in HPMC with the indomethacin molecules, which do not occur in the physical mixture.

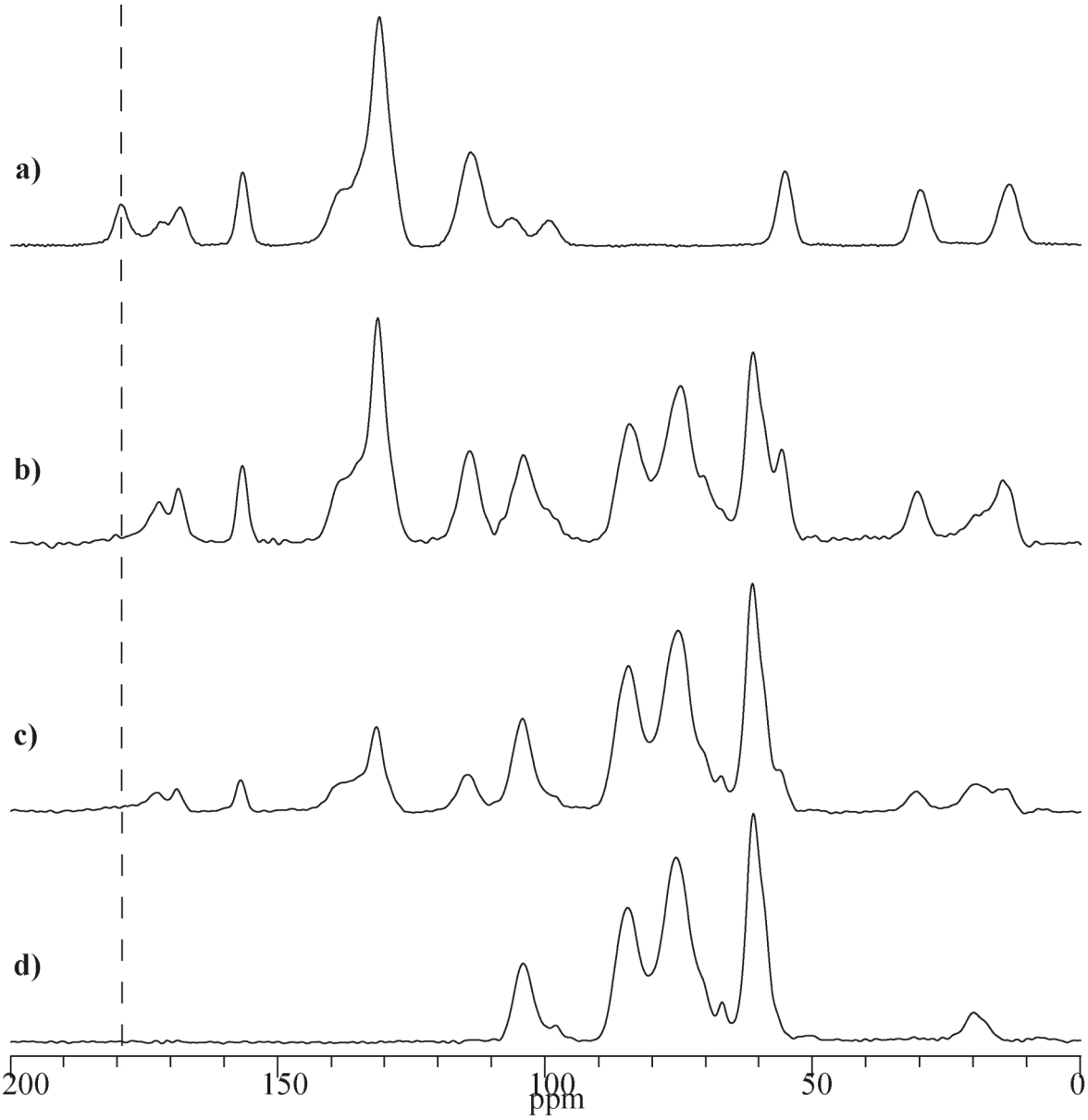

Figure 5.19. ^{13}C SSNMR spectra of indomethacin:HPMC melt-quenched mixtures: (a) melt-quenched amorphous indomethacin, (b) 1:1 indomethacin:HPMC, (c) 1:3 indomethacin:HPMC, and (d) HPMC.

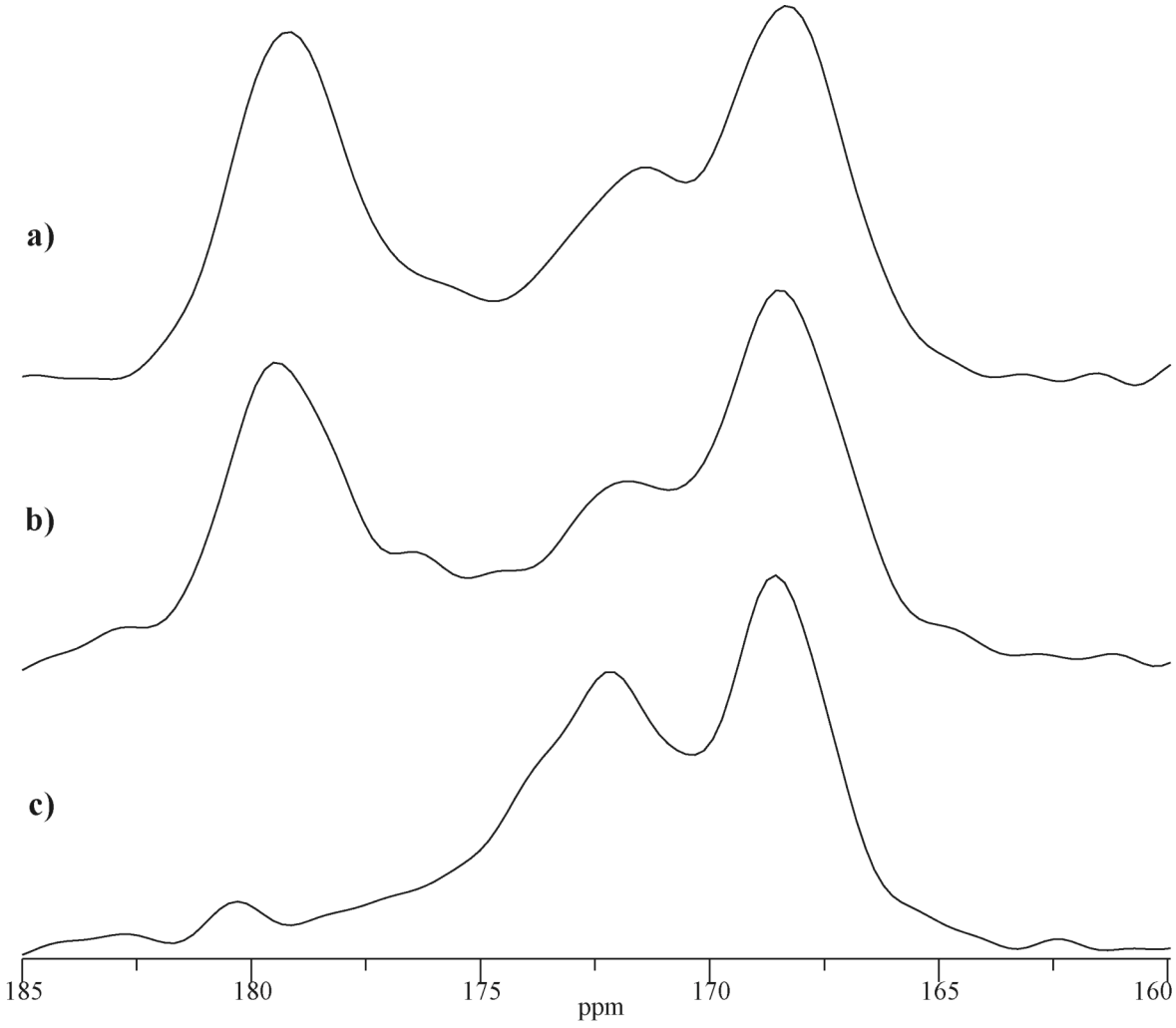

Figure 5.20. ^{13}C SSNMR spectra of (a) melt-quenched amorphous indomethacin, (b) 1:1 indomethacin:HPMC physical mixture, and (c) 1:1 indomethacin:HPMC melt-quenched mixture.

5.4 Discussion

Taylor et al. were the first to use spectroscopic analysis for the detection of hydrogen-bonding interactions between indomethacin and PVP in amorphous solid dispersions prepared via solvent evaporation.[6] Based on IR data, the authors concluded that indomethacin forms hydrogen bonds with PVP at the expense of cyclic dimer formation. Using a molecular weight of 111 to represent a PVP monomer unit, it was determined that a 1:1 molar ratio of PVP to indomethacin is present at 24% weight fraction PVP, which should be enough to completely hydrogen bond with all of the indomethacin molecules. However, changes in the IR spectra that occurred in excess of this weight fraction indicated that this was not the case. In our ^{13}C SSNMR spectroscopy studies, changes in the spectra of the melt-quenched indomethacin:PVP mixtures occurred in excess of 20% PVP (4:1 mixture). Elimination of cyclic dimers was not observed until the amount of PVP was raised to 50% weight fraction (1:1 mixture). These observations agree with those of Taylor and co-workers. Since the pioneering work of Taylor et al., other studies[4,18] have reported the use of IR spectroscopy to monitor the disruption of the cyclic dimer in indomethacin as a means of detecting interactions with an excipient such as PVP. However, very few studies have mentioned detection or disruption of the non-cyclic dimer hydrogen-bonding interactions that also occur in the amorphous form. The work presented here demonstrates the potential for using ^{13}C SSNMR spectroscopy to follow changes in these interactions as well as loss of the cyclic dimer. Additionally, the data presented here suggests that the interactions formed between indomethacin and PVP in amorphous

dispersions are not dependent on the preparation method used, as the spectral changes observed in the SSNMR spectra of the melt-quenched and solvent-evaporated indomethacin:PVP mixtures were the same.

Vibrational spectroscopy has also been used to detect interactions that occur between indomethacin and HPMC in amorphous solid dispersions. Ohara et al.[19] attributed peak shifts in the IR spectra of a 1:1:1 indomethacin:ethycellulose:HPMC mixture prepared by solvent evaporation to disruption of the indomethacin cyclic dimer in favor of hydrogen-bonding interactions with the HPMC. Gong and co-workers[20] used IR and Raman spectroscopy to detect hydrogen bonds between the carboxylic acid group of indomethacin and the -OH group of HPMC in a mixture prepared by supercritical carbon dioxide assisted impregnation. The ^{13}C SSNMR data presented here shows that these interactions also occur upon melt-quenching a mixture of indomethacin and HPMC, and that HPMC is able to completely disrupt the hydrogen bonds of the cyclic dimer at a weight percent of 50% or more using this preparation method. Potential future studies could involve analysis of mixtures containing a smaller percentage of HPMC, and comparison to solvent-evaporated mixtures.

The results of this study show that both PVP and HPMC form hydrogen bonds with indomethacin, which explains why the T_g values for all amorphous solid dispersions show negative deviations from ideality. However, the deviations observed in the indomethacin:HPMC mixtures (Table 5.2) are much greater than those of the amorphous dispersions prepared with PVP (Table 5.1). These differences can be explained through a

consideration of the thermodynamics of mixing. For molecular mixing of two components to occur, the free energy of mixing, ΔG_m, must be negative. The ΔG_m is given by the following equation:

$$\Delta G_m = \Delta H_m - T\Delta S_m$$

where ΔH_m is the enthalpy of mixing, ΔS_m is the entropy of mixing, and T is temperature. The entropy of mixing is always positive and, therefore, favorable. When the formation of hydrogen bonds between the two components results in an overall loss in the number or strength of hydrogen bonds, the enthalpy of mixing will be positive (unfavorable) but the entropy will be increased due to the disruption of the hydrogen-bonding interactions in the individual components. For example, Zografi and co-workers[21] suggested that the formation of hydrogen bonds between sucrose and PVP resulted in an increase in the entropy of the system since they were formed at the expense of extensive sucrose-sucrose hydrogen bonds, whereas the enthalpy of mixing was positive because the overall number or strength of bonds formed between sucrose and PVP was less than those in the sucrose. Mixing was thereby entropically driven, and the T_g value showed a negative deviation from ideality due to the formation of weaker or fewer bonds. In another study, Tong et al.[22] observed positive deviations from the theoretical T_g for a dispersion of amorphous indomethacin with its sodium salt, due to the stronger ionic interactions formed between the acid and the salt compared to those present in the individual components. When the energy of the bonds formed upon mixing is equal to the energy of the bonds present in the individual components, a T_g equal to that of the theoretical T_g will be observed. Thus, the

negative deviations from ideality observed in the indomethacin:PVP amorphous solid dispersions indicate that the strength and/or number of interactions between indomethacin and PVP is not as great as in indomethacin alone, but the increase in entropy upon mixing makes the formation of a solid dispersion favorable. Because the amide group of PVP is more basic than the amide or carboxylic acid group of indomethacin, hydrogen bonds between indomethacin and PVP should theoretically be stronger. However, because the indomethacin cyclic dimer is being disrupted, the overall number of hydrogen bonds likely decreases upon mixing, resulting in the negative deviation from ideality. The extreme deviation observed in the indomethacin:HPMC melt-quenched mixtures can be explained by the fact that intramolecular hydrogen bonding in HPMC can occur between the unsubstituted -OH groups, ether oxygen groups, and -OH groups introduced by substituents. Disruption of this self-association in both indomethacin and HPMC upon mixing of the two components results in an overall decrease in the number and strength of hydrogen bonds, causing a large negative deviation of the T_g from theoretically calculated values. The significant gain in entropy upon mixing is what drives the formation of an indomethacin:HPMC amorphous solid dispersion.

5.5 Conclusions

The nature of the hydrogen-bonding network in amorphous indomethacin was investigated using ^{13}C SSNMR spectroscopy and compared to that of the α and γ crystalline polymorphs. The results suggest that the amorphous form consists of both cyclic dimers as in the γ form and non-cyclic dimer hydrogen-bonding interactions similar to those observed in the α form. Cryogrinding indomethacin seemed to result in formation of amorphous material that differed from the melt-quenched material in terms of its ^{13}C SSNMR spectrum and its recrystallization behavior. Melt-quenching and solvent evaporation of indomethacin:PVP mixtures resulted in similar changes to the ^{13}C SSNMR spectra when compared to physical mixtures, indicating that similar interactions were taking place. Melt-quenching mixtures of indomethacin and HPMC resulted in amorphous solid dispersions exhibiting one T_g, the value of which did not change as a function of indomethacin:HPMC weight ratio. Both PVP and HPMC form hydrogen bonds with indomethacin, resulting in disruption of both the non-cyclic dimer and cyclic dimer hydrogen-bonding interactions. Deviations from ideal mixing indicate that the strength and/or number of the hydrogen bonds formed between indomethacin and each polymer are less than those occurring in indomethacin alone. The extremely low T_g values of the indomethacin:HPMC melt-quenched mixtures suggest that the addition of PVP is more likely to prevent crystallization of the amorphous indomethacin.

5.6 References

1. Hancock BC, Zografi G. 1997. Characteristics and significance of the amorphous state in pharmaceutical systems. J Pharm Sci 86(1):1-12.

2. Bhugra C. Pikal MJ. 2008. Role of thermodynamic, molecular, and kinetic factors in crystallization of the amorphous state in pharmaceutical systems. J Pharm Sci 97(4): 1329-1349.

3. Fujii M, Okada H, Shibata Y, Teramachi H, Kondoh M, Watanabe Y. 2005. Preparation, characterization, and tableting of a solid dispersion of indomethacin with crospovidone. Int J Pharm 293:145-153.

4. Matsumoto T, Zografi G. 1999. Physical properties of solid molecular dispersions of indomethacin with poly(vinylpyrrolidone) and poly(vinylpyrrolidone-co-vinyl-acetate) in relation to indomethacin crystallization. Pharm Res 16(11):1722-1728.

5. Newman A, Engers D, Bates S, Ivanisevic I, Kelly RC, Zografi G. 2008. Characterization of amorphous API:polymer mixtures using X-ray powder diffraction. J Pharm Sci 97(11):4840-4856.

6. Taylor LS, Zografi G. 1997. Spectroscpic characterization of interactions between PVP and indomethacin in amorphous molecular dispersions. Pharm Res 14(12):1691-1698.

7. Kaneniwa N, Otsuka M, Hayashi T. 1985. Physicochemical characteristics of indomethacin polymorphism and transformation kinetics in ethanol. Chem Pharm Bull 33(8):3447-3455.

8. Pines A, Gibby MG, Waugh JS. 1973. Proton-enhanced NMR of dilute spins in solids. J Chem Phys 59:569-590.

9. Andrew ER. 1971. Narrowing of NMR spectra of solids by high-speed specimen rotation and the resolution of chemical shift and spin multiplet structures for solids. Prog Nucl Mag Res 8:1-39.

10. Dixon WT, Schaefer J, Sefcik MD, Stejskal EO, McKay RA. 1982. Total suppression of sidebands in CPMAS carbon-13 NMR. J Magn Reson 49:341-345.

11. Fung BM, Khitrin AK, Ermolaev K. 2000. An improved broadband decoupling sequence for liquid crystals and solids. J Magn Reson 142:97-101.

12. Barich DH, Gorman EM, Zell MT, Munson EJ. 2006. 3-methylglutaric acid as a ^{13}C solid-state NMR standard. Solid State Nucl Magn Reson 30:125-129.

13. Yoshioka M, Hancock BC, Zografi G. 1994. Crystallization of indomethacin from the amorphous state below and above its glass transition temperature. J Pharm Sci 83(12):1700-1705.

14. Aceves-Hernandez J, Nicolas-Vazquez I, Aceves F, Hinojosa-Torres M, Castano V. 2009. Indomethacin polymorphs: experimental and conformational analysis J Pharm Sci 98(7):2448-2463.

15. Kistenmacher TJ, Marsh RE. 1972. Crystal and molecular structure of an antiinflammatory agent, indomethacin, 1-(p-chlorobenzoyl)-5-methoxy-2-methylindole-3-acetic acid. J Am Chem Soc 94:1340-1345.

16. Chen X, Morris KR, Griesser UJ, Byrn SR, Stowell JG. 2002. Reactivity of different indomethacin solid forms with ammonia gas. J Am Chem Soc 124:15012-15019.

17. Crowley KJ, Zografi G. 2002. Cryogenic grinding of indomethacin polymorphs and solvates: assessment of amorphous phase formation and amorphous phase physical stability. J Pharm Sci 91(2):492-507.

18. Forster AH, Apperley DC, Hempenstall J, Lancaster RW, Rades T. 2003. Investigation of the physical stability of amorphous drug and drug/polymer melts using variable temperature solid-state NMR. Pharmazie 58:761-762

19. Ohara T, Kitamura S, Kitagawa T, Terada K. 2005. Dissolution mechanism of poorly water-soluble drug from extended release solid dispersion system with ethylcellulose and hydroxypropylmethylcellulose. Int J Pharm 302: 95-102.

20. Gong K, Rehman IU, Darr JA. 2008. Characterization and drug release investigation of amorphous drug-hydroxypropylmethylcellulose composites made via supercritical carbon dioxide assisted impregnation. J Pharm Biomed Analysis 48: 112-119.

21. Taylor LS, Zografi G. 1998. Sugar-polymer hydrogen bond interactions in lyophilized amorphous mixtures. J Pharm Sci 87(12): 1615-1621.

22. Tong P, Zografi G. 2001. A study of amorphous molecular dispersions of indomethacin and its sodium salt. J Pharm Sci 90(12): 1991-2004.

Chapter 6

Insights into Miscibility and Molecular Mobility of Indomethacin Amorphous Solid Dispersions using SSNMR Spectroscopy

6.1 Introduction

In Chapter 5, ^{13}C SSNMR spectroscopy was used to investigate the structural properties and hydrogen-bonding interactions in amorphous indomethacin and in amorphous solid dispersions of indomethacin with excipients such as PVP and HPMC. While changes in peak position and intensity can provide valuable information about any structural changes that may occur, SSNMR relaxation measurements can give additional insight into the properties of amorphous solid dispersions. The purpose of this chapter is to demonstrate the potential for SSNMR relaxation measurements to provide information on indomethacin amorphous solid dispersions with regards to two key areas: miscibility and mobility.

A miscible binary system is one in which the API and polymer are intimately mixed on the molecular level, and only one, single amorphous phase exists. In contrast, a system with more than one amorphous phase present would have different regions with varying API:polymer ratios. These compositional differences can result in variations in the physical properties of each system. Currently, the major means of determining whether or not a miscible amorphous solid dispersion has been produced is to use DSC to measure any T_g associated with amorphous phases. If the system is completely miscible, one T_g intermediate to the T_g values of the individual components will be observed. The presence of two Tg values indicates phase separation. However, the individual T_g values must be about 10 °C apart and the size of the phase separated domains must be larger than ~30 nm

in order to be detected by DSC.[1] For example, Newman et al. recently reported that formation of phase-separated small domains (< 15-30 nm) in binary amorphous mixtures of trehalose and dextran resulted in failure to detect two distinct T_g values.[2] Thus, it is not always possible to determine whether an API-polymer amorphous mixture is miscible or phase separated based solely on the determination of T_g using DSC. Other techniques in addition to DSC are, therefore, often used in order to characterize the number of amorphous phases present.[3] As described in Chapter 2, SSNMR spectroscopy can be used to determine the degree of mixing of two components through the measurement of ^1H T_1 and $T_{1\rho}$ values. If more than one phase exists, the observation of more than one ^1H T_1 and $T_{1\rho}$ value will depend on the domain size of the phases. The three possible cases are outlined in Table 6.1, which shows that phase separation of domains that are less than 30 nm is possible using SSNMR spectroscopy, providing an advantage over DSC.[4]

Mobility is another key factor that affects the physical stability of an API formulated with a polymer as an amorphous solid dispersion. As stated in Chapter 1, an amorphous material in the non-equilibrium glassy state (below T_g) will experience gradual losses in enthalpy due to the coupling of molecular motions and the thermodynamic driving force towards the more stable crystalline state.[5] In the rubbery state (above T_g), the amorphous material will have an even higher mobility and, hence, greater propensity to recrystallize. A direct measure of the molecular mobility of amorphous materials is therefore extremely beneficial in terms of predicting physical stability. As described in Chapter 2, one of the unique advantages of SSNMR spectroscopy is its ability to provide

Table 6.1. Determination of the number of solid phases using SSNMR spectroscopy.

Number of ^1H T_1 Values	Number of ^1H $T_{1\rho}$ Values	Number of Phases
1	1	1 (domain size > 5 nm)
1	2	2 (domain size between 5-50 nm)
2	2	2 (domain size > 50 nm)

information on the dynamics of molecules in the solid state. A combination of cross polarization (CP) and single-pulse experiments can be very useful for looking at the mobility of amorphous solids and amorphous solid dispersions in the rigid, glassy state versus the rubbery state. ^{1}H T_1 values can also be used to probe the molecular mobility of the amorphous state as a function of temperature, thereby making SSNMR relaxation measurements a valuable addition to the thermal methods traditionally used to measure molecular mobility and physical stability.

Potential hydrogen-bonding interactions in indomethacin:PVP and indomethacin:HPMC amorphous mixtures were discussed in the previous chapter. In this chapter, SSNMR relaxation measurements will be used to further assess the miscibility of these systems. Additionally, the ^{1}H T_1 and $T_{1\rho}$ values of these systems at various temperatures will be examined in order to detect potential differences in mobility and physical stability of amorphous indomethacin as a function of the excipient used, the ratio of the two components, and the preparation method.

6.2 Experimental

6.2.1 Materials

Crystalline indomethacin (γ form) was purchased from Sigma (St. Louis, MO) and used as received. PVP (Kollidon 25, MW 28,000-34,000) was obtained from the BASF

Corporation and HPMC was purchased from Sigma. PVP and HPMC were dried for 12 hours at 105 °C before use. Amorphous indomethacin was prepared using the melt-quench method. Crystalline indomethacin (γ form) was held above its melting point at 170 °C for 10 minutes and then liquid N_2 was poured directly onto the melt to form the amorphous material. Formation of amorphous material was confirmed using DSC, PXRD, and SSNMR spectroscopy. The density of each amorphous material was measured using a Micromeritics AccuPyc 1330 helium pycnometer (Micromeritics Instrument Corporation, Norcross, GA) and was found to be 1.34, 1.21, and 1.28 g/cm^3 for melt-quenched indomethacin, PVP, and HPMC, respectively.

6.2.2 Preparation of physical mixtures

Physical mixtures of melt-quenched amorphous indomethacin and each excipient were prepared. For indomethacin:PVP mixtures, ratios of 4:1, 1:1, and 1:3 w/w were prepared. For indomethacin:HPMC mixtures, ratios of 1:1 and 1:3 w/w were prepared. In all cases, the two materials were lightly ground together in a mortar and pestle to ensure thorough mixing.

6.2.3 Preparation of amorphous solid dispersions

Amorphous solid dispersions of indomethacin:PVP and indomethacin:HPMC were prepared using the melt-quench method. Physical mixtures of indomethacin and each polymer were heated to 170 °C and held for 10 minutes before being quenched with liquid N_2, as described in section 5.3.1. Indomethacin:PVP amorphous dispersions were also

prepared using the solvent-evaporation method. Physical mixtures were dissolved in anhydrous methanol heated to 65 °C. The solvent was removed under vacuum at 50 °C using a Buchi Rotovapor R-215 (Buchi Laboratory Equipment, Switzerland). The recovered products were then dried at 30 °C and under vacuum for 12 hours to ensure complete solvent removal.

6.2.4 Thermal analysis

Modulated DSC (MDSC) analysis using a TA Q1000 (TA Instruments, New Castle, DE) was performed on all samples in order to detect T_g, crystallization, and melting events. Samples of approximately 5-10 mg were weighed into aluminum DSC pans and hermetically sealed. Three pinholes were put in the lid to allow water to escape. Samples were equilibrated at 20 °C and then heated to 200 °C at a rate of 2 °C/min while using a temperature modulation of ±0.5 °C every 60 sec.

Thermogravimetric analysis (TGA) was performed using a TA Q100 (TA Instruments, New Castle, DE) in order to measure the amount of water and/or residual solvent in the amorphous materials. Samples of approximately 10-15 mg were weighed into platinum pans and heated to 150 °C at a rate of 10 °C/min. Total change in sample weight was attributed to loss of water and/or residual solvent.

6.2.5 Solid-state NMR spectroscopy

Solid-state ^{13}C NMR spectra were acquired using a Chemagnetics CMX-300 spectrometer (Varian, Inc., Palo Alto, CA) operating at approximately 75 MHz for ^{13}C. Chemagnetics double-resonance probes equipped with Revolution NMR 7-mm spinning modules (Revolution NMR, LLC, Fort Collins, CO) were used to acquire all spectra. Samples were packed into zirconia rotors and sealed with Kel-F end caps. Spectra were acquired using ramped-amplitude CP[6], MAS[7] with TOSS[8], and SPINAL64[9] decoupling. Single-pulse experiments were performed with background suppression to reduce any signal coming from the spinning module material. 3-methylglutaric acid (MGA) was used to optimize the spectrometer settings and set the reference frequency.[10] A contact time of 2 ms, MAS frequency of 3.0-4.0 kHz, ^{1}H-decoupling field of approximately 55-65 kHz, and a pulse delay of 10-20 s was used to acquire all spectra. ^{1}H T_1 values were measured using saturation recovery experiments and Chemagnetics Spinsight software. ^{1}H $T_{1\rho}$ values were obtained through measurement of the signal intensity as a function of spin-lock duration time and using KaleidaGraph software. In order to perform variable-temperature studies, the temperature scale of the NMR probe when coupled to a variable-temperature stack was calibrated. The chemical shift of ^{207}Pb is known to be highly temperature dependent and has been used as a chemical shift thermometer for SSNMR.[11] Changes in the peak position of lead nitrate were monitored from 293 K to 453 K. A plot of the observed chemical shift versus temperature is shown in Figure 6.1. The experimental slope of 0.7483 ppm/K was found to agree well with theoretical values.

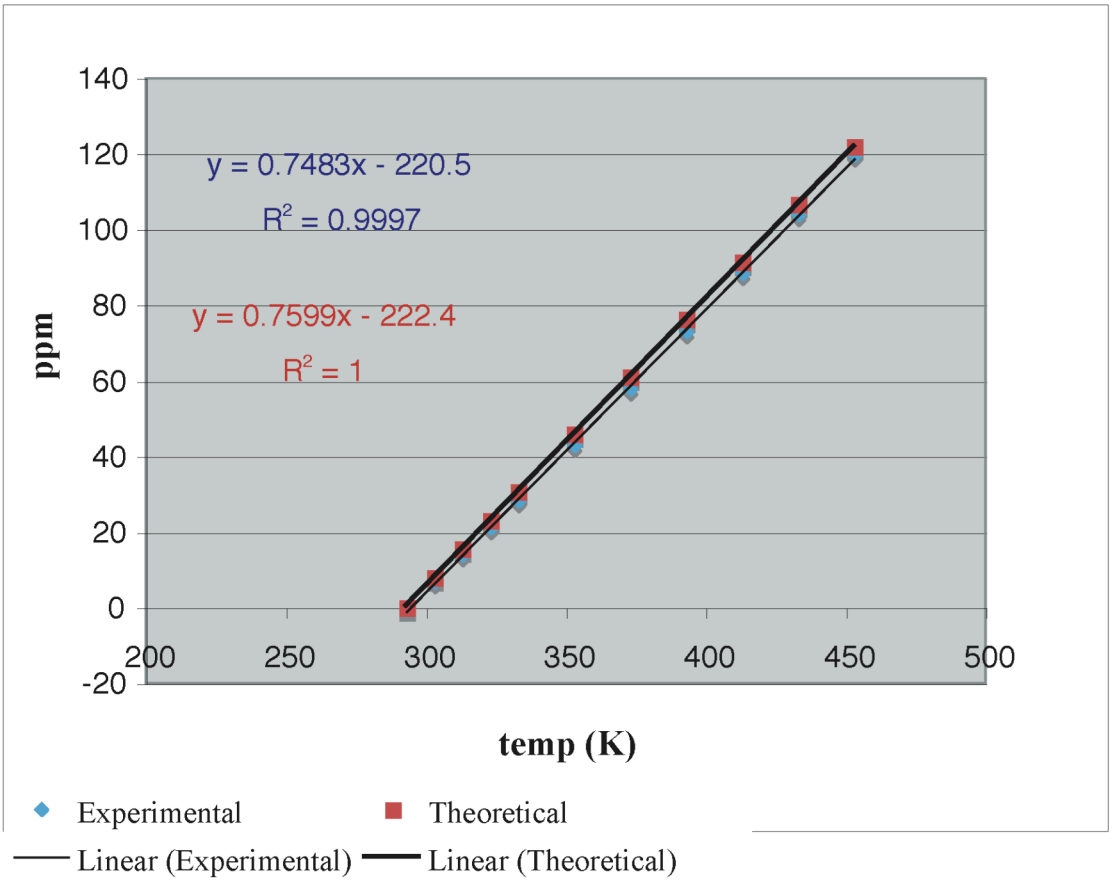

Figure 6.1. Plot of lead nitrate ^{207}Pb chemical shift versus the temperature indicated by the thermocouple on the variable-temperature stack.

6.3 Results and Discussion

6.3.1 Miscibility of indomethacin:PVP mixtures

The ^{13}C SSNMR spectra of melt-quenched amorphous indomethacin and PVP are shown in Figures 6.2a and 6.2b, respectively. The peaks used to measure the relaxation values are highlighted in each spectrum and were chosen based on the lack of interference from peaks of the other component, which avoids the potential for spectral overlap to affect the results. As shown in Figure 6.2, amorphous indomethacin and PVP have very similar ^{1}H T_1 values. Therefore, using T_1 as a measurement of miscibility is not feasible because a common T_1 value in amorphous solid dispersions of indomethacin and PVP does not necessarily indicate that one miscible phase exists. However, the $T_{1\rho}$ values of amorphous indomethacin and PVP were measured as 34 ms and 16 ms, respectively. This two-fold difference indicates that $T_{1\rho}$ relaxation measurements can be used to examine miscibility in amorphous mixtures of these two components.

The $T_{1\rho}$ values of indomethacin and PVP in physical mixtures and in melt-quenched mixtures are shown in Table 6.2a. In physical mixtures, the indomethacin and PVP have different $T_{1\rho}$ values, as expected for a phase-separated mixture. However, in the 1:1 indomethacin:PVP melt-quenched mixture, the $T_{1\rho}$ values of each component are essentially the same, which indicates that a miscible amorphous solid dispersion was formed. In the 4:1 melt-quenched mixture, the values are closer than in the 4:1 physical mixture but are not the same. This suggests that domains 5 to 50 nm in size are present in

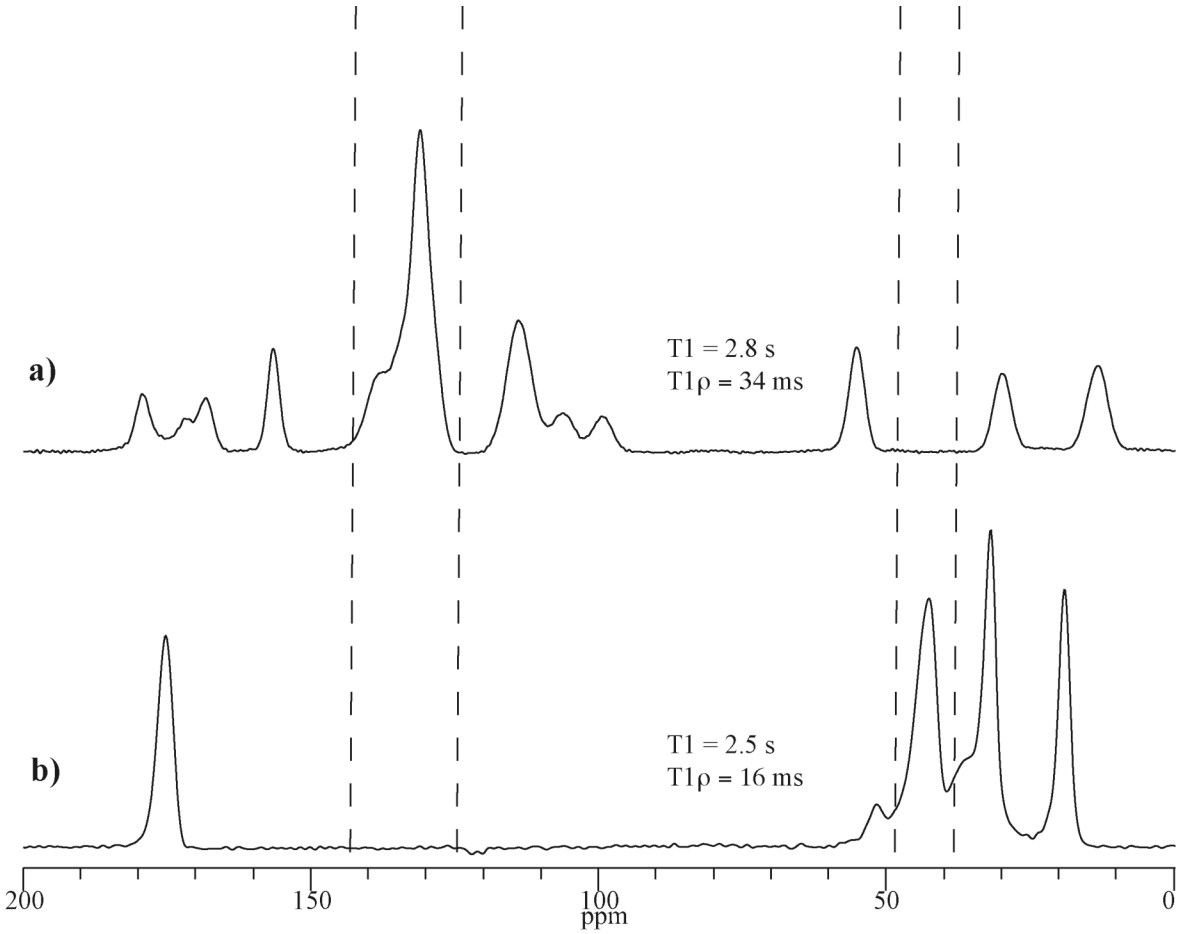

Figure 6.2. ^{13}C SSNMR spectra and relaxation times for (a) melt-quenched amorphous indomethacin and (b) PVP. Peaks used to calculate relaxation times are highlighted.

Table 6.2. Comparison of $T_{1\rho}$ values for indomethacin and PVP in (a) physical mixtures and melt-quenched mixtures, and (b) physical mixtures and solvent-evaporated mixtures. The numbers in parantheses indicate the error associated with fit.

a)

	Physical Mixtures		**Melt-Quenched Mixtures**	
Indomethacin:PVP (w:w)	**T1ρ (ms)**		**T1ρ (ms)**	
	Indomethacin	PVP	Indomethacin	PVP
4:1	24.9 (0.38)	13.0 (0.39)	33.9 (0.61)	27.7 (0.67)
1:1	28.6 (0.54)	12.2 (0.27)	31.8 (0.87)	31.3 (0.27)
1:3	31.3 (0.86)	13.3 (0.19)	17.6 (0.99)	13.8 (0.18)

b)

	Physical Mixtures		**Solvent-Evaporated Mixtures**	
Indomethacin:PVP (w:w)	**T1ρ (ms)**		**T1ρ (ms)**	
	Indomethacin	PVP	Indomethacin	PVP
1:1	28.6 (0.54)	12.2 (0.27)	19.9 (0.45)	17.7 (0.32)
1:3	31.3 (0.86)	13.3 (0.19)	10.5 (0.70)	9.5 (0.14)

the 4:1 melt-quenched mixture. The same holds true for the 1:3 melt-quenched mixture. While the components display different T_{1p} values than those observed in the 1:3 physical mixture, they do not display one common T_{1p} value. Results from MDSC analysis shown in Figure 6.3 suggest that all of the indomethacin:PVP melt-quenched mixtures are miscible, based on the observation of one T_g value which indicates the presence of one, single amorphous phase. However, the results from T_{1p} relaxation measurements indicate that the 1:1 melt-quenched mixture is the only one of the three that may be considered completely miscible. In the 1:3 and 4:1 melt-quenched mixtures, a pure amorphous phase of the component present in excess likely exists, which may be due to incomplete mixing.

The T_{1p} values of indomethacin and PVP in physical mixtures and in solvent-evaporated mixtures are shown in Table 6.2b. The solvent-evaporated mixtures appear to be better mixed than the melt-quenched mixtures, as indicated by the common T_{1p} values observed in both the 1:3 and the 1:1 mixtures. As observed with the melt-quenched mixtures, results from MDSC analysis of the solvent-evaporated mixtures (Figure 6.4) suggest that both of the solvent-evaporated mixtures consist of one amorphous phase, based on the observation of one, single T_g value. The higher T_g value of 107 °C for the 1:3 solvent-evaporated mixture compared to the value of 89 °C for the 1:3 melt-quenched mixture (Figure 6.3) is closer to the theoretical T_g value for ideal mixing predicted by the Gordon-Taylor equation, supporting the conclusion that better mixing of this ratio of components was achieved using solvent evaporation.

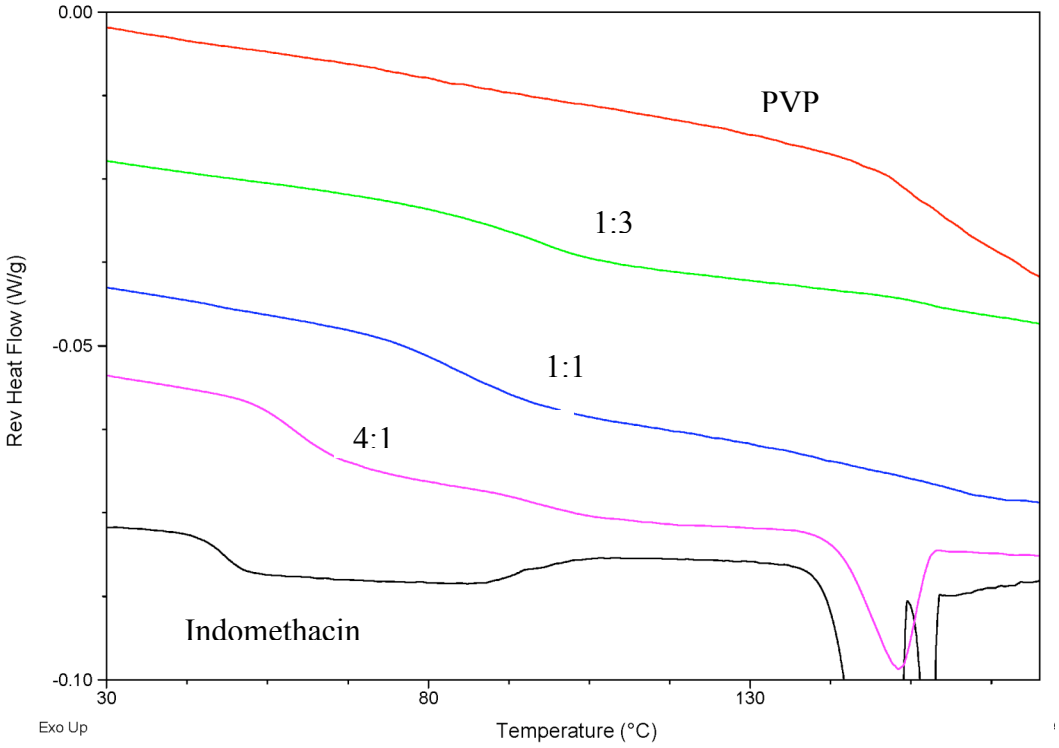

Figure 6.3. MDSC results showing the reversible heat flow and glass transition temperatures for indomethacin, PVP, and indomethacin:PVP melt-quenched mixtures.

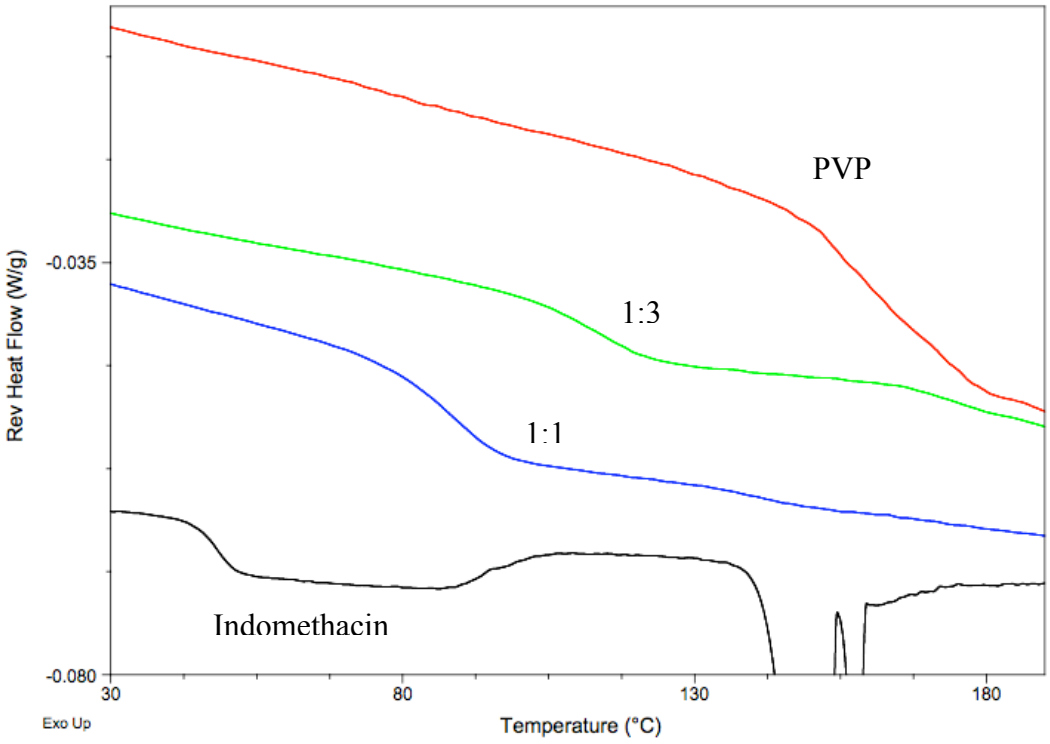

Figure 6.4. MDSC results showing the reversible heat flow and glass transition temperatures for indomethacin, PVP, and indomethacin:PVP solvent-evaporated mixtures.

6.3.2 Miscibility of indomethacin:HPMC mixtures

The ^{13}C SSNMR spectra of melt-quenched amorphous indomethacin and HPMC are shown in Figures 6.5a and 6.5b, respectively. The peaks used to measure the relaxation values are highlighted in each spectrum. The ^{1}H T_1 values of indomethacin and HPMC differ by more than 1 sec, meaning that T_1 relaxation measurements can be used to help determine miscibility, unlike in indomethacin:PVP systems. The $T_{1\rho}$ values of amorphous indomethacin and HPMC were also significantly different with values of 34 ms and 12 ms, respectively. Thus, measurement of both ^{1}H T_1 and $T_{1\rho}$ values can give insight into the number and domain size of amorphous phases present in indomethacin:HPMC mixtures.

The ^{1}H T_1 and $T_{1\rho}$ values of indomethacin and HPMC in physical mixtures and in melt-quenched mixtures are shown in Tables 6.3a and 6.3b, respectively. In physical mixtures, the indomethacin and HPMC have different T_1 and $T_{1\rho}$ values, as expected for a phase-separated mixture. However, in the indomethacin:HPMC melt-quenched mixtures, the two components display common values for both T_1 and $T_{1\rho}$. This evidence, along with the presence of one T_g value for both of these mixtures (Figure 6.6), indicates that both melt-quenched indomethacin:HPMC mixtures consist of one, miscible amorphous phase. This conclusion is further supported by the SSNMR data presented in the previous chapter, which showed complete disruption of the indomethacin hydrogen-bonding interactions when melt-quenched in the presence of HPMC.

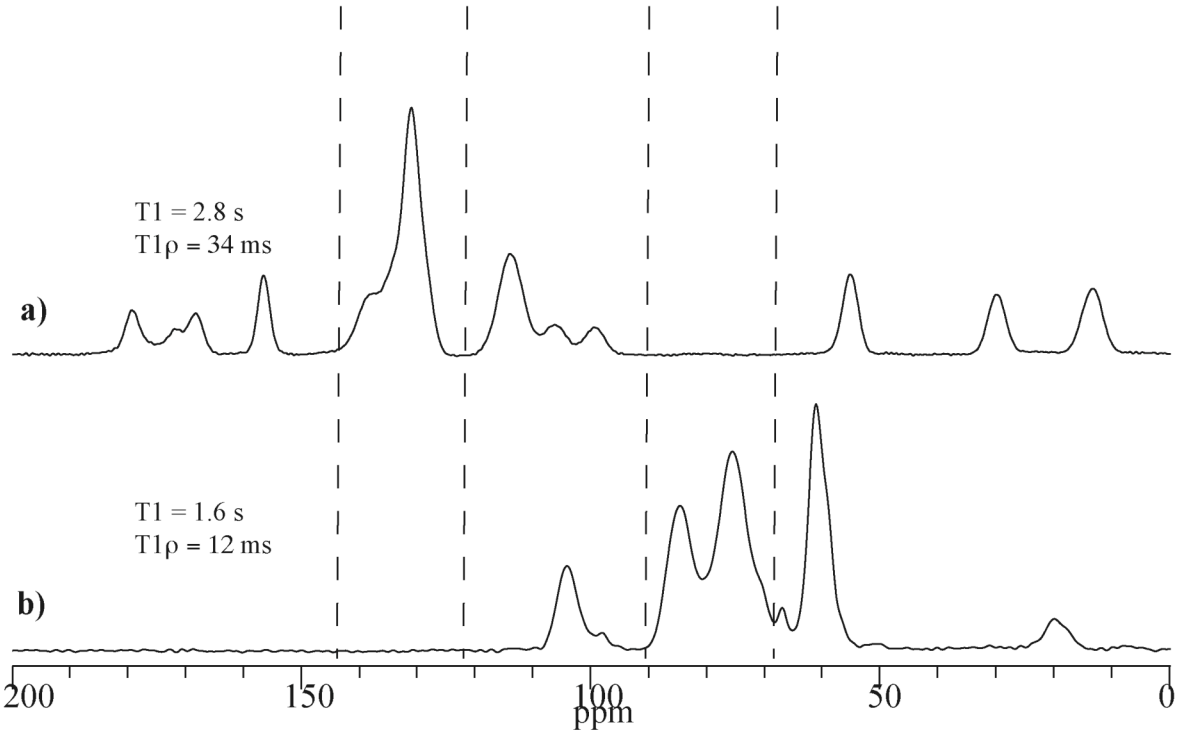

Figure 6.5. ^{13}C SSNMR spectra and relaxation times for (a) melt-quenched amorphous indomethacin and (b) HPMC. Peaks used to calculate relaxation times are highlighted.

Table 6.2. Comparison of relaxation values for indomethacin and HPMC in physical mixtures and melt-quenched mixtures: (a) T_1 values and (b) $T_{1\rho}$ values.

a)

	Physical Mixtures		**Melt-Quenched Mixtures**	
Indomethacin:HPMC (w:w)	**T1 (s)**		**T1 (s)**	
	Indomethacin	HPMC	Indomethacin	HPMC
1:1	2.7	1.6	2.1	1.9
1:3	2.5	1.6	2.3	2.2

b)

	Physical Mixtures		**Melt-Quenched Mixtures**	
Indomethacin:HPMC (w:w)	**T1ρ (ms)**		**T1ρ (ms)**	
	Indomethacin	HPMC	Indomethacin	HPMC
1:1	22.2 (0.50)	10.3 (0.17)	13.8 (0.29)	11.9 (0.18)
1:3	21.6 (0.48)	11.3 (0.15)	13.9 (0.61)	12.4 (0.31)

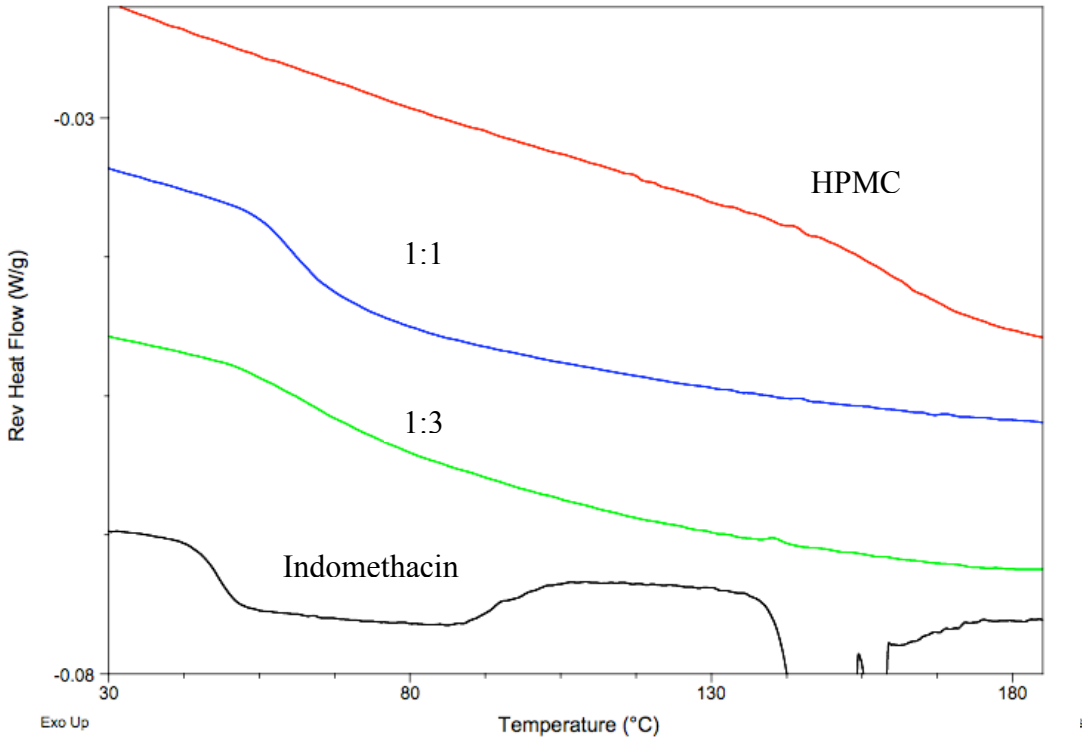

Figure 6.6. MDSC results showing the reversible heat flow and glass transition temperatures for indomethacin, HPMC, and indomethacin:HPMC melt-quenched mixtures.

6.3.3 Mobility of indomethacin in amorphous solid dispersions with PVP

The relaxation behavior of melt-quenched indomethacin, melt-quenched indomethacin:PVP mixtures, and solvent-evaporated indomethacin:PVP mixtures was measured as a function of temperature. Results are shown in Figure 6.7. The $T_{1\rho}$ value of the melt-quenched amorphous indomethacin at 20 °C is ~34 ms, as stated previously. As the temperature is increased, the mobility of the melt-quenched amorphous indomethacin increases dramatically, as indicated by the large decrease in $T_{1\rho}$. At 40 °C, the sample has gained sufficient mobility, and its $T_{1\rho}$ value has decreased to 25 ms. This observation suggests that even at temperatures below its T_g of 47 °C, the melt-quenched amorphous indomethacin displays significant mobility. As the temperature is further increased above the T_g, the $T_{1\rho}$ value continues to rapidly decrease. At 60 °C, which is only ~ 13 °C above T_g, the relaxation time has been reduced to a fraction of its original value. In the 1:1 indomethacin:PVP melt-quenched and solvent-evaporated mixtures, reduced mobility of the indomethacin is expected, because the results shown in this and the previous chapter suggest that stabilizing interactions between the two components result in the formation of a one-phase, miscible amorphous solid dispersion. Indeed, this is what was observed, as shown in Figure 6.7. The $T_{1\rho}$ values for the melt-quenched and solvent-evaporated mixtures do not show any significant decrease until after 60 °C, which indicates that at temperatures below T_g, the mobility of the indomethacin is significantly inhibited by the

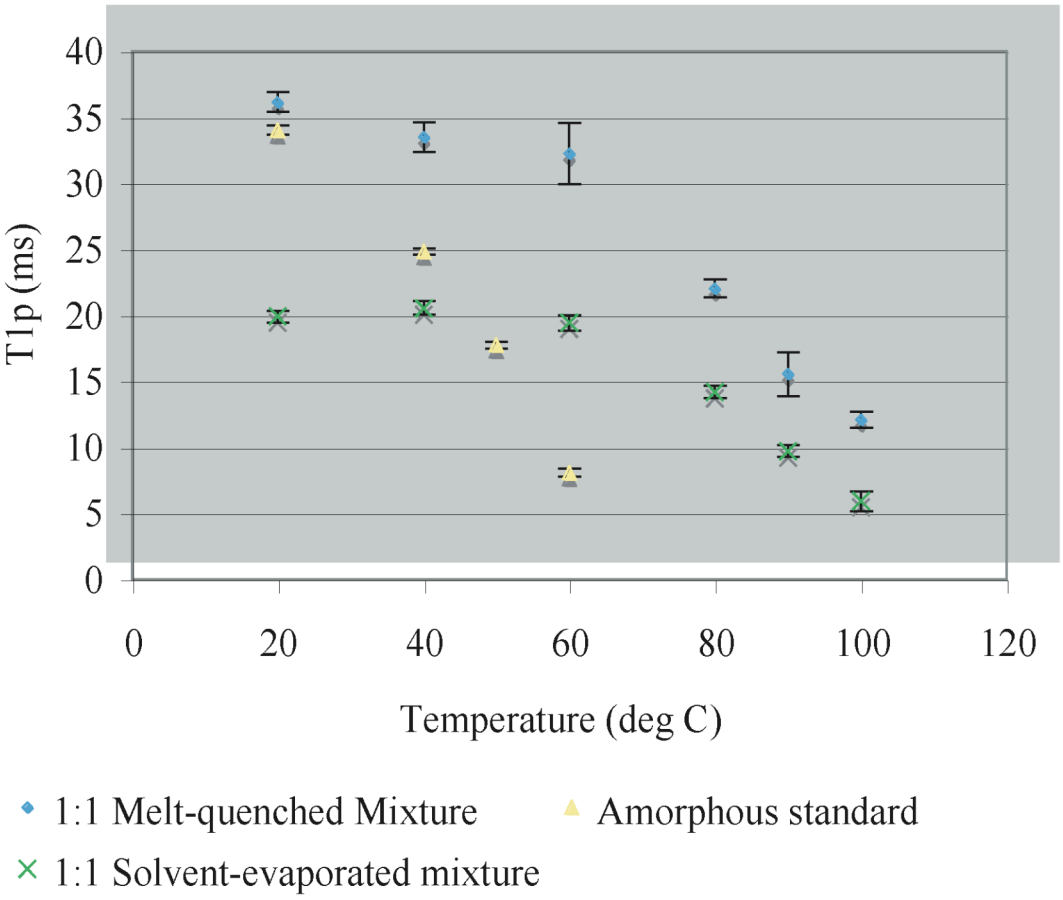

Figure 6.7. T1p values as a function of temperature for melt-quenched amorphous indomethacin, 1:1 indomethacin:PVP melt-quenched mixture, and 1:1 indomethacin:PVP solvent-evaporated mixture.

PVP. Mobility does not increase until temperatures above the T_g of the mixtures are reached. The melt-quenched and solvent-evaporated indomethacin:PVP mixtures appear to exhibit increased mobility at similar rates. This is not surprising when considering the T_g values of these two mixtures are very close (78 °C and 81 °C).

6.3.4 Mobility of indomethacin in amorphous solid dispersions with HPMC

The relaxation behavior of the melt-quenched indomethacin:HPMC mixtures was also measured as a function of temperature. Results are shown in Figure 6.8. The $T_{1\rho}$ value of the 1:1 melt-quenched mixture begins to decrease before the T_g of 56 °C is reached, and shows an increased rate of decline at temperatures above T_g. For instance, at 60 °C, which is only slightly above T_g, the relaxation time is less than half of its value at 20 °C. However, it is interesting that the 1:3 melt-quenched mixture does not appear to display this same behavior. Rather, the $T_{1\rho}$ value shows only a slight decrease with increased temperature, suggesting that the 1:3 melt-quenched mixture is much less mobile than the 1:1 melt-quenched mixture. At 60 °C, which is above the measured T_g, the $T_{1\rho}$ value is only slightly lower than what it was at 20 °C. This is significant because based on a common T_g value (Figure 6.6) and the similar SSNMR spectra shown in the previous chapter, one would expect these two melt-quenched indomethacin:HPMC mixtures to display identical behavior. However, the decreased mobility of the 1:3 melt-quenched mixture could potentially result in greater physical stability and lower tendency to

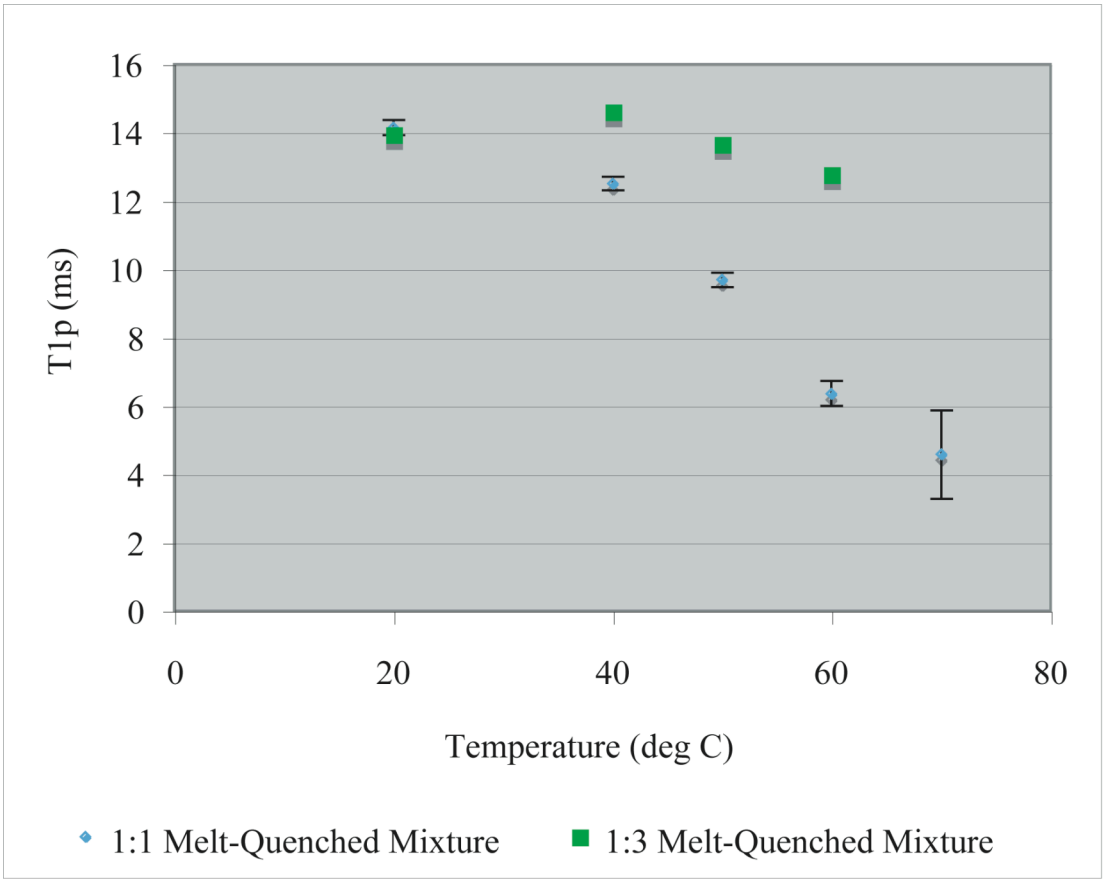

Figure 6.8. T1p values as a function of temperature for 1:1 indomethacin:HPMC and 1:3 indomethacin:HPMC melt-quenched mixtures.

recrystallize. Experiments to monitor the crystallization rate of these two melt-quenched mixtures over time would have to be performed in order to confirm or deny this, but previous studies have shown that SSNMR relaxation measurements do lead to an improved estimate of amorphous physical stability compared to DSC T_g determination.[12]

6.3.5 Comparison of SSNMR spectra collected using CP and single-pulse experiments

CP and single-pulse experiments are complementary techniques in that CP allows observation of rigid components whereas single-pulse experiments detect mobile components. Therefore, both CP and single-pulse experiments were performed on some of the amorphous indomethacin:excipient mixtures at temperatures below and above T_g. The SSNMR spectra of the 1:1 indomethacin:HPMC melt-quenched mixture collected using CP and at temperatures below T_g are shown in Figure 6.9. No significant changes between these spectra are observed. However, once above the T_g, the peaks corresponding to indomethacin being to drastically decrease in intensity, and essentially disappear at 70 °C, as shown in Figure 6.10. These peaks disappear because they are too mobile to be observed in the CP spectra. The single-pulse spectra collected at temperatures above the T_g are shown in Figure 6.11. Here, the mobile components are observed, and the "liquid-like" indomethacin peaks can be seen as sharp signals at a temperature of 120 °C, which indicates extremely high mobility. In the 1:1 melt-quenched indomethacin:PVP mixture, the loss of signal from the rigid components in the CP spectra does not occur until 120 °C,

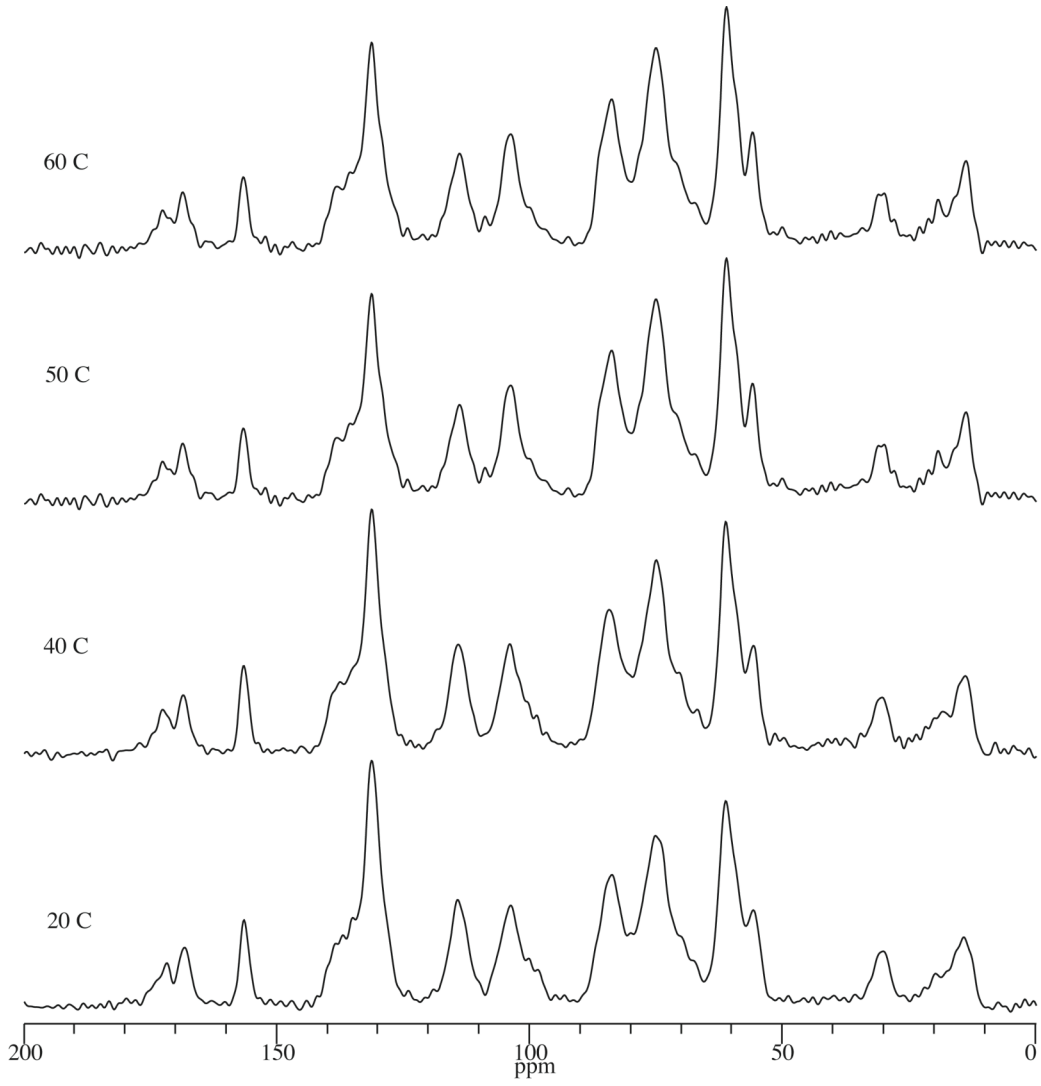

Figure 6.9. ^{13}C SSNMR spectra of the 1:1 indomethacin:HPMC melt-quenched mixture collected using CP and at temperatures below T_g.

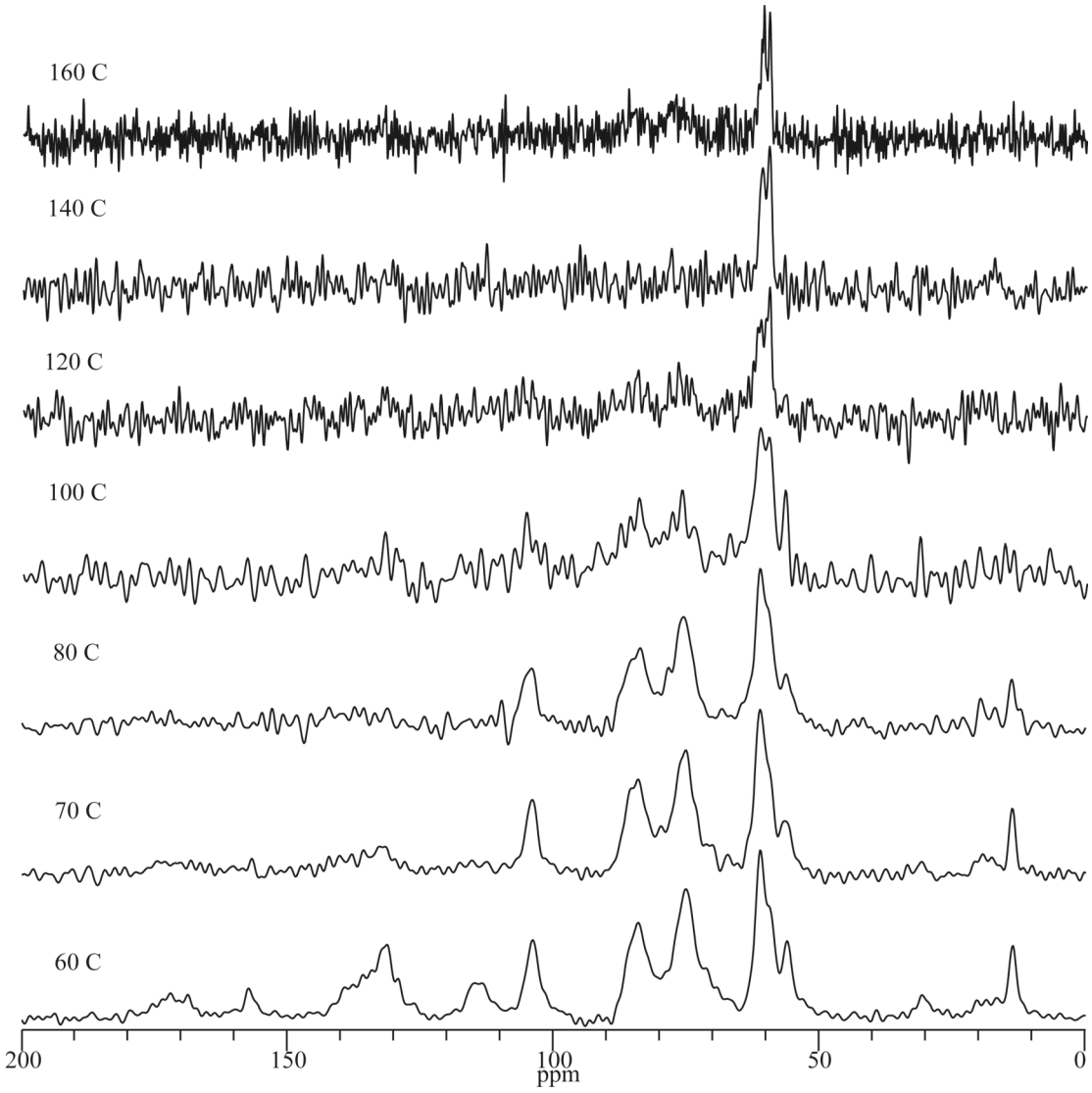

Figure 6.10. ^{13}C SSNMR spectra of the 1:1 indomethacin:HPMC melt-quenched mixture collected using CP and at temperatures above T_g.

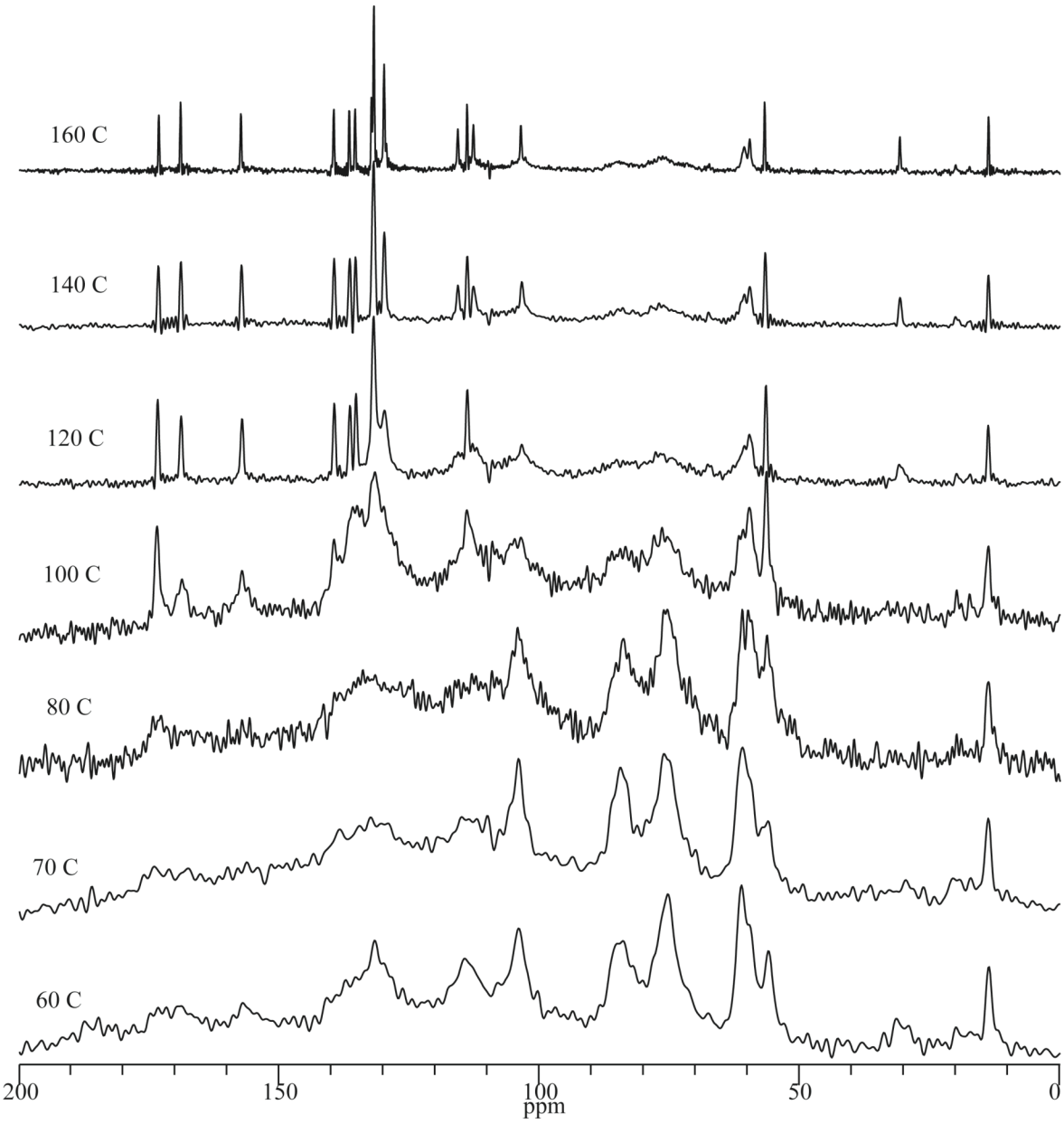

Figure 6.11. ^{13}C SSNMR spectra of the 1:1 indomethacin:HPMC melt-quenched mixture collected using single-pulse experiments and at temperatures above T_g.

and the mobile indomethacin peaks in the single-pulse experiments do not appear until a temperature of 160 °C is reached (data not shown). Therefore, it can be concluded that at temperatures above T_g the indomethacin:HPMC melt-quenched mixtures display greater mobility than the indomethacin:PVP melt-quenched mixtures.

6.4 Conclusions

Based on ^1H T_1 and $T_{1\rho}$ measurements, indomethacin appears to form a miscible amorphous solid dispersion with PVP in 1:1 and 1:3 solvent-evaporated mixtures and in a melt-quenched mixture when the weight ratio of the two componentsis 1:1. The melt-quenched indomethacin:PVP mixtures that were prepared at weight ratios of 1:3 and 4:1 appear miscible by DSC but only partially miscible by SSNMR relaxation measurements. Both of the melt-quenched indomethacin:HPMC mixtures consist of one amorphous phase by both DSC and SSNMR. The mobility of melt-quenched amorphous indomethacin is significantly reduced in the presence of both PVP and HPMC. However, with HPMC, the mobility of a 1:1 melt-quenched mixture appears to decrease slightly at temperatures below the T_g and more rapidly at temperatures above the T_g, while that of the 1:3 melt-quenched mixture does not show any significant decrease at all, suggesting that this weight ratio may result in improved physical stabilization of indomethacin in the amorphous state. CP and single-pulse experiments show that while amorphous indomethacin exhibits increased mobility at temperatures above T_g in both PVP and HPMC mixtures, the indomethacin

becomes extremely mobile and “liquid-like” at lower temperatures when melt-quenched with HPMC than when melt-quenched with PVP, suggesting that the PVP does a better job of reducing the mobility of indomethacin when prepared at a 1:1 ratio.

6.5 References

1. Krause, S, Iskander M. 1977. Phase separation in styrene-a-methyl styrene block copolymers. In Klempner D, Frisch KC, editors. Polymer science and technology. Vol. 10. New York: Plenum Press. p 231-243.

2. Newman A, Engers D, Bates S, Ivanisevic I, Kelly RC, Zografi G. 2008. Characterization of amorphous API:polymer mixtures using X-ray powder diffraction. J Pharm Sci 97(11):4840-4856.

3. Rumondor ACF, Ivanisevic I, Bates S, Alonzo DE, Taylor LS. 2009. Evaluation of drug-polymer miscibility in amorphous solid dispersion systems. Pharm Res 26(11):2523-2534.

4. Aso Y, Yoshioka S, Miyazaki T, Kawanishi T, Tanaka K, Kitamura S. 2007. Miscibility of nifedipine and hydrophilic polymers as measured by 1H-NMR spin-lattice relaxation. Chem Pharm Bull 55(8):1227-1231.

5. Hancock BC, Shamblin SL, Zografi G. 1995. Molecular mobility of amorphous pharmaceutical solids below their glass transition temperatures. Pharm Res 12(6):799-806.

6. Pines A, Gibby MG, Waugh JS. 1973. Proton-enhanced NMR of dilute spins in solids. J Chem Phys 59:569-590.

7. Andrew ER. 1971. Narrowing of NMR spectra of solids by high-speed specimen rotation and the resolution of chemical shift and spin multiplet structures for solids. Prog Nucl Mag Res 8:1-39.

8. Dixon WT, Schaefer J, Sefcik MD, Stejskal EO, McKay RA. 1982. Total suppression of sidebands in CPMAS carbon-13 NMR. J Magn Reson 49:341-345.

9. Fung BM, Khitrin AK, Ermolaev K. 2000. An improved broadband decoupling sequence for liquid crystals and solids. J Magn Reson 142:97-101.

10. Barich DH, Gorman EM, Zell MT, Munson EJ. 2006. 3-methylglutaric acid as a ^{13}C solid-state NMR standard. Solid State Nucl Magn Reson 30:125-129.

11. Bielecki A, Burum DP. 1995. Temperature dependence of ^{207}Pb MAS spectra of solid lead nitrate. An accurate, sensitive thermometer for variable-temperature MAS. J Magn Reson 116(2):215-220.

12. Forster AH, Apperley DC, Hempenstall J, Lancaster RW, Rades T. 2003. Investigation of the physical stability of amorphous drug and drug/polymer melts using variable temperature solid state NMR. Pharmazie 58:761-762.

Chapter 7

Summary and Future Work

7.1 Summary

Throughout this dissertation, solid-state NMR spectroscopy was used to examine the structure and properties of pharmaceutically relevant amorphous materials. Various types of solid-state NMR experiments were used to investigate numerous aspects of these materials, such as structure, crystalline/amorphous content, molecular weight, water content, interactions with other molecules, and molecular mobility. Results presented in this dissertation highlight the benefit of using solid-state NMR spectroscopy in conjunction with other techniques in order to gain a fuller understanding of the solid-state properties of pharmaceutical samples.

Chapter 1 supplied background information on the importance of studying pharmaceuticals in the solid state and described potential problems associated with oral solid dosage forms. The pharmaceutical prevalence of amorphous and/or semi-crystalline materials was outlined and the drawbacks and benefits of formulating a drug in the amorphous state were also explained. Commonly used techniques for analyzing these types of solid-state pharmaceuticals were described.

In Chapter 2, the basic theory of NMR spectroscopy was briefly outlined. Differences between solution-state and solid-state NMR spectroscopy were discussed, and the need to implement techniques such as cross polarization (CP), decoupling, magic-angle spinning (MAS), and total suppression of spinning sidebands (TOSS) when acquiring NMR data on solid samples was explained. Advantages and disadvantages of solid-state NMR spectroscopy in regards to its use during the drug development process were also

described and potential areas where solid-state NMR experiments could increase the pharmaceutical scientist's understanding of the nature of amorphous systems were highlighted.

Chapter 3 described the application of solid-state NMR spectroscopy to the analysis of common polysaccharide-based excipients. Naturally derived excipients that were studied included the following: alginic acid and sodium alginate, carrageenans, starch and starch hydrolysis derivatives such as maltodextrin and corn syrup solids, microcrystalline cellulose, and cellulose-based derivatives such as hydroxyethylcellulose, (HEC), hydroxypropylcellulose (HPC), and hydroxypropylmethylcellulose (HPMC). Results showed that although the peaks in the solid-state NMR spectra of these samples were broad, the resolution was sufficient for accurate form identification and differentiation. Relaxation measurements provided unique information on starch derivatives. As the extent of hydrolysis increased, the ^{1}H T_1 value also increased. A linear correlation between T_1, the peak area of new signals, and the DE value of maltodextrin and corn syrup solids samples was observed. This finding suggests that solid-state NMR spectroscopy could be an excellent non-destructive and rapid tool for determining and monitoring any changes in the relative degree of hydrolysis among multiple starch samples.

In Chapter 4, sodium alginate, an excipient presented in Chapter 3, was extensively studied. Experiments to explore the potential for solid-state NMR parameters to be correlated to important functionally related characteristics of sodium alginate were performed. The ability to detect variations in monomer content among different grades of sodium alginate using solid-state NMR was demonstrated. During these studies, hydration

of the alginate was found to be a fast and simple way to increase the resolution of signals in the solid-state NMR spectra. Differences in intrinsic viscosity and molecular weight of samples with similar monomer content were correlated to solid-state NMR relaxation times. Variations in water content were also detected using relaxation measurements. Solid-state NMR proved to be sensitive and selective enough to detect changes in sodium alginate when diluted with other excipients such as lactose and HPMC and compressed into a tablet.

Chapters 5 and 6 involved analysis of the poorly water-soluble drug indomethacin in the amorphous state and in amorphous solid dispersions with PVP and HPMC. Differences in the hydrogen-bonding networks of the crystalline γ and α forms and the melt-quenched amorphous form of indomethacin were analyzed. Disruptions of this network when intimately mixed with PVP or HPMC were detected. Solid-state NMR data supported the conclusion that indomethacin forms hydrogen bonds with PVP and HPMC at the expense of forming hydrogen bonds with other indomethacin molecules. Deviations from ideal mixing, reflected by experimental T_g values less than those theoretically predicted, indicated that the strength and/or number of the hydrogen bonds formed between indomethacin and each polymer are less than those occurring in indomethacin alone, but the significant increase in entropy upon mixing is what facilitates the formation of an amorphous solid dispersion.

In Chapter 6, the miscibility and mobility of the indomethacin amorphous solid dispersions analyzed in Chapter 5 was probed using solid-state NMR relaxation

measurements. Based on ^{1}H T_1 and $T_{1\rho}$ values, indomethacin appeared to form a miscible amorphous solid dispersion with HPMC at all conditions studied, with PVP in 1:1 and 1:3 solvent-evaporated mixtures, and in a 1:1 melt-quenched mixture with PVP. Melt-quenched indomethacin:PVP mixtures that were prepared at weight ratios of 1:3 and 4:1 appeared miscible by DSC but only partially miscible by SSNMR relaxation measurements, suggesting that better mixing of the two components was achieved through the solvent-evaporation technique. The mobility of melt-quenched amorphous indomethacin was significantly reduced in the presence of both PVP and HPMC. Differences in the mobility of indomethacin in amorphous solid dispersions were measured as a function of temperature. Results showed that solid-state NMR relaxation measurements are very useful for detecting differences in the mobility of amorphous solid dispersions both below and above T_g. Therefore, solid-state NMR experiments can potentially be used to predict the relative physical stability of amorphous solid dispersions as a function of excipient, weight ratio, and preparation method.

7.2 Future Work

The data presented in Chapter 3, while informative, barely scratches the surface in terms of what solid-state NMR spectroscopy can add to the current understanding of excipients. With the groundwork laid, future studies should involve larger sample sets and

principle component analysis in order to determine exactly which solid-state NMR variables, if any, can be related to an important property of the excipient. Ideally, the extensive analysis of sodium alginate (Chapter 4) that was done in attempts to correlate solid-state NMR parameters to characteristics affecting functionality should be performed on all types of excipients. For instance, in the case of sodium alginate, the factors affecting its function in pharmaceutical formulations are monomer content and molecular weight. In other excipients, such as microcrystalline cellulose, the factors affecting functionality are particle size and water content. The studies presented in this dissertation suggest that solid-state NMR relaxation measurements can be used to monitor changes in water content among microcrystalline cellulose samples, but an extensive study on multiple samples should be performed. Additionally, it would be interesting to see if some sort of correlation between flowability or compressibility of excipients such as microcrystalline cellulose or lactose and solid-state NMR parameters such as linewidths or relaxation times exists. The ultimate goal would be to create a database of solid-state NMR parameters that can be used to analyze variations in excipients and aid in excipient selection during formulation development.

Future work involving solid-state NMR spectroscopy of amorphous solid dispersions should be performed to address various aspects of these systems. For instance, correlation of solid-state NMR relaxation values to measured rates of recrystallization would be extremely useful for determining whether or not solid-state NMR can be used to predict the relative physical stability of multiple dispersions. Stability studies on the indomethacin amorphous solid dispersions discussed in this dissertation

should be performed and compared to the relative mobility determined using relaxation measurements. Additionally, it would be interesting to compare the melt-quench and solvent-evaporation techniques to other preparation methods such as ball milling or cryogrinding. As stated in Chapter 5, cryogrinding of indomethacin did not appear to create stable amorphous material. However, could cryogrinding in the presence of PVP or HPMC facilitate the production of the amorphous state through the formation of stabilizing drug-excipient interactions? If so, would this mixture display similar mobility and stability as mixtures prepared via other methods? These are just some of the potential questions that can be probed with further experimentation.

In order to better understand the nature of the hydrogen-bonding interactions in indomethacin:PVP and indomethacin:HPMC mixtures, additional mixtures prepared at various weight ratios encompassing those already discussed in this dissertation should be analyzed. Furthermore, it would be helpful to compare our solid-state NMR data to data obtained using IR and Raman spectroscopy. While water content was controlled and monitored during our studies, it would be interesting to analyze solid dispersions containing various amounts of water. Differences in peak shifts, linewidths, and relaxation measurements could potentially provide insight into the role of water in phase separation.

Finally, other model compounds besides indomethacin should be identified. Compounds that are known to phase separate or crystallize from amorphous solid dispersions would be ideal for solid-state NMR analysis, as information gained via variable-temperature studies and relaxation measurements could provide insight into changes in miscibility or mobility that occur.

Appendix

Investigations into Aspirin Polymorphism

A.1 Introduction

The question of whether or not aspirin exists in more than one crystal form has been heavily debated in the literature.[1-8] The existence of other aspirin forms is supported by theoretical calculations, but it has been difficult to generate pure forms experimentally. Analysis of polymorphs typically relies on having pure forms, as there are few analytical techniques with the ability to characterize complex mixtures. Therefore, characterization of potential aspirin polymorphs has been complicated and inconclusive. The purpose of this work was to use SSNMR spectroscopy combined with thermal and diffraction techniques to provide the physical evidence that is necessary to show that other aspirin polymorphs do or do not exist.

SSNMR spectroscopy is a particularly useful technique for the study of polymorphism because slight changes in molecular conformation or molecular arrangement can alter the local electronic environment and give rise to different chemical shifts. Therefore, SSNMR is sensitive to differences in both molecular conformation and in crystal packing. Molecular conformation can also be probed by using the chemical shift principal values to obtain detailed orientational information. Unlike PXRD, which is an averaging technique, SSNMR can be used to probe different functional groups of a molecule. While PXRD is highly sensitive to "long range" order, SSNMR is highly sensitive to local chemical environment. Stephenson et al. were able to show that different forms of erythromycin were discernible by SSNMR, but not by PXRD, most likely due to slight differences in crystallographic packing that were only observable by SSNMR.[9]

Padden et al. have investigated neotame polymorphs using both SSNMR and PXRD.[10] The authors found that ^{13}C CP-MAS SSNMR was able to detect several different forms, while PXRD was unable to detect any changes in diffraction patterns between forms. Thus, for thorough solid-state analysis, a combination of techniques is necessary, as data from only one technique can at times be insufficient.

As stated earlier, the polymorphism of aspirin has been heavily debated in the literature. The known crystal structure (Form 1) is based on centrosymmetric carboxylic acid dimers in a nonplanar conformation, as shown in Figure A.1. There are three bonds about which rotation is possible as well as opportunities for hydrogen bonding, all of which can allow for conformational polymorphism.

Mitchell and Saville demonstrated that commercial aspirin obtained from various sources displayed different dissolution rates but were unable to conclude if the differences were due to variations in crystal size and habit, crystal defects, or the existence of polymorphs.[1] Tawashi et al. reported the existence of aspirin in two polymorphic forms, based on different melting points and PXRD patterns.[2] However, when Mitchell and Saville repeated Tawashi's work, they were unable to produce aspirin crystals with distinguishable PXRD patterns.[3] Chang et al. investigated different crystal habits of aspirin, and were able to use ^{13}C CP-MAS SSNMR to show that the change in morphology was not due to a change in crystal packing, as the spectra of all the different habit forms were identical.[5] It has also been suggested by Mulley et al. that it is not polymorphism but rather the amount and location of salicylic acid impurity within the aspirin's crystal lattice that causes changes in melting point.[4]

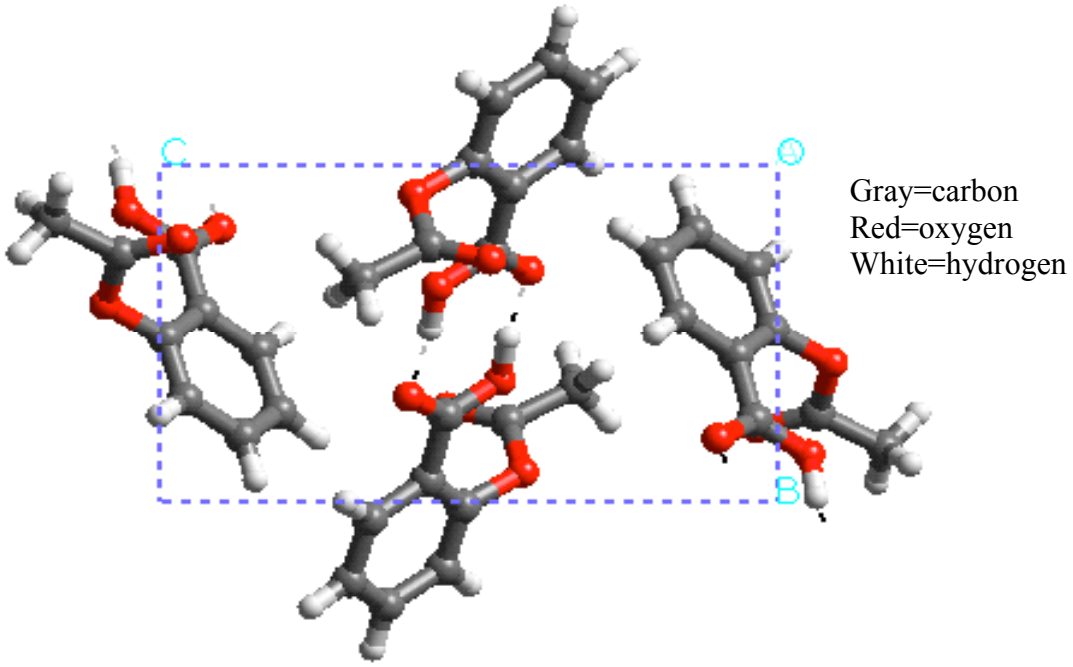

Figure A.1 Crystal structure of aspirin.

Due to the lack of conclusive physical data, numerous theoretical and experimental research groups are still investigating the existence of aspirin polymorphs. Computational chemists have reported that semi-empirical and *ab initio* calculations predict a number of other low energy structures based on a planar conformer.[11-12] More recently, Vishweshwar et al. have reported the isolation and structural characterization of a polymorph of aspirin, obtained by co-crystallization with levetiracetam or acetamide.[6] However, Bond et al. have stated that the error in the experimental diffraction data collected by Vishweshwar and co-workers is too great to conclude that a polymorph has been isolated.[7-8] During the course of an earlier research project in our laboratory, SSNMR data suggested formation of aspirin polymorphs during the lyophilization process. The work presented here was motivated by this interesting observation.

The overall objective of this work was to use SSNMR experiments to provide much needed insight into the conformation of aspirin produced by various techniques. Differences in chemical shifts indicate the formation and presence of polymorphs, and relaxation measurements can be used to determine if mixtures of polymorphs are intimately mixed, as intimate mixing results in similar T_1 relaxation times. Complementary techniques traditionally used for polymorph identification were also performed.

A.2 Experimental

A.2.1 Materials

Bulk aspirin was purchased from Sigma (St. Louis, MO). In attempts to generate polymorphs, aspirin samples were produced in two ways. The first was lyophilization from water at a concentration of 1 mg/mL, which was performed using a Virtis Advantage Benchtop Freeze Dryer (SP Industries, Warminster, PA). The second was rapid recrystallization from hot acetonitrile (75 °C). For two-dimensional and chemical shift tensor studies, aspirin with a ^{13}C labeled methyl group was synthesized from salicylic acid and labeled acetic anhydride according to the scheme outlined in Figure A.2.

A.2.2 Thermal analysis

Differential Scanning Calorimetry (DSC) was performed using a TA Q1000 (TA Instruments, New Castle, DE). Samples of 5-10 mg were packed into aluminum pans and heated from ambient temperature to 200 °C at a rate of 10 °C/min. Thermogravimetric analysis (TGA) was performed in order to determine the amount of solvent present in each sample. Samples of ~10-20 mg were heated to 200 °C at a rate of 10 °C/min. Total weight loss was attributed to loss of solvent.

A.2.3 X-ray diffraction

Bulk and lyophilized aspirin samples were analyzed using a Scintag X2 Powder X-ray Diffractometer (Scintag Inc., Cupertino, CA). Samples were packed into stainless steel

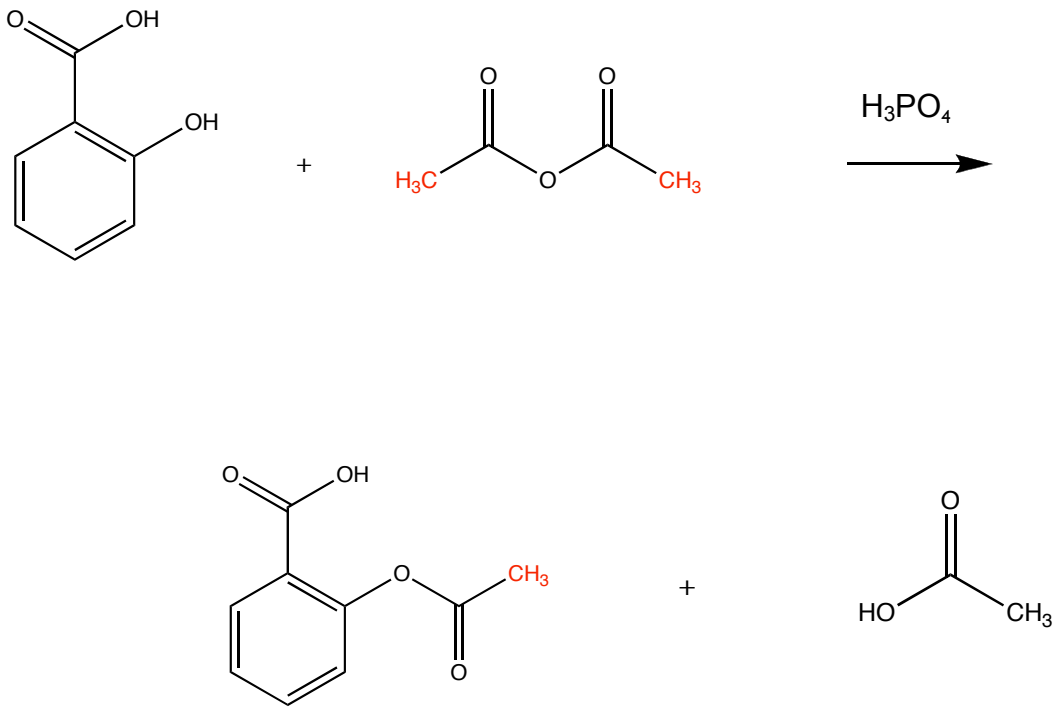

Figure A.2. Synthesis of aspirin with a ^{13}C labeled methyl group.

sample holders that were spun during data collection. Analysis was performed from 2.0 to 42.0 deg 2-theta using a scan rate of 0.02 deg 2-theta per minute and a dwell time of 2 sec. Synchrotron diffraction analysis of these samples was performed by Dr. Yuegang Zhang through the University of Minnesota.

A.2.4 Solid-state NMR spectroscopy

^{13}C solid-state NMR spectroscopy was performed using either a Chemagnetics CMX-300 (Varian, Inc., Fort Collins, CO) or Tecmag Apollo-HF-3 (Tecmag, Inc., Houston, TX) spectrometer operating at approximately 75 MHz for ^{13}C. Chemagnetics probes fitted with 7-mm Revolution NMR (Revolution NMR, LLC, Fort Collins, CO) spinning modules were used. Samples were packed in 7-mm zirconia rotors using Teflon endcaps and spun at the magic angle at a frequency of 4 kHz. Spectra were acquired using variable amplitude cross polarization (CP) or ramped CP, total sideband suppression (TOSS), and high power ^{1}H decoupling with two-pulse phase modulation (TPPM) or SPINAL-64 decoupling schemes. The effect of temperature on the SSNMR spectrum of lyophilized aspirin was also investigated. Two-dimensional SSNMR experiments, chemical shift tensor studies, and FIREMAT experiments were also performed. For chemical tensor studies, the ^{13}C labeled sample was lyophilized and spun at 250 Hz in order to yield enough spinning sidebands for accurate tensor component analysis. FIREMAT experiments were performed on natural abundance aspirin in order to compare the chemical shift tensor values of the two samples. Two-dimensional SSNMR experiments performed on the ^{13}C labeled lyophilized sample monitored the transfer of

magnetization between the two methyl carbons via proton-mediated spin diffusion. MAS speed of 4 kHz and a mixing time of 2 s was employed.

A.3 Results

Lyophilization of aspirin results in a mixture of two forms by SSNMR. Figure A.3 highlights the major differences seen between the SSNMR spectra of the bulk aspirin and the lyophilized sample. There is a distinct splitting in the methyl peak and appearance of a slight shoulder on a peak in the aromatic region of the SSNMR spectrum of the lyophilized form. The ^{1}H T_1 relaxation times were also measured. Aldrich aspirin has a relaxation time of ~60 s, while the lyophilized material has a relaxation time of ~10 s.

Differences in the diffraction patterns of the bulk material and the lyophilized material could not be observed using PXRD analysis. This suggests that the difference between the two forms is too small to cause a change in long-range order. Because of this, the materials were also analyzed using Synchrotron X-Ray Powder Diffraction, which is a more powerful technique. Synchrotron data presented in Figure A.4 clearly shows that a mixture of two forms exists in the lyophilized material, as evidenced by additional peaks at ~ 8 deg 2-theta and just above 10 deg 2-theta in the pattern of this sample compared to that of the bulk aspirin.

To complement the SSNMR and Synchrotron data, the material was also analyzed using DSC. The lyophilized material consistently melts ~6-7 °C lower than bulk Aldrich

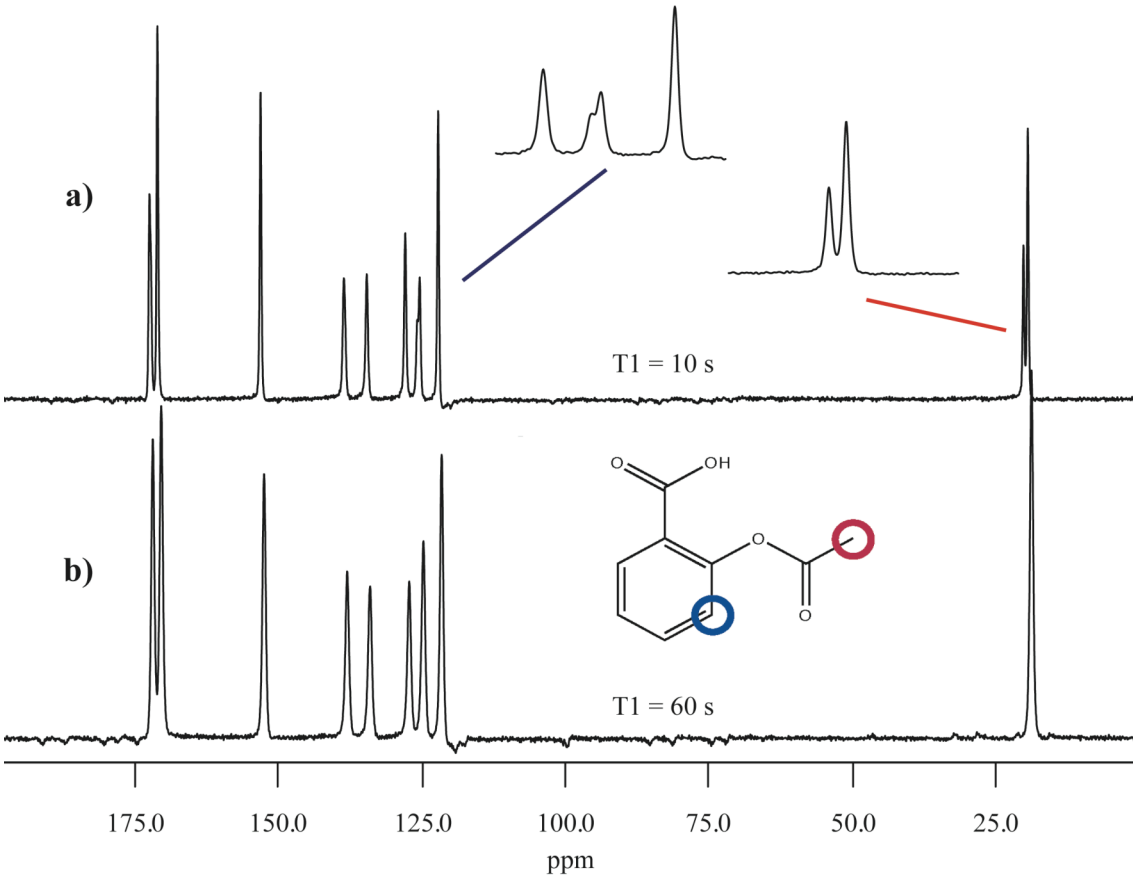

Figure A.3. SSNMR spectrum of (a) lyophilized aspirin and (b) bulk aspirin received from Sigma.

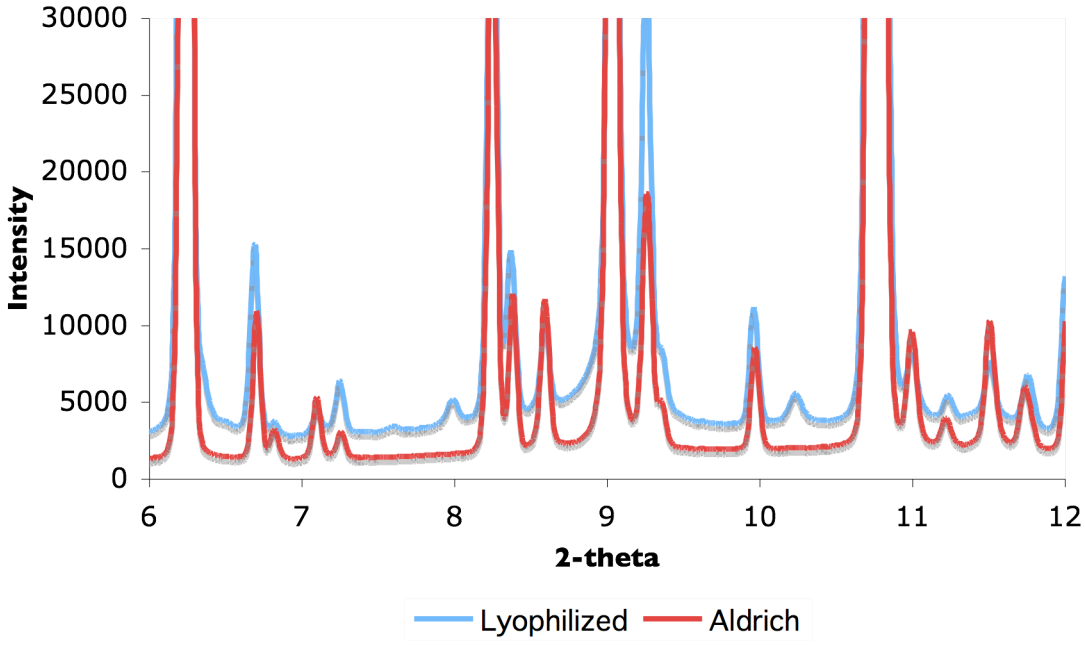

Figure A.4. Synchrotron diffraction analysis of bulk aspirin and lyophilized aspirin.

aspirin, as shown in Figure A.5. Unfortunately, aspirin degrades upon melting, so a distinct melt for each form that is present in the mixture is unable to be observed.

TGA and Karl Fischer analysis were performed to rule out the possibility of hydrate formation. The only weight loss observed by TGA corresponded to degradation upon melting, most likely due to the formation of volatile acetic acid. Karl Fischer analysis showed that the lyophilized material contains ~1.75% water compared to ~0.6% in Aldrich aspirin. This is not enough water to form a stoichiometric hydrate, as 9.1 and 4.55% water would be required for a monohydrate and a hemi-hydrate, respectively. Also, if the mixture did, in fact, contain a hydrate, a decrease in relaxation time, which is what is observed, would not be expected. If a tightly bound hydrate formed during lyophilization, hydrogen bonding would result in a rigid structure, which would be less mobile and, therefore, have a longer relaxation time.

Studies to determine whether or not the changes in DSC and SSNMR could be due to formation of crystal defects were also performed. In order to do this, aspirin was cryoground for various amounts of time. Shorter relaxation times were observed, which can be attributed to smaller particle size and crystal defects. However, no changes in the SSNMR spectral features were observed, even for samples that were cryoground for 60 minutes. DSC of the cryoground samples showed that the melting temperature of the cryogound samples did not differ from that of the original bulk aspirin material. These results suggest that the changes in the SSNMR spectrum and reduction in melt temperature

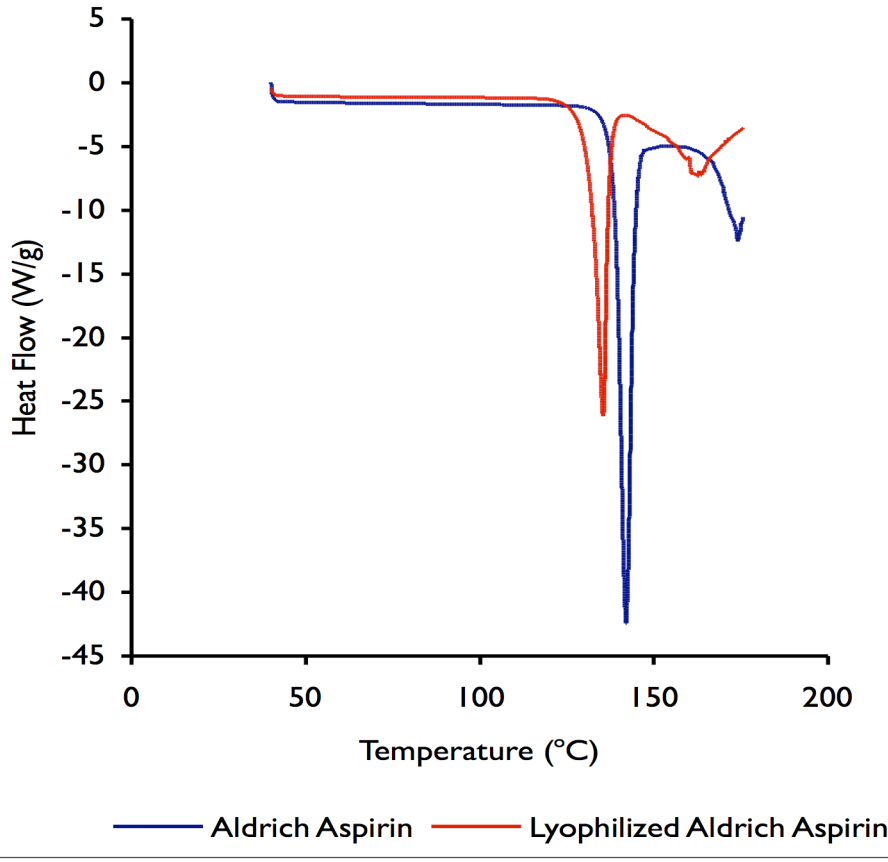

Figure A.5. DSC results showing melting of aspirin as received from Aldrich and after lyophilization. Bulk aspirin melts at ~138 °C and lyophilized aspirin melts at ~131 °C.

for the lyophilized aspirin are not due to crystal defects that may be produced during the lyophilization process.

To better investigate the conformation and possible interactions of the methyl group after lyophilization, aspirin with a ^{13}C labeled methyl group was synthesized from salicylic acid and ^{13}C labeled acetic anhydride (labeled at both methyl groups). The final product was analyzed using SSNMR, DSC, and HPLC to ensure that pure aspirin had been formed. The material was subsequently lyophilized and analyzed using SSNMR. The peak splitting and relaxation time were the same as the unlabeled lyophilized Aldrich aspirin, as shown in Figure A.6. The sample was then spun at 250 Hz to yield enough spinning sidebands for accurate tensor component analysis. The results indicate similar tensors for each methyl peak, as shown in Table A.1a. The chemical shift tensor values were also similar for the bulk aspirin (Table A.1b), indicating that the methyl groups in the lyophilized material experience similar environments to each other and to that of the methyl group in aspirin Form 1.

Initial two-dimensional SSNMR experiments with the ^{13}C labeled lyophilized material have been performed. Results from these studies are shown in Figure A.7. The observation of cross peaks indicates that the two types of methyl groups in the lyophilized aspirin are in close proximity to one another. Future work should involve performing additional two-dimensional SSNMR experiments that will allow determination of the distance between the methyl groups.

While SSNMR, Synchrotron, and DSC results show that lyophilization results in a mixture of aspirin forms, differences in the SSNMR spectrum of the aspirin recrystallized

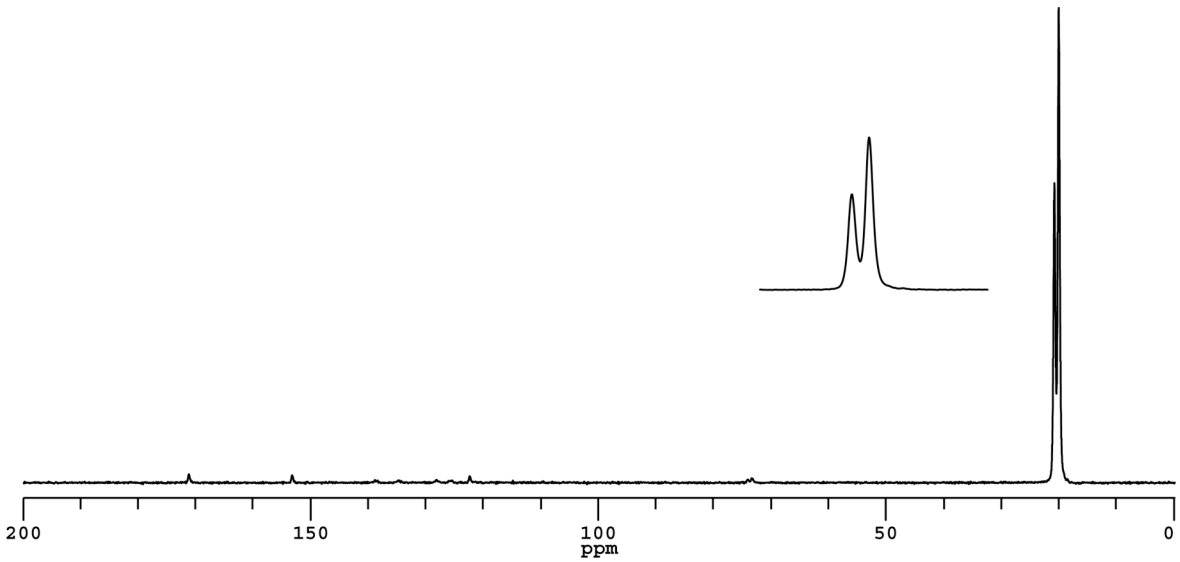

Figure A.6. SSNMR spectrum of ^{13}C labeled aspirin after lyophilization. An enlarged picture of the methyl peaks is included in order to show the splitting that occurs.

Table A.1. Principal values of the chemical shift tensor values for (a) ^{13}C lyophilized aspirin and (b) natural abundance bulk aspirin.

a)

Principal Values of the Chemical Shift Tensor for Aspirin Methyl			
Chemical Shift (ppm)	δ_{11}	δ_{22}	δ_{33}
20.8	37.79	28.83	-4.06
20.1	36.50	28.45	-4.78

b)

Principal Values of the Chemical Shift Tensor for Aspirin Methyl			
Chemical Shift (ppm)	δ_{11}	δ_{22}	δ_{33}
20.1	35.11	30.29	-4.86

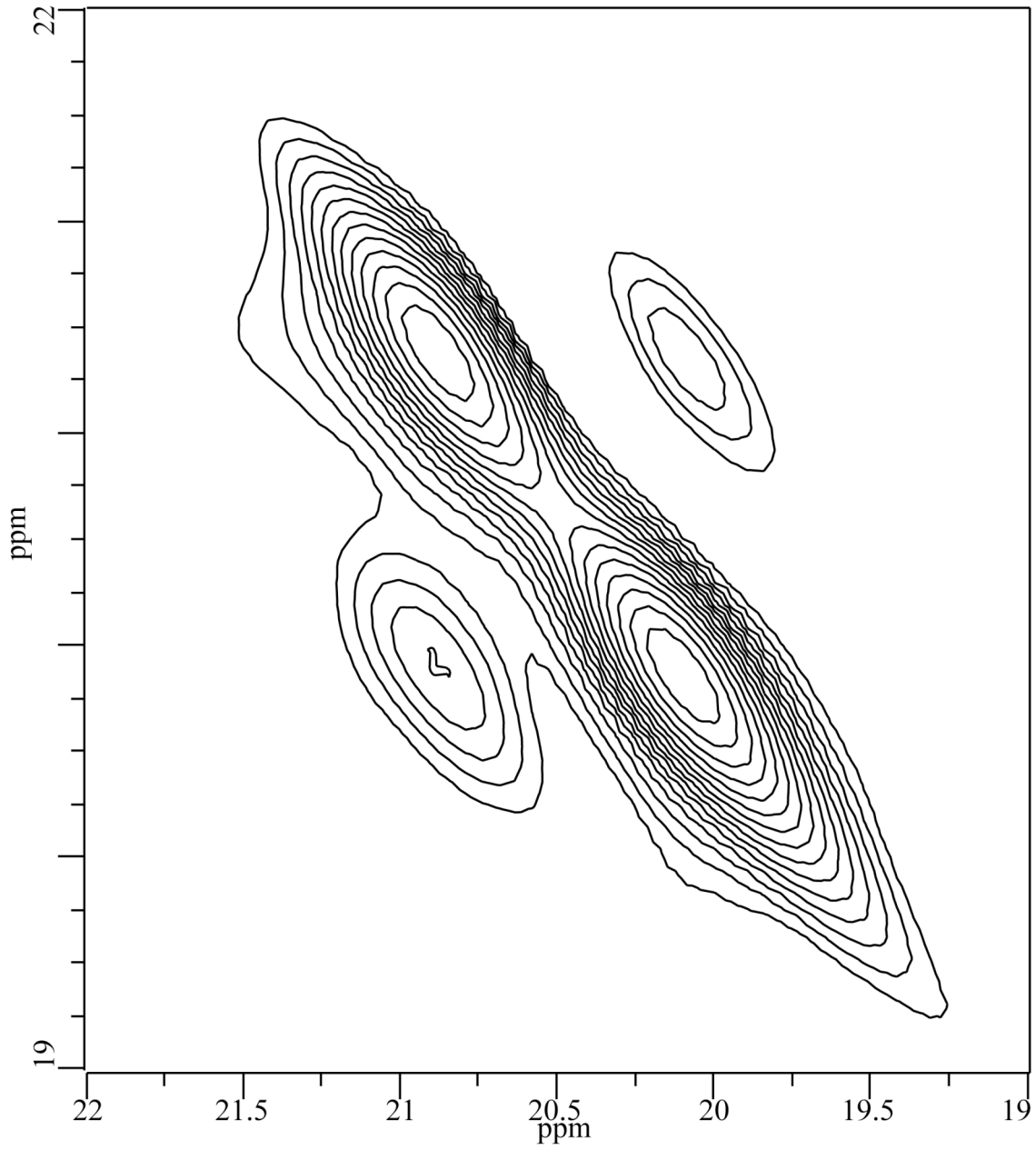

Figure A.7. 2D SSNMR results for ^{13}C labeled lyophilized aspirin.

from hot acetonitrile compared to the spectrum of the bulk aspirin were not observed. The relaxation times were also similar, with a T_1 value of 54 s for the recrystallized sample and a T_1 value of 60 s for the bulk aspirin. This suggests that this preparation method does not result in the same mixture of forms produced via lyophilization.

A.4 Discussion

Because of the uncertainty in the data presented by Vishweshwar[6], Bond and co-workers re-examined aspirin crystals using single-crystal X-ray diffraction.[13] The distinction between the two reported crystal structures was found to be slight. Both contain centrosymmetric dimers held together by O-H---O hydrogen bonds between their carboxyl groups. However, while the dimers are arranged in two-dimensional layers in both structures, the distinction lies in the way these two-dimensional layers are stacked. A relative translation by an amount equal to half the lattice repeat in one direction changes the way in which the methyl group of the acetyl substituent forms contacts with the carbonyl oxygen atom of a neighboring acetyl substituent. These two arrangements of layers are practically the same energy.

During the course of undertaking new crystallization experiments, the authors produced single crystals that displayed diffraction patterns of both the Form 1 and Form II structures simultaneously. The maximum amount of Form II observed in a sample was ~85%. Pure Form II could not be obtained.

These results can help explain some of the results observed in our laboratory. For instance, the fact that the two forms are essentially isoenergetic explains why their DSC melting temperatures were so close. The major change observed in the SSNMR spectrum of the lyophilized material is the splitting of the peak corresponding to the methyl group. The environment of the methyl carbon changes between the structures of the two forms, explaining why a new peak is observed in the SSNMR spectrum of the lyophilized material for this carbon, but peaks for most of the other carbons do not change. Chemical shift tensor experiments and two-dimensional SSNMR data support the conclusion that the two forms are not phase separated but rather co-exist as an intergrowth of two layers.

A.5 Conclusions

Lyophilization of aspirin produces a mixture of forms. It is likely that this mixture consists of aspirin Form I and the newly reported aspirin Form II. This is the first report of lyophilization as a means of producing the new form and of using SSNMR spectroscopy to characterize it. Future work should involve SSNMR spectroscopy analysis of aspirin crystals produced in the same way as reported by Vishweshwar and Bond.[6-8] These experiments would help to confirm the production of a mixture of aspirin Form I and aspirin Form II upon lyophilization.

A.6 References

1. Mitchell, A.G. and Saville, D.J. (1967). J. Pharm, Pharmac. 19, 729-734.

2. Tawashi, R. (1968). Science, N.Y., 160, 76.

3. Mitchell, A.G. and Saville, D.J. (1971). J. Pharm, Pharmac. 23, 534-535.

4. Mulley et al. (1971). J. Pharm, Pharmac. 23, 904.

5. Chang et al. (1986). Magnetic Resonance in Chemistry 24, 768-771.

6. Vishweshar, P. et al. (2005). J. Am. Chem. Soc. 127, 16802-16803.

7. Bond, A.D. et al. (2007). Angew Chem Int Ed. 46, 615-617.

8. Bond, A.D. et al. (2007). Angew Chem Int Ed. 46, 618-622.

9. Stephenson, G.A. et al. (1997) J. Pharm. Sci. 86 (11), 1239-1244.

10. Padden, B.E. et al. (1999) Anal. Chem. 71, 3325-3331.

11. Payne, R.S et al, (1999). J. Computational Chemistry, 20 (2), 262-273.

12. Ouvrard, C. et al, (2004). Crystal Growth and Design, 4 (6), 1119-1127.

13. Bond A.D. et al. (2007) Am. Pharm. Rev. *May/June*, 1-4.